

DOCTORAL THESIS

Energy Metabolism of Cancer: Unravelling Complexities Through Multiparameter Metabolic Analysis

Sten Miller

TALLINN UNIVERSITY OF TECHNOLOGY
DOCTORAL THESIS
34/2025

Energy Metabolism of Cancer: Unravelling Complexities Through Multiparameter Metabolic Analysis

STEN MILLER



TALLINN UNIVERSITY OF TECHNOLOGY
School of Science
Department of Chemistry and Biotechnology

NATIONAL INSTITUTE OF CHEMICAL PHYSICS AND BIOPHYSICS

Laboratory of Chemical Biology

This dissertation was accepted for the defence of the degree of Doctor of Philosophy in Chemistry on 06/05/2025

Supervisor: Tuuli Käämbre, PhD
Laboratory of Chemical Biology
National Institute of Chemical Physics and Biophysics
Tallinn, Estonia

Co-supervisor: Aleksandr Klepinin, PhD
(previously National Institute of Chemical Physics and Biophysics)
Institute of Genomics
University of Tartu
Tartu, Estonia

Opponents: Prof Emirhan Nemutlu, PhD
Department of Analytical Chemistry
Hacettepe University
Ankara, Turkey

Prof Sergei Kopantšuk, PhD
Chair of Bioorganic Chemistry, Institute of Chemistry
University of Tartu
Tartu, Estonia

Defence of the thesis: 10/06/2025, Tallinn

Declaration:

Hereby I declare that this doctoral thesis, my original investigation and achievement, submitted for the doctoral degree at Tallinn University of Technology has not been submitted for doctoral or equivalent academic degree.

Sten Miller

signature



European Union
European Regional
Development Fund



Investing
in your future

Copyright: Sten Miller, 2025

ISSN 2585-6898 (publication)

ISBN978-9916-80-303-5 (publication)

ISSN 2585-6901 (PDF)

ISBN 978-9916-80-304-2 (PDF)

DOI <https://doi.org/10.23658/taltech.34/2025>

Printed by EVG Print

Miller, S. (2025). *Energy Metabolism of Cancer: Unravelling Complexities Through Multiparameter Metabolic Analysis* [TalTech Press]. <https://doi.org/10.23658/taltech.34/2025>

TALLINNA TEHNIKAÜLIKOO
DOKTORITÖÖ
34/2025

**Energia metabolism vähis:
multiparametriline metaboolne
analüüs**

STEN MILLER



Contents

List of publications	7
Author's contribution to the publications	8
Introduction	9
Abbreviations	11
1 LITERATURE REVIEW	13
1.1 Overview of cancer metabolism	13
1.1.1 Historical perspective	13
1.1.2 Pathogenesis and traits of breast and colorectal cancer.....	13
1.1.3 Metabolic reprogramming in cancer	14
1.2 Metabolic pathways in cancer	16
1.2.1 Glycolytic pathway.....	16
1.2.2 OXPHOS and its regulation	17
1.2.3 Role of phosphotransfer networks in tumour formation	18
1.2.4 Mitochondrial Interactosome rearrangement in cancer cells	23
1.3 Experimental models for cancer metabolism research	24
1.4 Methodological approaches in cancer metabolism.....	25
1.4.1 Multiple analytical methods to study complex cancer metabolism	25
1.4.2 Stable isotope labeling in metabolic studies	26
1.4.3 ¹⁸ O labeling in metabolism research.....	28
1.4.4 Phosphometabolite analysis and quantification	30
2 AIMS OF THE STUDY	31
3 MATERIALS AND METHODS	32
3.1 Materials.....	33
3.1.1 Human post-operative samples.....	33
3.1.2 Cell cultures	33
3.1.3 Animals	33
3.1.4 Chemicals.....	34
3.2 Methods.....	34
3.2.1 Sample preparations.....	34
3.2.2 Chromatography.....	36
3.2.3 Analysis methods.....	37
3.2.4 Statistical analysis	40
4 RESULTS	41
4.1 Breast cancer cell lines metabolic profiling with ¹⁸ O method	41
4.1.1 Energetic status of cells	41
4.1.2 Profiling the creatine kinase pathway in breast cancer.....	41
4.1.3 Profiling the adenylate kinase pathway in breast cancer	42
4.2 Investigating CRC with oxygraphy and energy charges from adenine nucleotide quantification and enzyme kinetics	43
4.2.1 OXPHOS	43
4.2.2 OXPHOS across CRC progression	44
4.2.3 Adenine nucleotide quantifications.....	45
4.2.4 Glycolytic enzyme activities.....	46
4.3 NMR – Pure shift optimization, ATP from rat heart	48

5	DISCUSSION	49
5.1	Limitations of the study	56
	CONCLUSIONS	57
	List of Figures	58
	List of Tables	59
	References	60
	Acknowledgements.....	72
	Abstract.....	73
	Lühikokkuvõte.....	75
	Appendix 1	77
	Appendix 2	95
	Appendix 3	111
	Appendix 4	119
	Curriculum vitae.....	133
	Elulookirjeldus.....	135

List of publications

This thesis is based on the following publications:

- I Reinsalu, L*; **Miller, S***; Auditano, G. L ; Puurand, M ; Moreno-Sanchez, R; Käämbre, T (2025). The Energy Metabolism Profiling of Human Colorectal Tumors. *Journal of cellular and molecular medicine*, 29(5):e70462. doi:10.1111/jcmm.70462.
- II Klepinin, A; **Miller, S**; Reile, I; Puurand, M; Rebane-Klemm, E; Klepinina, L; Vija, H; Zhang, S; Terzic, A; Dzeja, P; Kaambre, T (2022). Stable Isotope Tracing Uncovers Reduced g/b-ATP Turnover and Metabolic Flux Through Mitochondrial-Linked Phosphotransfer Circuits in Aggressive Breast Cancer Cells. *Frontiers in oncology*, 12:892195. doi: 10.3389/fonc.2022.892195.
- III Kaup, K. K; Toom, L; Truu, L; **Miller, S**; Puurand, M; Tepp, K; Käämbre, T; Reile, I (2021). A line-broadening free real-time 31P pure shift NMR method for phosphometabolomic analysis. *The Analyst*, 146(22):7034. doi:10.1039/d1an90092g.
- IV Reinsalu, L; Puurand, M; Chekulayev, V; **Miller, S**; Shevchuk, I; Tepp, K; Rebane-Klemm, E; Timohhina, N; Terasmaa, A; Kaambre, T (2021). Energy Metabolic Plasticity of Colorectal Cancer Cells as a Determinant of Tumor Growth and Metastasis. *Frontiers in oncology*, 11:698951. doi: 10.3389/fonc.2021.698951.

* equal contribution

Author's contribution to the publications

Contribution to the papers in this thesis are:

- I The autor was involved in the conceptualization, conducted high-resolution respirometry, nucleotide quantification, Energy charge calculations, Enzyme activity assessments, handled data analysis and visualtization, and was responsible for writing and editing the original draft.
- II The autor participated in conceiving and designing the study, cultured cells, conducted isotope labelings, sample preparations, chromatographic separataions and quantifications, GC-MS experiments, data analysis, and visualization. The author also participated in writing and editing of the manuscript.
- III The author assisted conceptualization and conducting of experiments, conceptualized and performed the successful separation of ^{18}O labelled ATP molecule from biological sample and participated in writing and editin of the manuscript.
- IV The author participated in manuscript review and editing.

Introduction

As of today, cancer, more specifically, lung cancer is the fourth cause of death globally among noncommunicable diseases, ranking behind cardiovascular diseases, stroke, and chronic obstructive pulmonary disease respectively (WHO, 2024). According to estimates by the International Agency for Research on Cancer (IARC) in 2022, there were an estimated 20 million new cancer cases and 9.7 million deaths. The estimated number of people who were alive within 5 years following a cancer diagnosis was 53.5 million. About 1 in 5 people develop cancer in their lifetime, approximately 1 in 9 men and 1 in 12 women die from the disease. Lung cancer was the most commonly occurring cancer worldwide, with 2.5 million new cases, accounting for 12.4% of the total. Female breast cancer ranked second (2.3 million cases, 11.6%), followed by colorectal cancer (CRC) (1.9 million cases, 9.6%), prostate cancer (1.5 million cases, 7.3%), and stomach cancer (970 000 cases, 4.9%). Of the four most prevalent cancers, lung cancer has the highest mortality rate, with CRC, liver cancer, and breast cancer following in that order (IARC, 2022).

Cancer is characterized by notable alterations in cellular energy metabolism, enabling malignant cells to meet the increased demands for energy and biosynthetic precursors required for rapid growth and proliferation. One of the most well-known features of cancer metabolism is the Warburg effect, where cancer cells preferentially utilize aerobic glycolysis instead of relying on oxidative phosphorylation (OXPHOS) to produce Adenosine triphosphate (ATP), even in the presence of oxygen. However, recent research has revealed that this metabolic shift is more nuanced, involving complex interactions between glycolysis and mitochondrial respiration to support the metabolic needs of tumor cells (Alberghina, 2023).

The ever-changing nature of cancer metabolism, coupled with the heterogeneity of tumor biology, presents difficulties in fully understanding the metabolic reprogramming that occurs in different types of cancer. Traditional studies often focus on isolated systems that may not capture the full complexity of metabolic changes. To tackle these issues, there is a growing need for integrated methodological approaches that can offer a more exhaustive perspective of the metabolic alterations in cancer (J. Kim & DeBerardinis, 2019).

This study seeks to explore the metabolic reprogramming in cancer by employing a combination of advanced methodologies. These include ^{18}O isotope labeling to trace metabolic fluxes, high-resolution respirometry (oxygraphy) to assess mitochondrial function, and sophisticated metabolomic techniques such as ultra-performance liquid chromatography (UPLC), liquid chromatography (LC), and nuclear magnetic resonance (NMR). Applying these techniques to both human post-operative colorectal cancer samples and established cancer cell lines (Caco-2 for CRC, and MCF7, MDA-MB-231, and MCF10A for breast cancer) enables characterization of phosphotransfer networks (creatine kinase (CK), adenylate kinase (AK)), mitochondrial ATP synthesis rate, and activities of essential glycolysis pathway enzymes (hexokinase (HK) and lactate dehydrogenase (LDH)).

In addition, this study will explore how different experimental conditions, such as the application of metabolic inhibitors, affect cancer cell metabolism. Integrating findings from these diverse analytical approaches facilitates a detailed understanding of the energy metabolism in cancer cells, potentially uncovering novel metabolic vulnerabilities that could be targeted in therapeutic strategies.

This research contributes to the growing body of knowledge on cancer metabolism and offers perspectives that could influence the development of more effective cancer treatments by targeting the specific metabolic adaptations of cancer cells.

Abbreviations

α -KG	A-ketoglutarate
ADP	Adenosine diphosphate
AK	Adenylate kinase
AMP	Adenosine monophosphate
AMPK	AMP-activated protein kinase
ANC	Adenine nucleotide carrier
ANOVA	Analysis of variance
ANT	Adenine nucleotide translocator
ATP	Adenosine triphosphate
CK	Creatine kinase
CK-BB	Brain type creatine kinase
CK-MM	Muscle type creatine kinase
Cr	Creatine
CRC	Colorectal cancer
CSC	Cancer stem cell
Cyt c	Cytochrome c
DMEM	Dulbecco's modified Eagle medium
ETC	Electron transport chain
GC-MS	Gas chromatography-mass spectrometry
HK	Hexokinase
HPLC	High performance liquid chromatography
K _m	Apparent Michaelis-Menten constant
LC	Liquid chromatography
LDH	Lactate dehydrogenase
MIM	Mitochondrial inner membrane
MOM	Mitochondrial outer membrane
MtCK	Mitochondrial creatine kinase
NADH	Nicotinamide adenine dinucleotide
NMR	Nuclear magnetic resonance
OXPHOS	Oxidative phosphorylation
PCr	Phosphocreatine
Pi	Inorganic phosphate
SEM	Standard error of mean
sMtCK	Sarcomeric mitochondrial creatine kinase
TCA	Tricarboxylic acid

uMtCK	Ubiquitous mitochondrial creatine kinase
UPLC	Ultra high performance liquid chromatography
VDAC	Voltage-dependent anion channel
V_{\max}	Maximal mitochondrial respiration rate

1 LITERATURE REVIEW

1.1 Overview of cancer metabolism

1.1.1 Historical perspective

The study of cancer metabolism began with a pioneering discovery by Otto Warburg in the 1920s. Warburg observed that cancer cells exhibit a considerable preference for glycolysis over OXPHOS, even in the presence of sufficient oxygen, a phenomenon that became known as the Warburg effect (Warburg, 1956). This shift allows cancer cells to produce ATP less efficiently but at a faster rate, which supports their rapid proliferation. Warburg hypothesized that defects in mitochondrial respiration might be the cause of this metabolic reprogramming, and this theory dominated cancer metabolism research for several decades (Warburg, 1956).

In the following decades, research further explored the implications of the Warburg effect. It became clear that this metabolic shift also supports the biosynthetic demands of rapidly proliferating cancer cells, providing intermediates for the synthesis of nucleotides, lipids, and proteins. However, the idea that cancer cells universally rely on glycolysis, at the expense of mitochondrial function, began to be challenged as more advanced research tools became available (P. L. Pedersen, 1978).

By the early 2000s, advancements in molecular biology and metabolomics started to uncover the complexity of cancer metabolism, revealing that many cancer cells still maintain functional mitochondria and utilize OXPHOS in specific contexts (Vander Heiden et al., 2009; Ward & Thompson, 2012). Recent studies have shown that cancer cells can dynamically switch between glycolysis and mitochondrial respiration depending on the tumor microenvironment, nutrient availability, and stage of tumor development (Chelakkot et al., 2023).

This dual dependence on glycolysis and OXPHOS has led to the current understanding of metabolic plasticity in cancer cells. Rather than being limited to one pathway, cancer cells can utilize multiple metabolic strategies to adapt to various stressors such as hypoxia, limited glucose, or therapeutic interventions (Jia et al., 2018). For example, certain types of cancer, such as glioblastomas and pancreatic cancers, have been found to rely heavily on OXPHOS, especially during metastatic stages (Burban et al., 2023; Masoud et al., 2020). These findings shifted the focus of cancer metabolism research from a static view of glycolysis-dominated metabolism to a better overall understanding of metabolic flexibility.

1.1.2 Pathogenesis and traits of breast and colorectal cancer

While both CRC and breast cancer share common hallmarks, such as uncontrolled cell proliferation and evasion of apoptosis, their initiation and progression involve distinct molecular pathways and risk factors.

The average age of the population in developed societies is continuously increasing, which is also one of the reasons for the rising incidence of breast cancer. It has been established that the risk of developing the disease after the age of 65 is 5.8 times higher than before that age, and remarkably 150-fold higher compared to individuals under the age of 30 (Imyanitov & Hanson, 2004). Apart from age, several predispositions have been identified, which mostly fall into two categories: increased exposure to estrogens and deficiencies in maintaining genomic integrity, i.e., DNA damage. In addition to these, 5–10% of breast cancer cases are associated with inherited genetic mutations, primarily in the BRCA1 and BRCA2 genes (Feng et al., 2018).

Breast cancer can originate from milk ducts (ductal), lobules, or the surrounding tissues, and based on this, the cancer types can be broadly classified into carcinomas and sarcomas. Carcinomas, which make up the majority of breast cancers, are associated with breast epithelial tissue, such as lobular epithelial cells and the terminal parts of the milk ducts. These can further be classified into non-invasive, invasive, and metastatic carcinomas. Sarcomas, although quite rare, are typically associated with breast stromal tissue, which includes blood vessels and myofibroblasts. Often, breast cancer is a combination of both of these types (Feng et al., 2018).

From a molecular perspective, breast cancers are divided into four distinct subtypes, which are essential for treatment decisions and prognosis. 40% of breast cancers belong to the Luminal A subtype, which is estrogen receptor (ER) and/or progesterone receptor (PR) positive, human epidermal growth factor receptor 2 (HER2) negative, and expresses the proliferation marker Ki-67. About 20% are classified as Luminal B, which are ER and/or PR positive, HER2 negative or positive, and have a high Ki-67 level. HER2-positive breast cancers constitute 10–15% of cases, characterized by the absence of ER and PR expression, high HER2 expression, high proliferation gene cluster expression, and low luminal and basal cluster expression. Triple-negative breast cancers (TNBC) make up 20% of cases and are defined by the lack of ER, PR, and HER2 expression, making them the most aggressive subtype (Feng et al., 2018). The metabolic preference is least glycolytic in Luminal A, predominantly glycolytic in HER2 positive, leaning towards glycolytic and somewhere in between Luminal A and HER2 positive in Luminal B, and highly glycolytic in TNBC (García Vicente et al., 2013).

The development of CRC follows the “adenoma-carcinoma sequence”, in which normal colonic epithelium gradually transforms into an adenomatous polyp, serving as an intermediate stage, before progressing to adenocarcinoma (Morson, 1974). Mammalian cells have developed multiple protective mechanisms against potentially lethal mutations. Consequently, for tumorigenesis to be induced, mutations in multiple genes must occur simultaneously (Vogelstein & Kinzler, 2004). The heterogeneity of CRC is evident at the molecular level, over the past decades, various molecular phenotypes have been identified, including microsatellite instability (MSI), the CpG island methylator phenotype (CIMP), and somatic mutations in the oncogenes BRAF and KRAS (Cunningham et al., 2010; Kocarnik et al., 2015; Z. Yu & Yu, 2020). The first two phenomena manifest as global genomic dysfunction within CRC tumors, indicating genomic instability. In contrast, KRAS and BRAF mutations are point mutations that can act as initiators of CRC tumorigenesis (Kocarnik et al., 2015).

1.1.3 Metabolic reprogramming in cancer

The reprogramming of metabolism in cancer cells is widely believed to result from the progressive accumulation of genetic mutations (Amoedo et al., 2014). This reprogramming encompasses enhanced glycolysis, glutaminolysis, macromolecule biosynthesis, increased lipid and amino acid metabolism, mitochondrial biogenesis, and alterations in the pentose phosphate pathway (Hanahan & Weinberg, 2011).

Tumor cells exhibit elevated glycolysis, which also results in an increase in glucose uptake through the upregulation of glucose transporters (GLUT) such as GLUT1-GLUT5 (Ralph J. DeBerardinis et al., 2008). This characteristic is widely applied in medical diagnostics, particularly in Positron Emission Tomography (PET), where radiolabeled glucose analogs help visualize and locate tumors (Hsu & Sabatini, 2008). In healthy cells, glucose is typically converted to acetyl-CoA and enters the tricarboxylic acid (TCA) cycle.

In contrast, tumor cells convert glucose to lactate, with this excess lactate allowing glycolysis to continue by cycling nicotinamide adenine dinucleotide (NADH) back to NAD⁺, while the rest is expelled to create the tumor microenvironment (Figure 1). Although excess lactate production may seem wasteful, it is proposed that excreting excess lactate instead of converting it back to pyruvate helps prevent glycolytic slowdown caused by a high ATP/adenosine diphosphate (ADP) ratio, thereby maintaining a continuous supply of biosynthetic precursors essential for rapid cell division. Since proliferating cells often have abundant nutrients, maximizing ATP production is not always a primary concern (Vander Heiden et al., 2009). This topic is further explored in “1.2 metabolic pathways in cancer” and “1.2.4 mitochondrial interactosome rearrangement in cancer cells” sections of the thesis.

In glutaminolysis, glutamine is converted to glutamate and then to α -ketoglutarate, feeding into the TCA cycle. Tumor cells exploit TCA cycle intermediates to synthesize lipids, amino acids, and other essential molecules, while also generating electrons for the electron transport chain to produce ATP. Reprogramming glutaminolysis enhances both biomass production and energy synthesis (R. J. DeBerardinis & Cheng, 2010).

The pentose phosphate pathway is divided into two phases: oxidative and non-oxidative. The oxidative phase converts glucose-6-phosphate (G-6-P) into ribulose-5-phosphate, which is utilized for nucleotide synthesis, and nicotinamide adenine dinucleotide phosphate (NADPH), essential for biosynthesis reactions and managing oxidative stress. The non-oxidative phase produces fructose-6-phosphate (F-6-P) and glyceraldehyde-3-phosphate (G-3-P), with oxidative phase products supporting biosynthesis, glutathione production, and detoxification, while non-oxidative products feed into glycolysis. Tumor cells often upregulate the pentose phosphate pathway to resist radiation and chemotherapy, and to promote invasion and metastasis (Riganti et al., 2012).

Mitochondrial biogenesis is a key factor for tumor cells, as mitochondria are responsible for the majority of ATP production and assume critical functions in biosynthesis. Mitochondria regulate cellular homeostasis by maintaining redox balance and calcium (Ca²⁺) concentrations, establishing them as crucial for tumor growth and proliferation (Douglas C. Wallace, 2012). In cancer cells, mitochondria sometimes exhibit dysfunctions compared to normal cells. For instance, enhanced glycolysis in cancer cells supports survival by regulating cytochrome C (cyt C) and preventing apoptosis (Vaughn & Deshmukh, 2008). Mitochondria are also the primary source of reactive oxygen species (ROS) in the cell, and most cancers exhibit elevated ROS levels. ROS is implicated in various cellular processes, including cell cycle progression, survival, apoptosis, energy metabolism, cell morphology, adhesion, motility, angiogenesis, and the maintenance of tumor stemness (Liou & Storz, 2010).

Lipid biosynthesis is frequently upregulated in tumor cells, as they require a constant supply of new organelles and membranes. Changes in lipid composition and balance are commonly observed in cancer cells. Research has shown that lipid content can influence the formation and degradation of respiratory chain supercomplexes (Lenaz & Genova, 2012). Cholesterol levels in cancer cells are often elevated to promote cell proliferation and tumor growth (Gorin et al., 2012). Additionally, the lipid ganglioside has been identified in many tumors, where it supports angiogenesis and acts as an immunosuppressant (Lladó et al., 2014). Lipids are also involved in signaling, energy storage, and function as hormones. Alterations in lipid metabolism impact cell growth, proliferation, motility, and differentiation (Santos & Schulze, 2012). Tumor cells also tend to accumulate more lipid

droplets (Accioly et al., 2008). Obesity is one of the risk factors for cancer development. Elevated lipid levels induce insulin resistance, leading to increased secretion of insulin and insulin-like growth factors, which, in turn, promote cancer proliferation and survival (Rosenzweig & Atreya, 2010; Samuel & Shulman, 2012).

1.2 Metabolic pathways in cancer

1.2.1 Glycolytic pathway

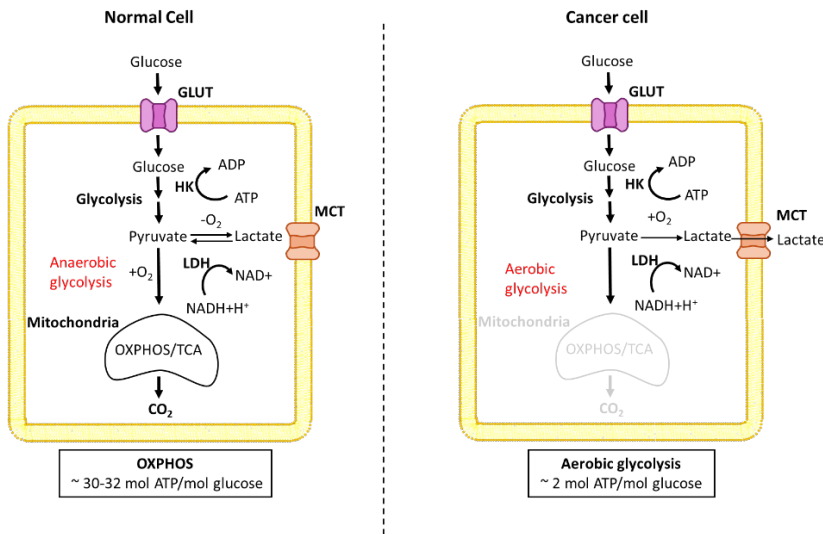


Figure 1. Glucose metabolism comparison of normal cells against cancer cells. Glucose is metabolized to pyruvate in normal cells, mainly for growth and survival, followed by complete oxidation of pyruvate to CO_2 through TCA cycle and OXPHOS in the mitochondria that generates 30-32 units of ATP. O_2 is essential, as it's the final acceptor of electrons, and when limited, pyruvate is metabolized to lactate. Cancer cells convert most glucose to lactate, regardless of O_2 availability (Warburg effect), which diverts glucose metabolites from energy production to anabolic process to speed up cell proliferation, generating only 2 units of ATP. Adapted from (with permission) (Marie & Shinjo, 2011).

Numerous glycolytic enzymes are overexpressed in cancer cells and tissues. The upregulation of GLUTs enhances glucose uptake in cancer, with GLUT1 and GLUT3 being notably overexpressed in various cancer types. The initial step of glycolysis, involving the conversion of glucose to glucose-6-phosphate (G-6-P) by the HK enzyme, is also frequently impacted. Mammals possess four isoforms of HK, among which HK2 is typically absent in most adult tissues, except for skeletal and adipose tissues. However, HK2 is overexpressed in numerous cancers and has been linked to poor clinical outcomes in various solid tumors (Y. Liu et al., 2016). Furthermore, the preferential mitochondrial localization of HK1 and HK2 not only grants direct access to ATP produced through OXPHOS but also plays a role in protecting cancer cells from apoptosis (Mathupala et al., 2006).

Another critical enzyme in the glycolytic pathway is pyruvate kinase (PK), which facilitates the conversion of phosphoenolpyruvate (PEP) to pyruvate. The M2 isoform of pyruvate kinase (PKM2) is upregulated in proliferating and cancer cells, supporting anabolic metabolic pathways (Israelson & Vander Heiden, 2015). The fate of pyruvate is influenced by the cellular state and microenvironmental conditions. In quiescent,

differentiated cells, pyruvate is transported into mitochondria, where it undergoes complete oxidation. In contrast, in cancer cells, pyruvate is converted into lactic acid, a process catalyzed by LDH (Figure 1). Elevated expression of LDH is observed in various cancer types and is linked to tumor growth, progression, and metastasis. Consequently, LDH is often regarded as a potential predictive biomarker for certain cancers and a promising therapeutic target for novel anticancer treatments (Gallo et al., 2015).

The reasons why cancer cells use aerobic glycolysis, a less efficient energy production pathway, remains largely unclear, despite being extensively studied for decades. One possible explanation for this metabolic shift is that enhanced glycolysis is a downstream effect of oncogene activation and tumor suppressor loss. For instance, mutations in the oncogene Ras drive glycolysis, while the loss of the tumor suppressor protein p53 disrupts mitochondrial function. Beyond genetic alterations, the tumor microenvironment plays a significant role in metabolic reprogramming. As tumors grow, the local blood supply becomes inadequate, leading to hypoxia and stabilization of hypoxia-inducible factor (HIF). HIF stimulates the expression of several glycolytic enzymes, glucose transporters, mitochondrial metabolism inhibitors, and angiogenesis-promoting factors, collectively enabling cancer cells to survive in low-oxygen conditions. Moreover, the altered glucose metabolism in cancer cells serves not only to sustain cell proliferation but also to supply essential intermediates for biosynthetic pathways. Increased glycolytic flux supports other cancer-critical processes, including resistance to apoptosis and the facilitation of cancer-specific signaling pathways (Hsu and Sabatini, 2008).

1.2.2 OXPHOS and its regulation

ATP is the predominant energy-storing and transferring molecule in cells, essential for the function of many energy-consuming processes, such as the biosynthesis of proteins and nucleotides, muscle contraction, signal transduction, and the transport of metabolites across the cell membrane. Aerobic organisms produce ATP primarily through glycolysis in the cytoplasm and OXPHOS in the mitochondria, and the preference or production ratio of each pathway depends largely on the cell type, its growth stage, and its microenvironment. Through OXPHOS, between 30–32 units of ATP can be produced (Figure 1), and under normal conditions, approximately 70% of ATP in cells is generated via OXPHOS (Nelson et al., 2021; Zheng, 2012).

The mitochondrion is an organelle that serves as the cell's main energy supplier. The mitochondrion is enclosed by two membranes, the inner membrane (MIM) and the outer membrane (MOM), which spatially differentiate the intermembrane space from the matrix. In the folds (cristae) formed by the inner membrane, the electron transport chain (ETC) establishes a proton gradient, and ATP is synthesized as a result of OXPHOS. The ETC comprises complexes that form the mitochondrial respiratory chain: (I) NADH coenzyme Q reductase, (II) succinate coenzyme Q reductase, (III) coenzyme Q-cytochrome c reductase, and (IV) cytochrome c oxidase. Electrons enter ETC complexes I and II on the inner membrane via NADH and succinate through the TCA cycle in the matrix. Electrons move from complexes I and II to coenzyme Q, which transfers them to complex III. Subsequently, via cyt c, electrons are transported to complex IV, where they are transferred to an acceptor (oxygen), reducing oxygen to water molecules.

During this thermodynamic reaction, the energy released pumps protons against their gradient from the matrix into the intermembrane space. To restore balance, protons flow back into the matrix through ATP synthase, generating an electrochemical

gradient that activates ATP synthase, converting ADP and inorganic phosphate into ATP (Figure 2) (Sousa et al., 2018).

The regulation of oxidative phosphorylation, as originally postulated by Kadenbach, occurs through the allosteric modulation of complex IV by nucleotides (Kadenbach, 1986). Later, it was found that it is not the intracellular levels of ATP or ADP, but rather the intracellular ATP/ADP ratio that affects the activity of complex IV and controls overall OXPHOS (Napiwotzki & Kadenbach, 1998). To prevent the inhibitory effects of nucleotides on OXPHOS, ATP molecules do not diffuse intracellularly; instead, the transfer of ATP's high-energy phosphoryl group to energy-consuming compartments occurs via enzymatic pathways. These enzymatic pathways for phosphoryl group transfer consist of fast, sequentially balanced chains of phosphorylation transfer reactions (Zeleznikar et al., 1995).

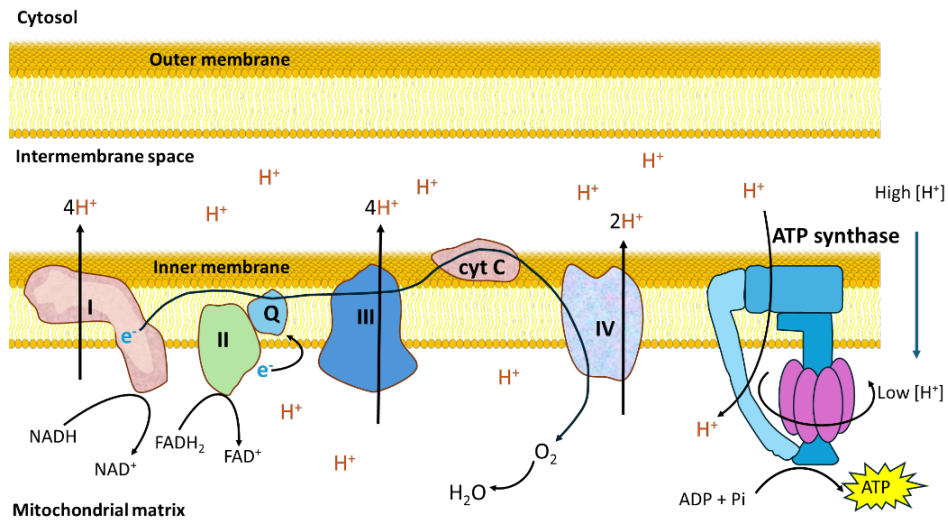


Figure 2. The mitochondrial respiratory chain facilitates proton transport across the inner mitochondrial membrane via complexes I, III, IV, and ATP synthase, using NADH and succinate to produce ATP. Electrons enter the electron transport chain located on the inner membrane through complex I via NADH and through complex II via FADH₂ oxidation to FAD⁺. The electrons then travel along the respiratory chain, where coenzyme Q (Q) and cytochrome c (cyt c) mediate their transfer to complex IV, where they reduce oxygen to form water. The energy released from these thermodynamically favorable reactions is used by complexes I, III, and IV to create a proton gradient. Protons then flow back into the matrix through ATP synthase (driven by the electrochemical gradient), which rotates the ATP synthase rotor, thereby synthesizing ATP from ADP and inorganic phosphate (Pi) Adapted from (with permission) (Sousa et al., 2018).

1.2.3 Role of phosphotransfer networks in tumour formation

The spatial coordination of intracellular ATP production and consumption processes is essential for maintaining cellular homeostasis. This coordination underpins various critical cellular functions, such as maintaining ion gradients across membranes, facilitating cell motility, and regulating nuclear processes like DNA replication and the transport of macromolecules across the nuclear membrane (Petras P. Dzeja et al., 2007).

Two primary theories describe the movement of nucleotides between different cellular compartments. The first theory proposes that adenine nucleotides diffuse

between sites of ATP production and consumption. However, this process is kinetically and thermodynamically inefficient, as it requires a substantial concentration gradient (P. P. Dzeja & Terzic, 2003).

According to the second theory, energy transfer between ATP-producing and ATP-consuming compartments is mediated by a phosphotransfer network. This mechanism is significantly more efficient than diffusion, as it relies on rapid, sequential reactions that transfer phosphoryl groups. The phosphotransfer network primarily involves CK, AK, and glycolytic enzymes (Figure 3) (P. P. Dzeja & Terzic, 2003).

CK catalyzes the transfer of a high-energy phosphoryl group between ATP and creatine (Cr) and between ADP and PCr (equation 1).



The primary functions of the creatine kinase network in cells are to act as an intracellular energy buffer and to prevent the excessive accumulation of intracellular ADP. This buffering mechanism ensures the maintenance of ATP/ADP balance across various cellular compartments, even under conditions of high energy demand (Wallimann et al., 1992). Another critical role of CK is the facilitation of energy transport. CK mediates the movement of energy in both directions: from ATP-consuming centers to the mitochondria and from the mitochondria back to ATP-consuming centers via a series of Cr/PCr reactions (Figure 3) (Wallimann et al., 1992).

In mammals, four genes encode CK, and CK enzymes are broadly classified into two categories: mitochondrial CK (MtCK) and cytosolic CK. MtCK is further divided into ubiquitous MtCK (uMtCK) and sarcomeric MtCK (sMtCK). The cytosolic forms include CK-BB (B-brain type) and CK-MM (M-muscle type), with homodimers that can also form the CK-MB heterodimer. CK expression is tissue-specific and predominantly occurs in tissues with high energy demand. uMtCK is typically co-expressed with cytosolic CK-BB, whereas sMtCK is exclusively expressed in muscle tissues, such as skeletal and cardiac muscle, where it is co-expressed with cytosolic CK-MM (Ishida et al., 1994; Wallimann et al., 1992).

In breast cancer and other malignant tumors, both CK-BB and uMtCK are frequently overexpressed, with elevated uMtCK levels particularly associated with poor survival outcomes in breast cancer (Li et al., 2013; X.-L. Qian et al., 2012). In CRC it has been shown that inhibiting activities of CK-BB and mtCK suppressed its growth, stemness, and metastasis. The study suggested that creatine shuttle via CK-BB and MtCK may supply ATP for phosphorylation (Kita et al., 2023). Similar findings were discussed in lung cancer research, where it was found that plasma levels of CK, along with LDH, were both independently and closely related to metastasis occurrence and patient survival. Specifically, plasma CK levels dramatically decreased in lung cancer patients, hypothetically being “recruited” by tumor cells to aid their growth (L. Liu et al., 2017). Another study suggested that CK, or specifically uMtCK, may also associate with glycolytic enzymes, such as HK2 to enhance glycolysis and ATP production in gastric cancer (Mi et al., 2023).

Experiments in a CK knockout mouse model have demonstrated that AK can maintain normal cellular homeostasis in the absence of CK, indicating a compensatory mechanism when CK is suppressed (P. P. Dzeja & Terzic, 1998; P. P. Dzeja et al., 2004).

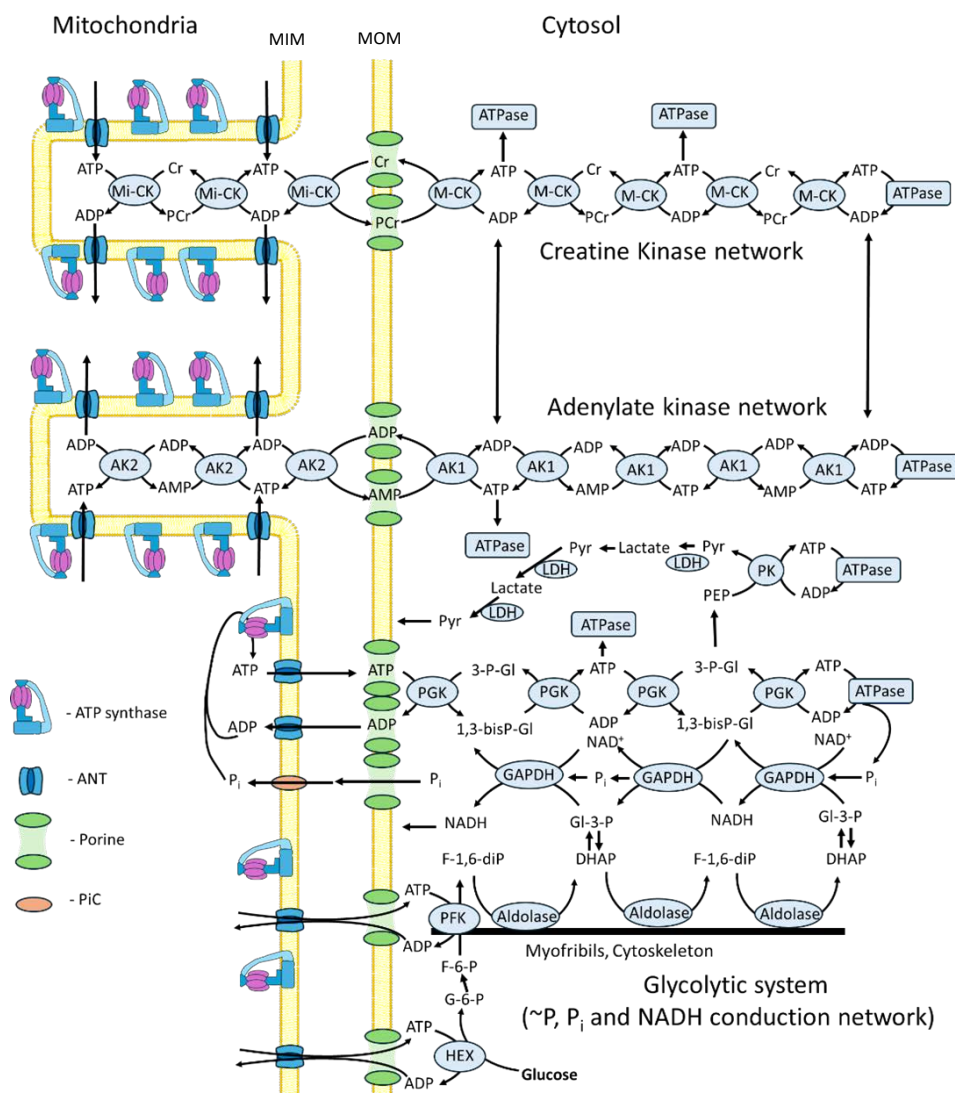


Figure 3. The intracellular phosphotransfer network is catalyzed by creatine kinase (CK) and adenylate kinase (AK), facilitating the transfer of phosphoryl groups between ATP-consuming and ATP-generating compartments, as well as mediating metabolic signal communication. CK catalyzes the transfer of phosphate groups between phosphocreatine (PCr) and ADP, while AK catalyzes the reversible transfer of phosphate groups between ATP and AMP. The mitochondrial isoforms of creatine kinase (MtCK) and adenylate kinase (AK2) supply oxidative phosphorylation (OXPHOS) with ADP through the adenine nucleotide translocator (ANT). Additionally, MtCK and AK2 facilitate the export of ATP from the mitochondria. The exported ATP is transferred to ATPases through a series of sequential reactions mediated by the cytosolic isoforms of creatine kinase (M-CK) and adenylate kinase (AK1). The glycolytic system also plays a role in intracellular energy transfer and metabolic signaling by generating ATP and assisting in the movement of high-energy phosphoryl groups. Key glycolytic enzymes near mitochondria, such as hexokinase (Hex) and phosphofructokinase (PFK), help integrate glycolysis into the phosphotransfer network. Additionally, reversible enzyme reactions contribute to maintaining cellular energy balance, especially under high metabolic demand. The organization of glycolytic enzymes within the cytoskeleton and other cellular structures ensures efficient energy distribution. Adapted from (with permission) (P. P. Dzeja et al., 2004).

In many organisms, AK is an evolutionarily conserved and ubiquitous enzyme that plays a crucial role in maintaining adenine nucleotide homeostasis. AK catalyzes a reversible reaction in which the γ -phosphoryl group from ATP is transferred to adenosine monophosphate (AMP), generating two molecules of ADP (equation 2).



A unique feature of AK is its ability to transfer not only the γ -phosphoryl group of ATP but also the β -phosphoryl group (Figure 4), effectively doubling the energetic potential of ATP. AK is distributed throughout various cellular compartments, where it monitors the intracellular ATP/ADP ratio (P. Dzeja & Terzic, 2009; Tanabe et al., 1993).

In humans, nine distinct AK isoforms (AK1-AK9) have been identified, numbered in the order of their discovery. These isoforms differ in molecular weight, tissue distribution, subcellular localization, substrate specificity, phosphate donor preferences, and kinetic properties (Panayiotou et al., 2014). This diversity and distribution are not random but have evolved to support specific cellular processes, such as muscle contraction, neuronal electrical activity, cell motility, and mitochondrial communication with other organelles (P. Dzeja & Terzic, 2009). In tissues with high energy demands, the predominant isoform is AK1, which is located in the cytosol and is primarily expressed in skeletal muscle, brain, and erythrocytes (Tanabe et al., 1993). AK2, on the other hand, is located in the intermembrane space of mitochondria and is mainly expressed in the liver, heart, skeletal muscle, spleen, and kidneys (Tanabe et al., 1993). Both isoforms catalyze the reversible reaction, with AK1 producing ATP and AMP during muscle contraction, for example. ATP supports ATPase activity, while AMP acts as a metabolic signal to synchronize ATP consumption and production rates (Figure 3). Even the smallest amount of AMP reaching the mitochondria is rapidly converted to ADP by AK2, which is then directed to the mitochondrial matrix (P. Dzeja & Terzic, 2009).

AK3 and AK4 isoforms are found in the mitochondrial matrix, and both are expressed in mitochondria-rich tissues such as the brain, heart, liver, and kidneys (Panayiotou et al., 2014). Despite their similar localization and high structural homology, these isoforms differ significantly in their catalytic activities. AK3 is a widely distributed GTPphosphotransferase involved in the catalytic reactions of the citric acid cycle, where GTP is converted to GDP (guanosine diphosphate) (Noma et al., 2001). Although AK4 exhibits lower activity than AK3, it has been shown to be strongly upregulated under stress conditions. Experiments in neuroblastoma cells have demonstrated that AK4 overexpression protects cells from H_2O_2 -induced cell death (R. Liu et al., 2009).

Studies dating back to the 1980s in a rat model linked elevated AK activity to the development of prostate cancer (Hall et al., 1985). AK1, an isoform predominantly expressed in tissues with high energy demand, has shown contrasting findings. Some studies suggest that the downregulation of AK1 may have a tumor-initiating effect, as demonstrated by the transformation of mouse embryonic fibroblasts into tumor cells (Vasseur et al., 2005). In contrast, another study suggested that upregulation of AK1 in breast cancer cell lines indicated tumorigenesis initiation (Choong et al., 2010).

Recent studies propose that the interplay between AK2 and MtCK in the mitochondrial intermembrane space may contribute to the plasticity of cellular energetics and the phosphotransfer system, which, in turn, is utilized by cancer cells to promote uncontrolled growth. (A. Klepinin et al., 2020). For example, when MtCK is downregulated, AK2 is

upregulated, as shown in studies with embryonal cancer cells (Lyudmila Ounpuu et al., 2017). It has also been demonstrated that the mitochondrial creatine kinase system is dysfunctional in CRC and instead depends on AK2 to sustain energetic homeostasis (Kaldma et al., 2014).

AK4 also exhibits tumorigenic properties. Notably, one study on HeLa cells proposes a model in which hypoxia increases AK4 expression, leading to its interaction with adenine nucleotide translocator (ANT), voltage-dependent anion channel (VDAC), and HK. This interaction forms a transmembrane complex that enhances ADP recycling, which is subsequently converted to ATP by ATP synthase. This plays a significant role in malignancy and development of drug resistance (Fujisawa et al., 2016).

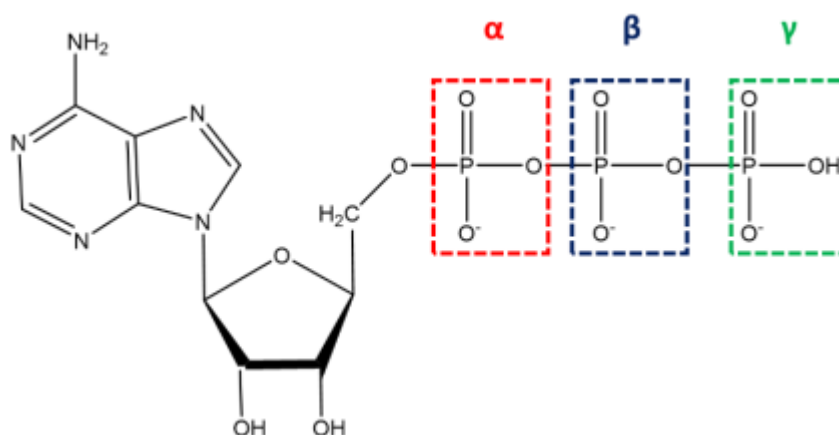


Figure 4. Labeling of the phosphoryl group positions in adenosine triphosphate (ATP). The figure illustrates the arrangement of the phosphate groups in ATP, where the dashed-line box indicates the positions of the phosphoryl groups: red represents the α-phosphoryl, blue represents the β-phosphoryl, and green represents the γ-phosphoryl.

1.2.4 Mitochondrial Interactosome rearrangement in cancer cells

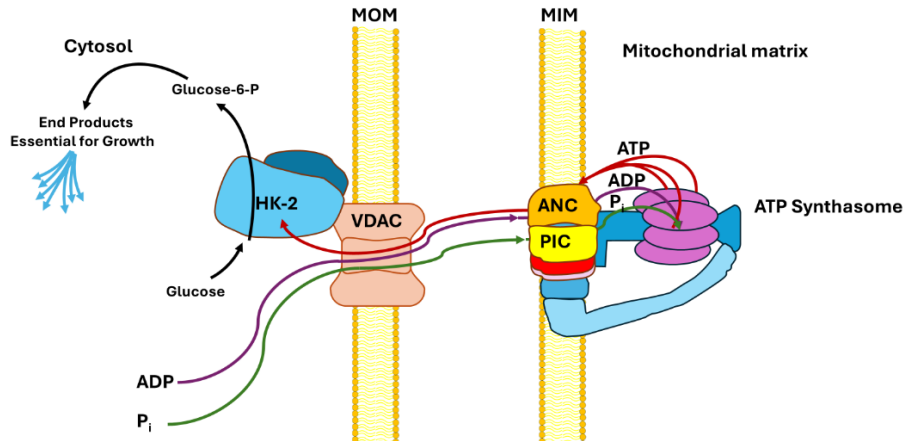


Figure 5. Diagram depicting the Pedersen model. HK2 associates with the VDAC channel, granting it direct access to ATP produced by ATP synthasome while also promoting ADP transport across MOM for ATP production. This interaction prevents HK2 from being inhibited by glucose-6-phosphate, its end product, effectively accelerating glycolysis. As a result, the majority of glucose is converted into lactate rather than pyruvate, which in healthy cells would support oxidative phosphorylation. Instead, the lactate is utilized for biomass production. Adapted from (with permission) (P. L. Pedersen, 2007)

In order to synthesize ATP in the mitochondrial matrix by ATP synthase, ADP from cytosol needs to be transported across both mitochondrial membranes. There are two critical components that mediate this adenine nucleotide exchange between the matrix and cytosol: ANT on the MIM and a class of porin, named VDAC on the MOM. The VDAC facilitates the flux of ATP, ADP, and P_i through the MOM, and as a result, OXPHOS is mainly controlled by it. Closure of this channel restricts the availability of essential substrates for mitochondrial respiration and inhibits the exchange of ADP and P_i for ATP, ultimately impairing the efficiency of OXPHOS (Lemasters & Holmuhamedov, 2006; D. C. Wallace, 1999)

The MOM itself represents a critical bottleneck for the transport and microcompartmentalization of adenine nucleotides and other energy metabolites due to its selective permeability, which in turn, is responsible for energy flux and feedback communication. Previous research on permeabilized cardiac muscle cells introduced the term “Mitochondrial Interactosome” (MI), referring to a multiprotein transmembrane supercomplex composed of ANT, VDAC, ATP synthasome, AK, HK, mtCK, and other associated proteins. This supercomplex is responsible for facilitating energy transfer fluxes and regulating mitochondrial respiration (Guzun et al., 2015). VDAC, as a component of this supercomplex, has been shown to play a pivotal role in adenine nucleotide regulation. This relationship has been demonstrated through the determination of the apparent affinity of mitochondria for exogenous ADP (K_m (ADP)), which was measured using high-resolution respirometry in permeabilized cells and tissues but not in isolated mitochondria. That is mainly because isolation of mitochondria disrupts their normal morphology and interactions with other cellular structures and cellular outer membrane permeability to metabolites is regulated and has diffusion restrictions (Puurand et al., 2018).

Prior studies have demonstrated that VDAC is a crucial regulator in determining the balance between OXPHOS and glycolysis in cancerous cells and could be a potential target for drug development (Maldonado, 2017).

The Pedersen model further describes how HK2 binding to VDAC on the MOM affects membrane permeability and adenine nucleotide transport. By anchoring to VDAC, HK2 prevents its closure, maintaining an open conformation that facilitates the exchange of ATP, ADP, Pi between the cytosol and intermembrane space. This structural organization enables efficient ATP supply to HK2, allowing it to drive high glycolytic activity while preventing product inhibition by G-6-P. By maintaining VDAC in an open state, this interaction facilitates ADP and ATP flux across the MOM, which is essential for sustaining the altered metabolism observed in cancer cells. This mechanism supports continuous energy production and plays a role in apoptosis resistance. (Figure 5) (P. L. Pedersen, 2007).

1.3 Experimental models for cancer metabolism research

Cancer research commonly relies on two principal models for studying tumor metabolism and evaluating therapeutic interventions: *in vitro* cancer cell lines and clinical materials such as tumor biopsies. Each model offers distinct advantages and limitations, influencing its utility in cancer metabolism research (Sinha et al., 2021).

Cancer cell lines are widely used due to their ability to be cultured indefinitely and their relative ease of use. Many cell lines retain key genetic and metabolic features of the tumors from which they were derived, making them valuable tools for investigating cancer biology and testing therapeutic strategies. These cell lines facilitate the study of metabolic pathways such as glycolysis, glutaminolysis, and OXPHOS, all of which are critical to cancer cell survival and proliferation (Mirabelli et al., 2019). However, genomic comparisons between cell lines and tumors reveal significant differences, particularly in epigenetic regulation and gene expression profiles. While many cell lines share similarities with primary tumors, these discrepancies highlight the limitations of cell lines in fully capturing the complexity of the tumor microenvironment (Sinha et al., 2021). For example, studies in breast cancer show that while some cell lines closely mimic certain subtypes of the disease, others exhibit far less resemblance to primary tumors, underscoring the need for careful selection of representative cell lines (Jiang et al., 2016).

In contrast, tumor biopsies provide a more accurate representation of cancer within its natural microenvironment. These samples retain the complete genomic, epigenetic, and metabolic characteristics of the tumor, including the interactions between cancer cells, stromal cells, and immune cells, which are often absent or altered in *in vitro* models (Dragic et al., 2024). Consequently, tumor biopsies are invaluable for understanding how cancer metabolism is influenced by the tumor microenvironment. However, the use of clinical materials is limited by their availability and the difficulty of maintaining them for extended research periods. Furthermore, unlike cancer cell lines, tumor biopsies cannot be cultured indefinitely, which restricts their use in long-term experiments. Despite these challenges, tumor biopsies remain crucial for investigating metabolic processes that are closely linked to tumor progression and therapeutic resistance (Potter et al., 2009).

One of the main challenges in cancer metabolism research are the observed discrepancies in gene expression and mutation profiles between *in vitro* cell lines and clinical tumor samples. These differences can limit the clinical relevance of findings derived from cell line-based studies. To address this issue, computational tools such as TumorComparer have been developed to match cell lines more accurately with tumor profiles, potentially improving the translational potential of cell line studies

(Sinha et al., 2021). In addition to computational solutions, advanced experimental models have emerged that aim to replicate the tumor microenvironment more faithfully. Three-dimensional (3D) culture systems and patient-derived xenografts (PDXs) are increasingly used to bridge the gap between cell lines and clinical materials. These models allow for the study of cancer metabolism in a more physiologically relevant context, better reflecting the heterogeneity of tumors and their response to metabolic therapies (Cortesi et al., 2024; Sablatura et al., 2020).

Both cancer cell lines and clinical tumor materials play essential roles in cancer metabolism research, each offering unique insights into the metabolic processes that drive tumor growth. However, with recent advancements in computational efficiency, a new modeling approach has emerged – computational modeling combined with systems biology. This approach has provided strong evidence of cancer’s ability to exist in a so-called ‘third state’, also known as hybrid metabolism, where cancer cells can simultaneously utilize both OXPHOS and aerobic glycolysis. This discovery highlights the need for new therapeutic strategies specifically targeting the hybrid state, as well as further investigation into how different metabolic pathways contribute to cancer cell survival and oncogenic potential (L. Yu et al., 2017). By integrating these models with advanced techniques such as 3D cultures and PDXs, researchers can gain a deeper understanding of cancer metabolism and enhance the translational relevance of preclinical studies.

1.4 Methodological approaches in cancer metabolism

1.4.1 Multiple analytical methods to study complex cancer metabolism

A combined approach in cancer research is justified due to the inherent complexity of cancer biology, where multiple interconnected molecular pathways influence disease progression and treatment response. Recent research on cancer stem cells (CSCs) has shown that genetic alterations and epigenetic events contribute to tumor heterogeneity. However, metabolism serves as a critical junction, integrating cumulative information from multiple signaling layers, including the genome, transcriptome, proteome, and microenvironment. CSC states can adapt, resist, or respond to these multi-omic influences through the differential regulation, synthesis, and availability of specific metabolites (Cuyàs et al., 2017). The metabolome, as the final downstream product of all omics layers, best represents the biological phenotype. Metabolomics bridges genome, transcriptome, proteome, and environmental influences, offering a powerful tool to clarify complex omics data. Cataloging a few homogeneous CSC metabolomic phenotypes could help decode tumor heterogeneity; however, metabolite fluxes (fluxomics) is an indispensable complementary tool, especially for tracking metabolic adaptations in response to treatment (Cuyàs et al., 2017). Previous research on biomarkers from blood samples of hepatocellular carcinoma patients has demonstrated that the integration of proteomic, glycomic, and metabolomic datasets significantly enhances the discovery of cancer biomarkers (M. Wang et al., 2016). A review by Srivastava and Creek highlighted how multi-omic analysis of plasma and serum identified biomarker panels with higher diagnostic accuracy for cancers like pancreatic and lung cancer. Key metabolites such as 2-hydroxyglutarate, glutamine, glycine, and serine were linked to cancer progression, underscoring the value of this approach for non-invasive biomarker discovery and clinical translation (Srivastava & Creek, 2019).

Another review by Benjamin et al. discusses how proteomics and enzyme activity profiling are used to understand metabolic reprogramming in cancer. It highlights

findings from studies on cancer cell lines, primary tumor tissues, and xenograft models, focusing on key enzymes like PKM2, PHGDH, MAGL, KIAA1363, and mutant IDH1/2. The review emphasizes methods such as ABPP, metabolic flux analysis, and post translational modifications profiling to study enzyme activity and showcases how dysregulation in glycolysis, amino acid metabolism, and lipid biosynthesis supports cancer progression and identifies potential therapeutic targets like PKM2 and MAGL (Benjamin et al., 2012).

In conclusion, these examples, among many others not mentioned here, highlight the importance of a combined methodological approach in cancer research. The integration of multiple analytical methods allows for a more comprehensive understanding of the complex molecular interactions that drive cancer progression.

1.4.2 Stable isotope labeling in metabolic studies

Metabolomic analyses of cells often require extensive, systematic, and simultaneous fingerprinting of multiple metabolites. These metabolites must be identified and quantified based on their cellular and systemic variations, which can be influenced by diseases, drugs, toxins, as well as genetic and environmental factors. Due to the vast differences in the physicochemical properties of various metabolites, a range of complementary analytical methods must be employed, as no universal platform exists as of today (Beckonert et al., 2007).

Advanced spectroscopic methods that provide diverse datasets are necessary for accurate metabolic profiling in metabolomic studies. These spectroscopic techniques are primarily based on NMR spectroscopy (^1H , ^{13}C , ^{31}P , ^{18}O , etc.) and mass spectrometry (MS) (Lenz & Wilson, 2007). However, metabolite concentrations alone may not reflect changes in their fluxes or turnover rates (Kruger & Ratcliffe, 2009). Therefore, to describe a comprehensive metabolic profile, it is not enough to measure metabolite concentrations; their turnover rates must also be determined, allowing for the calculation of metabolic fluxes and the overall dynamic profile. This complex analysis is enabled by methods based on stable isotope labeling (Emirhan Nemutlu et al., 2014).

Since the 1930s, when stable isotopes were first isolated, they have become indispensable tools in the study of disease-related metabolism, aging, and genetic disorders (Wilkinson, 2018). Stable isotopes are chemically and functionally identical to their primary elements but differ in mass due to varying numbers of neutrons in the atomic nucleus. Currently, over 6,000 compounds containing stable isotopes are available for metabolism research, with the primary isotopes being ^2H , ^{13}C , ^{15}N , ^{18}O , and ^{17}O (Table 1) (Bodamer & Halliday, 2001; Wilkinson, 2018).

A characteristic feature of many cancers is the upregulation of the glycolysis pathway compared to OXPHOS, which occurs even in the presence of sufficient oxygen (the Warburg effect). This process leads to lactate production, which acidifies the extracellular environment (Andrew N. Lane et al., 2019). In addition to glycolysis, tumors need to upregulate other metabolic pathways to support growth, metastasis, and survival in hostile environments, especially those related to the synthesis of precursors for nucleic acids, lipids, proteins, and carbohydrates. One example is $^2\text{H}_3$ -serine, a labeled compound used to study purine biosynthesis in tumor cell cultures through serine hydroxymethyltransferase, using ultra-high-resolution Fourier transform mass spectrometry (UHR-FTMS) (Yang et al., 2017).

Deuterium oxide ($^2\text{H}_2\text{O}$) is used for mass isotopomer analysis to determine the fractional biosynthesis of palmitate, stearate, and cholesterol in tumor cells (Lee et al.,

1994). Labeled glucose ([U-¹³C]-glucose) is employed to study glycolysis, the Krebs cycle, the pentose phosphate pathway, hexosamine biosynthesis, and nucleotide and lipid biosynthesis in tumor cells, utilizing NMR and mass spectrometry (A. N. Lane et al., 2017). Labeled lactate ([U-¹³C]-lactate) can be applied to investigate both the Krebs cycle and gluconeogenesis in lung cancer through phosphoenolpyruvate carboxykinase. This involves measuring isotopic enrichment in phosphoenolpyruvate using mass spectrometry after incubating cell cultures in labeled media (Leithner et al., 2015). The infusion of ¹⁵N₂-labeled arginine has been used in lung cancer studies through in vivo experiments in patients and healthy subjects. In these studies, blood samples were analyzed by mass spectrometry to investigate de novo arginine synthesis through the conversion of citrulline to arginine and nitrogen oxide synthesis through the conversion of arginine to citrulline (Engelen et al., 2016).

The oxygen isotope ¹⁷O has not found widespread use due to its very low natural abundance and high cost. However, it has been applied in the study of brain oxygen metabolism, which is severely disrupted following stroke or tumor formation. The cerebral metabolic rate of oxygen consumption (CMRO₂) is measured by ¹⁷O-labeled water (H₂¹⁷O) using ¹⁷O magnetic resonance imaging (MRI). H₂¹⁷O is the end product of oxygen metabolism when the subject breathes ¹⁷O-enriched gas (Kurzhunov et al., 2017).

Table 1. Common Stable Isotopes in Cancer Research. The table presents stable isotopes and their natural abundance (%) compared to the primary element, along with the labeled compound(s) and the corresponding metabolic pathways investigated using these isotopes. The table is adapted from (Kurzhunov et al., 2017; Andrew N. Lane et al., 2019; Wilkinson, 2018).

Stable Isotope	Natural abundance (%)	Labeled Compound(s)	Metabolic Pathways studied
² H	0,015	² H ₃ -serine	Serine and one-carbon metabolism, purine biosynthesis, lipids synthesis
		² H ₂ O	Lipids synthesis <i>in-vivo</i>
¹³ C	1,11	[U- ¹³ C]-glucose	Glycolysis, Krebs-cycle, pentose phosphate pathway, hexoamine biosynthesis pathway, serine glycine one-carbon metabolism, nucleotides and lipids synthesis
		[U- ¹³ C]-lactate	Krebs-cycle, gluconeogenesis
		[U- ¹³ C]-serine	Serine and one-carbon metabolism, purine biosynthesis, lipids synthesis
¹⁵ N	0,37	¹⁵ N arginine, citrulline	Arginine and nitrogen oxide metabolism
¹⁷ O	0,037	H ₂ ¹⁷ O	Brain oxygen metabolism
¹⁸ O	0,204	H ₂ ¹⁸ O	Hypoxia-sensitive pathway proteomics, Krebs-cycle intermediates

1.4.3 ^{18}O labeling in metabolism research

The oxygen isotope ^{18}O is a stable, non-radioactive, and naturally occurring isotope. ^{18}O labeling has previously been applied in cancer research, primarily in proteomics. Its usage involved the proteolytic labeling of plasma membrane proteins in melanoma cells grown under normoxic and hypoxic conditions, using trypsin to incorporate ^{18}O , followed by quantification via mass spectrometry (Castillo et al., 2014; Ye et al., 2013). Another, more recent application involves tracking oxygen exchange rates of Krebs cycle intermediates using ^{18}O stable isotope labeling combined with GC-MS analysis (Eylem et al., 2021). Outside of cancer research, ^{18}O isotope labeling has been used in the study of neurodegenerative, cardiac, and genetic diseases, particularly in analyzing the levels and fluxes of metabolites involved in energy metabolism, which is a crucial element in the integrated “omics” approaches (E. Nemutlu, Zhang, Juranic, et al., 2012).

When water containing the ^{18}O isotope at a known concentration (30%) is added to cell culture media, H_2^{18}O rapidly equilibrates with intracellular water. From there, ^{18}O is transferred from water to phosphoryl metabolites in proportion to the rate of enzyme-catalyzed reactions. The first transfer of ^{18}O occurs in the cytosol, where ATP hydrolysis by ATPase transfers ^{18}O to inorganic phosphate (Pi). Upon reaching the mitochondria, the ^{18}O -labeled Pi is incorporated into the γ -position of ATP ($\gamma\text{-ATP}[^{18}\text{O}]$) through the process of oxidative phosphorylation (OXPHOS). Within the mitochondria, CK reversibly transfers the ^{18}O -labeled phosphoryl group from $\gamma\text{-ATP}$ to creatine, resulting in the formation of ^{18}O -labeled phosphocreatine ($\text{PCr}[^{18}\text{O}]$). Additionally, AK2 catalyzes the reversible transfer of the ^{18}O -labeled phosphoryl group from $\gamma\text{-ATP}$ to AMP, producing ^{18}O -labeled $\beta\text{-ADP}$. The ^{18}O -labeled $\beta\text{-ADP}$ is then transported out of the mitochondria into the cytosol via the outer mitochondrial membrane. In the cytosol, AK1 mediates the reversible transfer of the phosphoryl group from unlabeled ADP to ^{18}O -labeled $\beta\text{-ADP}$, resulting in the formation of ^{18}O -labeled $\beta\text{-ATP}$ ($\beta\text{-ATP}[^{18}\text{O}]$) (Figures 3 and 6A) (Pucar et al., 2004).

The reaction rates between Pi, $\gamma\text{-ATP}$, and PCr in these sequential reactions are rapid, with ^{18}O saturation occurring within two minutes. However, the turnover rates for $\beta\text{-ADP}$ and $\beta\text{-ATP}$ are significantly slower, which may extend the labeling process to up to five minutes (Emirhan Nemutlu et al., 2014).

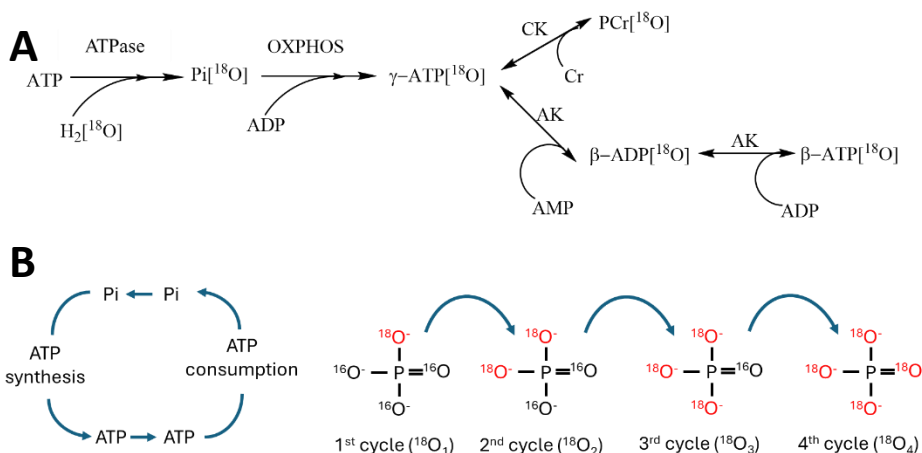


Figure 6. Overview of the ^{18}O labeling incorporation process. (A) Incorporation of ^{18}O into various phosphometabolites through a series of phosphorylation transfer reactions. First, ^{18}O is incorporated into inorganic phosphate (Pi) following ATP hydrolysis, catalyzed by ATPase, resulting in $\text{Pi}^{[18\text{O}]}$. Subsequently, ADP is converted into ATP via oxidative phosphorylation (OXPHOS), where $\text{Pi}^{[18\text{O}]}$ is added to ADP, forming $\gamma\text{-ATP}^{[18\text{O}]}$. Through creatine kinase (CK) activity, $\text{Pi}^{[18\text{O}]}$ is transferred from $\gamma\text{-ATP}$ to creatine (Cr), resulting in $\text{PCr}^{[18\text{O}]}$. Through adenylate kinase (AK) activity, $\text{Pi}^{[18\text{O}]}$ is transferred from $\gamma\text{-ATP}$ to AMP, producing $\beta\text{-ADP}^{[18\text{O}]}$, and subsequently, AK catalyzes the transfer of a phosphate group from $\beta\text{-ADP}^{[18\text{O}]}$ to ADP, forming $\beta\text{-ATP}^{[18\text{O}]}$. (B) During the ATP synthesis and consumption cycle, ^{18}O is incorporated into the phosphate group. In each cycle, ^{18}O replaces ^{16}O in Pi following ATP hydrolysis, as $\gamma\text{-ATP}^{[18\text{O}]}$ returns to ATPase. Pi – inorganic phosphate, $\text{Pi}^{[18\text{O}]}$ – turnover rate of ATP, $\gamma\text{-ATP}^{[18\text{O}]}$ – rate of mitochondrial ATP synthesis, $\text{PCr}^{[18\text{O}]}$ – flux through creatine kinase, $\beta\text{-ADP}^{[18\text{O}]} / \beta\text{-ATP}^{[18\text{O}]}$ – rate of AK phosphorylation transfer. The figure is adapted from (with permission) (E. Nemutlu et al., 2015; Pucar et al., 2004).

Since ^{18}O from the medium incorporates into phosphometabolites according to the rates of phosphotransfer reactions, it is possible to quantify the enzymatic fluxes in the respective metabolic pathways. The proportion of ^{18}O atoms that have replaced ^{16}O in the phosphoryl group of phosphometabolites can be determined using ^{31}P NMR or mass spectrometry (Pucar et al., 2001), where the percentage of ^{18}O incorporation corresponds to the integral of isotopomer peaks in the ^{31}P NMR spectrum or the chromatogram from GC-MS (Figure 8B) (Emirhan Nemutlu et al., 2014).

With each cycle of ATP hydrolysis mediated by ATPase, the Pi formed returns to the ATPase as $\gamma\text{-ATP}$ labeled with ^{18}O . After each cycle, new ^{18}O atoms replace ^{16}O until all four positions in Pi are filled with ^{18}O (Figure 8B), and the degree of this saturation indicates the ATP turnover rate (E. Nemutlu et al., 2015). Up to three ^{18}O atoms can be incorporated into different phosphoryl groups of monophosphates and oligophosphates. The percentage of ^{18}O labeling in the γ -phosphoryl group of adenosine triphosphate ($\gamma\text{-ATP}^{[18\text{O}]}$) represents the rate of ATP synthesis in the mitochondria. The AK phosphotransfer rate can be determined by the percentage of ^{18}O labeling in the β -phosphoryl group of adenosine triphosphate ($\beta\text{-ATP}^{[18\text{O}]}$). Energy flux through the CK pathway can be assessed based on the percentage of ^{18}O labeling in $\text{PCr}^{[18\text{O}]}$ (Emirhan Nemutlu et al., 2014).

The working principle of the ^{18}O labeling platform based on ^{31}P NMR is the chemical shift caused by the ^{18}O atom in the ^{31}P NMR spectrum. The primary advantage of this platform is that metabolites do not need to be separated or derivatized before analysis.

This method is stable, quantitative, and allows for the simultaneous analysis of the phosphoryl groups of multiple metabolites in a single run, including the different positions of phosphoryl groups within a single metabolite, such as the α -, β -, and γ -phosphoryls of ATP. The downside, compared to platforms like GC-MS, is that ^{31}P NMR requires a relatively large sample volume (300-400 μL) and is less sensitive (Emirhan Nemutlu et al., 2014).

The ^{18}O labeling platform based on gas chromatography-mass spectrometry (GC-MS) is more sensitive, requires a smaller sample volume, and has a shorter analysis time compared to ^{31}P NMR. However, sample preparation is more complex, involving several steps. Typically, this includes the chromatographic separation of metabolites, enzymatic transfer of phosphoryl groups from unstable monophosphates and oligophosphates to glycerol, and derivatization (Emirhan Nemutlu et al., 2014) (Figure 8A).

The electrospray ionization mass spectrometry (ESI-MS) platform for ^{18}O labeling offers even greater advantages over both ^{31}P NMR and GC-MS. The sample volume required for ESI-MS can be smaller than for GC-MS (in the range of 10 μL), and the time needed for sample preparation is shorter, as the need for enzymatic phosphoryl transfer is eliminated. The analysis time is also reduced, as all phosphoryl groups of the oligophosphate can be measured simultaneously. Furthermore, when coupled with liquid chromatography, there is no need for prior sample purification (E. Nemutlu, Juranic, et al., 2012).

1.4.4 Phosphometabolite analysis and quantification

It is well-established that tumors undergo metabolic reprogramming during their development, primarily to sustain the increased energy demands required for rapid proliferation. Adenine nucleotides (AMP, ADP, ATP) and phosphocreatine play central roles in the cellular energy currency, and fluctuations in their levels serve as indicators of how cells adapt to meet these elevated energy requirements (Kosmopoulou et al., 2020). However, it is not only the absolute levels of these molecules that represent alterations in energy metabolism; other factors, such as their ratios, play a critical role as well. For instance, changes in the ATP/ADP ratio significantly impact the activity of complex IV and the overall efficiency of OXPHOS (Napiwotzki & Kadenbach, 1998). Another approach is to calculate energy charge (EC) from adenine nucleotide concentrations. In 1967, Atkinson and Walton proposed that EC, derived from adenine nucleotide content, serves as a fundamental metabolic control parameter. EC provides a quantitative measure of the cellular energy state, reflecting the balance between energy availability and demand (Atkinson & Walton, 1967). More recent research has explored how EC may indicate alterations in cancer cell metabolism and mitochondrial functions that may influence their growth and survival (Iommarini et al., 2017).

There are numerous methods available for quantifying phosphometabolites such as adenine nucleotides and PCr. In terms of simplicity and reliability, enzymatic assays are commonly used and can perform comparably to chromatographic methods, in both being able to detect in picomolar range (Martens, 1992). However, over time, the cost of kits can accumulate, and these assays often exclude the quantification of AMP and ADP, requiring additional kits. For this reason, HPLC is considered a more favorable approach. Moreover, HPLC provides the ability to perform more complex analyses, despite the more challenging sample preparation process (Bhatt et al., 2012). In terms of matrices, HPLC outperforms most assay kits because of its reduced susceptibility to matrix effects (Berger et al., 1998; Wolff et al., 2009).

2 AIMS OF THE STUDY

The primary goal of this study is to develop and apply methodological approaches to investigate cancer energy metabolism, with a focus on colorectal and breast cancer. The specific aims are as follows:

1. **Characterize Key Metabolic Pathways and Quantify ATP Turnover:** Investigate metabolic reprogramming in cancer cells, focusing on OXPHOS, and phosphotransfer networks (CK, AK), and quantify ATP production and phosphotransfer rates using ^{18}O isotope labeling.
2. **Develop Analytical Techniques for Metabolic Profiling:** Apply and optimize analytical platforms for phosphometabolite detection using mass spectrometry (MS), nuclear magnetic resonance (NMR), liquid chromatography, high-resolution respirometry and enzyme activity measurements.
3. **Integrate and Compare Metabolic Profiles:** Compare metabolic adaptations in clinical colorectal cancer tissues and cancer cell lines to identify shared metabolic characteristics and system-specific differences.

3 MATERIALS AND METHODS

The summary of the applied approaches and techniques is illustrated in the figure below.

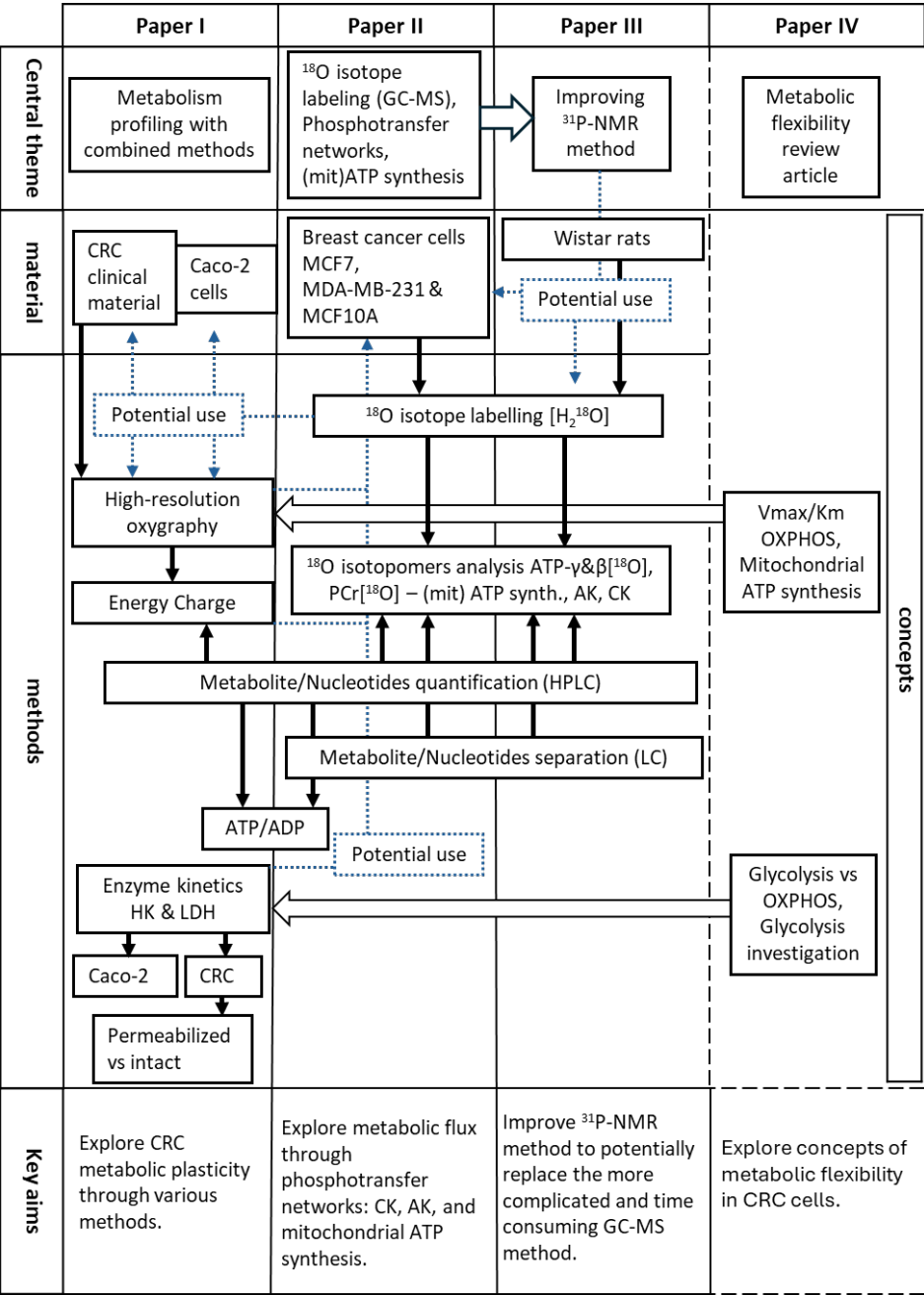


Figure 7. Design of the study.

3.1 Materials

3.1.1 Human post-operative samples

Post-operative samples, ranging from 0.1 to 0.3 grams, were sourced from the Oncology and Hematology Clinic at the North Estonian Medical Centre, Tallinn. Prior to experimentation, all samples underwent verification by a pathologist from the North Estonian Medical Centre. The study exclusively utilized primary tumors that had not been treated with radiation or chemotherapy. The colorectal cancer cohort comprised 34 patients, aged between 48 to 87 years. Normal tissue for colorectal cancer analysis was excised from areas 5 cm and 2 cm away from the tumors. Control tissues included colonocytes and smooth muscle cells. Within an hour of surgery, samples were transported to the Laboratory of Bioenergetics and analyzed within a 3-hour window. Transportation was conducted in pre-cooled Mitomedium–B solution, containing 0.5 mM EGTA, 3 mM $\text{MgCl}_2 \cdot 6\text{H}_2\text{O}$, 3 mM KH_2PO_4 , 20 mM taurine, 20 mM HEPES, 110 mM sucrose, 0.5 mM DTT, 60 mM K-lactobionate, 5 mg/ml BSA, and leupeptin. All experimental procedures received approval from the Medical Research Ethics Committee (decision numbers KK557 and KK558), adhering to the Helsinki Declaration and the Council of Europe's Convention on Human Rights and Biomedicine.

3.1.2 Cell cultures

The cell lines utilized in this study, including MCF7 (ATCC, HTB-22), MDA-MB-231 (ATCC, HTB26), MCF10A (ATCC, CRL-10317), and Caco-2 (HTB-37TM; p5), were all sourced from the American Type Culture Collection (ATCC). All cells were cultivated at 37 °C in 100 mm (seeding density 2.2×10^6 cells) or 35 mm (seeding density 0.3×10^6 cells) Petri dishes in a humidified incubator containing 95% air/5% CO_2 . Cells were sub-cultured every 5 days for MCF10A or every 2–3 days for MCF7, MDA-MB-231, and Caco-2 cells, using 1x trypsin-EDTA 0.5% solution in Dulbecco's Phosphate-Buffered Saline (DPBS, without calcium and magnesium). MDA-MB-231, MCF7, and Caco-2 cells were grown as adherent monolayers in high-glucose (25 mM) Dulbecco's Modified Eagle's Medium (DMEM) with stable L-glutamine and sodium pyruvate, supplemented with 10% heat-inactivated fetal bovine serum and 10 mg/mL human recombinant Zn insulin (Gibco). MCF10A cells were cultured in a lower glucose concentration (8 mM) in mammary epithelial growth medium (MEGM) supplemented with MEGM SingleQuots Supplements, 5% horse serum, and cholera toxin (100 ng/mL). All cell lines were maintained under conditions specified by the manufacturer.

For harvesting Caco-2 cells, the suspensions were centrifuged at $125 \times g$ for 5 minutes, and the supernatant was discarded. The cell number was determined using a Bürker Türk counting chamber, and aliquots of 17×10^6 cells were resuspended in 1 mL of DPBS in 2 mL Eppendorf tubes. The suspensions were then centrifuged as described previously, and after centrifugation, the supernatant was discarded. The resulting cell pellets were frozen in liquid nitrogen and stored at -80°C for further analysis.

For harvesting breast cancer cells, refer to the ^{18}O Labeling procedure for breast cancer cell lines in Methods.

3.1.3 Animals

Adult (3-month-old) male Wistar rats weighing about 300–400g were used in experiments. Rats were housed under standard laboratory conditions (at 22 °C constant temperature and a 12:12 h light/dark cycle with free access to food and water). Animal experiments

were approved by the Estonian National Board of Animal Experiments in accordance with the European Community Directive (86/609/EEC).

3.1.4 Chemicals

All chemicals were sourced from Merck (USA), if not stated otherwise. DMEM and DPBS (Ca/Mg free) were obtained from Corning (USA), MEGM SingleQuots Supplements (CC3151) were purchased from Lonza (Switzerland) whereas heat ubactuvated fetal bovine serum (FBS), peicillin-streptomycin solution (100x), trypsin-EGTA, and horse serum from Gibco (UK). TbHS was obtained from Acros (US), Oligomycin, PMSF and MSTFA were purchased from Thermo Fisher (US). oComplete protease inhibitors, glycerol kinase, creatine kinase, hexokinase, NADH, NADP⁺, and G6PDH were obtained from Roche (Switzerland). H₂¹⁸O water was received as a Cambridge Isotope Laboratories, Inc Research Award donation from the Cambridge Isotope Laboratories, Inc.

3.2 Methods

3.2.1 Sample preparations

3.2.1.1 ¹⁸O Labeling procedure for breast cancer cell Lines

Cultured cells underwent labeling with the ¹⁸O molecule, using H₂¹⁸O as a stable isotope source, in adherence to a protocol previously established (E. Nemutlu, Zhang, Gupta, et al., 2012) for determining the energetic profile of muscle cells. Upon reaching 70% confluency, the existing medium in the cultured cells was discarded and replaced with their respective regular media – DMEM for MCF7 and MDA-MB-231 cells, and MEGM for MCF10A cells (as outlined in the Cell Cultures section). This new medium was supplemented with 30% H₂¹⁸O, and the cells were subsequently incubated for 3 minutes at 37 °C. Cells that were not treated with H₂¹⁸O served as reference samples for unlabelled background control.

3.2.1.2 Cell processing for ¹⁸O breast cancer

The ¹⁸O labeling process was halted by swiftly removing the growth medium and rinsing the cells with saline, followed by quenching with either 0.6 M ice-cold HClO₄ or a 1:1 mixture of ice-cold methanol-water (100 µL for a 35 mm dish and 300 µL for a 100 mm dish). The Petri dishes containing the cells were immediately submerged in liquid nitrogen to halt cellular metabolism. Using a spatula chilled with liquid nitrogen, the cells were scraped off the dishes and transferred into cold microcentrifuge tubes, which were then promptly placed back into the liquid nitrogen. The samples were allowed to thaw just until the first signs of thawing appeared, after which they were centrifuged at 4 °C at 10,000 g for 5 minutes. For cells quenched with methanol-water, the supernatant was immediately frozen in liquid nitrogen and stored at –80 °C for later analysis by GC-MS. For cells quenched with HClO₄, the supernatant was transferred to a microcentrifuge tube containing 2 M KHCO₃ (35 µL for a 35 mm dish and 105 µL for a 100 mm dish) to neutralize the acid and bring the pH to approximately 7.4. These suspensions were then centrifuged at 10,000 g for 15 minutes at 4 °C to precipitate the salt. The supernatant was diluted to 1 mL with ultrapure water and stored at –80 °C until it could be analyzed. The remaining cell pellets were preserved in 300 µL of 1% SDS containing 0.1 M NaOH at –20 °C for protein quantification using the Pierce BCA Protein Kit.

3.2.1.3 Breast cancer cell cultures samples preparation with enzymatic reactions

Enzymatic processing reactions were used to transfer phosphoryl groups from ATP and PCr to glycerol after chromatographic isolation (Figure 8C). The g-phosphoryl of ATP was transferred to glycerol by glycerol kinase, and b-phosphoryls of ATP was transferred to glycerol by coupled catalytic reactions of adenylate kinase and glycerol kinase. The phosphoryl group of PCr was transferred to glycerol by combined catalytic reactions of creatine kinase and glycerol kinase (Figure 8C). Procedures in further detail: ATP (g-phosphoryl of ATP) fractions were lyophilized and reconstituted with a 200 μ L mixture of ultrapure water, 10mM TEAB (pH 8.8), 2mM MgCl₂, 5mM glycerol, and 1 μ L of glycerol kinase. The mixture was incubated at 37 °C for 1 hour, and fractions of G3P (g-phosphoryl of ATP) and ADP (b-phosphoryl of ATP) were collected by LC. ADP (b-phosphoryl of ATP) fractions were lyophilized and reconstituted with 200 μ L mixture of ultrapure water, 10mM TEAB (pH 8.8), 2mM MgCl₂, 5mM glycerol, 1 μ L of glycerol kinase, and 1 μ L of adenylate kinase (myokinase). The mixture was incubated at 37 °C for 2 hours, and the fraction of G3P (b-phosphoryl of ATP) was collected by LC. The phosphoryl group from PCr was transferred to G3P in a two-stage process: The phosphoryl from PCr was transferred to ADP. PCr fraction of a sample was lyophilized and reconstituted in 200 μ L mixture of ultrapure water, 25mM TEAB (pH 8.8), 1mM MgCl₂, 200 μ M ADP, 20 μ M diadenosine pentaphosphate, 1mM dithiothreitol, and 500 μ g/mL creatine kinase. The mixture was incubated 37 °C for 2 hours, and fractions of ATP were collected by LC. The phosphoryl from ATP was transferred to glycerol. ATP fractions were freeze-dried/lyophilized and reconstituted in 200 μ L mixture of ultrapure water, 10mM TEAB (pH 8.8), 2mM MgCl₂, 5mM glycerol, and 1 μ L of glycerol kinase. The mixture was incubated at 37 °C for 1 hour, and fractions of G3P (phosphoryl of PCr) were collected by LC.

3.2.1.4 Rat heart isolation

Wistar line male adult rats were anaesthetized by intraperitoneal injection of ketamine (75 mg/kg) and dexmedetomidin (1 mg/kg); the blood was protected against coagulation by injection of heparin. Hearts were rapidly excised, washed from blood, and used immediately for [¹⁸O] phosphoryl labelling.

3.2.1.5 [¹⁸O]Phosphoryl labeling of rat heart

The heart was quickly excised preserving a part of aorta and placed in an aerated perfusion solution, modified Krebs medium, with the following composition: 118 mM NaCl, 5.3 mM KCl, 1.2 mM MgSO₄, 0.5 mM EDTA, 25 mM NaHCO₃, 11 mM Glucose, and 2 mM CaCl₂ (pH 7.4). The heart was cannulated via aorta (Langendorf system) and perfused with the solution with a flow rate of 15 ml/min for 5 minutes. Then the heart was perfused for 10 minutes with the same solution where 30% of the H₂¹⁶O was replaced with H₂¹⁸O. The perfusate was continuously aerated and its temperature was kept at 37 °C. After that the heart was quickly frozen with liquid nitrogen (freeze clamp method) and the heart muscle was used for experiments.

3.2.1.6 NMR primary sample preparation from freeze clamped heart muscle

The heart tissue was ground in liquid nitrogen using a mortar and pestle. Then weighed and subjected to an extraction solution: 0.6 M HClO₄, 1 mM EDTA (1 mL extraction solution per 100 mg tissue), stirred vigorously and kept on ice for 5 min. The mixture was neutralized (pH 7.2) with 2 M KH₂CO₃ and centrifuged at 2253 x g for 10 min, at +4 °C. The supernatant was removed and treated with Chelex® 100 sodium form with constant stirring at +4 °C, overnight. The extract was centrifuged for 5 min 2253 x g at +4 °C the

supernatant was removed, frozen in liquid nitrogen and lyophilized. The dry residue was taken up in 300 μ L of D₂O, pH adjusted to 9.5 with NaOH aq and loaded into a Shigemi NMR tube.

3.2.1.7 Preparation of skinned tumor fibers

Skinned fibers were prepared using the protocol outlined by Kuznetsov and colleagues (Kuznetsov et al., 2008)(Figure 9A). Initially, tissue samples were dissected on ice into small bundles weighing 25–35 mg and then permeabilized in a chilled solution-A, which comprised 20 mM imidazole, 20 mM taurine, 3 mM KH₂PO₄, 5.7 mM ATP, 15 mM PCr, 9.5 mM MgCl₂*6H₂O, 49 mM K-MES, 2.77 mM K₂CaEGTA, 7.23 mM K₂EGTA, 1 μ M leupeptine, and 50 μ g/ml saponin, for 30 minutes at 4 °C. Subsequently, the permeabilized fibers underwent three 5-minute washes in a chilled mitomedium-B solution, containing 0.5 mM EGTA, 3 mM MgCl₂*6H₂O, 3 mM KH₂PO₄, 20 mM taurine, 20 mM HEPES, 110 mM sucrose, 0.5 mM DTT, 60 mM K-lactobionate, and 5 mg/ml BSA at pH 7.1. Post-washing, the samples were stored at 4 °C in mitomedium-B, ensuring their preservation and readiness for subsequent analyses.

3.2.1.8 Perchloric acid extraction for oxygraphic samples

2 mL of respiration media (mitomedium B) for both tumor and control were promptly collected from oxygraph after the experiments and processed immediately or kept in –80 °C for no longer than 2 weeks before processing. To precipitate proteins, 70% HClO₄ was added to the samples to 0.6M final concentration followed by centrifugation at 17000g (4 °C) for 10 minutes. The supernatant was collected and neutralized with 2M KHCO₃ (120–600 μ L depending on sample) and spun again at 17000g (4 °C) for 10 minutes after which the supernatants could directly be loaded into the HPLC for measurements, freeze-dried and resuspended in desired volume and solvent or kept in –20 °C for up to few weeks.

3.2.1.9 Preparation of CRC clinical materials and caco-2 cell lines for enzyme activity analysis

Clinical samples (10–100 mg ww) and caco-2 cells (approx. 15 x 10⁶ cells) were resuspended in 1 mL of 25 Mm Tris/ HCl buffer, pH 7.6, with 1 Mm EDTA, 5 Mm dithiothreitol, 1 Mm phenylmethanesulfonyl fluoride, 0.1–0.3% Triton-100X and 20x dilution of protease inhibitor mix (Roche). The samples were homogenized in Retsch MM400 ball mill homogenizer with 2 metal beads (3mm) for 2.5 minutes at 30Hz. The homogenized samples were then subjected to liquid nitrogen freezing and warm water bath thawing for 2–3 cycles to further facilitate breaking of cells and membranes. The samples were then centrifuged 5000g or higher for 1 minute at 4 °C followed by recovering the supernatant and keeping it on ice for enzymatic activity assays and protein determination.

3.2.2 Chromatography

3.2.2.1 Phosphometabolite Isolation

Cellular phosphometabolites (i.e. ATP and PCr) for breast cancer cell cultures and rat heart primary NMR sample were isolated by LC (GE Healthcare ÄKTAPrime Plus) using a Mono Q HR 5/5 ionexchange column (Pharmacia Biotech) with triethylammonium bicarbonate (TEAB) buffer pH 8.8 (gradient from 0–85%) at a 0.4 ml min⁻¹ flow-rate, equipped with a UV detector fixed at 280 nm (Figure 8A). All phosphometabolite fractions were collected by LC using this method, unless stated otherwise. For breast cancer cells, each sample was divided into two fractions, PCr and ATP, which were stored at –80 °C and –20 °C, respectively. For rat heart, ATP containing fractions were combined,

lyophilized, reconstituted in 300 μ L of D₂O, pH adjusted to 9.5 with NaOH aq and loaded into a Shigemi NMR tube.

3.2.2.2 Nucleotide separation

Separation and quantification of Adenine nucleotides was carried out with Waters Aquity UPLC with PDA detector for breast cancer cell samples and Agilent 1290 Infinity UPLC with PDA detector for CRC samples using reverse-phase column Tessek Separon SGX C18 5 μ m 3x150mm. The samples were eluted as described before (Seppet et al., 2001). For determining APT and PCr levels and ATP/ADP ratio in breast cancer cell samples, 50 μ L of the sample was used for 100mm dish and 20 μ L for 35mm dish. For determining ATP, ADP, and AMP concentrations in oxygraphic samples 100 μ L of sample was used (Figure 9C). The concentration of nucleotides was calculated from peak areas accounting for dilution factors where applied and normalized per mg protein for breast cancer samples and wet weight for CRC clinical material samples. Energy charge for CRC samples was calculated using the formula:

$$EC = [ATP] + 0.5 \times [ADP] / [ATP] + [ADP] + [AMP] \text{ (equation 3).}$$

3.2.3 Analysis methods

3.2.3.1 Analysis of ¹⁸O isotope distribution

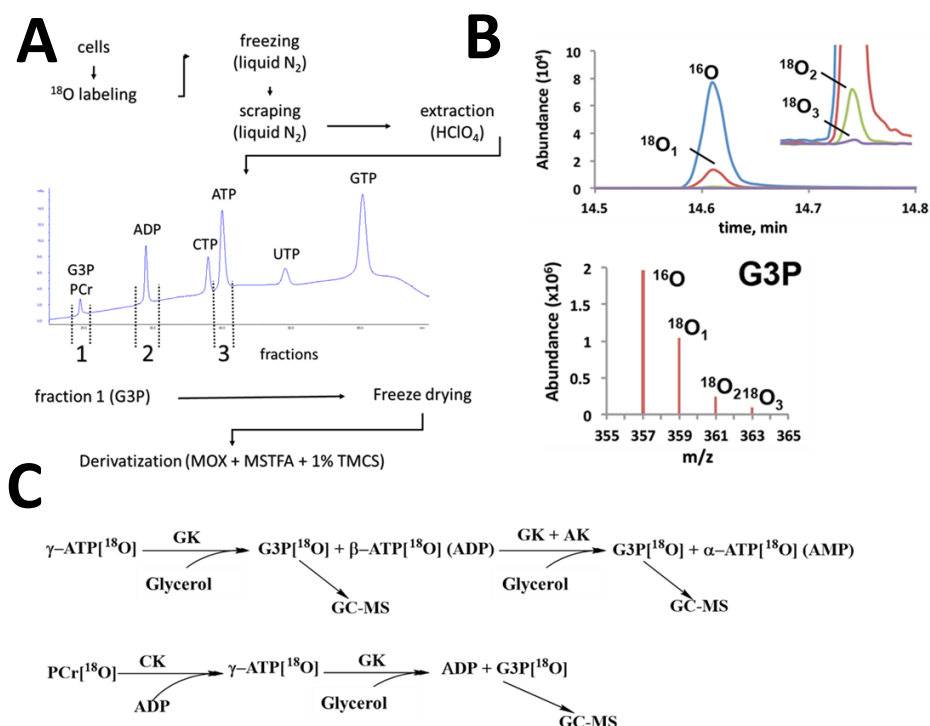


Figure 8. Sample preparation workflow for ¹⁸O-labelling based phosphometabolomics and metabolite ¹⁸O-labeling sequence. (A) Sample preparation, fractionation, and derivatization for GC-MS experiments. (B) Glycerol-3-phosphate (G3P) analysis via GC-MS. (C) Enzymatic reactions for γ - and β -ATP, as well as PCr, to analyze the distribution of ¹⁸O labeling in G3P using GC-MS. AK – adenylate kinase, GK – glycerol kinase, CK – creatine kinase, G3P – glycerol-3-phosphate, MOX – O-methoxyamine in pyridine, MSTFA + 1% TCMS – N-methyl-N-(trimethylsilyl) trifluoroacetamide with 1% trimethylsilyl chloride, ¹⁶O – oxygen, ¹⁸O₁, ¹⁸O₂, and ¹⁸O₃ – stable oxygen isotopes that have exchanged in one, two, or three positions within the phosphoryl group being studied. Figure adapted from (with permission) (Emirhan Nemutlu et al., 2014).

The PCr and γ - and β -ATP position samples, which were previously transferred to glycerol via enzymatic reactions, were lyophilized (VitRis SP Scientific Sentry 2.0) overnight and derivatized by silylation for GC-MS experiments. First, MOX (O-methoxylamine in pyridine) was added to all G3P samples, followed by incubation at 30°C in a thermoblock for 90 minutes. Next, MSTFA/1% TMCS (N-methyl-N-(trimethylsilyl) trifluoroacetamide with 1% trimethylsilyl chloride) was added to each sample, followed by incubation at 37 °C for 30 minutes (Figure 8A). In this study, a 1:4 ratio of MOX to MSTFA/1% TMCS was used.

After the final incubation, the samples were allowed to cool for 5 minutes and then centrifuged at 12,000 g for 3 minutes at room temperature (F. Wang et al., 2018). Following centrifugation, the supernatant was transferred to gas chromatography vials and analyzed using an Agilent 7890A/5975B inert XL MSD gas chromatograph-mass spectrometer. The column used was a DB-35ms 122-3832, 30m x 250 μ m x 0.25 μ m, with a split liner (split ratio 1:10) and helium as the carrier gas. The measurement conditions were: helium flow rate of 1.1 ml/min, inlet temperature of 250 °C, and an oven temperature gradient starting at 60°C, increasing to 325 °C at 10 °C/min (total analysis time: 42 minutes). GC-MS detected G3P signals at 357, 359, 361, and 363 m/z, corresponding to the exchange of oxygen isotopes ^{16}O with ^{18}O in one, two, or three positions within the phosphoryl group of the G3P molecule (Figure 8B).

The cumulative percentage of oxygen atoms replaced by ^{18}O in the phosphoryl groups can be calculated using the formula below (equation 4), where $\%^{18}\text{O}_1$, $\%^{18}\text{O}_2$, $\%^{18}\text{O}_3$, and $\%^{18}\text{O}_n$ represent the isotopomers and their percentages, and n represents the total number of oxygen atoms in the phosphoryl group of the metabolite. $\%^{18}\text{O H}_2\text{O}$ represents the percentage of isotope labeling in the water.

$$[\%^{18}\text{O}_1 + 2(\%^{18}\text{O}_2) + 3(\%^{18}\text{O}_3) + \dots n(\%^{18}\text{O}_n)]/[n(\%^{18}\text{O H}_2\text{O})] \text{ (equation 4)}$$

3.2.3.2 Colorectal cancer clinical samples workflow overview

General overview of CRC samples processing illustrated below.

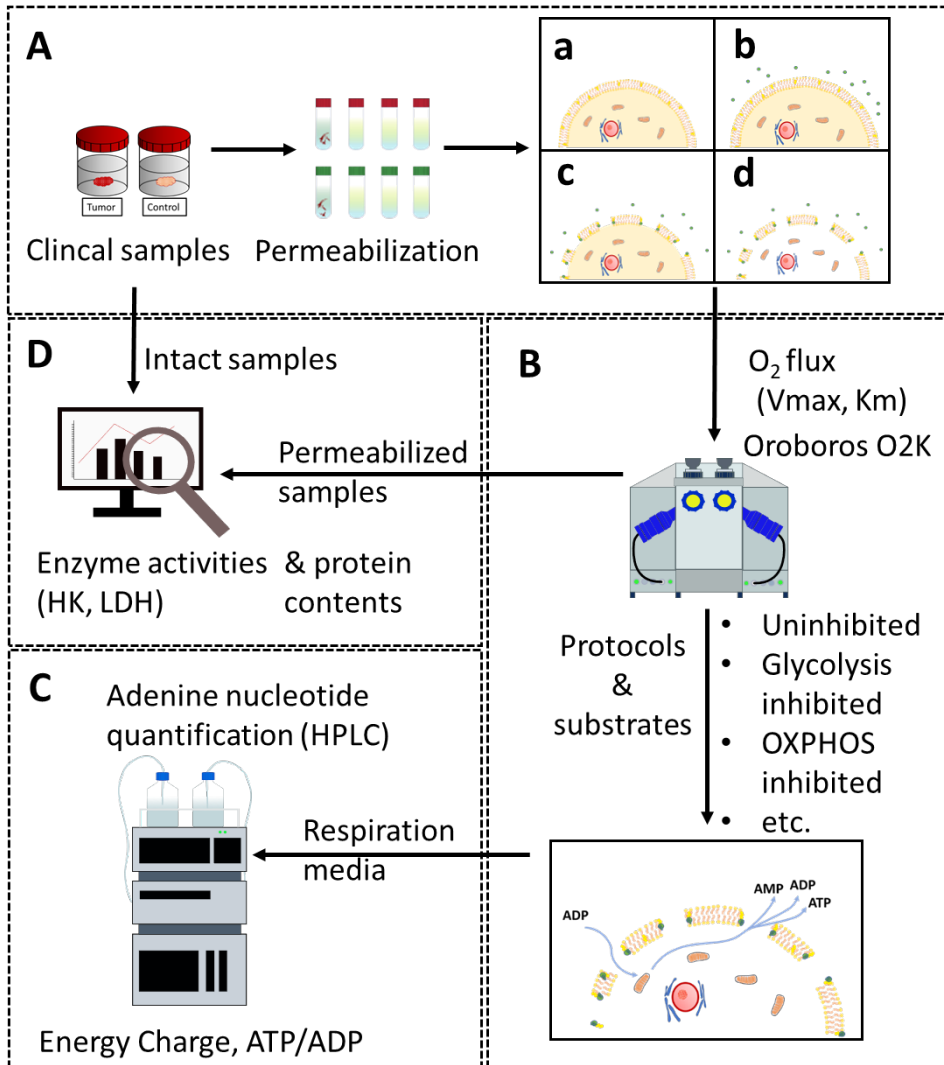


Figure 1. Overview of CRC clinical samples experiments. (A) preparation of clinical samples and permeabilization where during permeabilization: a - pre-prepared fiber is b - placed into a solution containing saponin, which c - binds to cholesterol forming cholesterol-saponin complexes and d - forms pores, washing out cytosolic contents and creating access for substrates to mitochondria. (B) permeabilized samples are transferred to high-resolution respirometer (Oroboros O2K), applied different protocols. (C) respiration media containing adenine nucleotides is processed and measured in HPLC (D) intact and permeabilized CRC clinical samples and Caco-2 cells are evaluated for enzyme activities for hexokinase and lactate dehydrogenase and protein contents.

3.2.3.3 Oxygraphic measurements

The mitochondrial respiration of permeabilized tissue samples was measured in mitomedium B at 25°C using a high-resolution respirometer Oxygraph-2k (Oroboros Instruments, Innsbruck, Austria) (Figure 9B). The medium was supplemented with 5 mM glutamate, 2 mM malate, and 10 mM succinate to fully activate respiratory chain complexes 1 and 2. To determine the relationship between respiration rate and exogenous ADP, increasing concentrations of ADP were added into the medium in the oxygraphic chamber. The collected data were then plotted as rates of O₂ consumption (the basal respiration rate of respiration was subtracted) *versus* ADP concentration. From these plots, the apparent affinity of mitochondria to exogenous ADP ($K_m(\text{ADP})$) and maximal respiration level (V_{\max}) values were calculated by nonlinear regression using Michaelis–Menten equation. Same experiments were conducted to calculate energy charges from adenylate nucleotide quantification with the exception of ADP being supplemented in 1 mM concentration. Additionally, other protocols were applied such as glycolysis activation and various inhibitions. To activate glycolysis (non-inhibited) 0,1 mM of ATP and 10 mM of glucose were added after glutamate, malate and succinate followed by addition of 1mM of ADP. To inhibit glycolysis 6–20 mM of 2-deoxyglucose and 0,5 mM of Iodoacetate were added before ADP and to inhibit OXPHOS 2,5 μM of rotenone, 10 μM of antimycin-A and 2 $\mu\text{g/ml}$ oligomycin were added before ADP.

3.2.3.4 Enzyme activities measurements

Activities of HK and LDH were determined spectrophotometrically (Cary Bio 100, Varian) at 37°C by following the NAD(P)⁺ reduction or NAD(P)H oxidation at absorbance of 340nm. Proteins were measured with BCA Protein Assay Kit (Thermo Fisher Scientific) according to the manufacturer's protocol (Figure 9D).

Assay for LDH was carried out in 1mL KME buffer (120 mM KCl, 20 mM MOPS, 1 mM EGTA, pH 7.2) including 0.2 mM NADH, 5–25 μL supernatant sample. The reaction was started by adding 1 mM pyruvate or increasing concentrations of pyruvate.

HK assay was carried out in 1mL KME buffer with 0.6 mM NADP⁺, 10 mM MgSO₄, 10 μL 1:10 Glc6PDH, 15–60 μL supernatant. 10mM of 0.3M ATP was added seconds before starting the reaction, this is done to avoid unspecific ATP hydrolysis by ATPases in the biological samples. The reaction was started by adding 2 mM glucose or increasing concentrations of glucose.

For the calculations of kinetic parameters (V_{\max} , K_m), all the enzyme activities normalized to protein content at variable substrate concentrations were fitted to the Michaelis-Menten equation by non-linear regression analysis using SigmaPlot 14.0 (Copyright © 2017 Systat Software, Inc.) by using NAD(P)H extinction coefficient 6.22mM⁻¹cm⁻¹ at 340nm and under initial-rate conditions.

3.2.4 Statistical analysis

Data are presented as the mean \pm SEM, aggregated from at least three independent experiments with a minimum of three technical replicates each. Differences among experimental groups were analyzed using ANOVA, followed by post-hoc Holm-Sidak tests for pairwise comparisons. Statistical significance was established at a p-value of less than 0.05.

4 RESULTS

4.1 Breast cancer cell lines metabolic profiling with ^{18}O method

4.1.1 Energetic status of cells

A fundamental parameter for all living cells is a high ATP/ADP ratio (10:1) (Hardie et al., 2003), and intracellular ATP concentration is one of the key indicators of the cell's energetic status (Nelson et al., 2008). To determine the ATP/ADP ratio and ATP concentration in cell lines, samples prepared from cell cultures were measured using UPLC, and ATP concentrations were calculated based on a calibration curve prepared with ATP standards ($R^2 = 0.99$). The experiment revealed no significant differences in the ATP/ADP ratio between cell lines, with values of 15.26 ± 0.5 for MCF10A, 14.34 ± 1.3 for MCF-7, and 16.00 ± 0.9 for MDA-MB-231 (Figure 10A). However, it was observed that the intracellular ATP reserves were significantly higher in the cancer cell subtypes (MCF-7 and MDA-MB-231) compared to the control cells (MCF10A). The intracellular ATP concentration in control cells was 17.3 ± 0.6 nM/mg of protein, while it was 24.9 ± 1.6 nM/mg of protein in MCF-7 cells and 23.0 ± 1.3 nM/mg of protein in MDA-MB-231 cells (Figure 10B). These changes in intracellular ATP concentration in breast cancer subtypes may indicate alterations in ATP synthesis and phosphotransfer pathways (P. P. Dzeja et al., 2004; Y. Qian et al., 2016). Therefore, ATP synthesis via OXPHOS, as well as CK and AK pathways, were subsequently investigated.

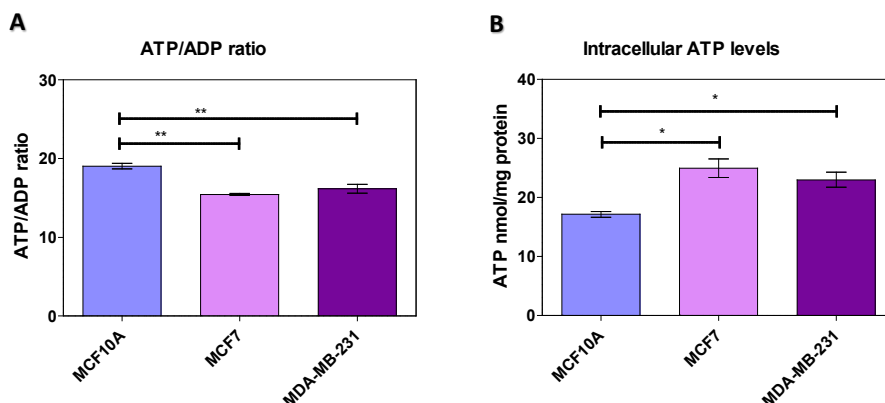


Figure 10. Assessment of cellular energetic status in breast cancer cells through (A) ATP/ADP ratio and (B) determination of intracellular ATP concentration. ATP and ADP were measured using hydrophobic interaction chromatography with UPLC, where nucleotides were detected at 254 nm using a photodiode array detector. MCF10A served as the control cell line, while MCF7 (Luminal A) and MDA-MB-231 (triple-negative) were the breast cancer cell lines. Results are presented as mean \pm SEM, $n = 3-5$, * $p < 0.05$ (Holm-Sidak), ANOVA.

4.1.2 Profiling the creatine kinase pathway in breast cancer

Previous studies have shown that the CK pathway is an important component of the phosphotransfer network in breast cancer, where the PCr level plays a crucial role in maintaining energy reserves in metabolically active cells (Kurmi et al., 2018). To assess the CK pathway profile in cells, PCr concentrations and energy flux through the CK pathway, referred to as the PCr turnover rate ($\text{PCr}^{[18}\text{O}]$), were measured. For the determination of

PCr concentration, samples prepared from cell cultures were analyzed using UPLC and calculated according to a calibration curve prepared with PCr standards ($R^2 = 0.99$). PCr $^{[18]O}$ was detected using GC-MS, based on the percentage of oxygen exchanged with ^{18}O in the PCr molecule.

The experimental results revealed differences in both intracellular PCr levels (Figure 11A) and PCr turnover rates (Figure 11B) across all studied cell lines. A significant difference in intracellular PCr levels was found between the control cell line (MCF10A) and the breast cancer subtypes (MCF7 and MDA-MB-231), where PCr concentrations were 30.0 ± 2.0 nM/mg of protein for MCF10A, 16.3 ± 0.6 nM/mg of protein for MCF-7, and 13.2 ± 0.6 nM/mg of protein for MDA-MB-231. Similarly to PCr levels, PCr turnover rates (PCr $^{[18]O}$) in the breast cancer subtypes were found to be twice as low as in the control cells. In MCF10A cells, the PCr turnover rate (PCr $^{[18]O}$) was $56.9 \pm 1.6\%$, compared to $24.1 \pm 0.1\%$ in MCF-7 cells and $18.1 \pm 0.3\%$ in MDA-MB-231 cells.

Lower PCr levels and reduced PCr turnover rates in breast cancer subtypes compared to the control cell line MCF10A suggest downregulation of the CK pathway in Luminal A and triple-negative breast cancers.

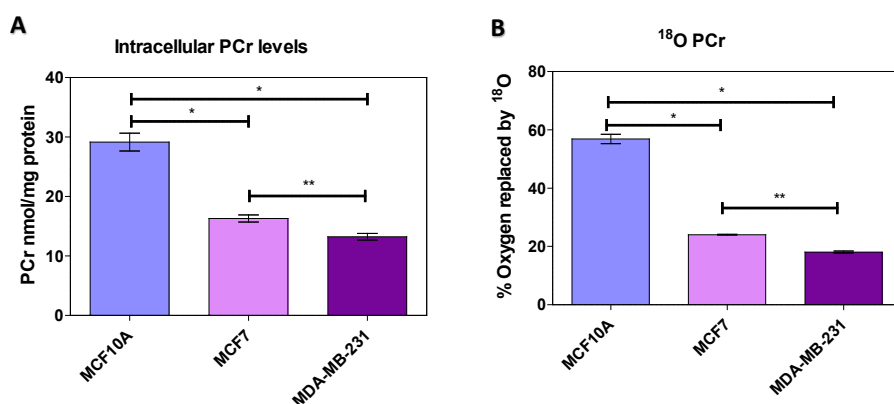


Figure 11. Determination of the energetic profile of the creatine kinase pathway in breast cancer cells through (A) measurement of PCr concentration and (B) measurement of PCr turnover rate/CK flux (PCr $^{[18]O}$). PCr was measured using hydrophobic interaction chromatography with UPLC, where the metabolite was detected at 210 nm using a photodiode array detector. The PCr turnover rate was measured using GC-MS, and the turnover rate was calculated based on the percentage of oxygen exchanged with ^{18}O in the phosphoryl group of PCr. MCF10A served as the control cell line, while MCF7 (Luminal A) and MDA-MB-231 (triple-negative) were the breast cancer cell lines. Results are presented as mean \pm SEM, $n = 3-5$, * $p < 0.001$, ** $p < 0.05$ (Holm-Sidak), ANOVA.

4.1.3 Profiling the adenylate kinase pathway in breast cancer

Experiments in a CK knockout mouse model have demonstrated that AK is capable of maintaining normal cellular homeostasis under conditions where CK is suppressed (E. Nemutlu, Zhang, Juranic, et al., 2012). Therefore, the AK pathway was subsequently investigated in breast cancer. To evaluate the AK profile, the proportion of mitochondrial ATP synthesis (γ -ATP $^{[18]O}$) and energy flux through the adenylate kinase pathway, specifically AK phosphotransfer rates (β -ATP $^{[18]O}$), were measured in the cells. Both γ -ATP $^{[18]O}$ and β -ATP $^{[18]O}$ were detected using GC-MS and calculated based on the percentage of oxygen exchanged with ^{18}O in the γ - or β -phosphoryl groups of ATP.

The results indicated that the proportion of mitochondrial ATP synthesis and AK phosphotransfer rates were significantly lower in the breast cancer subtypes MCF-7 and MDA-MB-231 compared to the control MCF10A cell culture (Figure 12 A,B). The mitochondrial γ -ATP[^{18}O] values were $64.4 \pm 0.8\%$ for MCF10A, $48.5 \pm 4.4\%$ for MCF-7, and $43.3 \pm 3.0\%$ for MDA-MB-231. Similarly, AK phosphotransfer rates were considerably lower in the breast cancer subtypes compared to the control cells. AK pathway activity in MCF10A cells was $59.9 \pm 8.8\%$, compared to $38.9 \pm 4.3\%$ in MCF-7 and $27.5 \pm 3.7\%$ in MDA-MB-231.

The significantly reduced mitochondrial ATP synthesis and AK phosphotransfer rates suggest a diminished contribution of these pathways to energy metabolism in Luminal A and triple-negative breast cancers.

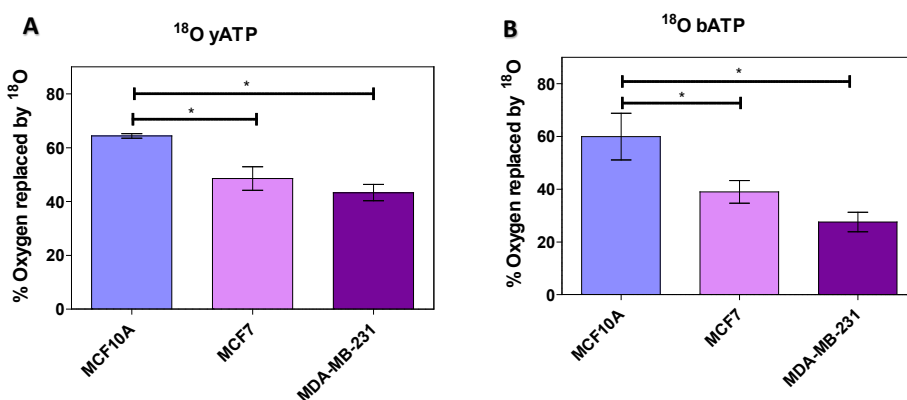


Figure 12. Determination of the metabolic profile of the adenylate kinase pathway in breast cancer cells through γ -ATP[^{18}O] and β -ATP[^{18}O]. Turnover rates were calculated based on the percentage of oxygen exchanged with ^{18}O in the γ - and β -phosphoryl groups of ATP, measured using GC-MS. MCF10A served as the control cell line, while MCF7 (Luminal A) and MDA-MB-231 (triple-negative) were the breast cancer cell lines. Results are presented as mean \pm SEM, $n = 3-5$, * $P < 0.05$ (Holm-Sidak), ANOVA.

4.2 Investigating CRC with oxygraphy and energy charges from adenine nucleotide quantification and enzyme kinetics

4.2.1 OXPHOS

High-resolution respirometry was utilized to investigate potential metabolic reprogramming in CRC by analyzing the kinetics of OXPHOS flux. This involved determining the values for maximal ADP-stimulated respiration (V_{\max}) and the apparent Michaelis-Menten constant for exogenously added ADP (K_{mADP}). A statistically significant difference was observed in V_{\max} between control and CRC tissues (Figure 13A), while no significant differences were found in K_{mADP} values (Figure 13B). The increased maximal ADP-stimulated respiration rate in CRC suggests an enhanced OXPHOS capacity. Additionally, the catalytic efficiency (V_{\max}/K_{mADP} ratio) of the entire OXPHOS pathway (Figure 13C) was $0.013 \text{ min}^{-1} \text{ mg}^{-1} \text{ mL}$ for control tissue and $0.026 \text{ min}^{-1} \text{ mg}^{-1} \text{ mL}$ for CRC tissue, indicating a more catalytically efficient system in tumor tissues.

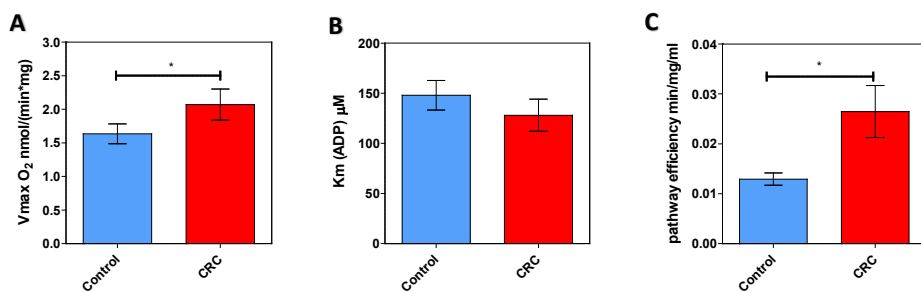


Figure 13. OXPHOS pathway analysis. Comparative analysis of (A) maximal ADP-stimulated respiratory rate (V_{max}) and (B) apparent Michaelis-Menten constant values for ADP (K_{mADP}) in control tissue ($n = 29$) and CRC tissue ($n = 29$). (C) The catalytic efficiency of OXPHOS pathway represented by V_{max}/K_{mADP} ratio was calculated from paired samples. Data are presented as mean \pm SEM, * $P < 0.05$ (Holm-Sidak), ANOVA.

4.2.2 OXPHOS across CRC progression

Next, OXPHOS flux of CRC cells was analyzed at different disease stages. When comparing V_{max} and K_{mADP} values across different CRC stages, no significant intergroup differences were observed. However, a close resemblance in V_{max} values was noted between control tissues and stage II CRC (Figure 14A). In addition, K_{mADP} values for stage II CRC looked higher than those of other stages (Figure 14B), suggesting a slight decrease in OXPHOS activity specifically in stage II of CRC (lower activity and lower affinity for substrate). The OXPHOS catalytic efficiencies at different CRC stages were clearly greater, $0.025 \text{ min}^{-1} \text{ mg}^{-1} \text{ mL}$ for stage 1, $0.031 \text{ min}^{-1} \text{ mg}^{-1} \text{ mL}$ for stage 2, and $0.021 \text{ min}^{-1} \text{ mg}^{-1} \text{ mL}$ for stage 3, than in the control colon tissue of $0.013 \text{ min}^{-1} \text{ mg}^{-1} \text{ mL}$ (Figure 14C).

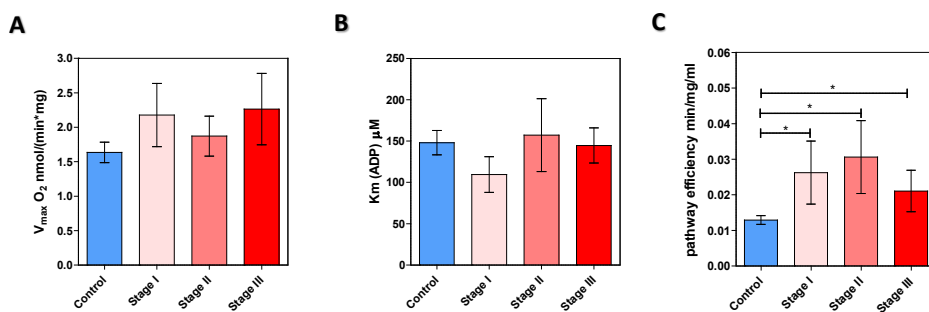


Figure 14. OXPHOS pathway analysis across CRC stages. Comparative analysis of (A) Maximal ADP-induced respiration rate (V_{max}), (B) apparent Michaelis-Menten constant values for exogenously added ADP (K_{mADP}) in control ($n = 27$) and tumor stages I–III ($n = 6, 12$ & 9), and (C) The catalytic efficiency of OXPHOS pathway represented by V_{max}/K_{mADP} ratio was calculated from paired samples. Data are presented as mean \pm SEM, * $P < 0.05$ (Holm-Sidak), ANOVA.

4.2.3 Adenine nucleotide quantifications

4.2.3.1 Energy charge and ATP/ADP changes in CRC

The analysis of adenine nucleotide concentrations revealed a slight increase in EC in both control and CRC samples when glycolysis was active (Figures 15 A,B). This indicates that the reliance on glycolysis affects cellular energy status in both healthy and cancerous tissues. However, the ATP/ADP ratio ranging between 0.2 and 0.25 showed no differences between tumor and control tissues (Figure 15C). In contrast, EC in control tissues was significantly affected by OXPHOS inhibition compared to the non-inhibited state (Figure 15B), with ATP/ADP ratios decreasing from 0.23 to 0.17 (Figure 15C) albeit not statistically significantly, demonstrating a strong dependence on OXPHOS to maintain energy homeostasis in non-cancerous cells. CRC tissues also displayed a notable decrease in EC (Figure 15B) and a tendency towards decrease in ATP/ADP ratios, from 0.25 to 0.15 (figure 15C) upon OXPHOS inhibition, indicating that energy production in cancer cells is similarly OXPHOS-dependent.

A significant reduction in EC was observed in the control group when comparing glycolysis inhibition to OXPHOS inhibition (Figure 15B), underscoring the distinct contributions of these metabolic pathways to cellular energy status. In contrast, CRC tissues did not show a significant change under the same conditions, suggesting greater metabolic flexibility or the presence of compensatory mechanisms that enable energy homeostasis when glycolysis is inhibited.

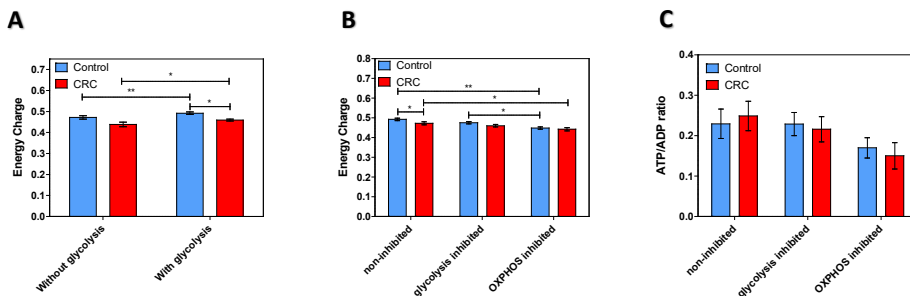


Figure 15. Energy charges and ATP/ADP ratios. Comparative analysis of (A) energy charges of control and tumor tissue without ($n = 15$) and with activated glycolysis ($n = 16$), (B) energy charges of non-inhibited ($n = 16$), glycolysis inhibited ($n = 17$) and OXPHOS inhibited ($n = 10$) states in control and tumor tissue, and (C) ATP/ADP ratios of non-inhibited ($n=16$), glycolysis inhibited ($n = 17$) and OXPHOS inhibited ($n = 10$) states in control and tumor tissue. Data are presented as mean \pm SEM, * $P < 0.05$, ** $P < 0.001$ (Holm-Sidak), ANOVA.

4.2.3.2 Energy charge and ATP/ADP changes across CRC progression

Energy charge measurements between samples without glycolysis activation showed no significant differences between control and CRC tissues, with values of 0.46 and 0.44, respectively (Figure 16A). However, when analyzed by cancer stage, a significant difference was observed between control and CRC stage II, with energy charges of 0.46 versus 0.41, respectively, and between CRC stages I and II, with values of 0.47 and 0.41, respectively (Figure 16B). This reflects a decrease in energy charge as the tumor progresses from stage I to stage II. The ATP/ADP ratios also showed significant differences between control and CRC (Figure 16C), as well as between control and stage II CRC (Figure 16D), indicating that cancer tissues and specifically stage II has more ATP available than control tissue.

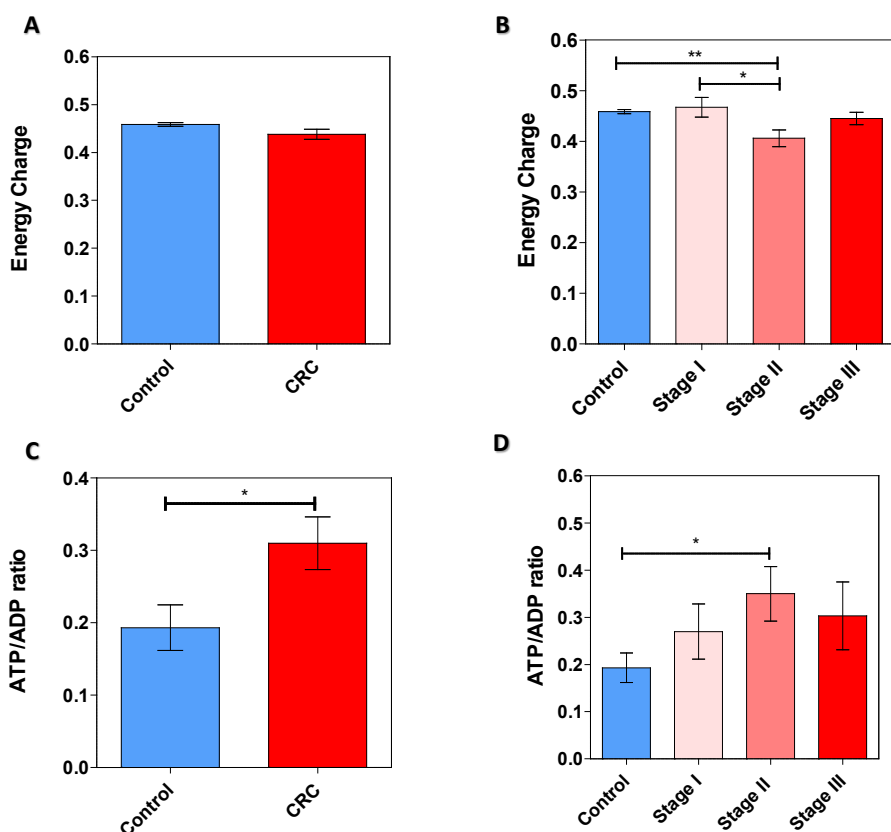


Figure 16. Energy charges and ATP/ADP ratios across CRC stages. (A) Energy Charges of control and tumor tissues without glycolysis activation (n = 15). (B) Energy charges in control (n = 15) and tumor stages I-III (n = 4, 5 & 6). (C) ATP/ADP ratio of control and tumor tissues without glycolysis (n = 15). (D) ATP/ADP ratios in control (n = 15) and tumor stages I-III (n = 4, 5 & 6). Data are presented as mean ± SEM, * P < 0.05, * P < 0.001 (Holm-Sidak), ANOVA.

4.2.4 Glycolytic enzyme activities

4.2.4.1 LDH activity in CRC and Caco-2

LDH activity showed significant differences between different tissue types (Figure 17A). Notably, a two-fold increase in LDH activity of intact control 747.5 ± 97.4 nmol/(min*mg) and intact tumor 2112.02 ± 278.2 nmol/(min*mg) samples was observed, suggesting higher potential of pyruvate processing in CRC. In contrast, no difference in LDH activity between permeabilized 979.2 ± 117.1 nmol/(min*mg) tumor and permeabilized control 963.5 ± 98.9 nmol/(min*mg) samples was attained. LDH activity in Caco-2 cells 3207.1 ± 151.9 nmol/(min*mg) was remarkably higher, exceeding that of the clinical samples by approximately 25%, with significant differences observed across all groups. The $K_{m_{\text{pyruvate}}}$ values had a tendency to be higher in all tumor and control samples compared to Caco-2 123.4 ± 27.4 μM $K_{m_{\text{pyruvate}}}$ and being significantly higher in intact tumor 215.3 ± 24.5 μM $K_{m_{\text{pyruvate}}}$ samples (Figure 17B), indicating Caco-2 cells' higher affinity for substrate ADP compared to clinical samples. Similar to LDH activity, the LDH

enzymatic efficiency calculations show that Caco-2 cells have 3-6 times more efficient LDH catalysis capability 29.7 ± 9.2 min/mg/ml than all clinical sample, and significantly higher enzymatic efficiency in intact tumors 9.9 ± 1.2 min/mg/ml compared to permeabilized tumors 5.1 ± 0.7 min/mg/ml can also be noted (Figure 17C).

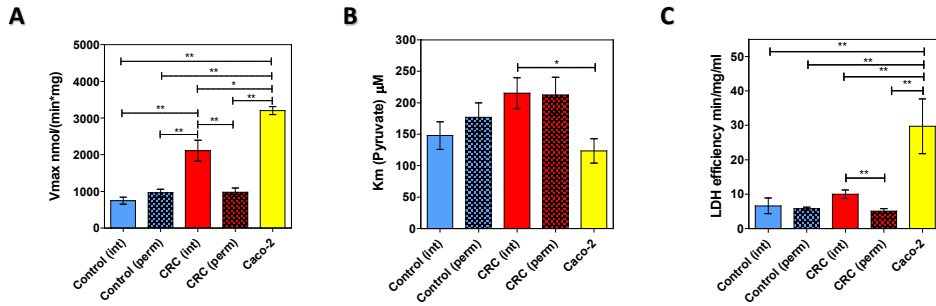


Figure 17. LDH activities. (A) LDH activity in intact control tissue (Control (int), $n = 7$), permeabilized control tissue (Control (perm), $n = 13$), intact colorectal cancer tissue (CRC (int), $n = 7$), permeabilized colorectal cancer tissue (CRC (perm), $n = 13$) and Caco-2 cells ($n = 4$). (B) apparent Michaelis-Menten constant values for exogenously added Pyruvate (Km_{Pyruvate}) and (C) the efficiency of LDH enzyme represented by $V_{\text{max}}/Km_{\text{Pyruvate}}$ ratio was calculated from paired samples. Data are presented as mean \pm SEM, * $p < 0.01$, ** $p < 0.001$ (Holm-Sidak) ANOVA.

4.2.4.2 HK activity in CRC and Caco-2

HK activity assays were carried out in both intact and saponin-treated control and tumor tissue, as well as in Caco-2 cells (Figure 18A). However, there were no significant HK activity differences between permeabilized control tissue and tumor intact or permeabilized tissue, and CaCo cells, except for intact control 0.2 ± 0.05 min/mg/ml and permeabilized control 0.4 ± 0.05 min/mg/ml. The Km_{glucose} values had a tendency of being higher in intact control tissues 98.1 ± 33.4 μM Km_{glucose} than the rest of the samples and caco-2 (Figure 18B). The HK enzymatic efficiency levels had no significant differences across all samples (Figure 18C).

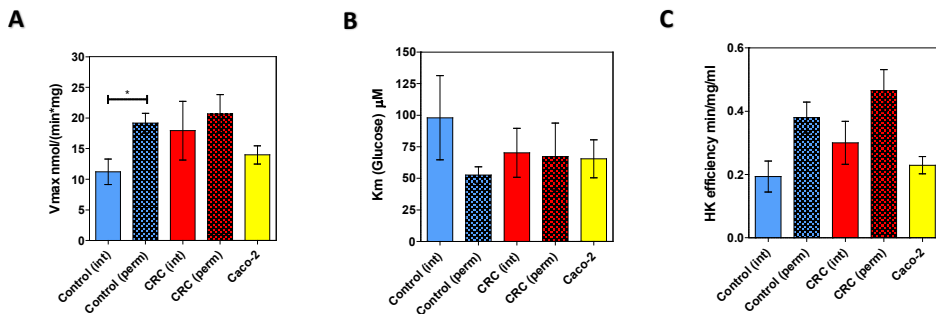


Figure 18. HK activities. (A) HK activity in intact control tissue (Control (int), $n = 7$), permeabilized control tissue (Control (perm), $n = 13$), intact colorectal cancer tissue (CRC (int), $n = 7$), permeabilized colorectal cancer tissue (CRC (perm), $n = 13$) and Caco-2 cells ($n = 4$). (B) apparent Michaelis-Menten constant values for exogenously added Glucose (Km_{Glucose}) and (C) the efficiency of HK enzyme represented by $V_{\text{max}}/Km_{\text{Glucose}}$ ratio was calculated from paired samples. Data are presented as mean \pm SEM, * $p < 0.01$, (Holm-Sidak) ANOVA.

4.3 NMR – Pure shift optimization, ATP from rat heart

This study advanced the pure shift NMR technique to condense multiplets into singlets for better interpretation and quantification of the NMR spectra, thus mitigating problems such as isotopomer overlap. Following the successful isolation of the ^{18}O -labeled ATP molecule from rat heart tissue, as detailed in the Materials and Methods section, the results of the technique's application are presented in Figure 19. The regular ^{31}P spectrum of the ^{18}O -labeled ATP molecule shows overlapping isotopomers for the β and γ phosphoryls (Figure 19A, B). By applying the pure shift technique, these multiplets collapse into singlets, thereby resolving the overlap and distinctly displaying both non-labeled (^{16}O) and labeled (^{18}O) isotopomers in a quantifiable manner. For more specifics refer to **Publication III**.

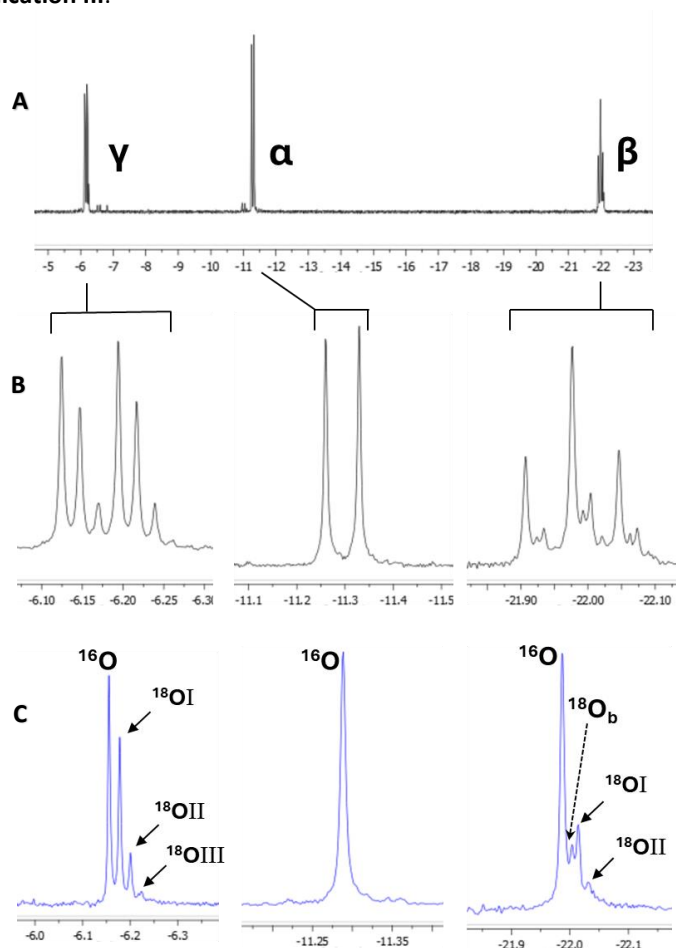


Figure 19. ^{31}P NMR spectra of partially ^{18}O -labelled ATP, isolated from a perfused rat heart. (A) Regular ^{31}P spectrum of the sample with ATP α , β , and γ positions indicated. (B) Segments of the regular ^{31}P spectrum with overlapping multiplets. (C) Pure shift spectrum that displays segments with a singlet for each isotopomer: ^{16}O indicates phosphate with all ^{16}O positions isotopomer, ^{18}OI for phosphate with one oxygen ^{18}O -labelled, ^{18}OII for two labelled oxygens, $^{18}\text{OIII}$ for three labelled oxygens. $^{18}\text{O}_b$ in the β -phosphate indicates a labelled oxygen that bridges adjacent phosphates. All spectra were acquired in 2048 scans, with spectrum (C) acquired in four 512-scan experiments of different SAPHIRE orders and the FIDs were added after LP extrapolation. Adapted from (Kaup et al., 2021) with permission.

5 DISCUSSION

I – Profiling the energy metabolism of breast cancer cell cultures with stable isotope ^{18}O -method

The first part of this study primarily focused on the optimization and application of a mass spectrometry-based method utilizing the stable isotope ^{18}O to investigate energy metabolism in breast cancer. The main area of interest was the analysis of phosphotransfer networks, specifically involving CK and AK pathways, as well as mitochondrial ATP synthesis. The goal was to describe these pathways by observing their fluxes, which would otherwise remain undetected through conventional metabolite quantification methods. The optimization of chromatographic separation of metabolites using standard compounds is crucial due to the specific characteristics of the column and instrument. As a result of the optimization, all required metabolites, including PCr and G3P, were separated and collected for subsequent experiments, despite having a similar retention time to AMP (Emirhan Nemutlu et al., 2014).

For the experiments, a GC-MS-based ^{18}O labeling platform was chosen, which offers greater sensitivity and requires smaller sample sizes compared to ^{31}P NMR. ^{31}P NMR requires approximately 18 million cells to measure mitochondrial ATP synthesis ($\gamma\text{-ATP}[^{18}\text{O}]$), AK flux ($\beta\text{-ATP}[^{18}\text{O}]$), and CK flux ($\text{PCr}[^{18}\text{O}]$) (Singer et al., 1995). This study demonstrated that the mass spectrometry-based method requires only 1–1.5 million cells to measure γ - and β -ATP ^{18}O and 5–10 million cells to measure PCr ^{18}O . Previously, this mass spectrometry platform was applied to study metabolic pathways and fluxes in aging-related cardiac defects (E. Nemutlu et al., 2015) and profiling oxygen exchange rates in Krebs-cycle intermediates in Caco-2 cell lines (Eylem et al., 2021). This study demonstrated that the same platform could be successfully used to investigate energy metabolism in breast cancer.

Cancer is a complex and heterogeneous disease where alterations in enzymatic pathways can depend on tumor location, stage, and progression from initial growth to the metastatic phase. The typical ATP/ADP ratio in unstressed living cells is 10:1 (Hardie et al., 2003). The ATP/ADP ratios measured in cancer cells were greater than 10:1 and showed no significant differences between cell lines, indicating that the cells were not under stress (Figure 10A).

Previous studies have shown that cancer is a metabolic disease associated with increased nucleotide metabolism. As a result, elevated nucleotide levels have been proposed as potential biomarkers for tumors (Zancan et al., 2010). In this study, intracellular ATP reserves were found to be elevated in Luminal A and triple-negative breast cancer cell lines compared to the control MCF10A cell line (Figure 10B). Literature has also reported elevated ATP levels in breast cancer (Zancan et al., 2010). In mammalian cells, ATP is primarily produced through OXPHOS and glycolysis (Zheng, 2012). This study found that $\gamma\text{-ATP}[^{18}\text{O}]$ levels were lower in Luminal A and triple-negative breast cancer cells compared to the control cells (Figure 12A), suggesting that mitochondrial ATP synthesis is downregulated in both breast cancer subtypes. Therefore, the increased ATP levels in breast cancer cells may be associated with upregulation of glycolysis. Indeed, previous studies have shown that the glycolytic pathway in breast cancer subtypes MCF-7 and MDA-MB-231 plays a significantly larger role compared to OXPHOS in control MCF10A cells (Zancan et al., 2010). While glycolysis is less efficient than OXPHOS (2 ATP vs. 36 ATP), it is approximately 100 times faster in producing ATP (Pfeiffer et al., 2001). Moreover, it has been found that glycolysis can contribute sufficiently to ATP production

to maintain a high intracellular ATP/ADP ratio (Vander Heiden et al., 2009). Although assessing elevated intracellular ATP levels as a marker could be valuable for breast cancer diagnosis, further studies are needed to determine the role of glycolysis in maintaining intracellular ATP reserves in breast cancer cells.

Although previous studies have indicated that the CK network plays a critical role in breast cancer progression (Kurmi et al., 2018), this study showed that CK function is altered in Luminal A and triple-negative breast cancer subtypes. Specifically, low PCr levels and reduced energy flux through the CK pathway (PCr[¹⁸O]) were observed in both Luminal A and triple-negative breast cancer cells (Figures 10A and B). Similar to the findings of this study, low PCr levels have been reported in metastatic breast cancer cells due to mitochondrial metabolic disruptions (Singer et al., 1995). According to the literature, there are differences in the expression profiles of mitochondrial CK (MtCK) and cytosolic CK-BB in breast cancer cells. Previously, Kurmi et al. demonstrated that MtCK is downregulated in triple-negative breast cancer (Kurmi et al., 2018), and the low PCr levels and PCr[¹⁸O] measured in this study also point to downregulation of this isoform. Although CK-BB has been shown to be overexpressed in triple-negative breast cancer subtypes (Zarghami et al., 1996), the low PCr levels and PCr[¹⁸O] observed in this study suggest that CK-BB's contribution to PCr synthesis is likely minimal. These findings suggest that the contribution of CK and its isoforms to energy metabolism may depend on the breast cancer subtype, and further research is needed to clarify the relationships between CK isoform expression levels and PCr fluxes.

According to the literature, cells have the ability to reprogram phosphotransfer networks to compensate for downregulated metabolic pathways (Emirhan Nemutlu et al., 2014). This has been previously demonstrated in transgenic mouse models with CK knockout, where the AK pathway compensated for downregulated CK pathways (Emirhan Nemutlu et al., 2014). Previous studies have shown that AK plays a crucial role in breast cancer progression (Aleksandr Klepinin et al., 2014). The low AK β -ATP[¹⁸O] levels measured in Luminal A and triple-negative breast cancer subtypes in this study (Figure 12B) indicate a reduced role of this metabolic pathway in these subtypes. Experiments with MCF-7 and MDA-MB-231 cell cultures in previous studies have indicated that these cells rely more heavily on glycolysis than control MCF10A cells (Zancan et al., 2010). Therefore, the reduced energy flux through the AK pathway observed in this study may be linked to increased glycolysis. A previous study demonstrated a correlation between increased glucose uptake and reduced AK activity, where activation of glycolysis in pancreatic cells decreased the contribution of the AK pathway (Olson et al., 1996). Another reason for the low AK phosphotransfer rates in breast cancer could be related to changes in the expression of AK isoforms. The literature contains diverse and sometimes contradictory data on the expression and functions of AK isoforms in breast cancer. Kim et al. found that high AK2 levels in breast cancer inhibit proliferation (H. Kim et al., 2014). Conversely, Speers et al. suggested that elevated AK2 levels in ER-negative breast cancer subtypes could make AK2 a potential drug target (Speers et al., 2009). Klepinin et al. demonstrated that the AK phosphotransfer pathway is the primary energy transfer mechanism in clinical breast cancer tissues, with AK1 and AK2 activity increasing during carcinogenesis (A. Klepinin et al., 2016). Recently, it was found that AK6 is overexpressed in breast cancer and is associated with a poorer prognosis (Bai et al., 2016). Since previous studies have not investigated AK phosphotransfer fluxes together with AK isoform expression in breast cancer, such a comprehensive study is needed, particularly using clinical material. This type of research could clarify which AK

isoforms are expressed in specific breast cancer subtypes and how they influence AK phosphotransfer fluxes. Moreover, similar studies could be used on colorectal cancer cell cultures and clinical material.

II – Improving ^{31}P -NMR method for stable isotope ^{18}O experiments

The second part of this study was a continuation of the first, aimed at improving the NMR method to make it more accessible and efficient. NMR spectroscopy, while undoubtedly expensive to both acquire and maintain, remains an invaluable tool in biochemical and metabolic research. When available, it is imperative to harness its extensive capabilities due to the depth of information it provides. Specifically, ^{31}P -NMR, although requiring larger sample volumes compared to techniques such as GC-MS, offers significant advantages (Singer et al., 1995).

One of its primary benefits is its non-destructive nature, which allows repeated measurements without compromising the integrity of the sample. Additionally, ^{31}P -NMR requires minimal sample preparation, reducing the complexity and potential errors associated with sample handling, a factor that is especially relevant when compared to the labor-intensive preparation required for GC-MS analysis (Emirhan Nemutlu et al., 2014).

However, there are challenges inherent to NMR, particularly when quantifying stable isotope turnover rates. These rates are typically derived from the formation of isotopomers, which can exhibit overlapping signals. Such overlaps complicate the accurate integration of these signals, leading to potential difficulties in interpreting isotopic enrichment data. This issue becomes particularly prominent when studying metabolic fluxes where high precision in isotopomer discrimination is critical for accurate flux analysis (Kaup et al., 2021).

The method introduced by Kaup and co-authors offers significant improvements to traditional ^{31}P NMR techniques, particularly in phosphometabolomic analysis. One of the main advancements is the enhanced resolution achieved by collapsing multiplets into singlets (Figure 19C), which simplifies spectra and makes signal interpretation more straightforward, especially when analyzing nucleotide triphosphates and isotopomers.

Additionally, the method reduces measurement time by integrating pure shift techniques with artifact suppression, allowing spectra to be recorded without substantial time penalties or line broadening. This improvement is particularly beneficial in biological samples where sample size and time are often limiting factors. Furthermore, the technique is possibly applicable to ^1H -NMR if additional resolution is sought after for very dilute samples (Kaup et al., 2021).

The emphasis in this thesis is on the non-destructive nature of the method. Given that clinical material is rare and difficult to obtain, its preservation becomes even more critical in future studies. Therefore, metabolic profiling should be conducted in a way that retains the sample whenever possible. A similar approach has been previously applied using NMR, specifically high-resolution magic angle spinning NMR (HR-MAS NMR), where a study (Mirnezami et al., 2014) highlighted the importance of non-destructive techniques and demonstrated cancer-specific metabolic signatures.

In conclusion, this improved method is expected to be both useful and efficient in future studies.

III – Profiling energy metabolism of colorectal cancer clinical material and Caco-2 cell cultures with combined methods

The third and final part of this thesis focuses on the study of colorectal cancer metabolism, primarily using clinical samples and, to a lesser extent, Caco-2 cell cultures for comparing enzyme activities to clinical material. A combination of methods, including high-resolution oxygraphy, adenine nucleotide quantification, and enzyme kinetics, was employed to explore alterations in OXPHOS and glycolysis in cancer. Each method complemented the others, providing a nuanced and comprehensive understanding of metabolic changes in colorectal cancer. Additionally, an effort was made to maximize the use of clinical material, treating it as an experiment in itself to determine how much data could be extracted from a single sample, given its uniqueness and rarity due to patient-to-patient variability (Figure 9).

Previous studies on mitochondrial respiration have revealed a significant difference in K_m ADP values between fast-twitch glycolytic and slow-twitch oxidative muscle tissues, with oxidative tissues showing a lower apparent K_m for ADP (Kuznetsov et al., 1996). In contrast, the current study found no significant difference in K_m ADP values between control and CRC tissues (Figure 13B) nor between control and stages I-III (Figure 14B), consistent with prior research indicating similar K_m ADP values in cancer and control tissues. However, these values were found to be higher in colorectal polyps, potentially reflecting early metabolic changes in the progression of CRC (Rebane-Klemm et al., 2023).

Despite the similar K_m ADP values, it has been previously shown that CRC tissues exhibit significantly higher V_{max} values compared to surrounding healthy tissues, which may suggest an increased energy demand due to a higher mitochondrial content (Chekulayev et al., 2015). This study corroborates these findings, demonstrating higher V_{max} values in CRC tissues (Figure 13A), but not when CRC is broken down into stages I-III (Figure 14A), however this could be due to small sample sizes. Furthermore, the elevated V_{max}/K_m ADP ratios observed in CRC tissues (Figure 13C) could indicate a more efficient pathway for mitochondrial ATP synthesis, potentially serving as a marker for a more aggressive disease (Rebane-Klemm et al., 2023). Similar differences were observed in analysis between control and CRC stages, where all the stages through I to III had significantly higher V_{max}/K_m ADP ratios (Figure 14C).

Recent studies have increasingly applied Atkinson's EC concept to explore cancer cell metabolism and mitochondrial function, suggesting that EC may indicate alterations that disrupt the energy balance in cancer cells, thereby affecting their growth and survival (Iommarini et al., 2017). EC values range from 0 to 1, with values close to 0 indicating that the adenine nucleotide pool mainly consists of AMP, 0.5 when ADP is predominant, and 1 when ATP is predominant. Previous studies have documented EC values within a narrow range of 0.7 to 0.95 across various organisms and cell types, including liver and muscle cells. These values typically decrease under stressful conditions (De la Fuente et al., 2014), such as during nutrient depletion, where they can drop from ≥ 0.8 to below 0.5 (Passman et al., 2023).

In the present studies, EC values were obtained by quantifying adenine nucleotides with HPLC and ranged between 0.4 and 0.5, from high-resolution respirometry media, that hosted the permeabilized clinical material during the experiment (Figure 9C). These values could be attributed to permeabilization process (Figure 9A), where there may be leakage of cytosolic proteins, including glycolytic enzymes, which could limit observable glycolytic activity, hence lowering the EC values. However, some glycolytic enzymes, such

as HK, remain bound to the cell's macromolecular structures, preserving a degree of glycolytic activity (Ouhabi et al., 1998) that can be explored through inhibition or activation. This pattern was observed in this study, where EC values were significantly higher in control tissues compared to CRC tissues when glycolysis was activated (Figures 14, B). Additionally, both control and CRC samples with activated glycolysis showed higher EC values than their non-activated glycolysis counterparts (Figure 15A). However, no significant difference was found between control and CRC samples where glycolysis was not activated (Figures 15A and 16A). To further investigate this pattern, glycolysis was activated and subsequently inhibited in some experiments, resulting in EC values similar to those observed in samples without prior glycolysis activation (Figure 15B). Interestingly, there was a significant difference in EC values, which were higher in glycolysis-activated, non-inhibited control and CRC samples compared to their OXPHOS-inhibited counterparts (Figure 15B). This finding aligns with previous studies suggesting that OXPHOS has a more substantial impact on cancer metabolism than previously thought (Chekulayev et al., 2015).

Another aspect worth mentioning is the relationship between EC and AMP-activated protein kinase (AMPK). The role of AMPK regarding tumorigenesis remains unclear, mainly because it can act as a tumor suppressant and an oncogene (Liang & Mills, 2013). AMPK's main role is to control catabolic and anabolic pathways by modulating key metabolic enzymes, under conditions where AMP levels rise and EC drops it activates catabolic pathways to mitigate ATP depletion. Whereas when EC is high, ATP consuming anabolic pathways are activated (Iommarini et al., 2017). A study on AMPK-deficient mouse embryonic fibroblasts (MEFs) demonstrated that ATP levels remained high despite the absence of AMPK, while EC levels were largely unaffected. Additionally, the cells exhibited a shift toward aerobic glycolysis (Faubert et al., 2013). While neither AMPK activity nor its levels were explored in this thesis, investigating them in the future would be worthwhile, as AMPK is potentially linked to the so-called hybrid metabolism concept, and could be a potential therapeutic target. (L. Yu et al., 2017).

When examining ATP/ADP ratios, they were relatively low in both non-inhibited and inhibited glycolysis-activated groups, with no significant differences observed (Figure 15C). This outcome may be attributed to the use of permeabilized cells. Although non-inhibited CRC samples had slightly higher ATP/ADP ratios than control samples, the differences were not statistically significant, possibly due to small sample size and high variability.

Interestingly, a different trend was observed in samples where glycolysis had not been activated. Despite there being no significant difference in EC values between control and CRC samples (Figure 16A), CRC samples showed significantly higher ATP/ADP ratios (Figure 16C). This finding contradicts previous research, which suggested that glycolysis typically contributes to elevated ATP/ADP ratios (Vander Heiden et al., 2009). This discrepancy is notable, especially since the present study has already demonstrated that remnant glycolytic activity can still be utilized in permeabilized tissues. Another explanation for the low ATP/ADP ratios observed in this part of the thesis is that, in most cases, these ratios are measured under optimal conditions in cell cultures or isolated mitochondria, where they typically range from 6–10:1 in healthy proliferating cells (Schwenke et al., 1981) or even reach 100:1 in the extramitochondrial space (Wanders et al., 1984), which differ with the conditions in this study. Also ATP/ADP are more sensitive to changes, making them fluctuate more in contrast to EC where AMP concentrations have a stabilizing effect (Kanamori et al., 1990).

Additionally, when the CRC samples were analyzed by stages (I to III), an even more nuanced picture emerged. The lower EC value observed in Stage II CRC samples (Figure 16B) along with their overall higher ATP/ADP ratio (Figure 16D) may indicate a critical shift in energy metabolism specific to this stage. According to the literature, Stage II CRC can have a poorer prognosis, especially if epithelial-mesenchymal transition (EMT) occurs, which enables cancer cells to detach from the primary tumor, facilitating invasion and metastasis (Kevans et al., 2011). This process is associated with tumor budding, a phenomenon that is more energy demanding, particularly in terms of OXPHOS activity (Burban et al., 2023; Masoud et al., 2020). Furthermore, modern therapeutic strategies for CRC have been standardized for Stages I and IV, but treatment approaches for Stage II remain a subject of considerable debate. Stage II is recognized as a heterogeneous category, with prognoses varying significantly, and 5-year overall survival rates ranging from 87.5% to 58.4%. In some cases, patients with Stage II CRC have a worse prognosis than those with low-risk Stage III cancer. Standard adjuvant chemotherapy, which typically involves 5-fluorouracil and leucovorin, offers only a modest improvement in 5-year survival rates, increasing by 2-5% (Parent et al., 2020). Overall, the data suggested that distinct energy metabolism profiles may emerge across different colorectal tumor stages, reflecting their progression from one stage to another. Although the metabolic differences among CRC stages I, II, and III appeared relatively minimal, this could be attributed to the limited sample size examined in this study. Notably, this study did not include cases of high-grade metastatic CRC, which, according to previous research, exhibit a significant increase in EC of approximately 26%. In contrast, CRC stages I and III have shown negligible changes in EC (Teo et al., 2017), consistent with the findings described here. Overall, indicators such as EC and the ATP/ADP ratio show promise in metabolic analysis and should be considered for broader use. Additionally, measuring adenine nucleotides from respiration media appears to provide valuable insights.

For the most part, this study utilized high-resolution oxygraphy to assess the mitochondrial respiration pathway in permeabilized clinical material, with some limited evaluation of glycolytic pathway remnants. To fully exploit the value of this unique material, additional experiments were conducted specifically to assess the glycolytic pathway, albeit in a constrained manner, by measuring the enzyme activities of LDH and HK. These experiments aimed to explore whether, and to what extent, clinical CRC samples differ from healthy colon tissue, CRC clinical material differs from Caco-2 cell cultures, and how non-permeabilized CRC samples compare to their permeabilized counterparts.

HK plays a pivotal role in cancer energy metabolism. As one of the key regulatory enzymes in glycolysis, HK serves as a major rate-limiting step in cancer cells (Roberts & Miyamoto, 2015). Additionally, HK2 has been identified as an independent prognostic marker for CRC (Katagiri et al, 2017). The interaction between HK2 and voltage-dependent anion channel (VDAC) has been suggested to facilitate the Warburg effect by directing mitochondria-generated ATP preferentially towards glycolysis (Peter L. Pedersen et al., 2002). This association provides several advantages to cancer cells, including increased permeability of the MOM for adenine nucleotides, heightened aerobic glycolysis, and enhanced resistance to apoptosis. Despite these benefits, the co-localization of HK2 with VDAC has been observed in both normal colorectal mucosa and CRC tissue (Kaldma et al., 2014; L. Ounpuu et al., 2018). LDH and monocarboxylate transporters (MCTs) are crucial enzymes responsible for lactate production and transport, respectively (Hatami et al., 2023). Both LDH and MCTs play key roles in the “lactate shuttle” hypothesis, which

describes the transfer of lactate from highly glycolytic tissues, such as muscles, to other organs like the liver or heart, where it can be used for energy production or converted back into glucose. Elevated levels of LDH are frequently found in the bloodstream of individuals with colon cancer (Casadei Gardini & Scarpi, 2020; Manerba et al., 2017; Xie et al., 2022).

In this study, the enzyme activity assessments did not differentiate between HK1 and HK2 isoforms, nor did they reveal any statistically significant differences in hexokinase activities between control and CRC clinical material, permeabilized and non-permeabilized samples, or between clinical material and Caco-2 cells. The exception was observed in permeabilized versus non-permeabilized control tissues (Figure 18A), where enzyme activity was notably higher in the permeabilized controls. Interestingly, all HK activities appeared higher in permeabilized clinical samples compared to their intact counterparts (Figure 18A). This may be attributed to the loss of cytosolic low molecular weight biomolecules during permeabilization, leaving only some glycolytic enzymes and organelles intact. In contrast, non-permeabilized tissues likely retain a greater overall amount of peptides and proteins, thus increasing their total protein content. Consequently, when enzyme activities are calculated, the remaining glycolytic proteins in permeabilized tissues exhibit greater activity per mg of protein due to the diminished background – in simpler terms, suspected protein dilution effect. In theory, the activities of permeabilized control and intact control should be similar, and same with CRC samples. Overall CRC samples have a non-significant trend to be higher in HK activity, Caco-2 slightly lower and healthy colon tissues the lowest (Figure 18A). Also, the $K_{m\text{Glucose}}$ seems the highest in intact control tissue and in theory should be similar in permeabilized (Figure 18B) whereas the CRCs and Caco-2 should have similar low values, meaning as tumors should have higher affinity towards substrate. A clearer distinction was observed with lactate dehydrogenase (LDH) activity, which varied significantly across all groups (Figure 18A), even when considering the potential effects of protein dilution. The results clearly indicate a marked difference between clinical material and Caco-2 cells, with the latter exhibiting LDH activity threefold higher than in control tissue and approximately 30% higher than in CRC samples. Additionally, the affinity for pyruvate in Caco-2 cells was much greater compared to the other groups with statistically significant difference between intact CRC samples (Figure 17B), and the efficiency of LDH enzyme in Caco-2 cells surpassed the others by more than twofold (Figure 17C). These findings are consistent with previous reports highlighting fundamental differences in energy metabolism between clinical material and cell cultures (Koitz et al., 2017). The other thing worth to point out is the discrepancy between enzyme activities between permeabilized CRC and intact CRC, in which there is twofold difference (Figure 17A), meaning that a significant portion of LDH enzymes may get washed out from the cytosol.

The high LDH activity observed in intact CRC samples reinforces the notion that CRC may exhibit significant metabolic plasticity. A review on CRC metabolism (Gharib & Robichaud, 2024) found that mutant KRAS signaling enhances LDHA expression, promoting a shift toward glycolysis at the expense of OXPHOS. This further underscores the need for additional studies focusing on glycolytic enzymes in clinical material.

5.1 Limitations of the study

The study has certain limitations that future research could aim to overcome. With stable isotope labeling, it is important to consider determining the expression levels of enzyme isoforms involved, as well as measuring glycolytic pathway activity.

The improved NMR method, while efficient and precise, has its drawbacks. Notably, ^{31}P -NMR requires larger sample sizes.

Variations in sample size across different CRC stages present an inherent challenge that cannot be eliminated but must instead be accounted for. Nonetheless, increasing the sample size could enhance the statistical power, potentially leading to more robust and statistically significant differences between groups. More parallel experiments should be conducted on Caco-2 cells in the future to better elucidate the extent of differences between clinical material and cell lines.

Thus far, the primary focus has been on OXPHOS and glycolysis. Expanding the scope of the study to include lipid metabolism or the pentose phosphate pathway could provide a more comprehensive understanding of CRC metabolism. Addressing these aspects would further enhance our knowledge of the metabolic reprogramming that occurs during cancer development.

CONCLUSIONS

1. The ^{18}O isotope labelling method provides precise measurements of ATP turnover and phosphotransfer fluxes (AK and CK fluxes), making it an effective tool for studying breast.
2. The improved NMR method simplifies phosphometabolite quantification, making it more efficient for metabolic studies.
3. Combining methods enhances research by providing complementary insights, facilitating a clearer understanding of underlying mechanisms, and aiding in the identification of actionable indicators for implementation.
 - a. High resolution respirometry showed high OXPHOS capability in CRC in contrast to normal tissue
 - b. Glycolysis activation affects EC both between tumor and control samples with activated glycolysis, as well as within tumor and control groups separately.
 - c. EC decreases in both tumor and control groups under inhibition, especially OXPHOS inhibition, compared to non-inhibited counterparts.
 - d. EC values without glycolysis activation were significantly lower in stage II compared to control and stage I.
 - e. ATP/ADP ratios in uninhibited tumor samples without glycolysis activation showed significant difference from control, and was significantly higher in stage II compared to control
 - f. Enzymatic activities indicate that CRC LDH activity is significantly higher compared to control
 - g. Pathway efficiency (V_{\max}/K_m) could be a good indicator to consider.
1. Combining high-resolution oxygraphy, isotope tracing, mass spectrometry, and NMR would enhance the resolution and reliability of metabolic profiling. Multi-platform integration would help uncover metabolic vulnerabilities in cancer that would remain undetected using isolated techniques.
2. Future research directions:
 - a. The combination of NMR and ^{18}O stable isotope labelling could be further developed for cancer clinical material, possibly providing greater metabolic insight and improving translational cancer research.
 - b. Additional research is needed to explore tumor heterogeneity and microenvironmental effects on energy metabolism

List of Figures

Figure 1. Glucose metabolism comparison of normal cells against cancer cells.	16
Figure 2. The mitochondrial respiratory chain.....	18
Figure 3. The intracellular phosphotransfer network.....	20
Figure 4. Labeling of the phosphoryl group positions in adenosine triphosphate (ATP). ..	22
Figure 5. Diagram depicting the Pedersen model.	23
Figure 6. Overview of the ^{18}O labeling incorporation process.....	29
Figure 7. Design of the study	32
Figure 8. Sample preparation workflow for ^{18}O -labelling based phosphometabolomics and metabolite ^{18}O -labeling sequence.	37
Figure 9. Overview of CRC clinical samples experiments.....	39
Figure 10. Assessment of cellular energetic status in breast cancer cells	41
Figure 11. Determination of the energetic profile of the creatine kinase pathway in breast cancer cells.....	42
Figure 12. Determination of the metabolic profile of the adenylate kinase pathway in breast cancer cells.....	43
Figure 13. OXPHOS pathway analysis..	44
Figure 14. OXPHOS pathway analysis across CRC stages.....	44
Figure 15. Energy charges and ATP/ADP ratios.	45
Figure 16. Energy charges and ATP/ADP ratios across CRC stages.	46
Figure 17. LDH activities.	47
Figure 18. HK activities.....	47
Figure 19. ^{31}P NMR spectra of partially ^{18}O -labelled ATP.	48

List of Tables

Table 1. Common Stable Isotopes in Cancer Research..... 27

References

- Accioly, M. T., Pacheco, P., Maya-Monteiro, C. M., Carrossini, N., Robbs, B. K., Oliveira, S. S., . . . Viola, J. P. (2008). Lipid bodies are reservoirs of cyclooxygenase-2 and sites of prostaglandin-E2 synthesis in colon cancer cells. *Cancer Research*, 68(6), 1732-1740. doi: 10.1158/0008-5472.can-07-1999
- Alberghina, L. (2023). The Warburg Effect Explained: Integration of Enhanced Glycolysis with Heterogeneous Mitochondria to Promote Cancer Cell Proliferation. *Int J Mol Sci*, 24(21). doi: 10.3390/ijms242115787
- Amoedo, N. D., Rodrigues, M. F., & Rumjanek, F. D. (2014). Mitochondria: are mitochondria accessory to metastasis? *International Journal of Biochemistry and Cell Biology*, 51, 53-57. doi: 10.1016/j.biocel.2014.03.009
- Atkinson, D. E., & Walton, G. M. (1967). Adenosine triphosphate conservation in metabolic regulation. Rat liver citrate cleavage enzyme. *Journal of Biological Chemistry*, 242(13), 3239-3241.
- Bai, D., Zhang, J., Li, T., Hang, R., Liu, Y., Tian, Y., . . . Zheng, X. (2016). The ATPase hCINAP regulates 18S rRNA processing and is essential for embryogenesis and tumour growth. *Nature Communications*, 7.
- Beckonert, O., Keun, H. C., Ebbels, T. M., Bundy, J., Holmes, E., Lindon, J. C., & Nicholson, J. K. (2007). Metabolic profiling, metabolomic and metabonomic procedures for NMR spectroscopy of urine, plasma, serum and tissue extracts. *Nat Protoc*, 2(11), 2692-2703. doi: 10.1038/nprot.2007.376
- Benjamin, D. I., Cravatt, B. F., & Nomura, D. K. (2012). Global profiling strategies for mapping dysregulated metabolic pathways in cancer. *Cell Metab*, 16(5), 565-577. doi: 10.1016/j.cmet.2012.09.013
- Berger, G., Girault, G., Pezenec, S., & Zimmermann, J. L. (1998). The use of HPLC for the Study of Chloroplast ATPase Enzymatic Activity and ATP Binding. *Journal of Liquid Chromatography & Related Technologies*, 21(13), 1925-1955. doi: 10.1080/10826079808006600
- Bhatt, D. P., Chen, X., Geiger, J. D., & Rosenberger, T. A. (2012). A sensitive HPLC-based method to quantify adenine nucleotides in primary astrocyte cell cultures. *Journal of Chromatography B*, 889-890, 110-115. doi: https://doi.org/10.1016/j.jchromb.2012.02.005
- Bodamer, O. A., & Halliday, D. (2001). Uses of stable isotopes in clinical diagnosis and research in the paediatric population. *Archives of Disease in Childhood*, 84(5), 444-448. doi: 10.1136/adc.84.5.444
- Burban, A., Sharanek, A., Bikfalvi, A., & Daubon, T. (2023). P02.04.B TARGETING METABOLIC VULNERABILITIES IN GLIOBLASTOMA. *Neuro-Oncology*.
- Casadei Gardini, A., & Scarpi, E. (2020). Prognostic role of a new index (multi inflammatory index) in patients with metastatic colorectal cancer: results from the randomized ITACa trial. 12, 1758835920958363. doi: 10.1177/1758835920958363
- Castillo, M. J., Reynolds, K. J., Gomes, A., Fenselau, C., & Yao, X. (2014). Quantitative protein analysis using enzymatic [¹⁸O]water labeling. *Curr Protoc Protein Sci*, 76, 23.24.21-23.24.29. doi: 10.1002/0471140864.ps2304s76
- Chekulayev, V., Mado, K., Shevchuk, I., Koit, A., Kaldma, A., Klepinin, A., . . . Kaambre, T. (2015). Metabolic remodeling in human colorectal cancer and surrounding tissues: alterations in regulation of mitochondrial respiration and metabolic fluxes. *Biochemistry and Biophysics Reports*, 4, 111-125. doi: 10.1016/j.bbrep.2015.08.020

- Chelakkot, C., Chelakkot, V. S., Shin, Y., & Song, K. (2023). Modulating Glycolysis to Improve Cancer Therapy. *International Journal of Molecular Sciences*, 24.
- Choong, L. Y., Lim, S., Chong, P. K., Wong, C. Y., Shah, N., & Lim, Y. P. (2010). Proteome-wide profiling of the MCF10AT breast cancer progression model. *PLoS One*, 5(6), e11030. doi: 10.1371/journal.pone.0011030
- Cortesi, M., Warton, K., & Ford, C. E. (2024). Beyond 2D cell cultures: how 3D models are changing the in vitro study of ovarian cancer and how to make the most of them. *PeerJ*, 12, e17603. doi: 10.7717/peerj.17603
- Cunningham, D., Atkin, W., Lenz, H.-J., Lynch, H. T., Minsky, B., Nordlinger, B., & Starling, N. (2010). Colorectal cancer. *The Lancet*, 375(9719), 1030-1047.
- Cuyàs, E., Verdura, S., Fernández-Arroyo, S., Bosch-Barrera, J., Martin-Castillo, B., Joven, J., & Menendez, J. A. (2017). Metabolomic mapping of cancer stem cells for reducing and exploiting tumor heterogeneity. *Oncotarget*, 8(59), 99223-99236. doi: 10.18632/oncotarget.21834
- De la Fuente, I. M., Cortés, J. M., Valero, E., Desroches, M., Rodrigues, S., Malaina, I., & Martínez, L. (2014). On the Dynamics of the Adenylate Energy System: Homeorhesis vs Homeostasis. *PLOS ONE*, 9(10), e108676. doi: 10.1371/journal.pone.0108676
- DeBerardinis, R. J., & Cheng, T. (2010). Q's next: the diverse functions of glutamine in metabolism, cell biology and cancer. *Oncogene*, 29(3), 313-324. doi: 10.1038/onc.2009.358
- DeBerardinis, R. J., Lum, J. J., Hatzivassiliou, G., & Thompson, C. B. (2008). The Biology of Cancer: Metabolic Reprogramming Fuels Cell Growth and Proliferation. *Cell Metabolism*, 7(1), 11-20.
- Dragic, H., Chaveroux, C., Cosset, E., & Manie, S. N. (2024). Modelling cancer metabolism in vitro: current improvements and future challenges. *The FEBS Journal*, 291(3), 402-411. doi: <https://doi.org/10.1111/febs.16704>
- Dzeja, P., & Terzic, A. (2009). Adenylate kinase and AMP signaling networks: Metabolic monitoring, signal communication and body energy sensing. *Int J Mol Sci*, 10(4), 1729-1772. doi: 10.3390/ijms10041729
- Dzeja, P. P., Chung, S., & Terzic, A. (2007). Integration of Adenylate Kinase and Glycolytic and Glycogenolytic Circuits in Cellular Energetics *Molecular System Bioenergetics* (pp. 265-301): Wiley-VCH Verlag GmbH & Co. KGaA.
- Dzeja, P. P., & Terzic, A. (1998). Phosphotransfer reactions in the regulation of ATP-sensitive K⁺ channels. *FASEB Journal*, 12(7), 523-529. doi: 10.1096/fasebj.12.7.523
- Dzeja, P. P., & Terzic, A. (2003). Phosphotransfer networks and cellular energetics. *Journal of Experimental Biology*, 206(Pt 12), 2039-2047.
- Dzeja, P. P., Terzic, A., & Wieringa, B. (2004). Phosphotransfer dynamics in skeletal muscle from creatine kinase gene-deleted mice. *Molecular and Cellular Biochemistry*, 256-257(1-2), 13-27. doi: 10.1023/b:mcbi.0000009856.23646.38
- Engelen, Mariëlle P. K. J., Safar, Ahmed M., Bartter, T., Koeman, F., & Deutz, Nicolaas E. P. (2016). Reduced arginine availability and nitric oxide synthesis in cancer is related to impaired endogenous arginine synthesis. *Clinical Science*, 130(14), 1185-1195. doi: <https://doi.org/10.1042/CS20160233>
- Eylem, C. C., Baysal, İ., Erikci, A., Yabanoglu-Ciftci, S., Zhang, S., Kir, S., . . . Nemutlu, E. (2021). Gas chromatography-mass spectrometry based (18)O stable isotope labeling of Krebs cycle intermediates. *Analytica Chimica Acta*, 1154, 338325. doi: 10.1016/j.aca.2021.338325

- Faubert, B., Boily, G., Izreig, S., Griss, T., Samborska, B., Dong, Z., . . . Jones, Russell G. (2013). AMPK Is a Negative Regulator of the Warburg Effect and Suppresses Tumor Growth In Vivo. *Cell Metabolism*, 17(1), 113-124.
- Feng, Y., Spezia, M., Huang, S., Yuan, C., Zeng, Z., Zhang, L., . . . Ren, G. (2018). Breast cancer development and progression: Risk factors, cancer stem cells, signaling pathways, genomics, and molecular pathogenesis. *Genes & Diseases*, 5(2), 77-106. doi: <https://doi.org/10.1016/j.gendis.2018.05.001>
- Fujisawa, K., Terai, S., Takami, T., Yamamoto, N., Yamasaki, T., Matsumoto, T., . . . Sakaida, I. (2016). Modulation of anti-cancer drug sensitivity through the regulation of mitochondrial activity by adenylate kinase 4. *Journal of Experimental and Clinical Cancer Research*, 35, 48. doi: 10.1186/s13046-016-0322-2
- Gallo, M., Sapio, L., Spina, A., Naviglio, D., Calogero, A., & Naviglio, S. (2015). Lactic dehydrogenase and cancer: an overview. *Front Biosci (Landmark Ed)*, 20(8), 1234-1249. doi: 10.2741/4368
- García Vicente, A. M., Soriano Castrejón, Á., León Martín, A., Chacón López-Muñiz, I., Muñoz Madero, V., Muñoz Sánchez Mdel, M., . . . González Ageitos, A. (2013). Molecular subtypes of breast cancer: metabolic correlation with ¹⁸F-FDG PET/CT. *Eur J Nucl Med Mol Imaging*, 40(9), 1304-1311. doi: 10.1007/s00259-013-2418-7
- Gharib, E., & Robichaud, G. A. (2024). From Crypts to Cancer: A Holistic Perspective on Colorectal Carcinogenesis and Therapeutic Strategies. *International Journal of Molecular Sciences*, 25(17). doi:10.3390/ijms25179463
- Gorin, A., Gabitova, L., & Astsaturov, I. (2012). Regulation of cholesterol biosynthesis and cancer signaling. *Current Opinion in Pharmacology*, 12(6), 710-716. doi: <https://doi.org/10.1016/j.coph.2012.06.011>
- Guzun, R., Kaambre, T., Bagur, R., Grichine, A., Usson, Y., Varikmaa, M., . . . Saks, V. (2015). Modular organization of cardiac energy metabolism: energy conversion, transfer and feedback regulation. *Acta Physiol (Oxf)*, 213(1), 84-106. doi: 10.1111/apha.12287
- Hall, M., Mickey, D. D., Wenger, A. S., & Silverman, L. M. (1985). Adenylate kinase: an oncodevelopmental marker in an animal model for human prostatic cancer. *Clinical Chemistry*, 31(10), 1689-1691.
- Hanahan, D., & Weinberg, R. A. (2011). Hallmarks of cancer: the next generation. *Cell*, 144(5), 646-674. doi: <https://doi.org/10.1016/j.cell.2011.02.013>
- Hardie, D. G., Scott, J. W., Pan, D. A., & Hudson, E. R. (2003). Management of cellular energy by the AMP-activated protein kinase system. *FEBS Letters*, 546(1), 113-120. doi: 10.1016/s0014-5793(03)00560-x
- Hatami, H., Sajedi, A., & Mir, S. M. (2023). Importance of lactate dehydrogenase (LDH) and monocarboxylate transporters (MCTs) in cancer cells. 6(1), e996. doi: 10.1002/hsr2.996
- Hsu, P. P., & Sabatini, D. M. (2008). Cancer cell metabolism: Warburg and beyond. *Cell*, 134(5), 703-707. doi: 10.1016/j.cell.2008.08.021
- IARC. (2022, 08.02.2022). Cancer Today. *Absolute numbers, Incidence, Both sexes, in 2022*. Retrieved 11.03, 2024, from https://gco.iarc.fr/today/en/dataviz/bars?mode=cancer&group_populations=1&key=total

- Imyanitov, E. N., & Hanson, K. P. (2004). Mechanisms of breast cancer. *Drug Discovery Today: Disease Mechanisms*, 1(2), 235-245. doi: <https://doi.org/10.1016/j.ddmec.2004.09.002>
- Iommarini, L., Ghelli, A., Gasparre, G., & Porcelli, A. M. (2017). Mitochondrial metabolism and energy sensing in tumor progression. *Biochim Biophys Acta Bioenerg*, 1858(8), 582-590. doi: 10.1016/j.bbabbio.2017.02.006
- Ishida, Y., Riesinger, I., Wallimann, T., & Paul, R. J. (1994). Compartmentation of ATP synthesis and utilization in smooth muscle: roles of aerobic glycolysis and creatine kinase. *Molecular and Cellular Biochemistry*, 133-134, 39-50.
- Israelsen, W. J., & Vander Heiden, M. G. (2015). Pyruvate kinase: Function, regulation and role in cancer. *Seminars in Cell and Developmental Biology*, 43, 43-51. doi: 10.1016/j.semcdb.2015.08.004
- Jia, D., Park, J. H., Jung, K. H., Levine, H., & Kaiparettu, B. A. (2018). Elucidating the Metabolic Plasticity of Cancer: Mitochondrial Reprogramming and Hybrid Metabolic States. *Cells*, 7.
- Jiang, G., Zhang, S., Yazdanparast, A., Li, M., Pawar, A. V., Liu, Y., . . . Cheng, L. (2016). Comprehensive comparison of molecular portraits between cell lines and tumors in breast cancer. *BMC Genomics*, 17(7), 525. doi: 10.1186/s12864-016-2911-z
- Kadenbach, B. (1986). Regulation of respiration and ATP synthesis in higher organisms: hypothesis. *Journal of Bioenergetics and Biomembranes*, 18(1), 39-54. doi: 10.1007/bf00743611
- Kaldma, A., Klepinin, A., Chekulayev, V., Mado, K., Shevchuk, I., Timohhina, N., . . . Kaambre, T. (2014). An in situ study of bioenergetic properties of human colorectal cancer: the regulation of mitochondrial respiration and distribution of flux control among the components of ATP synthasome. *International Journal of Biochemistry and Cell Biology*, 55, 171-186. doi: 10.1016/j.biocel.2014.09.004
- Kanamori, K., Weiss, R. L., & Roberts, J. D. (1990). Efficiency factors and ATP/ADP ratios in nitrogen-fixing *Bacillus polymyxa* and *Bacillus azotofixans*. *Journal of Bacteriology*, 172(4), 1962-1968. doi: 10.1128/jb.172.4.1962-1968.1990
- Kaup, K. K., Toom, L., Truu, L., Miller, S., Puurand, M., Tepp, K., . . . Reile, I. (2021). A line-broadening free real-time ³¹P pure shift NMR method for phosphometabolomic analysis. *Analyst*, 146(18), 5502-5507. doi: 10.1039/D1AN01198G
- Kevans, D., Wang, L. M., Sheahan, K., Hyland, J., O'Donoghue, D., Mulcahy, H., & O'Sullivan, J. (2011). Epithelial-Mesenchymal Transition (EMT) Protein Expression in a Cohort of Stage II Colorectal Cancer Patients With Characterized Tumor Budding and Mismatch Repair Protein Status. *International Journal of Surgical Pathology*, 19(6), 751-760. doi: 10.1177/1066896911414566
- Kim, H., Lee, H. J., Oh, Y., Choi, S. G., Hong, S. H., Kim, H. J., . . . Jung, Y. K. (2014). The DUSP26 phosphatase activator adenylate kinase 2 regulates FADD phosphorylation and cell growth. *Nat Commun*, 5, 3351. doi: <https://doi.org/10.1038/ncomms4351>
- Kim, J., & DeBerardinis, R. J. (2019). Mechanisms and Implications of Metabolic Heterogeneity in Cancer. *Cell Metabolism*, 30(3), 434-446. doi: 10.1016/j.cmet.2019.08.013

- Kita, M., Fujiwara-Tani, R., Kishi, S., Mori, S., Ohmori, H., Nakashima, C., . . . Kuniyasu, H. (2023). Role of creatine shuttle in colorectal cancer cells. *Oncotarget*, 14, 485-501. doi: 10.18632/oncotarget.28436
- Klepinin, A., Chekulayev, V., Timohhina, N., Shevchuk, I., Tepp, K., Kaldma, A., . . . Kaambre, T. (2014). Comparative analysis of some aspects of mitochondrial metabolism in differentiated and undifferentiated neuroblastoma cells. *Journal of Bioenergetics and Biomembranes*, 46, 17-31. doi: 10.1007/s10863-013-9529-5
- Klepinin, A., Ounpuu, L., Guzun, R., Chekulayev, V., Timohhina, N., Tepp, K., . . . Kaambre, T. (2016). Simple oxygraphic analysis for the presence of adenylate kinase 1 and 2 in normal and tumor cells. *Journal of Bioenergetics and Biomembranes*, 48(5), 531-548. doi: 10.1007/s10863-016-9687-3
- Klepinin, A., Zhang, S., Klepinina, L., Rebane-Klemm, E., Terzic, A., Kaambre, T., & Dzeja, P. (2020). Adenylate Kinase and Metabolic Signaling in Cancer Cells. *Front Oncol*, 10, 660. doi: 10.3389/fonc.2020.00660
- Kocarnik, J. M., Shiovitz, S., & Phipps, A. I. (2015). Molecular phenotypes of colorectal cancer and potential clinical applications. *Gastroenterology Report*, 3(4), 269-276. doi: 10.1093/gastro/gov046
- Koit, A., Shevchuk, I., Ounpuu, L., Klepinin, A., Chekulayev, V., Timohhina, N., . . . Kaambre, T. (2017). Mitochondrial Respiration in Human Colorectal and Breast Cancer Clinical Material Is Regulated Differently. *Oxid Med Cell Longev*, 2017, 1372640. doi: 10.1155/2017/1372640
- Kosmopoulou, M., Giannopoulou, A. F., Iliou, A., & Benaki, D. (2020). Human Melanoma-Cell Metabolic Profiling: Identification of Novel Biomarkers Indicating Metastasis. 21(7). doi: 10.3390/ijms21072436
- Kruger, N. J., & Ratcliffe, R. G. (2009). Insights into plant metabolic networks from steady-state metabolic flux analysis. *Biochimie*, 91(6), 697-702. doi: 10.1016/j.biochi.2009.01.004
- Kurmi, K., Hitosugi, S., Yu, J., Boakye-Agyeman, F., Wiese, E. K., Larson, T. R., . . . Hitosugi, T. (2018). Tyrosine Phosphorylation of Mitochondrial Creatine Kinase 1 Enhances a Druggable Tumor Energy Shuttle Pathway. *Cell Metab*, 28(6), 833-847.e838. doi: 10.1016/j.cmet.2018.08.008
- Kurzhunov, D., Borowiak, R., Reisert, M., Joachim Krafft, A., Caglar Özen, A., & Bock, M. (2017). 3D CMRO(2) mapping in human brain with direct (17)O MRI: Comparison of conventional and proton-constrained reconstructions. *NeuroImage*, 155, 612-624. doi: 10.1016/j.neuroimage.2017.05.029
- Kuznetsov, A. V., Tiivel, T., Sikk, P., Kaambre, T., Kay, L., Daneshrad, Z., . . . Saks, V. A. (1996). Striking differences between the kinetics of regulation of respiration by ADP in slow-twitch and fast-twitch muscles in vivo. *European Journal of Biochemistry*, 241(3), 909-915.
- Kuznetsov, A. V., Veksler, V., Gellerich, F. N., Saks, V., Margreiter, R., & Kunz, W. S. (2008). Analysis of mitochondrial function in situ in permeabilized muscle fibers, tissues and cells. *Nat Protoc*, 3(6), 965-976. doi: <https://doi.org/10.1038/nprot.2008.61>
- Lane, A. N., Higashi, R. M., & Fan, T. W. M. (2019). NMR and MS-based Stable Isotope-Resolved Metabolomics and applications in cancer metabolism. *TRAC Trends in Analytical Chemistry*, 120, 115322. doi: <https://doi.org/10.1016/j.trac.2018.11.020>

- Lane, A. N., Tan, J., Wang, Y., Yan, J., Higashi, R. M., & Fan, T. W. (2017). Probing the metabolic phenotype of breast cancer cells by multiple tracer stable isotope resolved metabolomics. *Metab Eng*, 43(Pt B), 125-136. doi: 10.1016/j.ymben.2017.01.010
- Lee, W. N., Bassilian, S., Guo, Z., Schoeller, D., Edmond, J., Bergner, E. A., & Byerley, L. O. (1994). Measurement of fractional lipid synthesis using deuterated water (2H₂O) and mass isotopomer analysis. *American Journal of Physiology*, 266(3 Pt 1), E372-383. doi: 10.1152/ajpendo.1994.266.3.E372
- Leithner, K., Hrzenjak, A., Trötz Müller, M., Moustafa, T., Köfeler, H. C., Wohlkoenig, C., . . . Olschewski, H. (2015). PCK2 activation mediates an adaptive response to glucose depletion in lung cancer. *Oncogene*, 34(8), 1044-1050. doi: 10.1038/onc.2014.47
- Lemasters, J. J., & Holmuhamedov, E. (2006). Voltage-dependent anion channel (VDAC) as mitochondrial governor--Thinking outside the box. *Biochimica et Biophysica Acta (BBA) - Molecular Basis of Disease*, 1762(2), 181-190.
- Lenaz, G., & Genova, M. (2012). Supramolecular Organisation of the Mitochondrial Respiratory Chain: A New Challenge for the Mechanism and Control of Oxidative Phosphorylation. *Advances in Experimental Medicine and Biology*, 748, 107-144. doi: 10.1007/978-1-4614-3573-0_5
- Lenz, E. M., & Wilson, I. D. (2007). Analytical strategies in metabolomics. *J Proteome Res*, 6(2), 443-458. doi: 10.1021/pr0605217
- Li, X.-H., Chen, X.-J., Ou, W.-B., Zhang, Q., Lv, Z.-R., Zhan, Y., . . . Zhou, H.-M. (2013). Knockdown of creatine kinase B inhibits ovarian cancer progression by decreasing glycolysis. *The International Journal of Biochemistry & Cell Biology*, 45(5), 979-986. doi: http://dx.doi.org/10.1016/j.biocel.2013.02.003
- Liang, J., & Mills, G. B. (2013). AMPK: a contextual oncogene or tumor suppressor? *Cancer Research*, 73(10), 2929-2935. doi: 10.1158/0008-5472.can-12-3876
- Liou, G. Y., & Storz, P. (2010). Reactive oxygen species in cancer. *Free Radical Research*, 44(5), 479-496. doi: 10.3109/10715761003667554
- Liu, L., He, Y., Ge, G., Li, L., Zhou, P., Zhu, Y., . . . Zhang, L. (2017). Lactate dehydrogenase and creatine kinase as poor prognostic factors in lung cancer: A retrospective observational study. *PLoS One*, 12(8), e0182168. doi: 10.1371/journal.pone.0182168
- Liu, R., Ström, A.-L., Zhai, J., Gal, J., Bao, S., Gong, W., & Zhu, H. (2009). Enzymatically inactive adenylate kinase 4 interacts with mitochondrial ADP/ATP translocase. *The International Journal of Biochemistry & Cell Biology*, 41(6), 1371-1380. doi: http://dx.doi.org/10.1016/j.biocel.2008.12.002
- Liu, Y., Wu, K., Shi, L., Xiang, F., Tao, K., & Wang, G. (2016). Prognostic Significance of the Metabolic Marker Hexokinase-2 in Various Solid Tumors: A Meta-Analysis. *PLoS One*, 11(11), e0166230. doi: 10.1371/journal.pone.0166230
- Lladó, V., López, D. J., Ibarguren, M., Alonso, M., Soriano, J. B., Escribá, P. V., & Busquets, X. (2014). Regulation of the cancer cell membrane lipid composition by NaChOleate: Effects on cell signaling and therapeutical relevance in glioma. *Biochimica et Biophysica Acta (BBA) - Biomembranes*, 1838(6), 1619-1627. doi: https://doi.org/10.1016/j.bbamem.2014.01.027
- Maldonado, E. N. (2017). VDAC-Tubulin, an Anti-Warburg Pro-Oxidant Switch. *Front Oncol*, 7, 4. doi: 10.3389/fonc.2017.00004

- Manerba, M., Di Ianni, L., Govoni, M., Roberti, M., Recanatini, M., & Di Stefano, G. (2017). Lactate dehydrogenase inhibitors can reverse inflammation induced changes in colon cancer cells. *European Journal of Pharmaceutical Sciences*, 96, 37-44. doi: 10.1016/j.ejps.2016.09.014
- Marie, S. K. N., & Shinjo, S. M. O. (2011). Metabolism and Brain Cancer. *Clinics*, 66, 33-43. doi: <https://doi.org/10.1590/S1807-59322011001300005>
- Martens, R. (1992). A comparison of soil adenine nucleotide measurements by hplc and enzymatic analysis. *Soil Biology and Biochemistry*, 24(7), 639-645. doi: [https://doi.org/10.1016/0038-0717\(92\)90042-V](https://doi.org/10.1016/0038-0717(92)90042-V)
- Masoud, R., Reyes-Castellanos, G., Lac, S., Garcia, J. T., Dou, S., Shintu, L., . . . Carrier, A. (2020). Targeting Mitochondrial Complex I Overcomes Chemoresistance in High OXPHOS Pancreatic Cancer. *Cell Reports Medicine*, 1.
- Mathupala, S. P., Ko, Y. H., & Pedersen, P. L. (2006). Hexokinase II: cancer's double-edged sword acting as both facilitator and gatekeeper of malignancy when bound to mitochondria. *Oncogene*, 25(34), 4777-4786. doi: 10.1038/sj.onc.1209603
- Mi, Y., Li, Q., Liu, B., Wang, D., Liu, Z., Wang, T., . . . Ding, Y. (2023). Ubiquitous mitochondrial creatine kinase promotes the progression of gastric cancer through a JNK-MAPK/JUN/HK2 axis regulated glycolysis. 26(1), 69-81. doi: 10.1007/s10120-022-01340-7
- Mirabelli, P., Coppola, L., & Salvatore, M. (2019). Cancer Cell Lines Are Useful Model Systems for Medical Research. *Cancers (Basel)*, 11(8). doi: 10.3390/cancers11081098
- Mirnezami, R., Jiménez, B., Li, J. V., Kinross, J. M., Veselkov, K., Goldin, R. D., . . . Darzi, A. (2014). Rapid diagnosis and staging of colorectal cancer via high-resolution magic angle spinning nuclear magnetic resonance (HR-MAS NMR) spectroscopy of intact tissue biopsies. *Annals of Surgery*, 259(6), 1138-1149. doi: 10.1097/SLA.0b013e31829d5c45
- Morson, B. (1974). President's address. The polyp-cancer sequence in the large bowel. *Proceedings of the Royal Society of Medicine*, 67(6 Pt 1), 451-457.
- Napiwotzki, J., & Kadenbach, B. (1998). Extramitochondrial ATP/ADP-ratios regulate cytochrome c oxidase activity via binding to the cytosolic domain of subunit IV. *Biological Chemistry*, 379(3), 335-339.
- Nelson, D. L., Cox, M. M., Hoskins, A. A., & Lehninger, A. L. (2021). *Lehninger principles of biochemistry* (8 ed.): W.H. Freeman And Company ; Houndmills, Basingstoke.
- Nelson, D. L., Lehninger, A. L., Cox, M. M., Osgood, M., & Ocorr, K. (2008). *Lehninger Principles of Biochemistry*: W.H. Freeman.
- Nemutlu, E., Gupta, A., Zhang, S., Viqar, M., Holmuhamedov, E., Terzic, A., . . . Dzeja, P. (2015). Decline of Phosphotransfer and Substrate Supply Metabolic Circuits Hinders ATP Cycling in Aging Myocardium. *PLoS One*, 10(9), e0136556. doi: 10.1371/journal.pone.0136556
- Nemutlu, E., Juranic, N., Zhang, S., Ward, L. E., Dutta, T., Nair, K. S., . . . Dzeja, P. P. (2012). Electron spray ionization mass spectrometry and 2D 31P NMR for monitoring 18O/16O isotope exchange and turnover rates of metabolic oligophosphates. *Anal Bioanal Chem*, 403(3), 697-706. doi: 10.1007/s00216-012-5899-5
- Nemutlu, E., Zhang, S., Gupta, A., Juranic, N. O., Macura, S. I., Terzic, A., . . . Dzeja, P. (2012). Dynamic phosphometabolomic profiling of human tissues and transgenic models by 18O-assisted (3)(1)P NMR and mass spectrometry. *Physiol Genomics*, 44(7), 386-402. doi: 10.1152/physiolgenomics.00152.2011

- Nemutlu, E., Zhang, S., Juranic, N. O., Terzic, A., Macura, S., & Dzeja, P. (2012). (18)O-assisted dynamic metabolomics for individualized diagnostics and treatment of human diseases. *Croatian Medical Journal*, 53(6), 529-534.
- Nemutlu, E., Zhang, S., Terzic, A., & Dzeja, P. (2014). 18O-assisted 31P NMR and Mass Spectrometry for Phosphometabolomic Fingerprinting and Metabolic Monitoring. In M. Grootveld (Ed.), *Metabolic Profiling: Disease and Xenobiotics* (pp. 0): The Royal Society of Chemistry.
- Noma, T., Fujisawa, K., Yamashiro, Y., Shinohara, M., Nakazawa, A., Gondo, T., . . . Yoshinobu, K. (2001). Structure and expression of human mitochondrial adenylate kinase targeted to the mitochondrial matrix. *Biochemical Journal*, 358(Pt 1), 225-232.
- Olson, L. K., Schroeder, W., Robertson, R. P., Goldberg, N. D., & Walseth, T. F. (1996). Suppression of adenylate kinase catalyzed phosphotransfer precedes and is associated with glucose-induced insulin secretion in intact HIT-T15 cells. *Journal of Biological Chemistry*, 271(28), 16544-16552. doi: 10.1074/jbc.271.28.16544
- Ouhabi, R., Boue-Grabot, M., & Mazat, J. P. (1998). Mitochondrial ATP synthesis in permeabilized cells: assessment of the ATP/O values in situ. *Analytical Biochemistry*, 263(2), 169-175. doi: 10.1006/abio.1998.2776
- Ounpuu, L., Klepinin, A., Pook, M., Teino, I., Peet, N., Paju, K., . . . Kaambre, T. (2017). 2102Ep embryonal carcinoma cells have compromised respiration and shifted bioenergetic profile distinct from H9 human embryonic stem cells. *Biochimica et Biophysica Acta (BBA) - General Subjects*, 1861(8), 2146-2154. doi: <https://doi.org/10.1016/j.bbagen.2017.05.020>
- Ounpuu, L., Truu, L., Shevchuk, I., Chekulayev, V., Klepinin, A., Koit, A., . . . Kaambre, T. (2018). Comparative analysis of the bioenergetics of human adenocarcinoma Caco-2 cell line and postoperative tissue samples from colorectal cancer patients. *Biochemistry and Cell Biology*, 1-10. doi: 10.1139/bcb-2018-0076
- Panayiotou, C., Solaroli, N., & Karlsson, A. (2014). The many isoforms of human adenylate kinases. *The International Journal of Biochemistry & Cell Biology*, 49, 75-83. doi: <https://doi.org/10.1016/j.biocel.2014.01.014>
- Parent, P., Cohen, R., Rassy, E., Svrcek, M., Taieb, J., André, T., & Turpin, A. (2020). A comprehensive overview of promising biomarkers in stage II colorectal cancer. *Cancer Treatment Reviews*, 88. doi: 10.1016/j.ctrv.2020.102059
- Passman, F. J., Schmidt, J., & Lewis, R. P. (2023). The relationship between microbial community vitality and ATP bioburden in bottom waters under fuel microcosms. *Access Microbiology*, 5(4). doi: <https://doi.org/10.1099/acmi.0.000411>
- Pedersen, P. L. (1978). Tumor mitochondria and the bioenergetics of cancer cells. *Progress in Experimental Tumor Research*, 22, 190-274.
- Pedersen, P. L. (2007). Warburg, me and Hexokinase 2: Multiple discoveries of key molecular events underlying one of cancers' most common phenotypes, the "Warburg Effect", i.e., elevated glycolysis in the presence of oxygen. *Journal of Bioenergetics and Biomembranes*, 39(3), 211-222. doi: 10.1007/s10863-007-9094-x
- Pedersen, P. L., Mathupala, S., Rempel, A., Geschwind, J. F., & Ko, Y. H. (2002). Mitochondrial bound type II hexokinase: a key player in the growth and survival of many cancers and an ideal prospect for therapeutic intervention. *Biochimica et Biophysica Acta (BBA) - Bioenergetics*, 1555(1-3), 14-20.

- Pfeiffer, T., Schuster, S., & Bonhoeffer, S. (2001). Cooperation and competition in the evolution of ATP-producing pathways. *Science*, 292(5516), 504-507. doi: 10.1126/science.1058079
- Potter, N. E., Phipps, K., Harkness, W., Hayward, R., Thompson, D., Jacques, T. S., . . . Warr, T. J. (2009). Astrocytoma derived short-term cell cultures retain molecular signatures characteristic of the tumour in situ. *Experimental Cell Research*, 315(16), 2835-2846. doi: <https://doi.org/10.1016/j.yexcr.2009.06.003>
- Pucar, D., Dzeja, P. P., Bast, P., Gumina, R. J., Drahl, C., Lim, L., . . . Terzic, A. (2004). Mapping hypoxia-induced bioenergetic rearrangements and metabolic signaling by 18O-assisted 31P NMR and 1H NMR spectroscopy. *Molecular and Cellular Biochemistry*, 256-257(1-2), 281-289. doi: 10.1023/b:mcbi.0000009875.30308.7a
- Pucar, D., Dzeja, P. P., Bast, P., Juranic, N., Macura, S., & Terzic, A. (2001). Cellular energetics in the preconditioned state: protective role for phosphotransfer reactions captured by 18O-assisted 31P NMR. *Journal of Biological Chemistry*, 276(48), 44812-44819. doi: 10.1074/jbc.M104425200
- Puurand, M., Tepp, K., Klepinin, A., Klepinina, L., Shevchuk, I., & Kaambre, T. (2018). Intracellular Energy-Transfer Networks and High-Resolution Respirometry: A Convenient Approach for Studying Their Function. *Int J Mol Sci*, 19(10). doi: 10.3390/ijms19102933
- Qian, X.-L., Li, Y.-Q., Gu, F., Liu, F.-F., Li, W.-D., Zhang, X.-M., & Fu, L. (2012). Overexpression of ubiquitous mitochondrial creatine kinase (uMtCK) accelerates tumor growth by inhibiting apoptosis of breast cancer cells and is associated with a poor prognosis in breast cancer patients. *Biochemical and Biophysical Research Communications*, 427(1), 60-66. doi: <https://doi.org/10.1016/j.bbrc.2012.08.147>
- Qian, Y., Wang, X., Li, Y., Cao, Y., & Chen, X. (2016). Extracellular ATP a New Player in Cancer Metabolism: NSCLC Cells Internalize ATP In Vitro and In Vivo Using Multiple Endocytic Mechanisms. *Mol Cancer Res*, 14(11), 1087-1096. doi: 10.1158/1541-7786.mcr-16-0118
- Rebane-Klemm, E., Reinsalu, L., Puurand, M., Shevchuk, I., Bogovskaja, J., Suurmaa, K., . . . Kaambre, T. (2023). Colorectal polyps increase the glycolytic activity. *Front Oncol*, 13, 1171887. doi: 10.3389/fonc.2023.1171887
- Riganti, C., Gazzano, E., Polimeni, M., Aldieri, E., & Ghigo, D. (2012). The pentose phosphate pathway: An antioxidant defense and a crossroad in tumor cell fate. *Free Radical Biology and Medicine*, 53(3), 421-436. doi: <https://doi.org/10.1016/j.freeradbiomed.2012.05.006>
- Roberts, D. J., & Miyamoto, S. (2015). Hexokinase II integrates energy metabolism and cellular protection: Acting on mitochondria and TORCing to autophagy. *Cell Death and Differentiation*, 22(2), 248-257. doi: 10.1038/cdd.2014.173
- Rosenzweig, S. A., & Atreya, H. S. (2010). Defining the pathway to insulin-like growth factor system targeting in cancer. *Biochemical Pharmacology*, 80 8, 1115-1124.
- Sablatura, L. K., Bircsak, K. M., Shepherd, P., Queiroz, K., Farach-Carson, M. C., Constantinou, P. E., . . . Harrington, D. A. (2020). Enhanced Viability for Ex vivo 3D Hydrogel Cultures of Patient-Derived Xenografts in a Perfused Microfluidic Platform. *J Vis Exp*(166). doi: 10.3791/60872

- Samuel, Varman T., & Shulman, Gerald I. (2012). Mechanisms for Insulin Resistance: Common Threads and Missing Links. *Cell*, 148(5), 852-871. doi: <https://doi.org/10.1016/j.cell.2012.02.017>
- Santos, C. R., & Schulze, A. (2012). Lipid metabolism in cancer. *Febs j*, 279(15), 2610-2623. doi: 10.1111/j.1742-4658.2012.08644.x
- Schwenke, W. D., Soboll, S., Seitz, H. J., & Sies, H. (1981). Mitochondrial and cytosolic ATP/ADP ratios in rat liver in vivo. *Biochemical Journal*, 200(2), 405-408. doi: 10.1042/bj2000405
- Seppet, E. K., Kaambre, T., Sikk, P., Tiivel, T., Vija, H., Tonkonogi, M., . . . Saks, V. A. (2001). Functional complexes of mitochondria with Ca,MgATPases of myofibrils and sarcoplasmic reticulum in muscle cells. *Biochimica et Biophysica Acta*, 1504(2-3), 379-395. doi: S0005272800002693 [pii]
- Singer, S., Souza, K., & Thilly, W. G. (1995). Pyruvate utilization, phosphocholine and adenosine triphosphate (ATP) are markers of human breast tumor progression: a 31P- and 13C-nuclear magnetic resonance (NMR) spectroscopy study. *Cancer Research*, 55(22), 5140-5145.
- Sinha, R., Luna, A., Schultz, N., & Sander, C. (2021). A pan-cancer survey of cell line tumor similarity by feature-weighted molecular profiles. *Cell Reports Methods*, 1(2), 100039. doi: <https://doi.org/10.1016/j.crmeth.2021.100039>
- Sousa, J. S., D'Imprima, E., & Vonck, J. (2018). Mitochondrial Respiratory Chain Complexes. *Sub-Cellular Biochemistry*, 87, 167-227. doi: 10.1007/978-981-10-7757-9_7
- Speers, C., Tsimelzon, A., Sexton, K., Herrick, A. M., Gutierrez, C., Culhane, A., . . . Brown, P. (2009). Identification of novel kinase targets for the treatment of estrogen receptor-negative breast cancer. *Clinical Cancer Research*, 15(20), 6327-6340. doi: 10.1158/1078-0432.ccr-09-1107
- Srivastava, A., & Creek, D. J. (2019). Discovery and Validation of Clinical Biomarkers of Cancer: A Review Combining Metabolomics and Proteomics. *Proteomics*, 19(10), 1700448. doi: <https://doi.org/10.1002/pmic.201700448>
- Zancan, P., Sola-Penna, M., Furtado, C. M., & Da Silva, D. (2010). Differential expression of phosphofructokinase-1 isoforms correlates with the glycolytic efficiency of breast cancer cells. *Molecular Genetics and Metabolism*, 100(4), 372-378. doi: 10.1016/j.ymgme.2010.04.006
- Zarghami, N., Giai, M., Yu, H., Roagna, R., Ponzzone, R., Katsaros, D., . . . Diamandis, E. P. (1996). Creatine kinase BB isoenzyme levels in tumour cytosols and survival of breast cancer patients. *British Journal of Cancer*, 73(3), 386-390.
- Zelevnikar, R. J., Dzeja, P. P., & Goldberg, N. D. (1995). Adenylate kinase-catalyzed phosphoryl transfer couples ATP utilization with its generation by glycolysis in intact muscle. *Journal of Biological Chemistry*, 270(13), 7311-7319. doi: 10.1074/jbc.270.13.7311
- Zheng, J. (2012). Energy metabolism of cancer: Glycolysis versus oxidative phosphorylation (Review). *Oncol Lett*, 4(6), 1151-1157. doi: 10.3892/ol.2012.928
- Tanabe, T., Yamada, M., Noma, T., Kajii, T., & Nakazawa, A. (1993). Tissue-specific and developmentally regulated expression of the genes encoding adenylate kinase isozymes. *J Biochem*, 113(2), 200-207.
- Teo, Z., Sng, M. K., Chan, J. S. K., Lim, M. M. K., Li, Y., Li, L., . . . Tan, N. S. (2017). Elevation of adenylate energy charge by angiopoietin-like 4 enhances epithelial-mesenchymal transition by inducing 14-3-3 γ expression. *Oncogene*, 36(46), 6408-6419. doi: 10.1038/onc.2017.244

- Wallace, D. C. (1999). Mitochondrial diseases in man and mouse. *Science*, 283(5407), 1482-1488. doi: 10.1126/science.283.5407.1482
- Wallace, D. C. (2012). Mitochondria and cancer. *Nat Rev Cancer*, 12(10), 685-698.
- Wallimann, T., Wyss, M., Brdiczka, D., Nicolay, K., & Eppenberger, H. M. (1992). Intracellular compartmentation, structure and function of creatine kinase isoenzymes in tissues with high and fluctuating energy demands: the 'phosphocreatine circuit' for cellular energy homeostasis. *Biochemical Journal*, 281 (Pt 1), 21-40.
- Vander Heiden, M. G., Cantley, L. C., & Thompson, C. B. (2009). Understanding the Warburg Effect: The Metabolic Requirements of Cell Proliferation. *Science*, 324(5930), 1029-1033. doi: 10.1126/science.1160809
- Wanders, R. J., Van den Berg, G. B., & Tager, J. M. (1984). A re-evaluation of conditions required for an accurate estimation of the extramitochondrial ATP/ADP ratio in isolated rat-liver mitochondria. *Biochimica et Biophysica Acta*, 767(1), 113-119. doi: 10.1016/0005-2728(84)90085-9
- Wang, F., Zhang, S., Vuckovic, I., Jeon, R., Lerman, A., Folmes, C. D., . . . Herrmann, J. (2018). Glycolytic Stimulation Is Not a Requirement for M2 Macrophage Differentiation. *Cell Metab*, 28(3), 463-475.e464. doi: 10.1016/j.cmet.2018.08.012
- Wang, M., Yu, G., & Resson, H. W. (2016). Integrative Analysis of Proteomic, Glycomic, and Metabolomic Data for Biomarker Discovery. *IEEE Journal of Biomedical and Health Informatics*, 20(5), 1225-1231. doi: 10.1109/JBHI.2016.2574201
- Warburg, O. (1956). On the origin of cancer cells. *Science*, 123(3191), 309-314.
- Ward, Patrick S., & Thompson, Craig B. (2012). Metabolic Reprogramming: A Cancer Hallmark Even Warburg Did Not Anticipate. *Cancer Cell*, 21(3), 297-308. doi: <http://dx.doi.org/10.1016/j.ccr.2012.02.014>
- Vasseur, S., Malicet, C., Calvo, E. L., Dagorn, J. C., & Iovanna, J. L. (2005). Gene expression profiling of tumours derived from rasV12/E1A-transformed mouse embryonic fibroblasts to identify genes required for tumour development. *Molecular Cancer*, 4(1), 4. doi: 10.1186/1476-4598-4-4
- Vaughn, A., & Deshmukh, M. (2008). Glucose metabolism inhibits apoptosis in neurons and cancer cells by redox inactivation of cytochrome c. *Nat Cell Biol*, 10(12), 1477-1483.
- WHO. (2024). *World Health Statistics 2024: Monitoring Health for the SDGs*: World Health Organization.
- Wilkinson, D. J. (2018). Historical and contemporary stable isotope tracer approaches to studying mammalian protein metabolism. *Mass Spectrometry Reviews*, 37(1), 57-80. doi: 10.1002/mas.21507
- Vogelstein, B., & Kinzler, K. W. (2004). Cancer genes and the pathways they control. *Nature Medicine*, 10(8), 789-799. doi: 10.1038/nm1087
- Wolff, F., El Khattabi, C., Bourdon, F., & Willems, D. (2009). Comparison of high-performance liquid chromatography with fluorescence detection versus enzymatic assay to measure blood pyruvate in clinical practice. *Clinical Biochemistry*, 42(10), 1099-1103. doi: <https://doi.org/10.1016/j.clinbiochem.2009.03.028>
- Xie, Z., Zhou, H., Wang, L., & Wu, Y. (2022). The Significance of the preoperative lactate dehydrogenase/albumin Ratio in the Prognosis of Colon Cancer: a retrospective study. *PeerJ*, 10, e13091. doi: 10.7717/peerj.13091

- Yang, Y., Fan, T. W., Lane, A. N., & Higashi, R. M. (2017). Chloroformate derivatization for tracing the fate of Amino acids in cells and tissues by multiple stable isotope resolved metabolomics (mSIRM). *Analytica Chimica Acta*, 976, 63-73. doi: 10.1016/j.aca.2017.04.014
- Ye, X., Chan, K. C., Prieto, D. A., Luke, B. T., Johann, D. J., Jr., Stockwin, L. H., . . . Blonder, J. (2013). Trypsin-mediated $^{18}\text{O}/^{16}\text{O}$ labeling for biomarker discovery. *Methods in Molecular Biology*, 1002, 133-149. doi: 10.1007/978-1-62703-360-2_12
- Yu, L., Lu, M., Jia, D., Ma, J., Ben-Jacob, E., Levine, H., . . . Onuchic, J. N. (2017). Modeling the Genetic Regulation of Cancer Metabolism: Interplay between Glycolysis and Oxidative Phosphorylation. *Cancer Research*, 77(7), 1564-1574. doi: 10.1158/0008-5472.CAN-16-2074
- Yu, Z., & Yu, H. (2020). Nomograms for Prediction of Molecular Phenotypes in Colorectal Cancer. *13*, 309-321. doi: 10.2147/ott.s234495

Acknowledgements

I would like to express my deepest gratitude to my supervisor, Tuuli Käämbre, for all the unwavering support she has given me. She is a remarkable role model in many ways, and above all, I greatly admire her resilience and wish I possessed her remarkable strength. I am sincerely grateful to my co-supervisor, Aleksandr Klepinin, whose assistance has been so extensive that I've lost count. Without his guidance, navigating the complexities of challenging science would have been significantly more difficult.

My heartfelt thanks go to Marju Puurand and Kersti Tepp for their invaluable help with countless questions and challenges. You are truly the best colleagues one could ever wish for.

I would like to give special mention to Rafael Moreno-Sanchez. I deeply admire your knowledge and aspire to reach your level of expertise one day. I am also truly grateful for the life wisdom you have shared with me – a gift even more valuable than knowledge itself.

Special thanks go to the team and other members of the institute: Anton Terasmaa, Igor Sevchuk, Indrek Reile, Heiki Vija, Giuseppe Leonardo Auditano, Ain Toim, and Tõnu Tolk.

And finally, I could not have done this without the unwavering support of my family and loved ones. A special thanks to my children, Mirko and Mirtel Lily and to my father Inno and grandmother Malle – you are my pillars.

I also wish to thank and acknowledge the Education and Youth Board (Haridus- ja Noorteamet) for providing me with a stipend through the Dora Pluss T1.2 program (5.10-6.1/22/73-2), which enabled me to travel to the UK, advance my research, and gain new knowledge.

Abstract

Energy metabolism of cancer: unravelling complexities through multiparameter metabolic analysis

Cancer is currently the fourth leading cause of death worldwide among non-communicable diseases. Female breast cancer is the second most common malignancy, followed by colorectal cancer (CRC) in third place, while lung cancer remains the most prevalent.

Cancer alters cellular energy metabolism to meet increased energy and biosynthetic demands for rapid growth. A key metabolic reprogramming is the Warburg effect, where cancer cells favor aerobic glycolysis over oxidative phosphorylation (OXPHOS) for adenosine triphosphate (ATP) production. However, recent studies suggest a more complicated metabolic shift, involving a complex interplay between glycolysis and OXPHOS. The complexity of cancer metabolism and tumor heterogeneity challenges our understanding of metabolic reprogramming in tumor development. Traditional studies on isolated methodologies may overlook key metabolic changes, emphasizing the need for integrated approaches to gain deeper insights.

Various analytical techniques were developed, including the application of an analytical platform for phosphometabolite detection using nuclear magnetic resonance (NMR), liquid chromatography, high-resolution respirometry, and enzyme activity measurements. In this thesis, several methods were combined to investigate metabolic adaptations in intact and permeabilized CRC clinical material and Caco-2 cells.

This thesis aimed to develop and apply methodological approaches to study cancer energy metabolism, focusing on breast cancer cell lines (MCF7, MDA-MB-231, and MCF10A as a control) and CRC clinical material and the Caco-2 cell line. Phosphotransfer networks involving adenylate kinase (AK), creatine kinase (CK), and ATP production were characterized in breast cancer cell lines (MCF7, MDA-MB-231, and MCF10A) using ^{18}O isotope labeling in combination with gas chromatography-mass spectrometry (GC-MS).

The results suggest that the ^{18}O isotope labeling method is a reliable approach for studying phosphotransfer networks. Findings indicate that ATP production in breast cancer cell lines may primarily rely on glycolysis and that intracellular ATP levels could serve as a potential biomarker.

Optimization of the NMR method showed promise in significantly simplifying ^{18}O isotope labeling experiments by enabling the collapse of multiplets into singlets, thereby improving data acquisition and interpretation.

Combining high-resolution respirometry, nucleotide quantification, and enzyme activity measurements demonstrated that careful experimental planning can maximize sample utilization for multiple analyses. CRC clinical material showed higher OXPHOS capacity as indicated by parameters derived from Michaelis-Menten kinetics, including increased V_{\max} , reduced $K_m(\text{ADP})$, and greater pathway efficiency (V_{\max}/K_m) across all stages compared to controls. Despite this, a significant dependence on glycolysis was evident from elevated lactate dehydrogenase (LDH) activity. This suggests a high degree of metabolic plasticity, and pathway efficiency (V_{\max}/K_m) could serve as a valuable metabolic indicator.

Adenine nucleotide quantification from respiration media, along with energy charge (EC) and ATP/ADP ratio calculations, could be valuable for metabolic analysis. Findings in this thesis demonstrated reliance on OXPHOS, residual glycolytic activity in permeabilized tissue, and stage-specific metabolic changes in stage II CRC.

Enzyme activity measurements further highlighted differences between clinical material and in cell cultures, exemplified by significantly higher LDH activity in Caco-2 cells.

To summarize, this study highlights cancer's complexity, advocating for an integrated approach using both cell cultures and clinical material. This comprehensive method has revealed previously unnoticed instances that may be difficult to detect with conventional or isolated research strategies. Additionally, this work may offer a potential framework for developing improved approaches to study cancer metabolism. Even small discoveries can contribute to a better understanding and potential improvements in cancer treatment and development of new biomarkers.

Lühikokkuvõte

Energia metabolism vähis: keerukuse lahtiharutamine multiparameetrilise metaboolse analüüsi abil

Tänase päeva seisuga on vähk mittenakkushaiguste seas neljas peamine surma põhjus kogu maailmas. Kõige sagedasem pahaloomuline kasvaja on kopsuvähk, teisel kohal, eeskätt naiste seas, on rinnavähk ning kolmandal kohal kolorektaalvähk (CRC).

Vähi üks olulisimaid omadusi on kohandada raku energiametabolismi suurenenud energiavajaduse, biosünteesi, kiire kasvu ja kontrollimatu jagunemise vajaduste rahuldamiseks. Üks peamistest muutustest on Warburgi efekt, mille puhul vähirakud eelistavad aeroobset glükolüüsi oksüdatiivsele fosforüleerimisele (OXPHOS) adenosiin trifosfaadi (ATP) tootmiseks, kuid hiljutised uuringud viitavad keerukamale metaboolsele nihkele, mis hõlmab glükolüüsi ja OXPHOS-i vahelist koosmõju. Vähi metabolismi keerukus ja heterogeensus seavad väljakutse meie arusaamisele metaboolsest ümberprogrammeerimisest kasvaja arengus. Traditsioonilistele metodoloogiatele keskendunud uuringud võivad olulisi metabolismis tekkinud muutusi tähelepanuta jätta, mistõttu on vajalik kombineerida uusi erinevaid meetodeid.

Arendati mitmeid bioanalüütika meetodeid, sealhulgas fosfometaboliitide tuvastamiseks välja töötatud analüütilise platvormi rakendamine tuumamagnetresonantsi (NMR), vedelikukromatograafia, kõrglahutusega respiromeetria ja ensüümiaktiivsuse mõõtmise kaudu. Erinevaid meetodeid kombineerides uuriti metaboolseid kohandumisi terviklikus ja permeabiliseeritud CRC kliinilises materjalis ning Caco-2 rakuliinides.

Käesoleva doktoritöö eesmärk oli välja töötada ja rakendada uudseid meetodilisi lähenemisviise vähi energiametabolismi uurimiseks, keskendudes rinnavähi rakuliinidele (MCF7, MDA-MB-231 ja kontrollina MCF10A), samuti CRC kliinilisele materjalile ja Caco-2 rakuliinile. Rinnavähi rakuliinides (MCF7, MDA-MB-231 ja MCF10A) iseloomustati adenülaatkinaasi (AK), kreatiinkinaasi (CK) ja ATP tootmisega seotud fosforülekandevõrgustikke, kasutades ^{18}O isotoobiga märgistamist kombinatsioonis gaaskromatograafia-massispektromeetria (GC-MS).

Tulemused viitavad sellele, et ^{18}O isotoobimärgistuse meetod on usaldusväärne lähenemine fosforülekandevõrgustike uurimiseks. Andmetest nähtub, et ATP tootmine rinnavähi rakuliinides võib tuleneda peamiselt glükolüüsist ning rakusisene ATP tase võib olla potentsiaalne kasvaja pahaloomulisuse biomarker.

NMR-meetodi optimeerimine andis paljulubavaid tulemusi. Meetod lihtsustab oluliselt ^{18}O isotoobimärgistuse eksperimente, kuna võimaldab multipllettide muutmist singlettideks, parandades seeläbi andmete tõlgendamist.

Kõrglahutusega respiromeetria, nukleotiidide kvantifitseerimise ja ensüümiaktiivsuse mõõtmise kombineerimine näitas, et hoolikas eksperimentide planeerimine võimaldab proove maksimaalselt ära kasutada. CRC kliiniline materjal näitas suuremat OXPHOS-i võimekust Michaelis-Menteni kineetikast saadud parameetrite analüüsil. Kõigis vähi staadiumides oli tõusnud oli V_{\max} -i ja metaboolse raja tõhususe (V_{\max}/K_m) ning vähenenud näilise K_m -i osad võrreldes kontrollkoega. Kuid samas ilmnes ka oluline sõltuvust glükolüüsist, mida kinnitas laktaadi dehüdrogenaasi (LDH) aktiivsus. Need tulemused viitavad suurenenud metaboolsele plastilisusele ning ühtlasi ka metaboolse raja tõhusus (V_{\max}/K_m) võiks olla väärtuslik indikaator kasvajate metabolismi kohta.

Mõõtelahusest adeniinnukleotiidide kvantifitseerimine koos energialaengu (EC) ja ATP/ADP suhte arvutamiseiga võivad olla kasulikud näitajad metaboolsetes analüüsides.

Käesolevas töös saadud tulemused näitasid OXPHOS-i domineerimist, jääglükolüüsi aktiivsust permeabiliseeritud koes ja staadiumispetsiifilisi metaboolseid muutusi II staadiumi CRC-s.

Ensüümiaktiivsuse mõõtmised tõid esile täiendavad erinevused kliinilise materjali ja rakuliinide proovide vahel, mida ilmestas oluliselt suurem LDH aktiivsus Caco-2 rakkudes.

Kokkuvõttes antud töö tõi esile vähi komplitseerituse, toetades meetodite kombineerimist ning kliinilise materjali ja ka rakukultuuride kasutamist. See laiaulatuslik meetodite rakendamine avaldas vähi kohta nüansse, mida oleks olnud konventsionaalsete uurimistrateegiatega keeruline tuvastada. Lisaks võib antud töö anda baasi ka tulevikus tehtavatele uuringutele. Ka pisemad avastused võivad anda uusi ja väärtusilke teadmisi vähi kohta ning panustada ravistrateegiate või biomarkerite arendamisse.


Appendix 1

Publication I

Reinsalu, L*; **Miller, S***; Auditano, G. L ; Puurand, M ; Moreno-Sanchez, R; Käämbre, T (2025). The Energy Metabolism Profiling of Human Colorectal Tumors. Journal of cellular and molecular medicine, 29(5):e70462. doi:10.1111/jcmm.70462.

ORIGINAL ARTICLE OPEN ACCESS

Energy Metabolism Profiling of Human Colorectal Tumours

Leenu Reinsalu^{1,2}  | Sten Miller^{1,2} | Giuseppe Leonardo Auditano^{1,2} | Marju Puurand¹ | Rafael Moreno-Sanchez^{1,3} | Emma Saavedra⁴ | Vahur Valvere⁵ | Tuuli Käämbre¹

¹Laboratory of Chemical Biology, National Institute of Chemical Physics and Biophysics, Tallinn, Estonia | ²Department of Chemistry and Biotechnology, Tallinn University of Technology, Tallinn, Estonia | ³Laboratorio de Control Metabólico, Carrera de Biología, Facultad de Estudios Superiores- Iztacala, UNAM, Tlanepantla, Estado de México, Mexico | ⁴Departamento de Bioquímica, Instituto Nacional de Cardiología Ignacio Chávez, México City, Mexico | ⁵Oncology and Hematology Clinic, North Estonia Medical Centre, Tallinn, Estonia

Correspondence: Leenu Reinsalu (leenu.reinsalu@kbfi.ee) | Sten Miller (sten.miller@taltech.ee)

Received: 30 April 2024 | **Revised:** 26 January 2025 | **Accepted:** 19 February 2025

Funding: This work was supported by National Institute of Chemical Physics and Biophysics, institutional grants.

Keywords: colorectal cancer | energy metabolism | glycolysis | oxidative phosphorylation

ABSTRACT

Colorectal cancer (CRC) is a significant global health burden, and its early detection is crucial. Novel diagnostic and prognostic methods are required for improving patient treatment, survival and quality of life. One promising approach is the analysis and understanding of the metabolic reprogramming undergone by cancer cells. Here, by analysing the changes in transcript and protein contents, activities, pathway flux and energy metabolite ratios in post-operative CRC tumours, in comparison to adjacent healthy tissue, the energy metabolism was characterised at the molecular and functional levels. Greater expression of glucose transporter 1 and lactate dehydrogenase A (LDH), together with increased protein content and activity of LDH in tumours, suggested a higher glycolytic capability. Hexokinase transcripts, protein and activity were similar, whereas monocarboxylate transport transcripts and protein contents were lower in tumours. The creatine kinase transcripts and the adenylate kinase protein contents were lower in tumours, suggesting a functional decrease in the CRC energy transfer pathway. Notwithstanding this, oxidative phosphorylation was fully functional and exhibited higher catalytic efficiency ($V_{max}/K_{m_{ADP}}$) in tumours, whereas the cellular energy charge was slightly lower in tumours. Remarkably, higher OxPhos catalytic efficiency correlated with advancing CRC clinical stage. The data revealed that CRC tumours exhibit a hybrid energy metabolism phenotype where both glycolysis and oxidative phosphorylation are highly active.

1 | Introduction

In 2020, 18.1 million people worldwide were diagnosed with cancer; among these, colorectal cancer (CRC) stands as the third most prevalent form and ranks second in cancer-related mortality following lung cancer [1]. Only 5%–10% of CRC cases occurred due to genetic predisposition, emphasising the relevant influence

of environmental factors on cancer development risks. Despite the advancements in screening strategies and technology, only about 33% of all CRC cases are diagnosed at the early localised stage, and around a fifth of all diagnosed incidences already show distant metastases upon diagnosis [2]. Considering the stark contrast in the 5-year survival rates between localised and metastasised CRC (88% vs. 16%, respectively), there is an imperative and

Abbreviations: AK, adenylate kinase; AMPK, AMP-activated protein kinase; CK, creatine kinase; CRC, colorectal cancer; EC, energy charge; GLUT1, glucose transporter 1; HK, hexokinase; LDH, lactate dehydrogenase; MCT, monocarboxylate transporter; OxPhos, Oxidative phosphorylation; RT-qPCR, Quantitative reverse transcription polymerase chain reaction; VDAC, voltage-dependent anion channel.

Leenu Reinsalu and Sten Miller contributed equally to this work.

This is an open access article under the terms of the [Creative Commons Attribution](https://creativecommons.org/licenses/by/4.0/) License, which permits use, distribution and reproduction in any medium, provided the original work is properly cited.

© 2025 The Author(s). *Journal of Cellular and Molecular Medicine* published by Foundation for Cellular and Molecular Medicine and John Wiley & Sons Ltd.

urgent public health need to enable earlier CRC detection. In that regard, metabolomics approaches to identify diagnostic biomarkers in blood or urine have been pursued [3, 4]; however, many of the proposed metabolites are not specific for CRC. Therefore, a comprehensive understanding of the metabolic reprogramming undergone during CRC development should be achieved in order to identify enzymes and/or metabolites that are more specific for early detection and prognosis of CRC development.

Living cells rely on a constant supply of energy, which they produce by converting food-sourced fuels into usable cellular energy carrier metabolites (e.g., ATP and creatine- phosphate). In cancer cells, energy metabolism, i.e., glycolysis and oxidative phosphorylation (OxPhos), undergoes significant reprogramming to sustain the accelerated cell proliferation and growth typical of neoplastic disease [5]. The predominant energy production pathway in different cancer cell types has not been completely established. The most widespread notion, the Warburg effect, suggests that cancer cells favour glycolytic energy production even in the presence of oxygen [6]. However, there is increasing evidence demonstrating that several cancer cell types exhibit high OxPhos rates [7–9]. Furthermore, cancer cells may adopt a hybrid energy metabolic state, simultaneously depending on both glycolysis and OxPhos pathways. This dynamic adaptive capacity of cancer cells has been termed metabolic plasticity [10]. Nonetheless, most of the mechanisms underlying this plasticity remain largely unknown.

Understanding the CRC development requires a comprehensive analysis at several levels, including changes in gene expression (transcript levels) and protein levels, enzyme activities, pathway fluxes, isoform profiles and their roles in cellular function [11]. While cancer has been historically considered solely as a genetic disease, it is now evident that extensive alterations occur in several cellular subsystems involved in functions like protein expression and activities, signalling and metabolic pathways, many of which cannot be solely attributed to genetic causes. Traditionally, molecular biology and biomedical research have focused on the study of single genes, individual protein targets, single metabolites or specific signalling pathways. However, an integral approach that considers the complex interplay of these components provides a more promising direction for uncovering changes in metabolic networks, diseases and understanding the mechanisms of drug effects [11]. Furthermore, significant cancer metabolic research is conducted primarily on 2D cancer cell line cultures; however, cell metabolism is profoundly influenced by the microenvironment. For instance, the metabolic phenotype of cultured cells can be modified by the conditions in which they are grown [12]. While these studies with cancer cell lines may offer valuable insights, they fail to fully represent the cancer clinical situation. Therefore, in the present study, energy metabolism reprogramming in post-operative tumour material obtained from CRC patients was analysed.

2 | Methods

2.1 | Clinical Material

Human patient post-operative tissue material samples were provided immediately after tumour removal by surgery by the Oncology and Hematology Clinic at the North Estonian Medical

Centre (NEMC, Tallinn, Estonia). Only primary and treatment-naïve tumours were examined. In addition, samples of non-cancerous mucosa tissue located at least 5 cm away from the tumour were also provided. Samples were collected in plastic containers with Mitomedium B solution (0.5 mM EGTA, 3 mM MgCl₂, 60 mM K-lactobionate, 20 mM taurine, 3 mM KH₂PO₄, 110 mM sucrose, 0.5 mM dithiothreitol, 20 mM HEPES, 5 µM leupeptin, 2 mg/mL fatty acids-free bovine serum albumin, pH 7.1), stored on ice and immediately transported to the laboratory. To ensure that the control colorectal tissue was healthy, patho-histology examination of all samples was expertly provided by NEMC pathologists. All patients were informed about the study and their respective signed informed consent letters were obtained. Coded identity protection was applied to protect the identity of the subjects. All actions concerning human subjects and follow-up protocols have been approved by the Tallinn Medical Research Ethics Committee (decision numbers KK557 and KK558) and are in accordance with the Helsinki Declaration and Convention of the Council of Europe on Human Rights and Biomedicine.

2.2 | RNA Extraction

To preserve cellular RNA integrity, a fraction of approximately 40% of each tissue sample was suspended in RNALater solution (Qiagen) for transportation. Upon arrival at the laboratory, the sample was frozen in liquid nitrogen and stored at –80°C. RNA was later extracted following the protocol by Untergasser [13]. The frozen tissue samples were homogenised using the TRIzol reagent (Ambion); the RNeasy Mini Kit (Qiagen) was used for RNA isolation. RNase-free DNase I Solution (Qiagen) was used to eliminate DNA. Finally, RNA was eluted from the spin column with 30 L of RNase-free water, and the total concentration of RNA was determined with a BioSpec-Nano spectrophotometer (Shimadzu). The isolated RNA was stored at –80°C.

2.3 | cDNA Synthesis and Real-Time Quantitative Polymerase Chain Reaction

All reagents used for cDNA synthesis and quantitative reverse transcription polymerase chain reaction (RT-qPCR) were from Applied Biosynthesis. cDNA was synthesised from 2 g of RNA using the High-Capacity cDNA Reverse Transcription Kit with the RNase inhibitor following the protocol provided by the manufacturer. Reverse transcription reaction incubation was performed in an Eppendorf 5332 Mastercycler thermocycler.

RT-qPCR was performed using a LightCycler 480 II instrument (Roche). The reaction mix contained TaqMan Gene Expression Master Mix (Thermo Fisher Scientific) and the FAM-labelled TaqMan probes: actin-β (Hs01060665_g1), for adenylate kinase AK1 (Hs00176119_m1), AK2 (Hs01123132_g1), AK4 (Hs03405743_g1), and AK6 (Hs00360444_g1); for creatine kinase CK-BB (Hs00176483_m1), CK-MT1 (Hs00179727_m1) and CK-MT2 (Hs00176502_m1); for hexokinases HK1 (Hs00175976_m1) and HK2 (Hs00606086_m1); for glucose transporter 1 GLUT1 (Hs00892681_m1); for lactate dehydrogenase LDHA (Hs03405707_g1); for MCTs MCT1 (Hs00161826_m1), MCT2 (Hs04332706_m1) and MCT4 (Hs00358829_m1);

and for 5'-AMP-activated protein kinase catalytic subunit alpha-1 PRKAA1 (Hs01562315_m1). Milli-Q water was used as a no-template control to check for extraneous nucleic acid contamination. Transcript differences were estimated by the $\Delta\Delta C_t$ method, using the β -actin transcript for normalisation.

2.4 | Protein Extraction for Western Blot

To extract proteins for Western blotting, the snap-frozen samples were first ground in liquid nitrogen using a mortar and pestle. The resulting powder was transferred into 2 mL Lysing Matrix A tubes (RotaPrep) filled with radioimmunoprecipitation assay (RIPA) buffer consisting of 50 mM Tris-HCl pH 8.0, 150 mM NaCl, 2 mM EDTA, 1% NP-40, 0.1% SDS and supplemented with a protease inhibitor cocktail (Roche) following the manufacturer's instructions. For homogenisation, the sample was processed three times for 10 s using the Monolyzer (RotaPrep) at maximum speed. Subsequently, the homogenates were maintained under constant agitation for 2 h at 4°C, followed by centrifugation for 20 min at 16 000×g at 4°C. The resulting tissue extracts were collected, aliquoted and stored at -80°C until protein quantification, using the BCA Protein Assay Kit (Thermo Fisher Scientific) according to the manufacturer's protocol.

2.5 | Western Blot

Proteins (30 µg) from lysates were separated by 10% sodium dodecyl sulfate polyacrylamide gel electrophoresis followed by overnight electroblotting onto Immobilon P PVDF membranes, pore size 45 µm (Merck Millipore) and blocking for 30 min with phosphate-buffered saline containing 0.05% Tween 20 (PBS-T) and 5% bovine serum albumin (BSA) at room temperature. Next, the blot was incubated with primary antibodies (Table 1) for 2 h at 4°C in PBS-T with 2% BSA, washed with PBS-T and incubated with secondary antibodies using either goat anti-rabbit IgG (H + L)-horse radish peroxidase (Invitrogen) diluted 1:2000 or 1:4000 or rabbit

anti-mouse IgG H&L-HRP (Abcam) diluted 1:5000 for 1 h at room temperature.

Chemiluminescence was detected using the Super Signal West Femto Maximum Sensitivity substrate (Thermo Fisher Scientific) and imaged with the Biospectrum multispectral imaging system. Protein levels were quantified using ImageJ software. The unspecific background signal was subtracted, and the area for each protein blot was determined. The levels of protein of interest were normalised to the total protein level obtained from Ponceau S staining signal. The relative quantity of the target in each sample was assessed by comparing the normalised target quantity in each sample to the normalised target quantity in the reference sample.

2.6 | Cell Culture

The colorectal adenocarcinoma cell line Caco-2 (ATCC) was cultured in 100 mm diameter Falcon Corning cell culture dishes using Dulbecco's Modification of Eagle's Medium (Corning, 10-013-CV), which contains 4.5 g/L glucose, 584 mg/L L-glutamine and 110 mg/L sodium pyruvate and supplemented with 1% 100× penicillin/streptomycin solution (Capricorn Scientific) and 10% fetal bovine serum (FBS Xtra, sourced from South America, Capricorn Scientific). Cell aliquots stored in liquid nitrogen were unfrozen for cell growth. Culturing was conducted in a CO2 incubator maintained at 37°C under 95% air/5% CO2. Sub-culturing of cells was performed every 2 days by trypsinisation using 1× trypsin-EDTA 0.5% solution (Capricorn Scientific) in DPBS (Dulbecco's Phosphate-Buffered Saline, without calcium and magnesium, Corning).

Subsequently, the cell suspensions were centrifuged at 125×g for 5 min, and the supernatant was discarded. Then, the cell number was determined using a Bürker-Türk counting chamber; aliquots of 15–20×10⁶ cells were resuspended in 1 mL of DPBS in 2 mL Eppendorf tubes and centrifuged as described previously. Following centrifugation, supernatants were discarded, and cell pellets were stored at -80°C for further analysis.

TABLE 1 | Antibodies used for Western blot analysis.

Protein	Catalogue number	Manufacturer	Dilution	Host species
HK1	PA5-117986	Invitrogen	1:1000	Rabbit
HK2	PA5-29326	Invitrogen	1:2500	Rabbit
LDHA	PA5-27406	Invitrogen	1:2000	Rabbit
MCT1	PA5-72957	Invitrogen	1:500	Rabbit
MCT2	Sc-50322	Santa Cruz Biotechnology	1:500	Rabbit
MCT4	Sc-367101	Santa Cruz Biotechnology	1:500	Mouse
AK1	Sc-365316	Santa Cruz Biotechnology	1:500	Mouse
AK2	PA5-28611	Invitrogen	1:500	Rabbit
AK4	PA5-61978	Invitrogen	1:500	Rabbit
AK6	10544-1-AP	Proteintech	1:200	Rabbit

2.7 | Enzyme Activities

To extract proteins for enzyme activity determinations from intact and saponin-treated human tissue samples (10–100 mg semidried weight) and CaCo2 cells ($15\text{--}20 \times 10^6$), the samples were resuspended in 1 mL of 25 mM Tris-HCl buffer pH 7.6, with 1 mM EDTA, 5 mM dithiothreitol, 0.1%–0.3% Triton X-100, and a 20× dilution of protease inhibitor mix (Roche) in 1.5 mL Eppendorf tubes. Then, the samples were homogenised in a Retsch MM400 ball mill homogeniser with 2 metal beads (3 mm diameter) for 2.5 min at 30 Hz. The homogenised samples were then subjected to 2–3 cycles of liquid nitrogen freezing and warm water bath thawing to further facilitate the breaking of cells and membranes for complete enzyme release. After each procedure step, strong vortexing for 1 min was applied to the cell or tissue suspensions. The samples were then centrifuged at $14,000 \times g$ for 2 min at 4°C, followed by recovering the supernatant and keeping it on ice for immediate enzymatic activity assays. Total protein contents were determined with the BCA protein assay kit (Thermo Fisher Scientific) according to the manufacturer's protocol, correcting for the DTT side reaction. To make rigorous comparisons with the protein content determinations and OxPhos measurements, glycolytic enzyme activities were analysed in both intact and saponin-treated control and tumour tissue samples. All the enzymatic assays were determined under conditions of initial velocity.

Activities of HK and LDH were determined spectrophotometrically by following the NADP⁺ reduction and NADH oxidation absorbance at 340 nm, respectively, using a spectrophotometer Cary Bio 100 (Varian).

Assay for LDH activity was carried out at 37°C in 1 mL KME buffer (120 mM KCl, 20 mM MOPS, 1 mM EGTA, pH 7.2) including 0.2 mM NADH and 10–40 µg protein sample. The reaction was started by adding 1 mM pyruvate or increasing concentrations of pyruvate.

HK assay was carried out at 37°C in 1 mL KME buffer with 0.6 mM NADP⁺, 10 mM MgSO₄, 1–2 units Glc6PDH, 50–200 µg protein supernatant. 10 mM ATP was added seconds before starting the reaction to avoid unspecific ATP hydrolysis by ATPases in the biological samples. The reaction was started by adding 2 mM glucose or increasing concentrations of glucose.

For the calculations of kinetic parameters (V_{\max} , K_m , V_{\max}/K_m), all the enzyme activities normalised to protein content at variable substrate concentrations were fitted to the Michaelis–Menten equation by non-linear regression analysis using SigmaPlot 14.0 (Systat Software Inc.) and a NAD(P)H extinction coefficient of $6.22 \text{ mM}^{-1} \text{ cm}^{-1}$ at 340 nm.

2.8 | Sample Preparation for Respirometry

Upon arrival at the laboratory (within 60 min after surgery), the tissue samples were placed into pre-cooled (4°C) medium A (3 mM KH₂PO₄, 20 mM taurine, 5.7 mM ATP, 15 mM phosphocreatine [PCr], 9.5 mM MgCl₂, 49 mM MES, 7.23 mM K₂EGTA, and 2.77 mM K₂CaEGTA, pH 7.1). Blood vessels and fat were removed from the tissue samples, which were then dissected into small samples (5–15 mg wet weight). These

were permeabilised in medium A containing 50 µg saponin/mL for 30 min at 4°C under 360° rotatory mixing. The permeabilised samples were then washed three times for 5 min in pre-cooled Mitomedium B without leupeptin and kept at 4°C until use in oxygraphic analyses. This saponin treatment allows for selective plasma membrane permeabilisation, leaving cholesterol-lacking intracellular organelle membranes rather intact [14]. Such a permeabilisation procedure was required to make freely available oxidisable substrates and ADP to the mitochondria of human tissue samples.

2.9 | Oxygraphic Measurements

Mitochondrial respiration of permeabilised tissue samples was measured in Mitomedium B at 25°C using a high-resolution respirometer Oxygraph-2k (Oroboros Instruments, Innsbruck, Austria). The medium was supplemented with 5 mM glutamate, 2 mM malate and 10 mM succinate to fully activate respiratory chain complexes I and II. To determine the relationship between respiration rate and exogenous ADP, increasing concentrations of ADP were added to the medium in the oxygraphic chamber. The collected data were then plotted as rates of O₂ consumption and OxPhos (the basal respiration rate attained in the absence of added ADP was subtracted from the ADP-stimulated respiration) versus ADP concentration. From these plots, the apparent affinity of OxPhos for exogenous ADP ($K_m\text{ADP}$) and maximal OxPhos rate (V_{\max}) values were calculated by non-linear regression using the Michaelis–Menten equation. Respirometry medium aliquots were withdrawn to calculate energy charges from adenine nucleotide quantification.

To activate glycolysis flux in the samples incubated in the respirometer, 0.1 mM of ATP and 10 mM of glucose were added after glutamate, malate and succinate, followed by the addition of 1 mM of ADP. To inhibit glycolysis, 6–2020 mM of 2-deoxyglucose and 0.5 mM of iodoacetate were added before ADP. To inhibit OxPhos, 2.5 µM of rotenone, 10 µM of antimycin-A and 2 µg/mL of oligomycin were added before ADP.

2.10 | Adenine Nucleotide Quantification

Two millilitres from both tumour and control tissue respirometry medium assays was collected from the oxygraph chambers after the experiments and processed immediately or kept at –80°C for no longer than 2 weeks before processing. For protein precipitation, 70% HClO₄ was added to the samples to a final concentration of 0.6 M final concentration followed by centrifugation at $17,000 \times g$ for 10 min at 4°C. The supernatant was collected and neutralised with 2 M KHCO₃ (120–600 µL depending on sample) and spun again, after which the supernatants were either directly loaded into a UPLC apparatus for measurements or freeze-dried and resuspended in the desired volume and solvent and kept at –20°C for up to a few weeks before analysis.

Separation and quantification of adenine nucleotides was carried out with an Agilent 1290 Infinity UPLC apparatus using a reverse-phase column Separon SGX C18 5 µm 3×150 mm (Tessek, Czechia). The samples were eluted as described before [14]. The concentrations of the nucleotides in neutralised oxygraphic

samples were calculated from the peak areas, accounting for all dilution factors and normalised to the wet weight of tissue. The energy charge (EC) was calculated using the formula:

$$EC = [ATP] + 0.5 \times [ADP] / [ATP] + [ADP] + [AMP]$$

2.11 | Data Analysis

Data in text and figures are presented as mean \pm standard error (SEM). All plots were made by using SigmaPlot 14.0. The results were analysed using one-way analysis of variance (ANOVA), and p -values < 0.05 were considered significant.

3 | Results

3.1 | Glycolysis Proteins

3.1.1 | Glucose Transporters

Glucose enters the cells via glucose transporters (GLUTs). Among the 14 members of the GLUT family, alterations of GLUT1 have been predominantly shown in various types of tumours [15–17]. To investigate whether glucose transport gene transcription could be affected in CRC cells, the transcript levels of the *SLC2A1* gene, which encodes GLUT1 protein, were assessed using RT-qPCR. The results revealed a more than two-fold increase in transcript levels in tumours compared to control colon tissue (Figure 1A), suggesting a higher content of GLUT1 protein and a heightened glucose uptake by cancer cells.

3.1.2 | Hexokinases

Hexokinase (HK) may couple with the voltage-dependent anion channel (VDAC) in the outer mitochondrial membrane, thereby modulating adenine nucleotides permeability. The transcript levels of one of the main controlling steps of glycolysis, catalysed by HK1 and HK2, were evaluated (Figure 1B). While *HK1* transcript remained similar in both tissue types, *HK2* expression was 35% lower in CRC tumours. This observation supports our earlier findings showing lower *HK2* expression in CRC compared to healthy colon tissue [18, 19].

To further explore changes in HKs, their protein levels were compared. No significant differences were observed between the CRC and control tissue for each isoform (Figure 1C); however, it is noted that HK2 was detected in only four tumour samples out of nine (44%) examined, supporting the notion of HK2 downregulation in CRC. Finally, HK activity assays were carried out in both intact and saponin-treated control and tumour tissues, as well as in Caco-2 cells (Figure 1D). However, there were no significant HK activity differences between permeabilised control tissue and tumour intact or permeabilised tissue, and CaCo2 cells.

3.1.3 | Lactate Dehydrogenase

LDHA converts pyruvate into lactate in the cytosol, thus its activity in this compartment may modulate whether pyruvate is preferentially directed towards mitochondria or transformed to

lactate in the cytosol. The transcript level of *LDHA* was higher in CRC compared to control tissue (Figure 2A).

Although LDHA protein levels appeared generally higher in tumour tissue, no statistically significant difference was apparent (Figure 2B), due to considerable heterogeneity among clinical samples and a statistically insufficient sample size ($n = 9$). Notwithstanding this, LDH activity showed significant differences between different tissue types (Figure 2C). Notably, a two-fold increase in LDH activity of intact tumour vs. intact control samples was observed.

In contrast, no difference in LDH activity between permeabilised tumour and permeabilised control samples was attained. LDH activity in Caco-2 cells was remarkably higher, exceeding that of the CRC clinical samples by approximately 30%, with significant differences observed across all groups.

3.1.4 | Monocarboxylate Transporters

The MCT family consists of 14 transmembrane proteins, but only MCT1, MCT2, MCT3 and MCT4 exhibit high affinity for lactate. Therefore, the transcript levels of *SLC16A1*, *SLC16A7* and *SLC16A3*, encoding for MCT 1, 2 and 4 isoforms, respectively, were analysed (Figure 3A). While the transcripts of *MCT2* and *MCT4* were similar between control and tumour tissues, the *MCT1* transcript in cancer was two-fold lower than in control colon tissue. The transcript pattern did not agree with the protein level pattern of MCT1 and MCT4, where MCT1 protein levels were nearly identical between control and CRC tissues, whereas the protein levels of both MCT2 and MCT4 were significantly decreased in CRC (Figure 3B).

3.2 | Energy Transfer Pathways

The energy metabolism consists of the two ATP-producing pathways, glycolysis and OxPhos. However, besides production by these pathways, ATP must be efficiently delivered to the consumption sites. Such a required energy transfer pathway consists of the mitochondrial and cytosolic isoforms of adenylate kinase (AK) and creatine kinase (CK). To achieve a full understanding of how cancer cell energy metabolism operates and is regulated, changes in the energy transfer pathway must also be identified.

Alterations in the CK system have been observed in many cancer types [20], including CRC. The transcript levels of three CK isoforms were determined via RT-qPCR (Figure 4A). The results demonstrated significantly decreased levels of *CKBB* and *CKMT1* in CRC compared to control tissue. This last observation was in agreement with previous studies from our group showing that the CK activity decreases approximately two-fold in CRC compared to normal colon tissue [19]. Interestingly, the expression of the second mitochondrial isoform *CKMT2* gene was higher in CRC tissue, although its overall expression remains low compared to other isoforms.

Downregulation of CKs could be compensated by upregulating the AK system. In this regard, it has been shown that the AK activities largely increase in CRC compared to normal colon tissue

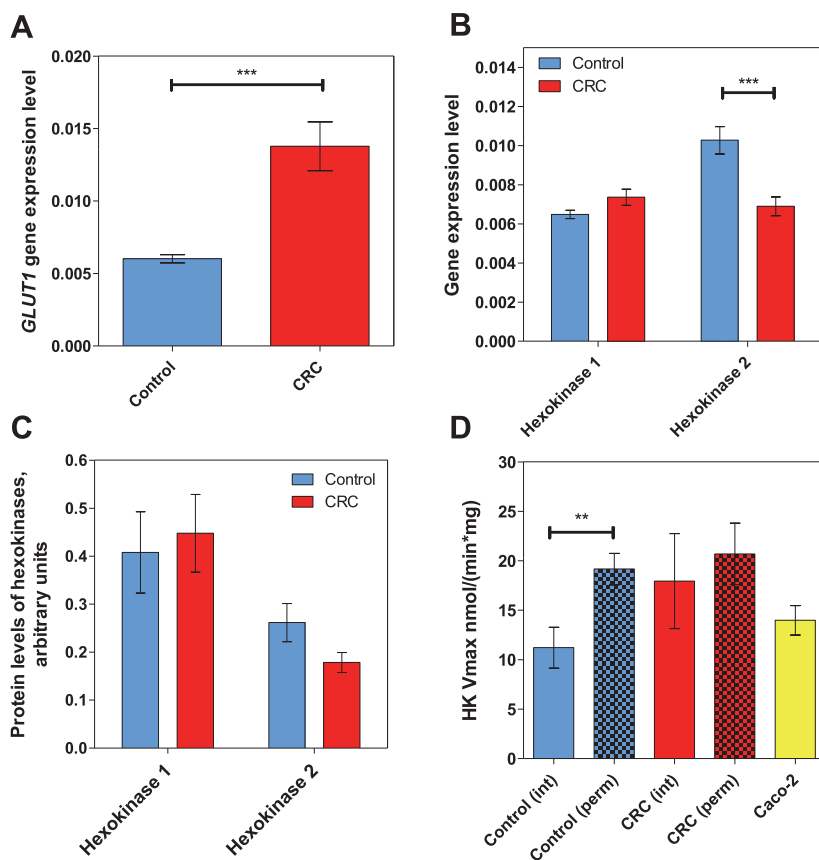


FIGURE 1 | The characteristics of glucose transporter 1 (GLUT1) and hexokinases (HKs) in healthy and colorectal tumour tissue. The transcript levels of (A) *GLUT1* and (B) *HK1* and *HK2* were determined by RT-qPCR in control colon tissue ($n=24$) and CRC tissue ($n=24$). (C) The protein levels of HK1 and HK2 measured by Western blot in control ($n=8$ and $n=7$, respectively) and CRC tissues ($n=8$ and $n=4$, respectively). (D) HK activity in intact control tissue (Control (int), $n=7$), permeabilised control tissue (Control (perm), $n=12$), intact colorectal cancer tissue (CRC (int), $n=7$), permeabilised colorectal cancer tissue (CRC (perm), $n=12$) and Caco-2 cells soluble clarified cell extract ($n=4$). $**p<0.01$, $***p<0.001$ (one-way ANOVA).

[20]. AKs catalyse the reversible transfer of phosphate groups between ADP, AMP and ATP. Nine isoforms of AKs have been identified and characterised in mammalian tissues so far [21]. Four isoforms were analysed in this study: cytosolic AK1, mitochondrial AK2 and AK4 and nucleus-located AK6. Contrary to the hypothesis, cancer cells did not show any change in the AK transcripts (Figure 4B). Furthermore, while no statistically significant differences were observed in protein levels of AK isoforms (Figure 4C), there appears to be a trend of lower AK1 levels in cancer tissue, supporting the similar finding in transcript levels.

In addition to AKs, another central regulator of cellular energy homeostasis is AMP-activated protein kinase (AMPK). AMPK is activated by low ATP and high AMP concentrations, conditions that could be caused by nutrient deprivation, hypoxia or oxidative stress. Once activated, AMPK shifts metabolism towards catabolism by phosphorylating proteins in multiple pathways [22]. Its role in cancer is still unclear. Here, the transcript level of 5'-AMP-activated protein kinase catalytic subunit

alpha-1 (*PRKAA1*) was assessed and shown to be downregulated (Figure 4D).

3.3 | Oxidative Phosphorylation Kinetic Characteristics

Next, high-resolution respirometry was applied to analyse the kinetics of the OxPhos flux: the values for maximal ADP-stimulated respiration rate (V_{max}) and the apparent Michaelis-Menten constant for exogenously added ADP (K_{mADP}) were determined (Figure 5).

A statistically significant difference in V_{max} values between control and CRC tissue was found (Figure 5A), but no differences in K_{mADP} values (Figure 5B). The higher maximal ADP-stimulated respiration rate in CRC suggests an increased OxPhos capacity. Further, the catalytic efficiency (V_{max}/K_{mADP} ratio) of the whole OxPhos pathway (Figure 5C) for control tissue was

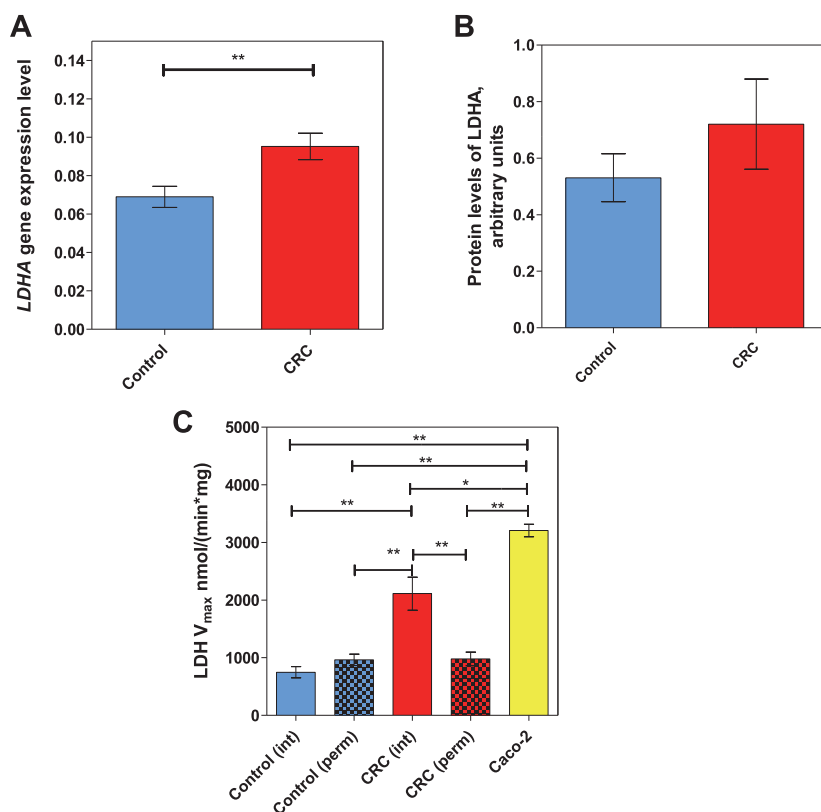


FIGURE 2 | The characteristics of lactate dehydrogenase (LDH) in colorectal tumours. (A) The transcript level of *LDHA* measured by RT-qPCR in control colon tissue ($n=24$) and CRC tissue ($n=24$). (B) The protein level of LDHA determined by Western blot in control colon tissue ($n=9$) and CRC tissue ($n=9$). (C) LDH activity in intact control tissue (Control (int), $n=7$), permeabilised control tissue (Control (perm), $n=13$), intact colorectal cancer tissue (CRC (int), $n=7$), permeabilised colorectal cancer tissue (CRC (perm), $n=13$) and Caco-2 cells ($n=4$). ** $p < 0.01$, *** $p < 0.001$ (one-way ANOVA).

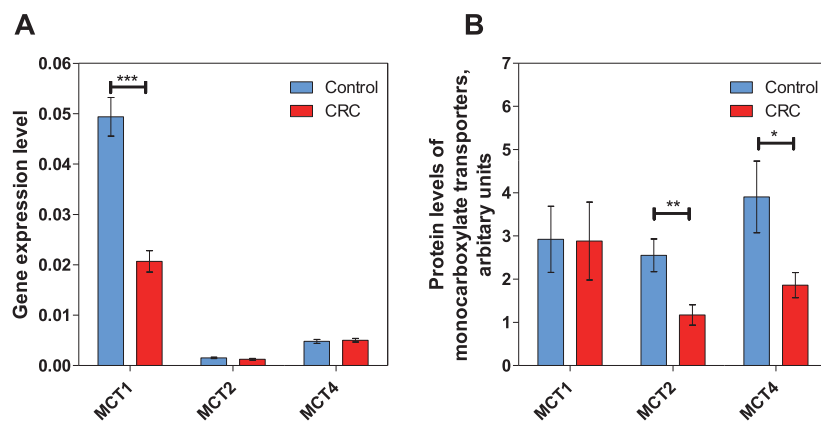


FIGURE 3 | The characteristics of monocarboxylate transporters (MCTs) in colorectal tumour tissue. (A) Transcript levels ($n=24$) and (B) protein levels ($n=9$) of monocarboxylate transporters 1, 2 and 4 in control colon tissue and colorectal cancer tissue. * $p < 0.05$, ** $p < 0.01$ and *** $p < 0.001$ (one-way ANOVA).

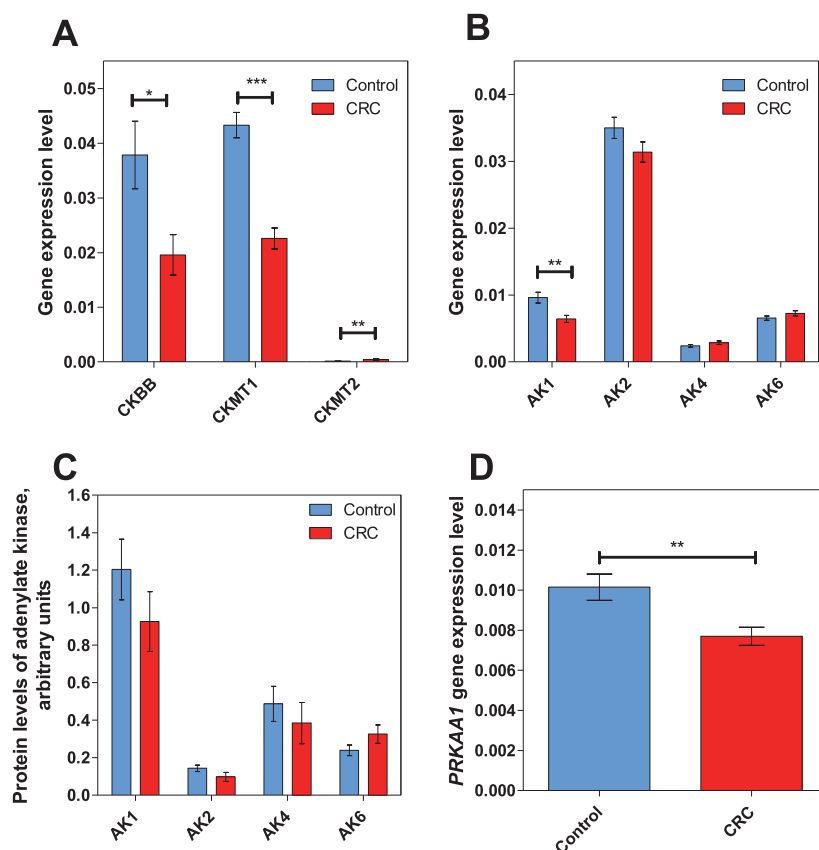


FIGURE 4 | Characteristics of the energy transfer pathways in colorectal tumours. The transcript levels of (A) creatine kinase isoforms *CKBB*, *CKMT1* and *CKMT2* and (B) adenylate kinase isoforms *AK1*, *AK2*, *AK4* and *AK6* in control colon tissue ($n=24$) and CRC tissue ($n=24$). (C) The protein levels of adenylate kinase isoforms *AK1*, *AK2*, *AK4* and *AK6* in control colon tissue ($n=8$) and CRC tissue ($n=8$). (D) The transcript level of 5'-AMP-activated protein kinase catalytic subunit alpha-1 (*PRKAA1*) in control colon tissue ($n=24$) and CRC tissue ($n=24$). * $p < 0.05$, ** $p < 0.01$ and *** $p < 0.001$ (one-way ANOVA).

significantly lower ($0.013 \text{ min}^{-1} \text{ mg}^{-1} \text{ mL}$) than that for CRC ($0.026 \text{ min}^{-1} \text{ mg}^{-1} \text{ mL}$), indicating a more catalytically efficient system in tumour tissue.

3.4 | Energy Charge

Analysis of the adenine nucleotide contents revealed that both control and CRC samples experienced a small increase in EC when glycolysis was active (Figure 5D,E). This suggested that reliance on glycolysis indeed affected cell energy status in healthy and cancerous tissue. In contrast, the ATP/ADP ratio (0.2–0.25 value range) showed no differences between tumour and control tissue, with or without glycolysis activated (data not shown).

However, EC in control tissues was significantly impacted by OxPhos inhibition compared to the non-inhibited state (Figure 5E), as well as the ATP/ADP ratios (from 0.23 down to 0.17; data not shown), indicating a substantial reliance on OxPhos for maintaining energy homeostasis in non-cancerous

cells. A significant decrease was noted in the control group when comparing glycolysis inhibition to OxPhos inhibition, highlighting the distinct contributions of these metabolic pathways to cellular energy status. CRC samples also showed a significant decrease in EC (and ATP/ADP ratios from 0.25 to 0.15) with OxPhos inhibition, suggesting OxPhos-dependent energy production in cancer cells. In contrast, CRC samples did not demonstrate a significant EC change under glycolysis-inhibited conditions, indicating a more pronounced metabolic flexibility or a compensatory mechanism enabling energy maintenance when glycolysis is inhibited (Figure 5E).

3.5 | OxPhos and Energy Charge Along CRC Progression

Searching for possible prognostic markers for aggressive cancer, OxPhos flux of CRC samples was analysed at different disease stages (Figure 6). When comparing V_{max} , K_{mADP} and EC values (and ATP/ADP ratios) across different CRC

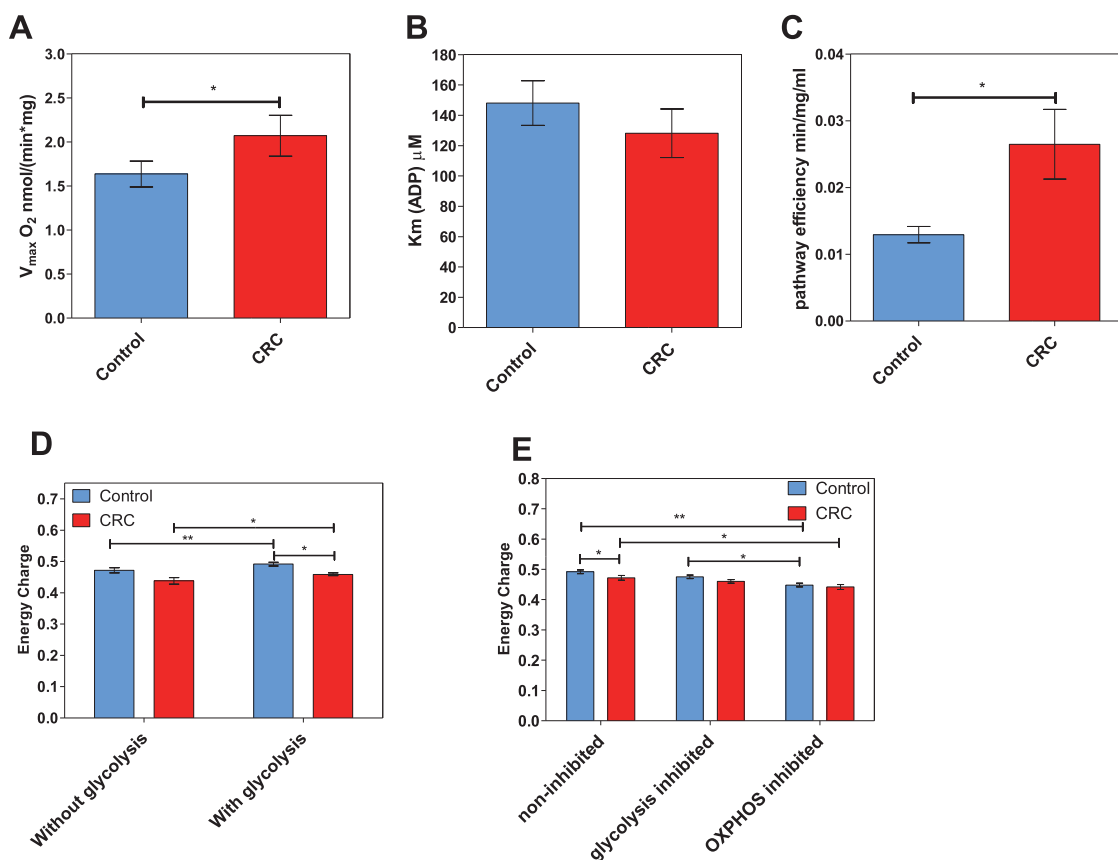


FIGURE 5 | Kinetic characteristics of oxidative phosphorylation in colorectal tumours. Comparative analysis of (A) maximal ADP-stimulated respiratory rate (V_{max}) and (B) apparent Michaelis–Menten constant values for ADP (K_{mADP}) in control tissue ($n=29$) and CRC tissue ($n=29$). (C) The catalytic efficiency of the OxPhos pathway represented by the V_{max}/K_{mADP} ratios, which were calculated from paired samples. (D) Energy charges of control and tumour tissue without ($n=15$) and with activated glycolysis ($n=16$), and (E) energy charges of non-inhibited ($n=16$), glycolysis-inhibited ($n=17$) and OxPhos-inhibited ($n=10$) states in control and tumour tissue. * $p < 0.05$, ** $p < 0.01$.

stages, no significant intergroup differences were observed, probably due to the intrinsic high sample heterogeneity among each group. Notwithstanding, a close resemblance in V_{max} values was noted between control tissues and Stage II CRC (Figure 6A). In addition, K_{mADP} values for Stage II CRC were higher than those of other stages (Figure 6B). The slight differences in these individual OxPhos kinetic parameters make the OxPhos catalytic efficiencies (V_{max}/K_m) clearly greater in the CRC stages than in the control colon tissue (Figure 6C). This suggested an enhanced OxPhos capability in CRC tumours.

Regarding EC without glycolysis activation (Figure 6D,E), control tissues showed significantly higher values compared to Stage II CRC, and there was a notable decrease between Stage I and Stage II CRC, pointing to a decrease in energy charge as the tumour progresses from Stage I to Stage II.

Finally, EC evaluations across control and CRC Stages I–III, under various metabolic conditions—non-inhibited, glycolysis-inhibited and OxPhos-inhibited—revealed no significant

differences between the groups (Figure 6D,E). A similar pattern of EC dependence on energy pathway was observed in control and Stage I tissues, whereas in Stages II and III, the pattern of changes seems slightly different from control.

3.6 | OxPhos and Energy Charge Profiles of CRC Patients

Previous work with data from 32 patients showed that CRC patients who had succumbed to the disease presented significantly higher OxPhos V_{max} values [23]. Here, additional disease progression data for all patients after 2017 were gathered, and a long-term disease progression analysis was conducted. Among the cohort of 57 patients, a total of 12 fatalities were observed. Out of these 12 patients, 10 had initially been diagnosed with Stage 0–II CRC and 2 with Stage III–IV CRC. It is important to note that the very small number of Stage III–IV patients is because we only collected samples from patients who had not received any systemic therapy before surgery.

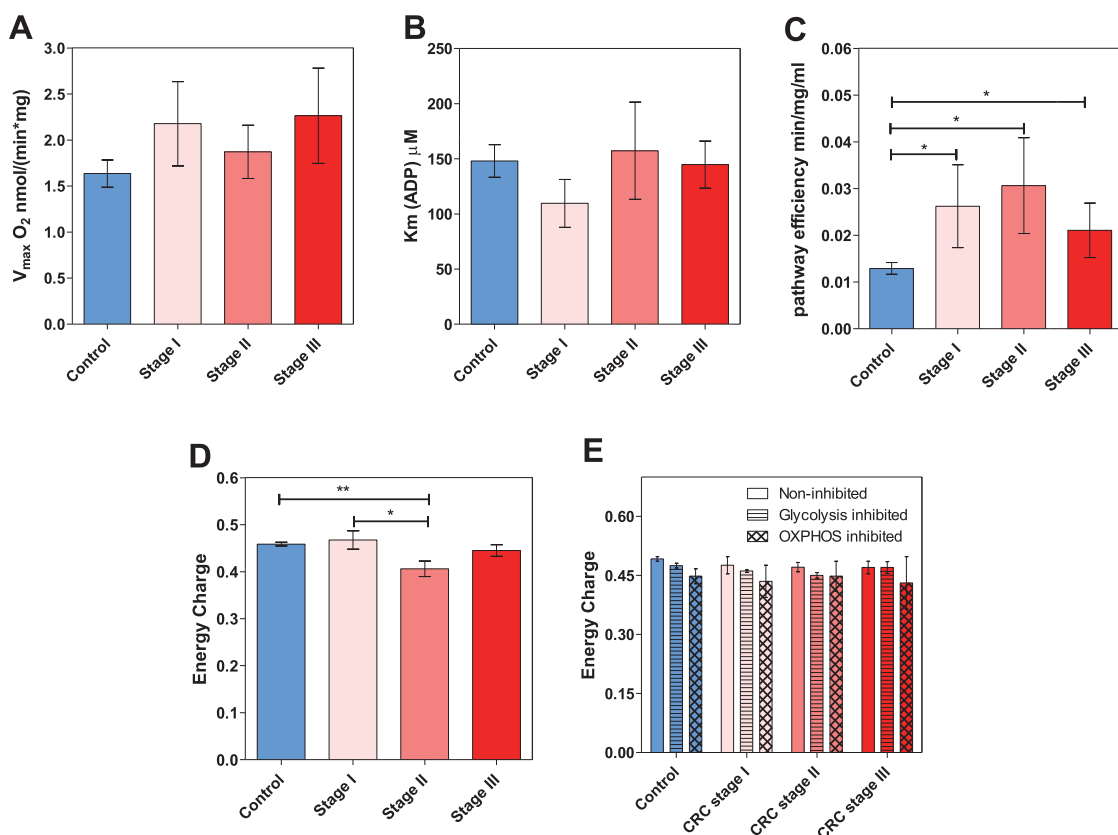


FIGURE 6 | Oxidative phosphorylation and energy charge values between different colorectal cancer stages. (A) Maximal ADP-induced respiration rate (V_{max}) and (B) apparent Michaelis–Menten constant values for exogenously added ADP (K_m ADP) in control and tumour Stages I–III. (C) The catalytic efficiency (V_{max}/K_m) of the OxPhos pathway for control and tumour Stages I–III. (D) Energy charges of control tissue and tumour Stages I–III without glycolysis activation ($n = 17$) and (E) energy charges of tumour stages under non-inhibited ($n = 16$), glycolysis-inhibited ($n = 17$) and OxPhos inhibited ($n = 10$) conditions. * $p < 0.05$, ** $p < 0.01$.

According to common clinical practice, patients with advanced disease mostly require some systemic therapy to achieve a resectable tumour size.

This updated analysis showed again a significantly lower average V_{max} value for alive patients compared to patients who had succumbed to the disease (Figure 7A). In addition, a higher average K_m ADP value was noted among the living patients (Figure 7B). The catalytic efficiency for the alive group was 0.012, whereas for the lethal groups, it was 0.042–0.043, indicating a more efficient OxPhos in the latter patients.

4 | Discussion

4.1 | Glycolysis

HK is one of the main rate-controlling steps of cancer glycolysis [8, 24] and HK2 has been proposed as an independent CRC prognostic factor [25]. Coupling between VDAC and HK2 promotes the Warburg effect by channelling

mitochondria-generated ATP preferentially towards glycolysis [26]. However, co-localisation of HK2 with VDAC has been detected in both normal colorectal mucosa and CRC [19, 27]. Thus, it is likely that the frequency and abundance of the HK–VDAC interaction depend on the cancer cell type. However, the changes observed in the present study on the transcript and protein levels of two HK isoforms in colorectal tumour and control colorectal tissue samples were not reflected in changes in total cellular HK activity. This observation suggested that the HK protein content changes were rather small or that HK1 (the most abundant HK isoform) predominated for total cellular activity over HK2.

Elevated LDH levels are often observed in the bloodstream of individuals with colon cancer [28–30]. The permeabilisation process, which presumably preserves high molecular weight proteins and mitochondria while removing cytosolic low-molecular weight contents, resulted in a substantial decrease in LDH activity in permeabilised tumour samples compared to their intact counterparts. This observation suggested that LDH is loosely bound to intracellular components like microtubules in tumour

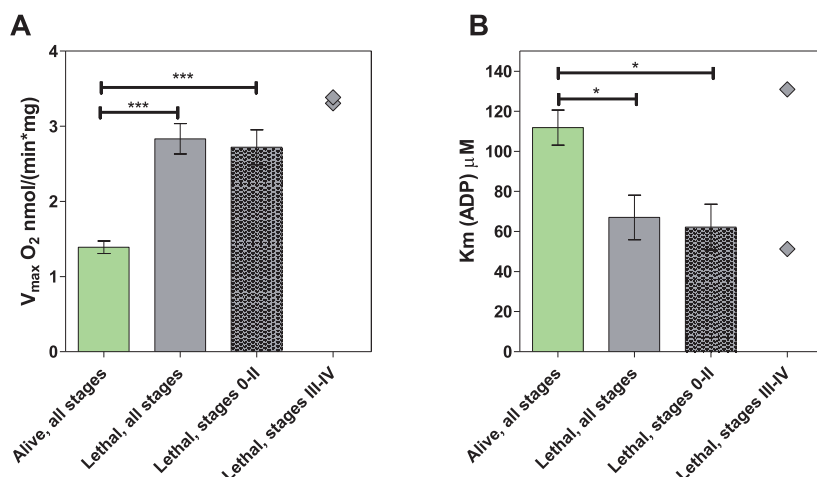


FIGURE 7 | (A) Maximal ADP-induced respiratory rate (V_{\max}) and (B) apparent Michaelis-Menten constant for exogenously added ADP (K_m ADP) in patients who are alive ($n=45$, all stages including Stage IV) or have passed away ($n=12$; Stage 0–II $n=10$ and Stage III–IV $n=2$) since their tumour samples were collected. * $p < 0.05$, *** $p < 0.001$.

cells. In addition, the results showed increased transcription of the *LDHA* gene together with a trend of higher LDHA protein levels and elevated LDH activity in cancer tissue, suggesting an increased lactate production capability in CRC compared to healthy colon tissue. The higher LDH activity in CaCo2 cells underscored a fundamental difference between cancer cell culture models and actual human tumours [31].

On the other hand, MCTs facilitate the transport of monocarboxylates, glycolytic intermediates like lactate, pyruvate and short-chain carboxylic acids across the plasma cell membrane [32]. In colon tissue, the most important isoform is MCT1, which is primarily responsible for the uptake of butyrate and lactate, and MCT4, which removes intracellular lactate produced by glycolysis. The release of lactate into the tumour microenvironment contributes to an acidic pH, fostering tumour growth, invasion, and metastasis. The lactate shuttle facilitated by MCTs may serve as an energy source for metastatic cancer cells in distant organs.

Since butyrate is primarily transported into the cell via MCT1, elevated transcript levels and high protein content may partly lead colon cells to depend on short-chain carboxylic acids supply. The higher protein content of MCT1, over that of MCT2 and MCT4, in CRC suggested an increased dependence on such short-chain carboxylic acids supply, which may be linked to increased acetate metabolism in CRC cells [33]. The discrepancy between MCT gene and protein levels may be related to their different regulation mechanisms at the transcriptional and translational levels and cautions against over-interpretation of their physiological meaning; hence, direct determination of activity is deemed necessary [11].

We previously demonstrated a substantial decrease in *MCT2* transcript in CRC while *MCT4* transcript was higher in CRC compared to control tissue [18]. The current study did not show a similar outcome at the level of mRNA. However, the decreased

MCT2 protein level correlated with prior results. MCT2 and MCT4 have been shown to translocate to mitochondria in breast cancer cell lines [34].

4.2 | Energy Transfer Pathways

A highly organised and efficient phosphoryl transfer system is essential to mediate intracellular communication between ATP-consuming and ATP-producing cellular processes for cell maintenance, growth and differentiation. During tumorigenesis, cells develop specific expression profiles of AK and CK isoforms that correlate with their oncometabolic phenotype [19, 35]. CK isoforms [19, 27, 36] catalyse the transfer of the high-energy phosphate of ATP to creatine in the mitochondrial intramembrane space and the reverse transfer from phosphocreatine to ADP, thus synthesising ATP in the cell energy-consuming sites and facilitating the intracellular diffusion of energy, avoiding the unspecific ADP and ATP protein binding. On the other hand, the AK family includes nine isoforms, each exhibiting distinct intracellular localisations and functional properties [21, 37, 38]. Similar to CK, the primary role of the AK system is to maintain the ATP/ADP ratio across various intracellular compartments [39]. AKs act as homeostatic metabolic regulators in both glycolysis and OxPhos, catalysing the efficient interconversion of adenine nucleotides (ATP, ADP and AMP), thereby ensuring a consistent and adequate ATP supply to fulfil cellular energy demands.

It has been demonstrated that cytosolic CK, associated with glycolytic enzymes, may support the Warburg effect by maintaining ATP homeostasis at glycolytic sites [39, 40]. However, changes in the mitochondrial outer membrane (MOM) permeability can influence the interplay between CKMTs and adenine nucleotide translocase, which catalyses the exchange of newly synthesised ATP to the cytosol by ADP entry into mitochondria. Growth of CRC is associated with upregulation of the AK

system and, in parallel, with a decrease in total CK and CKMT activities [41]. Indeed, the downregulation of the CK genes in colorectal tumours was found, which was accompanied by similar AK transcripts and protein levels to those of control colorectal tissue.

Furthermore, there is a significant increase in the coupling of mitochondrial AK with OxPhos in CRC [10, 41]. Oxidative stress, accompanied by a decline in ATP levels and an ADP increase (and hence decreased ATP/ADP ratios), induces increased AK activity, leading to an elevation in intracellular AMP. In turn, AMP, acting as a secondary messenger, may activate the energy stress-responsive AMP-dependent protein kinase (AMPK) that stimulates ATP production through catabolic processes while inhibiting the ATP-consuming processes involved in growth. The role of AMPK in cancer remains controversial [42, 43]. The observed slightly lower AMPK expression in colorectal tumours, whether mirrored in active protein content, suggests changes in metabolism, favouring catabolic over anabolic fluxes.

AMPK has been recognised as a tumour suppressor in certain cancers [44–47] by inhibiting protein synthesis, cell proliferation and growth, since it regulates the mTORC1 pathway. However, AMPK has also been described as a contextual oncogene due to its ability to promote tumour progression, chemoresistance upon activation and cancer cell survival by maintaining NADPH homeostasis [48–50].

4.3 | Energy Charge and ATP/ADP Ratios in CRC

In 1967, Atkinson and Walton proposed that EC derived from the adenine nucleotides contents is a fundamental metabolic thermodynamic parameter because it provides a quantitative value of the cellular energy state, reflecting the balance between energy supply and demand [51]. More recent research has delved into the intricacies of how EC reflects cancer cell metabolism and mitochondrial function, suggesting that alterations in EC can indicate disruptions in the energy balance of cancer cells, influencing their growth and survival [52].

Indeed, colorectal tumours exhibited slightly lower EC values than control tissue. EC values are established to range from 0 to 1, being close to 0 when the adenine nucleotide pool is made up of mainly AMP, 0.5 when ADP is the predominant adenine nucleotide and 1 if ATP is predominant [53]. Previous studies have documented EC values within a narrow range of 0.7–0.95, across various organisms and cell types, including liver and muscle cells. These values usually decrease under stressful conditions [52], for instance decreasing from ≥ 0.8 to less than 0.5 under nutrient depletion [54]. In contrast, our experiments consistently showed EC values ranging between 0.4 and 0.5. The estimated ATP/ADP ratio values were also lower than those determined for experiments with isolated mitochondria and intact cells and tissues.

The lower and narrower range of EC values and ATP/ADP ratios may be attributed to the use of permeabilised tissues in our experiments, which presumably retain high molecular weight enzymes that are preferentially bound to intracellular structures

such as membranes, organelles and microtubules. Thus, leakage of cytosolic proteins (glycolytic enzymes) may be induced by saponin permeabilisation, thereby limiting the observable portion of glycolytic activity. In addition, tissue permeabilisation may induce increased ATPase activity. Indeed, pooling together data from saponin-treated colorectal tumour and control tissue not subjected to lengthy incubations revealed ATP/ADP ratios of 0.3 for tumours and 0.2 for control tissues. Future research should include additional experiments using intact tumour and control clinical samples specifically for the determination of EC values, ATP/ADP ratios and glycolytic flux. Understanding such metabolic shifts could offer new avenues for cancer treatment by targeting the energy metabolism regulation mechanisms and main flux-controlling steps [8, 11, 24, 53].

4.4 | Kinetics of Oxidative Phosphorylation in CRC Progression and Patient Outcome

Our group has previously shown a significant difference in *KmADP* values between glycolytic and oxidative muscle tissue [55]. The oxidative tissue shows higher *KmADP* values, indicating a shift in the regulation of the MOM permeability by VDAC. In addition, we have also demonstrated that while control colon tissue and CRC tend to have similar *KmADP* values, which are in agreement with those found in the present study, benign colon polyps showed a significantly lower *KmADP* [18], suggesting an early energy metabolism switch, mediated by changes in the energy transfer pathway during CRC development.

Moreover, the higher *Vmax* values and *Vmax/KmADP* ratios in CRC suggested an increased OxPhos capacity and efficiency. These data confirmed the earlier findings [18], suggesting that high OxPhos *Vmax* values (and *Vmax/KmADP* ratios) could be a marker for a more aggressive disease. There was one recent CRC patient among the group of alive patients who showed a high *Vmax* value of 4.21, which was left out of the calculations as an outlier. However, it could be interesting to follow this patient's disease progression to validate the hypothesis of high *Vmax* being a prognostic marker.

There are several possible explanations for why the lethal Stage III–IV group did not show a significant difference in *KmADP*. Firstly, the group contained only two patients; secondly, advanced stage tumours have grown into nearby tissues including muscle tissue in the colon wall, meaning that these samples may include some muscle tissue that is characterised by a high *KmADP*. As described before, a lower *KmADP* value could indicate a shift to glycolytic metabolism. In turn, a high *Vmax* may derive from an advanced vascularisation in more aggressive malignant tumours and from an enhanced energy demand for metastatic processes. Interestingly, our previous work has shown a similar high *Vmax*—low *KmADP* metabolic profile in colon polyps, which are benign growths in the colon mucosa [18].

Although therapeutic strategies for Stage I, III and IV CRC are well established, the treatment approach for Stage II remains a subject of debate. Stage II is recognised as a heterogeneous category, with prognoses varying significantly. The search for more effective therapeutic strategies has led to the exploration of

various biomarkers [56]. Our results suggested the surge of a critical metabolic anomaly within Stage II CRC, perhaps reflecting changes in energetic needs and epithelial-mesenchymal transition onset that warrants further investigation into the specifics of its energy metabolism and energy-dependent metastasis events.

Furthermore, the data suggested that distinct energy metabolism profiles may emerge for the various colorectal tumour stages and their progression from one stage to another. Although the metabolic differences among CRC Stages I, II and III might seem inherently minimal, this may have derived from the relatively small sample size examined. Our study did not include cases of high-grade metastatic CRC, which previous research has shown to exhibit a notable increase in EC by approximately 26%, whereas CRC Stages I and III have shown negligible changes in EC [57], like the ones described here.

The lack of significant differences in the kinetic parameters of the ADP-stimulated respiration rate (V_{max} and K_m) across CRC stages observed in this study may be explained by the high heterogeneity of the samples and limited patient grouping. Specifically, the current study used treatment-naïve patients that are typically categorised as Stage I or II, while Stages III and IV are rarely surgically treated without prior chemotherapy or radiotherapy. These factors may have contributed to masking the subtle variations in EC that could otherwise indicate stage-specific metabolic alterations. Hence, a larger and more comprehensively designed cohort may be essential to further refine this approach and accurately identify differences in EC associated with CRC progression. Nevertheless, when the V_{max}/K_m ratio or catalytic efficiency is considered (cf. Figure 6C), or the EC values of Stage II are compared to those of control tissue samples (cf. Figure 6D), statistical significance emerged. Therefore, it seems the V_{max}/K_m ratio is a more sensitive parameter which might be able to help distinguish differences in the energy metabolism status of the different CRC stages. Let us recall that the catalytic efficiency comprises both catalytic capacity and substrate affinity, the two main kinetic parameters of an enzyme or metabolic pathway.

It is noted that EC and ATP/ADP ratio values were obtained from fully ADP-stimulated OxPhos samples. Then, to get a closer physiological view of colorectal cancer, a similar analysis should be undertaken for tumour samples under glycolysis and under both OxPhos and glycolysis to resemble actual microenvironmental changes undergone by CRC.

From the results described, it is clear that energy metabolism undergoes reprogramming throughout CRC development. We hypothesise that benign colon polyps increase glycolytic activity to support the increased proliferation by mainly supplying anabolic precursors such as Glc6P, Fru6P, DHAP, 3PG and Pyr and helping with the elevated energy demand under hypoxic conditions [8]. As the cell number increases and the tumour grows in size, the cells become deprived of oxygen and nutrients; consequently, new blood vessels are generated in the tissue to restore the supply.

Hanahan and Weinberg have proposed induced angiogenesis as one of the hallmarks of cancer [58]. While angiogenesis is usually dormant in adults, it is reinduced in early stages of tumorigenesis to further support cell growth and proliferation. As

the cancer progresses even further, cancer tissue will become more and more heterogeneous. Some cells will persist in hypoxic conditions and rely predominantly on glycolysis, while others, benefiting from sufficient oxygen availability, utilise lactate produced by the former cells as a substrate for ATP production via OxPhos [8, 59, 60]. Thus, it has become apparent that there is metabolic heterogeneity and plasticity within solid tumours [10, 61–63] and there is growing evidence of hybrid energy metabolism phenotypes in several cancer cell lines and tumours [7–10, 62]. Depending on the microenvironment, glycolysis or OxPhos or both may become predominant for energy supply [7–9, 59, 60, 63].

5 | Conclusion

The data of the present study showed that colorectal human tumours display altered expression, protein contents and enzyme activities of their energy metabolism, including the energy transfer pathway. The contents and activities of some glycolytic proteins, the changes in the energy charge values, enhanced OxPhos flux and catalytic efficiency suggested that colorectal tumours have highly active glycolysis and OxPhos; therefore, they seem to display a hybrid energy metabolism phenotype. Such a hybrid metabolic phenotype in CRC indicates drug targeting of both pathways, either with multi-site drugs or a combination of drugs, to achieve successful treatment schemes. Drugs preferentially or specifically targeting cancer mitochondria and glycolysis, particularly lipophilic cationic, vitamin E analogues or cholesterol-binding molecules, should be tested [7, 8, 11].

Moreover, the present study underscores the complex nature of cancer, advocating for an integral approach that employs both cancer cell cultures and tumour clinical material. This comprehensive approach has unveiled instances previously unseen, which might be challenging or even impossible to discern through more conventional or isolated research strategies. The present findings highlight the importance of combining diverse experimental models to fully understand the multifaceted biological behaviours of cancer.

Author Contributions

Leenu Reinsalu: conceptualization (equal), formal analysis (equal), investigation (equal), methodology (equal), visualization (equal), writing – original draft (equal). **Sten Miller:** conceptualization (equal), formal analysis (equal), investigation (equal), methodology (equal), visualization (equal), writing – original draft (equal). **Giuseppe Leonardo Auditano:** formal analysis (equal), investigation (supporting), methodology (supporting), writing – review and editing (equal). **Marju Puurand:** formal analysis (supporting), investigation (supporting). **Rafael Moreno-Sanchez:** conceptualization (equal), funding acquisition (equal), writing – review and editing (equal). **Emma Saavedra:** writing – review and editing (equal). **Vahur Valvere:** methodology (equal), resources (equal). **Tuuli Käämbre:** conceptualization (equal), funding acquisition (equal), supervision (equal), writing – review and editing (equal).

Ethics Statement

The studies involving human participants were reviewed and approved by the Research Ethics Committee of the National Institute for Health

Development in Estonia (decision numbers KK557 and KK558) and followed the Helsinki Declaration and Convention of the Council of Europe on Human Rights and Biomedicine. All participants were informed about the study and provided their written informed consent to participate in the study.

Conflicts of Interest

The authors declare no conflicts of interest.

Data Availability Statement

The data that support the findings of this study are available from the corresponding author upon request.

References

- World Health Organization, "Cancer," (2022).
- Centers for Disease Control and Prevention, "U.S. Cancer Statistics Colorectal Cancer Stat Bite," (2023).
- R. Udo, K. Katsumata, H. Kuwabara, et al., "Urinary Charged Metabolite Profiling of Colorectal Cancer Using Capillary Electrophoresis-Mass Spectrometry," *Scientific Reports* 10, no. 1 (2020): 21057, <https://doi.org/10.1038/s41598-020-78038-2>.
- F. di Cesare, A. Vignoli, C. Luchinat, L. Tenori, and E. Saccenti, "Exploration of Blood Metabolite Signatures of Colorectal Cancer and Polyposis Through Integrated Statistical and Network Analysis," *Metabolites* 13 (2023): 296, <https://doi.org/10.3390/metabo13020296>.
- D. Hanahan and R. A. Weinberg, "Hallmarks of Cancer: The Next Generation," *Cell* 144, no. 5 (2011): 646–674, <https://doi.org/10.1016/j.cell.2011.02.013>.
- O. Warburg, "On the Origin of Cancer Cells," *Science* 123, no. 3191 (1956): 309–314, <https://doi.org/10.1126/science.123.3191.309>.
- R. Moreno-Sanchez, S. Rodriguez-Enriquez, A. Marin-Hernandez, and E. Saavedra, "Energy Metabolism in Tumor Cells," *FEBS Journal* 274, no. 6 (2007): 1393–1418, <https://doi.org/10.1111/j.1742-4658.2007.05686.x>.
- R. Moreno-Sanchez, A. Marin-Hernandez, E. Saavedra, J. P. Pardo, S. J. Ralph, and S. Rodriguez, "Enriquez: Who Controls the ATP Supply in Cancer Cells? Biochemistry Lessons to Understand Cancer Energy Metabolism," *International Journal of Biochemistry & Cell Biology* 50 (2014): 10–23, <https://doi.org/10.1016/j.biocel.2014.01.025>.
- R. Moreno-Sánchez, D. X. Robledo-Cadena, S. C. Pacheco-Velázquez, J. L. Vargas Navarro, J. A. Padilla-Flores, and S. Rodríguez-Enriquez, "Estimation of Energy Pathway Fluxes in Cancer Cells—Beyond the Warburg Effect," *Archives of Biochemistry and Biophysics* 739 (2023): 109559, <https://doi.org/10.1016/j.abb.2023.109559>.
- L. Reinsalu, M. Puurand, V. Chekulayev, et al., "Energy Metabolic Plasticity of Colorectal Cancer Cells as a Determinant of Tumor Growth and Metastasis," *Frontiers in Oncology* 11 (2021): 698951, <https://doi.org/10.3389/fonc.2021.698951>.
- R. Moreno-Sánchez, E. Saavedra, J. C. Gallardo-Pérez, F. D. Rumjanek, and S. Rodríguez-Enriquez, "Understanding the Cancer Cell Phenotype Beyond the Limitations of Current Omics Analyses," *FEBS Journal* 283, no. 1 (2016): 54–73, <https://doi.org/10.1111/febs.13535>.
- M. V. Golikov, V. T. Valuev-Elliston, O. A. Smirnova, and A. V. Ivanov, "Physiological Media in Studies of Cell Metabolism," *Molecular Biology* 56, no. 5 (2022): 629–637, <https://doi.org/10.1134/s0026893322050077>.
- A. Untergasser, *RNAprep – Trizol Combined With Columns*, vol. 2023 (*Untergasser's Lab*, 2008).
- E. K. Seppet, T. Kaambre, P. Sikk, et al., "Functional Complexes of Mitochondria With ca, MgATPases of Myofibrils and Sarcoplasmic Reticulum in Muscle Cells," *Biochimica et Biophysica Acta* 1504, no. 2–3 (2001): 379–395.
- P.-B. Ancey, C. Contat, G. Boivin, et al., "GLUT1 Expression in Tumor-Associated Neutrophils Promotes Lung Cancer Growth and Resistance to Radiotherapy," *Cancer Research* 81, no. 9 (2021): 2345–2357, <https://doi.org/10.1158/0008-5472.can-20-2870>.
- P.-B. Ancey, C. Contat, and E. Meylan, "Glucose Transporters in Cancer – From Tumor Cells to the Tumor Microenvironment," *FEBS Journal* 285, no. 16 (2018): 2926–2943, <https://doi.org/10.1111/febs.14577>.
- H. Xiao, J. Wang, W. Yan, et al., "GLUT1 Regulates Cell Glycolysis and Proliferation in Prostate Cancer," *Prostate* 78, no. 2 (2018): 86–94, <https://doi.org/10.1002/pros.23448>.
- E. Rebane-Klemm, L. Reinsalu, M. Puurand, et al., "Colorectal Polyps Increase the Glycolytic Activity," *Frontiers in Oncology* 13 (2023): e1171887, <https://doi.org/10.3389/fonc.2023.1171887>.
- A. Kaldma, A. Klepinin, V. Chekulayev, et al., "An In Situ Study of Bioenergetic Properties of Human Colorectal Cancer: The Regulation of Mitochondrial Respiration and Distribution of Flux Control Among the Components of ATP Synthasome," *International Journal of Biochemistry & Cell Biology* 55 (2014): 171–186, <https://doi.org/10.1016/j.biocel.2014.09.004>.
- J. Joseph, A. Cardesa, and J. Carreras, "Creatine Kinase Activity and Isoenzymes in Lung, Colon and Liver Carcinomas," *British Journal of Cancer* 76, no. 5 (1997): 600–605.
- C. Panayiotou, N. Solaroli, and A. Karlsson, "The Many Isoforms of Human Adenylate Kinases," *International Journal of Biochemistry & Cell Biology* 49 (2014): 75–83, <https://doi.org/10.1016/j.biocel.2014.01.014>.
- C.-C. Hsu, D. Peng, Z. Cai, and H.-K. Lin, "AMPK Signaling and Its Targeting in Cancer Progression and Treatment," *Seminars in Cancer Biology* 85 (2022): 52–68, <https://doi.org/10.1016/j.semcancer.2021.04.006>.
- A. Koit, I. Shevchuk, L. Ounpuu, et al., "Mitochondrial Respiration in Human Colorectal and Breast Cancer Clinical Material Is Regulated Differently," *Oxidative Medicine and Cellular Longevity* 2017 (2017): 1372640, <https://doi.org/10.1155/2017/1372640>.
- A. Marín-Hernández, J. C. Gallardo-Pérez, S. Rodríguez-Enriquez, R. Encalada, R. Moreno-Sánchez, and E. Saavedra, "Modeling Cancer Glycolysis," *BBA-Bioenergetics* 1807 (2011): 755–767.
- M. Katagiri, H. Karasawa, K. Takagi, et al., "Hexokinase 2 in Colorectal Cancer: A Potent Prognostic Factor Associated With Glycolysis, Proliferation and Migration," *Histology and Histopathology* 32, no. 4 (2017): 351–360, <https://doi.org/10.14670/HH-11-799>.
- P. L. Pedersen, S. Mathupala, A. Rempel, J. F. Geschwind, and Y. H. Ko, "Mitochondrial Bound Type II Hexokinase: A Key Player in the Growth and Survival of Many Cancers and an Ideal Prospect for Therapeutic Intervention," *Biochimica et Biophysica Acta (BBA) Bioenergetics* 1555, no. 1 (2002): 14–20, [https://doi.org/10.1016/S0005-2728\(02\)00248-7](https://doi.org/10.1016/S0005-2728(02)00248-7).
- L. Ounpuu, L. Truu, I. Shevchuk, et al., "Comparative Analysis of the Bioenergetics of Human Adenocarcinoma Caco-2 Cell Line and Postoperative Tissue Samples From Colorectal Cancer Patients," *Biochemistry and Cell Biology* 96, no. 6 (2018): 808–817, <https://doi.org/10.1139/bcb-2018-0076>.
- Z. Xie, H. Zhou, L. Wang, and Y. Wu, "The Significance of the Pre-operative Lactate Dehydrogenase/Albumin Ratio in the Prognosis of Colon Cancer: A Retrospective Study," *PeerJ* 10 (2022): e13091, <https://doi.org/10.7717/peerj.13091>.
- A. Casadei-Gardini, E. Scarpi, P. Ulivi, et al., "Prognostic Role of a New Inflammatory Index With Neutrophil-To-Lymphocyte Ratio and Lactate Dehydrogenase (CII: Colon Inflammatory Index) in Patients With Metastatic Colorectal Cancer: Results From the Randomized Italian Trial in Advanced Colorectal Cancer (ITaCa) Study," *Cancer Management and Research* 11 (2019): 4357–4369, <https://doi.org/10.2147/CMAR.S198651>.

30. M. Manerba, L. di Ianni, M. Govoni, M. Roberti, M. Recanatini, and G. di Stefano, "Lactate Dehydrogenase Inhibitors Can Reverse Inflammation Induced Changes in Colon Cancer Cells," *European Journal of Pharmaceutical Sciences* 96 (2017): 37–44, <https://doi.org/10.1016/j.ejps.2016.09.014>.
31. R. Moreno-Sanchez, J. L. Vargas-Navarro, J. A. Padilla-Flores, et al., "Energy Metabolism Behavior and Response to Microenvironmental Factors of the Experimental Cancer Cell Models Differ From That of Actual Human Tumors," *Mini Reviews in Medicinal Chemistry* 25, no. 4 (2024), <https://doi.org/10.2174/0113895575322436240924101642> Epub ahead of print.
32. V. L. Payen, E. Mina, V. F. van Hee, P. E. Porporato, and P. Sonveaux, "Monocarboxylate Transporters in Cancer," *Molecular Metabolism* 33 (2020): 48–66, <https://doi.org/10.1016/j.molmet.2019.07.006>.
33. S. Rodríguez-Enríquez, D. X. Robledo-Cadena, J. C. Gallardo-Pérez, et al., "Acetate Promotes a Differential Energy Metabolic Response in Human HCT 116 and COLO 205 Colon Cancer Cells Impacting Cancer Cell Growth and Invasiveness," *Frontiers in Oncology* 11 (2021): e697408, <https://doi.org/10.3389/fonc.2021.697408>.
34. R. Hussien and G. A. Brooks, "Mitochondrial and Plasma Membrane Lactate Transporter and Lactate Dehydrogenase Isoform Expression in Breast Cancer Cell Lines," *Physiological Genomics* 43, no. 5 (2011): 255–264, <https://doi.org/10.1152/physiolgenomics.00177.2010>.
35. V. Chekulayev, K. Mado, I. Shevchuk, et al., "Metabolic Remodeling in Human Colorectal Cancer and Surrounding Tissues: Alterations in Regulation of Mitochondrial Respiration and Metabolic Fluxes," *Biochemistry and Biophysics Reports* 4 (2015): 111–125, <https://doi.org/10.1016/j.bbrep.2015.08.020>.
36. U. Schlattner, M. Tokarska-Schlattner, and T. Wallimann, "Mitochondrial Creatine Kinase in Human Health and Disease," *Biochimica et Biophysica Acta* 1762, no. 2 (2006): 164–180, <https://doi.org/10.1016/j.bbadis.2005.09.004>.
37. P. Dzeja and A. Terzic, "Adenylate Kinase and AMP Signaling Networks: Metabolic Monitoring, Signal Communication and Body Energy Sensing," *International Journal of Molecular Sciences* 10, no. 4 (2009): 1729–1772, <https://doi.org/10.3390/ijms10041729>.
38. D. M. Bai, J. F. Zhang, T. T. Li, et al., "The ATPase hCINAP Regulates 18S rRNA Processing and Is Essential for Embryogenesis and Tumour Growth," *Nature Communications* 7 (2016): 12310, <https://doi.org/10.1038/ncomms12310>.
39. Y.-B. Yan, "Creatine Kinase in Cell Cycle Regulation and Cancer," *Amino Acids* 48, no. 8 (2016): 1775–1784, <https://doi.org/10.1007/s00726-016-2217-0>.
40. S. M. Mooney, K. Rajagopalan, B. H. Williams, et al., "Creatine Kinase Brain Overexpression Protects Colorectal Cells From Various Metabolic and Non-Metabolic Stresses," *Journal of Cellular Biochemistry* 112, no. 4 (2011): 1066–1075, <https://doi.org/10.1002/jcb.23020>.
41. A. Klepinin, S. Zhang, L. Klepinina, et al., "Adenylate Kinase and Metabolic Signaling in Cancer Cells," *Frontiers in Oncology* 10 (2020): 660, <https://doi.org/10.3389/fonc.2020.00660>.
42. J. Liang and G. B. Mills, "AMPK: A Contextual Oncogene or Tumor Suppressor?," *Cancer Research* 73, no. 10 (2013): 2929–2935, <https://doi.org/10.1158/0008-5472.CAN-12-3876>.
43. W. Wang and K. L. Guan, "AMP-Activated Protein Kinase and Cancer," *Acta Physiologica* 196, no. 1 (2009): 55–63, <https://doi.org/10.1111/j.1748-1716.2009.01980.x>.
44. B. Faubert, G. Boily, S. Izreig, et al., "AMPK Is a Negative Regulator of the Warburg Effect and Suppresses Tumor Growth In Vivo," *Cell Metabolism* 17, no. 1 (2013): 113–124.
45. G. Rehman, A. Shehzad, A. L. Khan, and M. Hamayun, "Role of AMP-Activated Protein Kinase in Cancer Therapy," *Archiv der Pharmazie* 347, no. 7 (2014): 457–468, <https://doi.org/10.1002/ardp.201300402>.
46. D. G. Hardie, F. A. Ross, and S. A. Hawley, "AMP-Activated Protein Kinase: A Target for Drugs Both Ancient and Modern," *Chemistry & Biology* 19, no. 10 (2012): 1222–1236, <https://doi.org/10.1016/j.chembiol.2012.08.019>.
47. H. U. Park, S. Suy, M. Danner, et al., "AMP-Activated Protein Kinase Promotes Human Prostate Cancer Cell Growth and Survival," *Molecular Cancer Therapeutics* 8, no. 4 (2009): 733–741, <https://doi.org/10.1158/1535-7163.MCT-08-0631>.
48. A. S. Khan and D. E. Frigo, "Regulation, Role and Therapeutic Targeting of AMPK in Prostate Cancer," *Nature Reviews. Urology* 14, no. 3 (2017): 164–180, <https://doi.org/10.1038/nrurol.2016.272>.
49. X. Huang, X. Li, X. Xie, et al., "High Expressions of LDHA and AMPK as Prognostic Biomarkers for Breast Cancer," *Breast* 30 (2016): 39–46, <https://doi.org/10.1016/j.breast.2016.08.014>.
50. L. Collavin, D. Lazarevič, R. Utrera, S. Marzinotto, M. Monte, and C. Schneider, "Wt p53 Dependent Expression of a Membrane-Associated Isoform of Adenylate Kinase," *Oncogene* 18, no. 43 (1999): 5879–5888, <https://doi.org/10.1038/sj.onc.1202970>.
51. D. E. Atkinson and G. M. Walton, "Adenosine Triphosphate Conservation in Metabolic Regulation: Rat Liver Citrate Cleavage Enzyme," *Journal of Biological Chemistry* 242, no. 13 (1967): 3239–3241, [https://doi.org/10.1016/S0021-9258\(18\)95956-9](https://doi.org/10.1016/S0021-9258(18)95956-9).
52. L. Iommarini, A. Ghelli, G. Gasparre, and A. M. Porcelli, "Mitochondrial Metabolism and Energy Sensing in Tumor Progression," *Biochimica et Biophysica Acta (BBA) Bioenergetics* 1858, no. 8 (2017): 582–590, <https://doi.org/10.1016/j.bbabi.2017.02.006>.
53. I. M. de la Fuente, J. M. Cortés, E. Valero, et al., "On the Dynamics of the Adenylate Energy System: Homeorhesis vs Homeostasis," *PLoS One* 9, no. 10 (2014): e108676, <https://doi.org/10.1371/journal.pone.0108676>.
54. Frederick Jay Passman, Jordan Schmidt, and Russell P Lewis, "The Relationship Between Microbial Community Vitality and ATP Bioburden in Bottom Waters Under Fuel Microcosms," *Access Microbiology* 5, no. 4 (2023): acmi000411, <https://doi.org/10.1099/acmi.0.000411>.
55. A. V. Kuznetsov, T. Tiivel, P. Sikk, et al., "Striking Differences Between the Kinetics of Regulation of Respiration by ADP in Slow-Twitch and Fast-Twitch Muscles In Vivo," *European Journal of Biochemistry* 241, no. 3 (1996): 909–915, <https://doi.org/10.1111/j.1432-1033.1996.00909.x>.
56. P. Parent, R. Cohen, E. Rassy, et al., "A Comprehensive Overview of Promising Biomarkers in Stage II Colorectal Cancer," *Cancer Treatment Reviews* 88 (2020): e102059, <https://doi.org/10.1016/j.ctrv.2020.102059>.
57. Z. Teo, M. K. Sng, J. S. K. Chan, et al., "Elevation of Adenylate Energy Charge by Angiopoietin-Like 4 Enhances Epithelial–Mesenchymal Transition by Inducing 14-3-3 γ Expression," *Oncogene* 36, no. 46 (2017): 6408–6419, <https://doi.org/10.1038/nc.2017.244>.
58. D. Hanahan and R. A. Weinberg, "The Hallmarks of Cancer," *Cell* 100, no. 1 (2000): 57–70, [https://doi.org/10.1016/S0092-8674\(00\)81683-9](https://doi.org/10.1016/S0092-8674(00)81683-9).
59. S. J. Ralph, S. Rodríguez-Enríquez, J. Neuzil, E. Saavedra, and R. Moreno-Sánchez, "The Causes of Cancer Revisited: 'Mitochondrial Malignancy' and ROS-Induced Oncogenic Transformation – Why Mitochondria Are Targets for Cancer Therapy," *Molecular Aspects of Medicine* 31, no. 2 (2010): 145–170.
60. R. Moreno-Sanchez, E. Saavedra, S. Rodríguez-Enríquez, J. C. Gallardo-Perez, H. Quezada, and H. V. Westerhoff, "Metabolic Control Analysis Indicates a Change of Strategy in the Treatment of Cancer," *Mitochondrion* 10, no. 6 (2010): 626–639, <https://doi.org/10.1016/j.mito.2010.06.002>.
61. C. T. Hensley, B. Faubert, Q. Yuan, et al., "Metabolic Heterogeneity in Human Lung Tumors," *Cell* 164, no. 4 (2016): 681–694, <https://doi.org/10.1016/j.cell.2015.12.034>.

62. D. Jia, J. H. Park, K. H. Jung, H. Levine, and B. A. Kaipparettu, "Elucidating the Metabolic Plasticity of Cancer: Mitochondrial Reprogramming and Hybrid Metabolic States," *Cells* 7, no. 3 (2018): 21, <https://doi.org/10.3390/cells7030021>.
63. S. Rodríguez-Enríquez, T. Kaambre, and R. Moreno-Sánchez, "Editorial: Metabolic Plasticity of Cancer," *Frontiers in Oncology* 10 (2020): 599723, <https://doi.org/10.3389/fonc.2020.599723>.

Appendix 2

Publication II

Klepinin, A; **Miller, S**; Reile, I; Puurand, M; Rebane-Klemm, E; Klepinina, L; Vija, H; Zhang, S; Terzic, A; Dzeja, P; Kaambre, T (2022). Stable Isotope Tracing Uncovers Reduced g/b-ATP Turnover and Metabolic Flux Through Mitochondrial-Linked Phosphotransfer Circuits in Aggressive Breast Cancer Cells. *Frontiers in oncology*, 12:892195. doi: 10.3389/fonc.2022.892195.



Stable Isotope Tracing Uncovers Reduced γ/β -ATP Turnover and Metabolic Flux Through Mitochondrial-Linked Phosphotransfer Circuits in Aggressive Breast Cancer Cells

Aleksandr Klepinin^{1,2*}, Sten Miller^{1,3}, Indrek Reile⁴, Marju Puurand¹, Egle Rebane-Klemm^{1,3}, Ljudmila Klepinina^{1,3}, Heiki Vija⁵, Song Zhang², Andre Terzic^{6,7}, Petras Dzeja² and Tuuli Kaambre^{1*}

OPEN ACCESS

Edited by:

Ubaldo Emilio Martinez-Outschoorn,
Thomas Jefferson University,
United States

Reviewed by:

Riccardo Filadi,
Institute of Neuroscience (CNR), Italy
Eva Ramón-Gallegos,
Instituto Politécnico Nacional (IPN),
Mexico

*Correspondence:

Aleksandr Klepinin
aleksandr.klepinin@kbfi.ee
Tuuli Kaambre
tuuli.kaambre@kbfi.ee

Specialty section:

This article was submitted to
Cancer Metabolism,
a section of the journal
Frontiers in Oncology

Received: 08 March 2022

Accepted: 03 May 2022

Published: 31 May 2022

Citation:

Klepinin A, Miller S, Reile I, Puurand M,
Rebane-Klemm E, Klepinina L,
Vija H, Zhang S, Terzic A, Dzeja P
and Kaambre T (2022) Stable
Isotope Tracing Uncovers
Reduced γ/β -ATP Turnover and
Metabolic Flux Through Mitochondrial-
Linked Phosphotransfer Circuits in
Aggressive Breast Cancer Cells.
Front. Oncol. 12:892195.
doi: 10.3389/fonc.2022.892195

¹ Laboratory of Chemical Biology, National Institute of Chemical Physics and Biophysics, Tallinn, Estonia, ² Department of Cardiovascular Medicine and Center for Regenerative Medicine, Mayo Clinic, Rochester, MN, United States, ³ Department of Chemistry and Biotechnology, School of Science, Tallinn University of Technology, Tallinn, Estonia, ⁴ Laboratory of Chemical Physics, National Institute of Chemical Physics and Biophysics, Tallinn, Estonia, ⁵ Laboratory of Environmental Toxicology, National Institute of Chemical Physics and Biophysics, Tallinn, Estonia, ⁶ Department of Molecular Pharmacology and Experimental Therapeutics, Mayo Clinic, Rochester, MN, United States, ⁷ Department of Clinical Genomics, Mayo Clinic, Rochester, MN, United States

Changes in dynamics of ATP γ - and β -phosphoryl turnover and metabolic flux through phosphotransfer pathways in cancer cells are still unknown. Using ^{18}O phosphometabolite tagging technology, we have discovered phosphotransfer dynamics in three breast cancer cell lines: MCF7 (non-aggressive), MDA-MB-231 (aggressive), and MCF10A (control). Contrary to high intracellular ATP levels, the ^{18}O labeling method revealed a decreased γ - and β -ATP turnover in both breast cancer cells, compared to control. Lower β -ATP [^{18}O] turnover indicates decreased adenylate kinase (AK) flux. Aggressive cancer cells had also reduced fluxes through hexokinase (HK) G-6-P [^{18}O], creatine kinase (CK) CrP [^{18}O], and mitochondrial G-3-P [^{18}O] substrate shuttle. Decreased CK metabolic flux was linked to the downregulation of mitochondrial MTCK1A in breast cancer cells. Despite the decreased overall phosphoryl flux, overexpression of HK2, AK2, and AK6 isoforms within cell compartments could promote aggressive breast cancer growth.

Keywords: triple-negative breast cancer, 18 O stable isotope labeling technology, γ - and β -ATP phosphoryl turnover, adenylate kinase, creatine kinase, oxidative phosphorylation, glycolysis, phosphotransfer network

1 INTRODUCTION

One of the cancer hallmarks is the ability to reprogram energy metabolism to support malignant cell proliferation and metastatic activity (1, 2). However, despite significant advances, the molecular mechanisms and logic of such metabolic rearrangements and adjustments are still a mystery (3). It is unknown how mitochondrial ATP production is connected with sites of ATP utilization in different

cellular compartments to support the growth of malignant cells. Unveiling ATP production and ATP consumption dynamics in cancer cells will facilitate the development of a new therapeutic strategy for human breast cancer (HBC), the most diagnosed tumor and the second cause of death among females worldwide (4). Recently, the hybrid glycolysis/oxidative phosphorylation (OXPHOS) metabolic model for aggressive Triple-negative breast cancer (TNBC) cells has been proposed (5). The metabolic hybrid cancer phenotype is one of the reasons why malignant cells incline to metastasis and are cancer therapy-resistant (6). Understanding how OXPHOS interacts with glycolysis will give us new insights into the metabolic plasticity of breast cancer cells.

In cellular energetics, mitochondria are integrated with specialized phosphotransfer circuits that distribute energy from mitochondria and deliver it to ATP consumption sites to support constant undisturbed metabolic homeostasis (7–9). ATP delivery phosphotransfer circuits are mainly comprised of creatine kinase (CK), adenylate kinase (AK), and glycolytic/glucogenolytic enzymes, along with the associated mitochondrial substrate shuttles such as glycerol-3-phosphate (G-3-P) dehydrogenase/glycerol kinase (GPDH/GK) (9–11).

The enzyme AK, which catalyzes the reaction $2\text{ADP} \rightleftharpoons \text{AMP} + \text{ATP}$, is the central mediator of intracellular nucleotide exchange and AMP metabolic signaling (12). Importantly, AK can deliver both γ - and β -phosphoryl groups of ATP and make them available for utilization, thus doubling the ATP energetic potential (8). Evidence is accumulating that different AK isoforms are involved in cancer development and cell proliferation (13–15). However, it is unknown how changes in the AK-mediated β -ATP turnover and phosphotransfer flux within cell compartments are related to the aggressiveness of the TNBC subtype.

Glycolytic enzymes distributed throughout the cell can also comprise a phosphotransfer network. Hexokinases 1 and 2 (HK1 & HK2), enzymes catalyzing the first step of glycolysis, can relay mitochondrially generated ATP to energy-consumption sites (11, 16). Upregulation of HK2, which has a higher affinity to mitochondria, has been associated with enhanced aerobic glycolysis and promotion of tumor growth in many types of cancers, including HBC (17, 18). It is still unknown how the HK expression pattern correlates with glucose-6-phosphate (G-6-P) turnover and phosphoryl flux through the glycolytic pathway. Such data should provide valuable information about the integration of glycolytic phosphotransfer network into the bioenergetics of HBC.

Another phosphotransfer enzyme, mitochondrial creatine kinase MtCK, which is localized in the mitochondrial inner membrane compartment, facilitates phosphate transfer from mitochondrial ATP to the phosphocreatine (PCr). PCr serves as a dynamic cellular high-energy phosphoryl distributor and buffers during increased energy demand (7, 10). In the epithelial cells, the ubiquitous uMtCK (gene MtCK1) is co-expressed with the cytosolic brain-type CK (B-CK, gene CKB) (7), which is usually up-regulated during malignant epithelial transformation (19). Recent *in vivo* and *in vitro* studies demonstrate that CK's role in breast cancer progression depends on HBC subtypes (20).

However, it is unknown how remodeling of the CK isoform network affects the CrP metabolic flux and energetics of HBC and aggressiveness of TNBC cells.

^{18}O is a natural, stable and non-radioactive isotope of oxygen with a natural abundance of 0.2% (21) and more importantly it is not toxic for humans (22). In the cells the newly developed ^{18}O isotope-based metabolite tagging technology allows monitoring phosphotransfer dynamics by simultaneously determining their intracellular phosphometabolite levels and turnover rates (23, 24). In metabolically active cells, ^{18}O atoms from H_2^{18}O incorporate into phosphoryl groups during each event of ATP hydrolysis. Next, within the cellular phosphotransfer network, the ^{18}O -labeled phosphoryls are distributed among phosphate-carrying molecules (23). The resulting ^{18}O -labeled phosphates can be detected by gas chromatography-mass spectrometry (GC-MS) or ^{18}O -assisted ^{31}P NMR, which allows simultaneous detection labeling of G-6-P, G-3-P, PCr, ATP, and other phosphate metabolites (23, 24).

The aim of this study was to adapt ^{18}O stable isotope labeling technology for cancer cell cultures to discover how changes in ATP γ - and β -phosphoryl turnover and energy distribution between phosphotransfer pathways affects cancer cell aggressiveness. The current study demonstrates that the ^{18}O -based metabolite tagging technology revealed simultaneous depression of rates of ATP synthesis as well as AK, CK, and HK catalyzed phosphotransfer, together with the activity of mitochondrial substrate G-3-P shuttle in aggressive cancer MDA-MB-231 cells representing TNBC. Decreased CK metabolic flux and downregulation of mitochondrial MTCK1A in breast cancer cells indicate rewiring of phosphotransfer circuits. Discovered overexpression of HK2, AK2, and AK6 isoforms in mitochondrial and nuclear compartments suggests that aggressive cancer cells use a strategy of microcompartmentation to support specific cellular functions and promote tumor growth. This study uncovers new features of cancer cell energetics and provides unique insights into the remodeling of the phosphotransfer enzyme network in breast cancer cells that could be used to facilitate the development of new treatment strategies for TNBC.

2 MATERIALS AND METHODS

2.1 Chemicals, Kits and Reagents

All cell lines were obtained from the American Type Culture Collection and were maintained under conditions described by the manufacturer: MCF7 (ATCC, HTB-22), MDA-MB-231 (ATCC, HTB26), MCF10A (ATCC, CRL-10317). MEGM Single Quots Supplements (CC-3151) were purchased from Lonza (Switzerland). Dulbecco's modified Eagle's medium (DMEM), heat inactivated horse serum and human re-combinant Zn insulin were purchased from Gibco (UK). Sodium pyruvate and fetal bovine serum (FBS) were purchased from Corning (USA). Trizol reagent solution was purchased from Life Technologies (Thermo Fisher Scientific, USA). The RNeasy Mini kit was obtained from QIAGEN Sciences (Germany). The High Capacity cDNA Reverse Transcription Kit with RNase Inhibitor was acquired from Applied Biosystems (Thermo Fisher Scientific, USA). H_2^{18}O water was

received as a Cambridge Isotope Laboratories, Inc Research Award donation from the Cambridge Isotope Laboratories, Inc Sodium pyruvate were purchased from Capricorn Scientific GmbH. Creatine kinase (rabbit muscle) was purchased from Roche Diagnostics GmbH (Mannheim, Germany). The myokinase (rabbit muscle), glycerol kinase (*Bacillus stearothermophilus*), methanol, glycerol and cholera toxin from *Vibrio cholerae* were purchased from Sigma Aldrich (USA). Tetra-n-butylammonium hydrogen sulfate (TBHS) was purchased from Acros Organics (New Jersey, USA), MOX (n-Methoxyamine) and MSTFA+1%TMCS derivatization reagents and Pierce BCA Protein Kit from Thermo Fisher Scientific (USA).

2.2 Isolation of RNA, cDNA Synthesis, and qPCR

The expression pattern of phosphotransfer network was determined by analyzing the mRNA level. The total RNA from $\sim 10^6$ cells MCF10A, MCF7 and MDA-MB-231 was isolated using the Trizol reagent. RNA purification was performed by RNeasy Mini Kit with DNase treatment. RNA purity at $A_{260/280}$ ratio (range 2.0–2.1) and concentration at 260 nm were measured by a Nanodrop spectrophotometer. 350 ng of total RNA was used for cDNA synthesis, cDNA was synthesized using a High Capacity cDNA Reverse Transcription Kit with RNase Inhibitor. Synthesized cDNA was subjected to quantitative PCR analysis using the TaqMan® Gene Expression Master Mix and FAM-labelled specific primers (Applied Biosystems/Thermo Fisher Scientific, USA): actin beta – Hs01060665_g1; hexokinase I – Hs00175976_m1; hexokinase II – Hs000606086_m1; creatine kinase brain-type HS00176484_m1; creatine kinase, mitochondrial 1B – Hs00179727_m1; adenylate kinase 1 HS00176119_m1; adenylate kinase 2 HS01123132_g1; adenylate kinase 4 HS03405743_g1. All qPCR experiments were performed on a LightCycler 480 II Real-Time PCR System (Roche, Basel, Switzerland). Reactions were carried out in four replicates for each of three independent experiments. Threshold cycles (Ct) were automatically calculated by the LightCycler 480 software (Roche, Basel, Switzerland). Data were analyzed with the formula $2^{-\Delta\Delta Ct}$ (25), normalized to the endogenous control ActB and expressed as fold change over MCF10A samples.

2.3 Immunoblotting

Cells were washed twice with Ca/Mg-free PBS and then treated with a Tris-Triton X lysis buffer consisting of: 10 mM Tris pH 7.4, 100 mM NaCl, 1 mM EDTA, 1% Triton X-100, 10% glycerol, 0.1% SDS) supplemented with protease inhibitor cocktail (Roche). Lysates were homogenized by a Retsch Mixer Mill at 25 Hz for 2 min, incubated for 20 min on ice, and clarified by centrifugation at 21,000 g for 30 min at 4°C. The concentration of the isolated proteins is determined using the Pierce™ BCA Protein Assay Kit (Thermo Scientific, Rockford, U.S.A.). Protein samples (35 µg) were separated by a 12% Tris-Glycine SDS-PAGE and electrophoretically transferred onto Immobilon® -P PVDF membrane pore size 45 µm (Merck Millipore, Tullagreen, Ireland) by Trans- Blot Semi-Dry Transfer system (Bio-Rad). Membranes were then incubated with the primary antibodies against AK2 (sc374095) or AK6 (10544-1-AP, Proteintech) and

α -tubulin (ab7291) and the HRP conjugated secondary antibodies Goat Anti-Mouse IG (ab97040) and Goat Anti-Mouse IG (ab6721). Mouse kidney homogenate was used as a positive control for AK2. MCF7 serves as a positive control for AK6 recommended by the antibody manufacturer. Blots were developed using SuperSignal™ West Femto Maximum Sensitivity Substrate (Thermo Scientific, Rockford, U.S.A.) and imaged with Biospectrum Multispectral imaging system (Biospectrum 510, UVP, Cambridge, UK).

2.4 Phosphometabolomics Analysis

Experimental work towards analyzing the phosphometabolomic flux through energy production pathways was divided into 4 distinct stages (Stage I – Stage IV). The general workflow is depicted in **Figure 1** and described in technical detail further below.

2.4.1 Stage I: Cell Culturing and Labeling

2.4.1.1 Cell Culturing

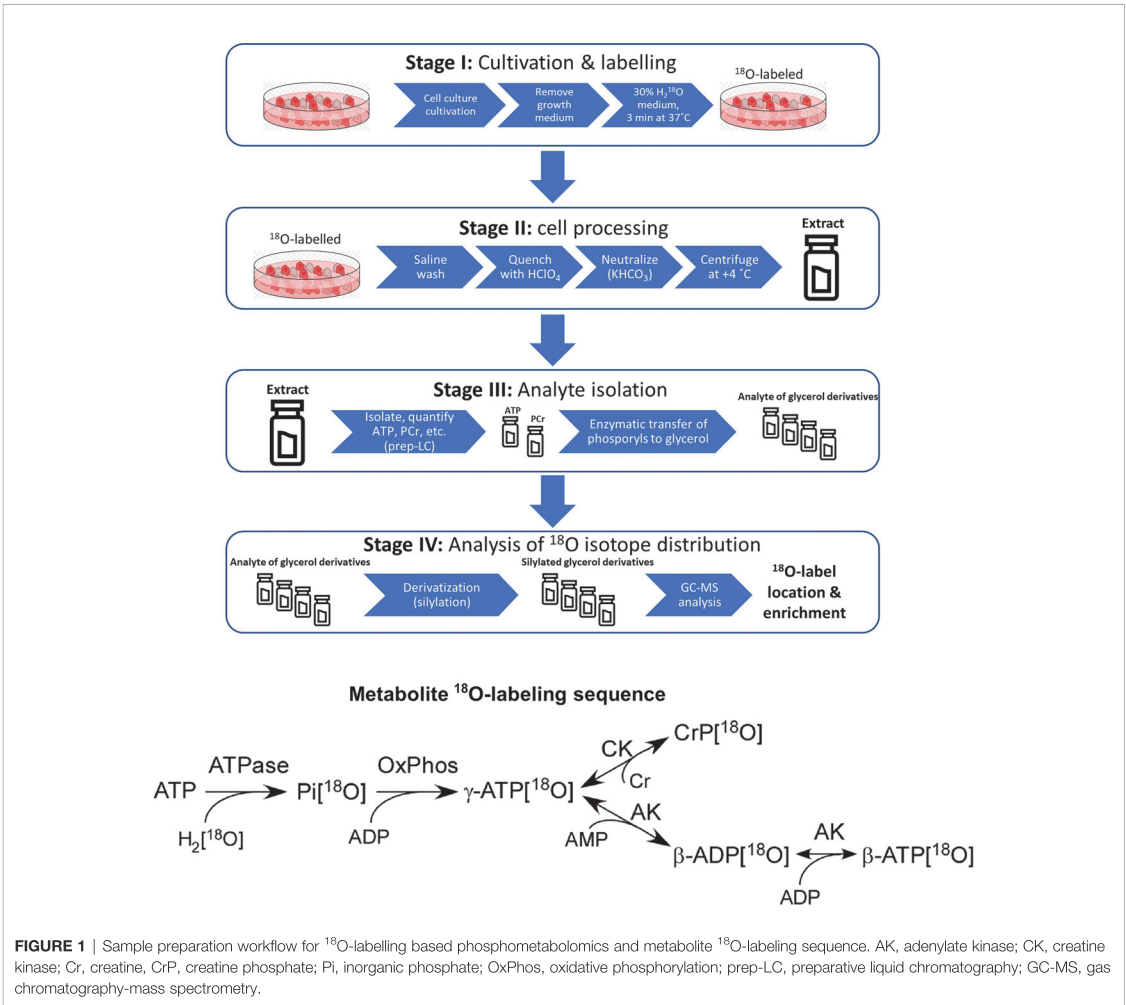
All cells were cultivated at 37°C in 100 mm (seeding density 2.2×10^6 cells) or 35 mm (seeding density 0.3×10^6 cells) Petri dishes in a humidified incubator containing 5% CO₂ in air and were cultured at 5 days (MCF10A) or 2–3 days (MDA-MB-231 and MCF7) intervals. MDA-MB-231 and MCF7 cells were grown as adherent monolayers in high glucose (25 mM) Dulbecco's modified Eagle's medium (DMEM) with stable L-glutamine and sodium pyruvate, supplemented with 10% heat-inactivated fetal bovine serum and 10 µg/mL human recombinant Zn insulin. MCF10A cells were grown in a lower level of glucose (8 mM) in mammary epithelial growth medium (MEGM) supplemented with MEGM SingleQuots Supplements, 5% horse serum and cholera toxin (100 ng/mL). All cell lines were cultured under conditions described by the manufacturer.

2.4.1.2 ¹⁸O Labeling Procedure for Cell Lines

Cultured cells were labelled with ¹⁸O molecule (H₂¹⁸O as a stable isotope source) followed a protocol previously described for establishing the energetic profile of muscle cells (24). After reaching 70% of confluency, medium from cultured cells was removed and replaced with regular medium (DMEM for MCF7 and MDA-MB-231 cells and MEGM for MCF10A cells (see *Cell Culturing* section)) enriched with 30% of H₂¹⁸O, then cells were incubated for 3 min at 37°C. Cells not treated with H₂¹⁸O served as the reference unlabeled background control samples.

2.4.2 Stage II: Cell Processing

The ¹⁸O labeling process was terminated by rapid removal of the growth medium, washing cells with saline, and quenching with 0.6 M ice-cold HClO₄ or ice-cold methanol-water (1:1, v:v) (100 µL for 35 mm dish and 300 µL for 100 mm dish). Petri dishes with cells were immediately frozen in liquid nitrogen to quench the cells' metabolism. Cells were scraped from the Petri dishes with a liquid nitrogen cooled spatula and transferred into cold microcentrifuge tubes, which were immediately placed into liquid nitrogen. Samples were briefly allowed to warm until first signs of thawing could be observed, then centrifuged at 4°C at 10,000 g for 5 min. The supernatant of methanol-water quenched cells was immediately



placed into liquid nitrogen, and samples were stored at -80°C until they were analyzed by GC-MS. The supernatant of HClO_4 quenched cells was removed and transferred to a microcentrifuge tube containing 2 M KHCO_3 35 μL for 35 mm dish and 105 μL for 100 mm dish to neutralize the acid and adjust pH to approximately 7.4. The resulting suspensions were centrifuged at 10,000 g for 15 min at 4°C to remove the salt. The supernatant was adjusted to 1 mL with ultrapure water and stored at -80°C until analysis. The remaining pellets were stored in 300 μL of 1%SDS containing 0.1 M NaOH at -20°C for protein assay with Pierce BCA Protein Kit.

2.4.3 Stage III: Analyte Quantification and Isolation

2.4.3.1 Analyte Quantification

50 μL of the sample was used for phosphometabolite quantification for 100mm dish and 20 μL for 35mm dish. ATP and PCr levels and ATP/ADP ratios were determined by a UPLC method adapted and

modified from (15, 26). Analytes were resolved on a reversed-phase C18 column (Separon SGX 5 μm 3x150 mm, Tessek, Czech Republic) on a Waters Acquity UPLC equipped with a PDA detector. The mobile phase consisted of a phosphate buffer (100 mM) with TBHS (10 mM) and methanol [water:methanol; 60:40 (v:v)] at 0.4 mL \cdot min $^{-1}$ flow rate. Gradient elution was applied, and all metabolites were separated in 30 min, where water: methanol percentage was raised from zero to 90%. PCr and nucleotides were simultaneously detected at 210 nm and 254 nm, respectively. ATP and PCr levels were normalized per mg of cell protein.

2.4.3.2 Quantitative Analysis of Oxidative Phosphorylation and Glycolysis Contribution to Total ATP Production

To estimate ATP production through mitochondrial respiration and glycolysis, we measured ATP/ADP ratios in the presence of OXPHOS (rotenone, antimycin A and oligomycin 1 $\mu\text{g}/\text{mL}$) or glycolysis (2-deoxyglucose) inhibitors, as described previously

(27). As 2-deoxyglucose is a competitive inhibitor, it was used at equimolar concentrations with medium glucose levels for MCF7, MDA-MB-231, and MCF10A.

2.4.3.3 Phosphometabolite Isolation

Cellular phosphometabolites (i.e. ATP and PCr) were isolated by LC (GE Healthcare ÄKTAPrime Plus) using a Mono Q HR 5/5 ion-exchange column (Pharmacia Biotech) with triethylammonium bicarbonate (TEAB) buffer pH 8.8 (gradient from 0-85%) at a 0.4 ml min⁻¹ flow-rate, equipped with a UV detector fixed at 280 nm. All phosphometabolite fractions were collected by LC using this method, unless stated otherwise. Each sample was divided into two fractions, PCr and ATP, which were stored at -80 and -20°C, respectively.

Enzymatic processing reactions were used to transfer phosphoryl groups from ATP and PCr to glycerol. The γ -phosphoryl of ATP was transferred to glycerol by glycerol kinase, and β -phosphoryls of ATP was transferred to glycerol by coupled catalytic reactions of adenylate kinase and glycerol kinase. The phosphoryl group of PCr was transferred to glycerol by combined catalytic reactions of creatine kinase and glycerol kinase. Particular procedures in further detail:

ATP (γ -phosphoryl of ATP) fractions were lyophilized and reconstituted with a 200 μ L mixture of ultrapure water, 10mM TEAB (pH 8.8), 2mM MgCl₂, 5mM glycerol, and 1 μ L of glycerol kinase. The mixture was incubated at 37 °C for 1 hour, and fractions of G3P (γ -phosphoryl of ATP) and ADP (β -phosphoryl of ATP) were collected by LC.

ADP (β -phosphoryl of ATP) fractions were lyophilized and reconstituted with 200 μ L mixture of ultrapure water, 10mM TEAB (pH 8.8), 2mM MgCl₂, 5mM glycerol, 1 μ L of glycerol kinase, and 1 μ L of adenylate kinase (myokinase). The mixture was incubated at 37°C for 2 hours, and the fraction of G3P (β -phosphoryl of ATP) was collected by LC.

The phosphoryl group from PCr was transferred to G3P in a two-stage process:

The phosphoryl from PCr was transferred to ADP. PCr fraction of a sample was lyophilized and reconstituted in 200 μ L mixture of ultrapure water, 25mM TEAB (pH 8.8), 1mM MgCl₂, 200 μ M ADP, 20 μ M diadenosine pentaphosphate, 1mM dithiothreitol, and 500 μ g/mL creatine kinase. The mixture was incubated 37°C for 2 hours, and fractions of ATP were collected by LC.

The phosphoryl from ATP was transferred to glycerol. ATP fractions were freeze-dried/lyophilized and reconstituted in 200 μ L mixture of ultrapure water, 10mM TEAB (pH 8.8), 2mM MgCl₂, 5mM glycerol, and 1 μ L of glycerol kinase. The mixture was incubated at 37°C for 1 hour, and fractions of G3P (phosphoryl of PCr) were collected by LC.

2.4.4 Stage IV: Analysis of ¹⁸O Isotope Distribution

Distinct samples containing phosphoryls of γ -ATP, β -ATP, PCr enzymatically transferred to G3P and G6P, G3P (extracted by methanol-water) were converted to respective trimethylsilyl derivatives with Tri-Sil as the derivatization agent. ¹⁸O

incorporation rate into phosphometabolites was determined with a GC-MS operated in select ion-monitoring mode (Agilent 7890 GC connected to an Agilent 6890 MSD, equipped with a 5 m deactivated precolumn and a 30m HP-5MS analytical column.

To perform derivatization reactions: Samples containing phosphoryls of γ -ATP β -ATP, PCr enzymatically transferred to G3P and G6P, G3P (extracted by methanol-water) were lyophilized and reconstituted with 10 μ L of MOX (20 mg/mL in pyridine), vortexed thoroughly for 15 seconds and incubated at 30°C for 90 min. 40 μ L of MSTFA+1%TMCS was added, vortexed for 15 seconds, and incubated at 37°C for 30 min. Samples were cooled to room temperature for 5 minutes, centrifuged at 12000 g for 3 minutes, and transferred (supernatant) to vials (200 μ L inserts) for GC-MS analysis.

The instrument was operated in split injection mode with a temperature gradient of 60°C to 325°C with the rate of 10°C/min, hold time 10 min. Injection volume was 5 μ L, split ratio 10:1, inlet temperature 250°C and flow rate (He) 1.1 mL/min in scan mode: For G3P ions were selected at 357, 359, 361, and 363 m/z and for G6P were selected at 387, 389, 391 and 393 m/z, which represent the isotopes of ¹⁶O replaced with ¹⁸O at one, two or three positions in the phosphoryl group. Isotope abundances were derived from integrals of their peak areas, which correspond to the fractions of the replaced oxygens.

The cumulative percentage of phosphoryl oxygens replaced by ¹⁸O in the metabolites was calculated using the formula:

$$\begin{aligned} & [\%^{18}\text{O}_1 + 2(\%^{18}\text{O}_2) + 3(\%^{18}\text{O}_3) + \dots + \\ & n(\%^{18}\text{O}_n) / [n(\%^{18}\text{O in H}_2\text{O})], \end{aligned}$$

where n is the total number of phosphoryl oxygen sites in the metabolite

2.5 Bioinformatics Analysis

AK2 and MtCK1A gene analysis of primary HBC was based on the Cancer Genome Atlas (TCGA) platform (<http://www.cbioportal.org/>) where the Pan-Cancer Atlas database was used. Further information on parameters and conclusions is available in **Figures 4, 5**.

To perform Kaplan–Meier (K–M) analysis on AK2 and AK6 gene we used an open access online survival analysis tool (28). We primarily analyzed data from Lymph node positive and TNBC patients. For breast cancer patients' hazard-ratios were calculated using best auto-selected cutoff. K–M curves were created using the online K–M plotter (<https://kmplot.com/analysis/index.php?p=service&cancer=breast>). The latest 2021 version of the database was utilized for all these analyses.

2.6 Statistical Analysis

Data are expressed as mean \pm SEM of taken over ≥ 3 independent experiments, ≥ 3 technical replicates per experiment. Differences between experimental groups were determined by ANOVA followed by Holm–Sidak tests and for K–M analysis Log-rank test was performed. A p value of less than 0.05 was considered significant.

3 RESULTS

3.1 Bioenergetic Status of HBC Cells: Increased Intracellular ATP Level, Reduced ATP Turnover and Shift of ATP Production From OXPHOS to Glycolysis

Unlike in normal cells, hybrid metabolic state, where glycolysis and OXPHOS are simultaneously active, was observed in TNBC cells (5). Hence, the bioenergetic status of HBC cells was evaluated by measuring the static intracellular ATP levels and ATP/ADP ratios. Moreover, to assess the dynamics of energy fluxes *via* OXPHOS, we applied ^{18}O -labeling of ATP by labeling of γ -ATP [^{18}O]. Labeling of γ -ATP [^{18}O] predominantly occurs in mitochondria by phosphorylating ADP with inorganic phosphate Pi [^{18}O] derived from cellular ATPase reactions ($\text{ATP} + \text{H}_2^{18}\text{O} \rightarrow \text{ADP} + \text{Pi}^{18}\text{O}$). Measurements revealed a significant reduction in the ^{18}O -labeling of γ -ATP of MCF7 and MDA-MB-231 cell lines compared to control cells (Figure 2A), indicating a decrease in OXPHOS activity. Diminished γ -ATP [^{18}O] turnover is a new feature of breast cancer cell metabolism, reflecting intrinsic rearrangements in energetic networks.

Analysis of intracellular ATP levels revealed an increase in ATP content in both cancer cell lines (Figure 2B). A slightly diminished ATP/ADP ratio was observed in both HBC cell lines (Figure 2C), indicating a different energy state. The contribution of glycolysis or OXPHOS into energy metabolism was assessed using the respective inhibitors and by observing changes in the ATP/ADP ratio. We observed apparent differences between cancer and control cells. A substantial decrease in the ATP/ADP ratio in the presence of a glycolysis inhibitor (2-deoxyglucose) in MCF7 and MDA-MB-231 cells, compared to MCF10A, suggests that glycolysis plays a significant role in energy production in HBC cells (Figure 2D). At the same time, inhibition of OXPHOS (with oligomycin, rotenone, and antimycin A) had the weakest effect on the ATP/ADP ratio in MDA-MB-231 cells and the strongest in the MCF10A cells (Figure 2D). Based on the pattern of changes in ATP/ADP ratios, we conclude that in MCF7 and MDA-MB-231 cells, most ATP (70%) was produced *via* the glycolytic pathway, indicating a metabolic shift compared to MCF10A cells, where the main provider of ATP was OXPHOS (Figure 2D).

3.2 Glycolytic Flux, HK Expression Pattern in MDA-MB-231 Cells, and Mitochondrial Substrate Shuttle as a Link Between OXPHOS and Glycolysis in MCF7 Cells

As we observed an increased contribution of glycolytic pathway to energy production in breast cancer cells compared to control cells. Therefore, we evaluated the HK expression pattern in those cells. Figure 2A illustrated that TNBC cells (MDA-MB-231) had four times higher HK2 mRNA expression levels than had Luminal A (MCF7) and normal breast epithelial cells (MCF10A). Nevertheless, no difference in HK1 expression level was observed between MDA-MB-231 cells and control cell lines (MCF10A cells) (Figure 3A). For MCF7 cells, even slightly lower

HK1 expression level was observed compare to MDA-MB-231 cells (Figure 3A).

Next, we estimated how distinct HK pattern (Figure 3A) and increased glycolytic activity (Figure 2D) of breast cancer cells is related with glycolytic flux. Observation of the ^{18}O -labeling of G-6-P [^{18}O], which reflects the glucose consumption rate of energy metabolism, does not reveal any difference between MCF10 and MCF7 cells (Figures 3B, D).

The glycolytic flux, however, was significantly lower in MDA-MB-231 cells compared to MCF10 cells. At the same time, inhibition of glycolysis in MDA-MB-231 cells had a similar suppressive effect on the ATP/ADP ratio as in MCF7 cells (Figure 2D), indicating nearly equal activity of glycolysis in these cells. This discrepancy could be due to the lower turnover and labeling of γ -ATP [^{18}O], a precursor for G-6-P [^{18}O]. Yet, this was not the case in MCF7 cells, which also had lower γ -ATP [^{18}O]. Moreover, we did not observe correlation between HK level and G6P flux in MDA-MB-231 cells (Figures 3A, B).

Metabolic flux through the G-3-P shuttle, which reflects the mitochondrial substrate shuttle (Figure 3D), is an important supplier of reducing equivalents to mitochondria, especially for MCF7 cells. We observed that the MCF7 cell line is clearly distinguished by its high levels of labeled G-3-P [^{18}O] (Figure 3C). Since HK2 expression in MCF7 cells was low, it can be assumed that the interaction between OXPHOS and glycolysis is realized *via* the G-3-P shuttle in these cells.

3.3 A Decreased CK Metabolic Flux and a Lower PCr Level Is Associated With Downregulation of Mitochondrial CKMT1A in Breast Cancer Cells

Recently, Kurmi et al. reported that the PCr energy shuttle has an important role in maintaining breast cancer cell homeostasis (20). In current work, diminished energy flux of PCr was observed in both Luminal A and TNBC cells compare to normal breast epithelia cells (Figures 4A, B). Labeling of PCr [^{18}O] revealed approximately three-fold lower CK metabolic flux in MCF7 and MDA-MB-231 cells than in MCF10A cells (Figure 4B). Also, MCF7 and MDA-MB-231 cells had two-fold lower intracellular PCr levels compared to control cells (Figure 4A). An analysis of CKB and CKMT1A genes was conducted to evaluate how the decreased fluxes are associated with changes in CK gene expression. Analysis of mRNA level for all examined groups (Figures 4C, D) revealed that in both cancer cell lines CKMT1A was downregulated compared to MCF10A cells (Figure 4C). In contrast, mRNA levels of cytosolic CK-B were significantly overexpressed in both cancer cell lines (50- and 800-fold in MCF7 and MDA-MB-231, respectively) (Figure 4D). In addition, analysis of the TCGA database revealed that CKMT1A mRNA levels are elevated only in 5% of HBC patients. Furthermore, an elevation of CKMT1A expression levels was associated with amplification of CKMT1A copy number (Figure S1). Out of high MTCK1A level, 31% belong to the TNBC group and 20% of patients to Luminal A group, whereas most (49%) belong to Luminal B and HER2-positive groups (Figure 4E). Nevertheless, the only statistically significant

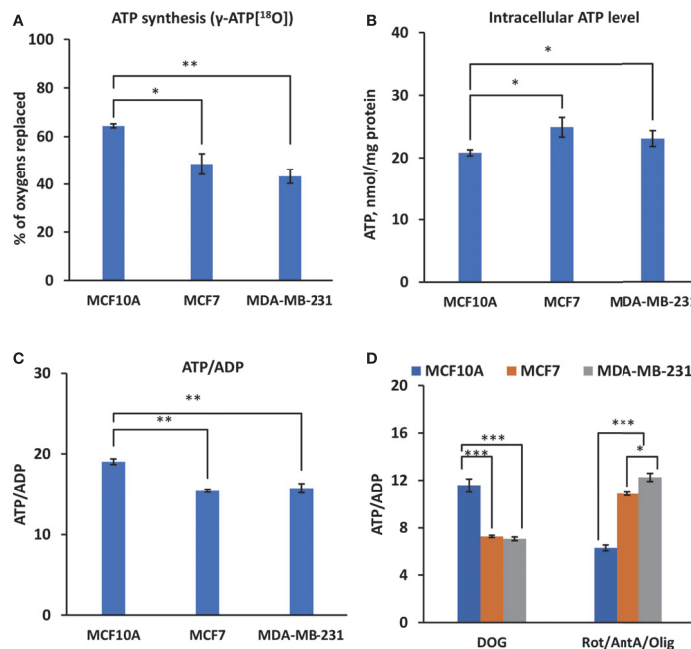


FIGURE 2 | Assessment of γ -ATP[^{18}O] turnover and bioenergetic profile in Luminal A, Triple-negative breast cancer cells, and control cells. Comparative analysis of intracellular (A) ^{18}O -metabolic labeling of γ -ATP, reflecting ATP synthesis via OXPHOS. (B) Changes in ATP level and (C) ATP/ADP ratio between Luminal A (MCF7), Triple-negative (MDA-MB-231) breast cancer, and control cells (MCF10A). (D) Effect of glycolysis and OXPHOS inhibition on the intracellular ATP/ADP ratio. All data presented as mean \pm SEM (ANOVA followed by Holm-Sidak test $n=3-5$). *, ** and *** indicate a statistically significant differences between the mean values; $p < 0.05$, $p < 0.01$ and $p < 0.001$, respectively. AntA – antimycin A, DOG – 2-deoxyglucose, Olig – oligomycin, Rot – rotenone.

difference in CKMT1A expression was observed between the primary HER2-positive breast cancer subtype and normal tissue (Figure 4F and Figure S2). According to the TCGA database, CKMT1A is deleted in 40% of breast cancer patients (Figure 4G), most of them are belonging to TNBC and Luminal A groups (71% and 22%, respectively). Altogether, this data indicates that PCr circuit is disrupted and displays low activity in Luminal A and TNBC cells, probably due to downregulation of CKMT1A.

3.4 Decreased AK Flux and AK2 and AK6 Isoform Overexpression in MDA-MB-231 Cells

Analysis of the four AK genes (AK1, AK2, AK4, and AK6) mRNA expression in breast cancer cells revealed several alterations in the composition of the AK network. Reprogramming of the AK network in MDA-MB-231 cells (Figure 5A) is associated with the upregulation of AK2 and the nuclear/cytosolic AK6 isoforms. At the same time, expression of the cytosolic AK1 isoform and mitochondrial AK4 were lower in MCF7 and MDA-MB-231, compared to MCF10A (control). Analysis of the TCGA database revealed that the AK2 mRNA level is elevated only among 6% of HBC patients. Yet, most

patients with high AK2 mRNA levels are in the TNBC group (80%), while only 5% are in the Luminal A group (Figure 5C). To strengthen results statistical analysis was performed. Only in AK2 gene expression statistical differences were found between TNBC and normal breast tissue (Figure 5B and Figure S3). In addition, expression of AK6 and AK2 at the protein level in all cell lines studied was demonstrated by western blot (Figure S4). We did not noticed correlation between protein level and Ak2 and Ak6 gene expression level (Figure S4). To evaluate the clinical significance of AK2 and AK6, we used K-M survival analysis (Figures 5D, E). Interestingly, high AK2 levels of tumors were associated with poor outcome of distant metastasis-free survival in breast cancer patients with positive lymph node compared to those tumors which have low level of AK2 (Figure 5D). Moreover, we found that AK6 affected recurrence-free survival among TNBC patient (Figure 5E). Survival analysis showed that TNBC patients with high AK6 have poor outcome compared to TNBC patients with low level of AK6 (Figure 5E). These results indicate that AK2 and AK6 gene expression could have considerable clinical significance in diagnosing aggressive breast cancer. A unique property of AK catalysis is the ability to allow cellular utilization of the second high-energy phosphoryl of ATP ($\text{A-}\alpha\text{P-}\beta\text{P-}\gamma\text{P}$). ^{18}O -metabolic

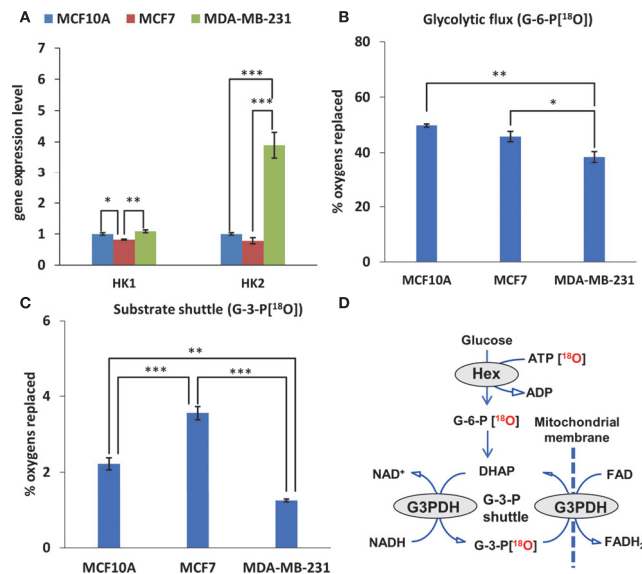


FIGURE 3 | Glycolytic and mitochondrial substrate shuttle profile of Luminal A, Triple-negative breast cancer cells, and breast control cells. **(A)** HK (fold change of the mRNA level) isoform expression pattern in Luminal A (MCF7), Triple-negative (MDA-MB-231) breast cancer cells, and breast control cells (MCF10A). ¹⁸O-metabolic labeling of **(B)** G-6-P [¹⁸O] and **(C)** G-3-P [¹⁸O] reflecting glycolytic and substrate shuttle activities, respectively. **(D)** Schematic representation of metabolite ¹⁸O-labeling allowing for tracking glycolytic and G-3-P substrate shuttle dynamics. All data are presented as mean ± SEM (ANOVA followed by Holm-Sidak test $n=3$). *, ** and *** indicate statistically significant difference between the mean values, $p < 0.05$, $p < 0.01$, and $p < 0.001$, respectively. HK – hexokinase; G-6-P – glucose-6-phosphate; G-3-P – glyceral-3-phosphate.

labeling of β -ATP revealed a reduced β -ATP turnover in MCF7 and MDA-MB-231 cells, compared to control MCF10A cells. This suggests a decreased AK flux in breast cancer cells (Figure 5F). Altogether, this data indicates that decreased AK flux is probably associated with the downregulation of AK1 and AK4 in HBC cells. The current study revealed that both AK6 and AK2 are promising biomarkers for TNBC.

4 DISCUSSION

The stable isotope (²H, ¹³C, ¹⁵N, ¹⁸O) tracer-based metabolomics technologies are used for metabolic research (29, 30). Water-based ¹⁸O-labeling has several advantages over ¹³C and ¹⁵N labeling. Firstly, the cellular water uptake is fast because water has a high diffusion coefficient (2.3 $\mu\text{m}^2/\text{ms}$). Secondly, ¹⁸O labeling period is very short compared to the time it takes to do ¹³C or ¹⁵N labeling (30). Based on the Encyclopedia of Genes and Genomes (KEGG) database, approximately 3000 enzyme reactions used water as a substrate (30). In general, stable isotope-labeled water (²H₂O, H₂¹⁸O, and ²H₂¹⁸O) have been used to study cellular anabolic and catabolic processes, including in cancer cells (30–32). Most important, numerous studies have shown that usage of ¹⁸O-enriched water is safe for humans (22).

It is well known that the backbone of cellular energy metabolism is high-energy phosphoryl turnover and dynamics of ATP synthesis and hydrolysis in OXPHOS and glycolytic pathways, and phosphoryl exchange through phosphotransfer pathways (9). However, knowledge about flexibility of phosphotransfer network in cancer cells has been limited. It is first time when ¹⁸O labeling method was applied to study dynamics of ATP γ - and β -phosphoryl turnover and metabolic flux through phosphotransfer pathways in cancer cells. The objective of this work was to apply the ¹⁸O isotope labeling technology and GC-MS-based phosphometabolite analysis to study the dynamics of the HBC energy metabolism. We directly demonstrate that compare to normal breast cells, HBC cells have a lower γ/β -ATP [¹⁸O] turnover rate. The lower γ -ATP [¹⁸O] turnover rate was associated with reduced OXPHOS activity in those cells. As a result, we observed energy metabolism shifting towards glycolysis in HBC cells. Moreover, we also monitored alterations in fluxes through HK (G-6-P [¹⁸O]) CK (PCr [¹⁸O]) and AK (β -ATP [¹⁸O]) phosphotransfer pathways as well as mitochondrial substrate shuttle (G-3-P [¹⁸O]) in HBC cells.

Recent work has demonstrated that high-ATP breast cancer cells has an aggressive phenotype with inclination to metastasis and they are multi-drug resistance, as well (33). Similarly, we observed, in both HBC cell lines, elevated intracellular ATP levels

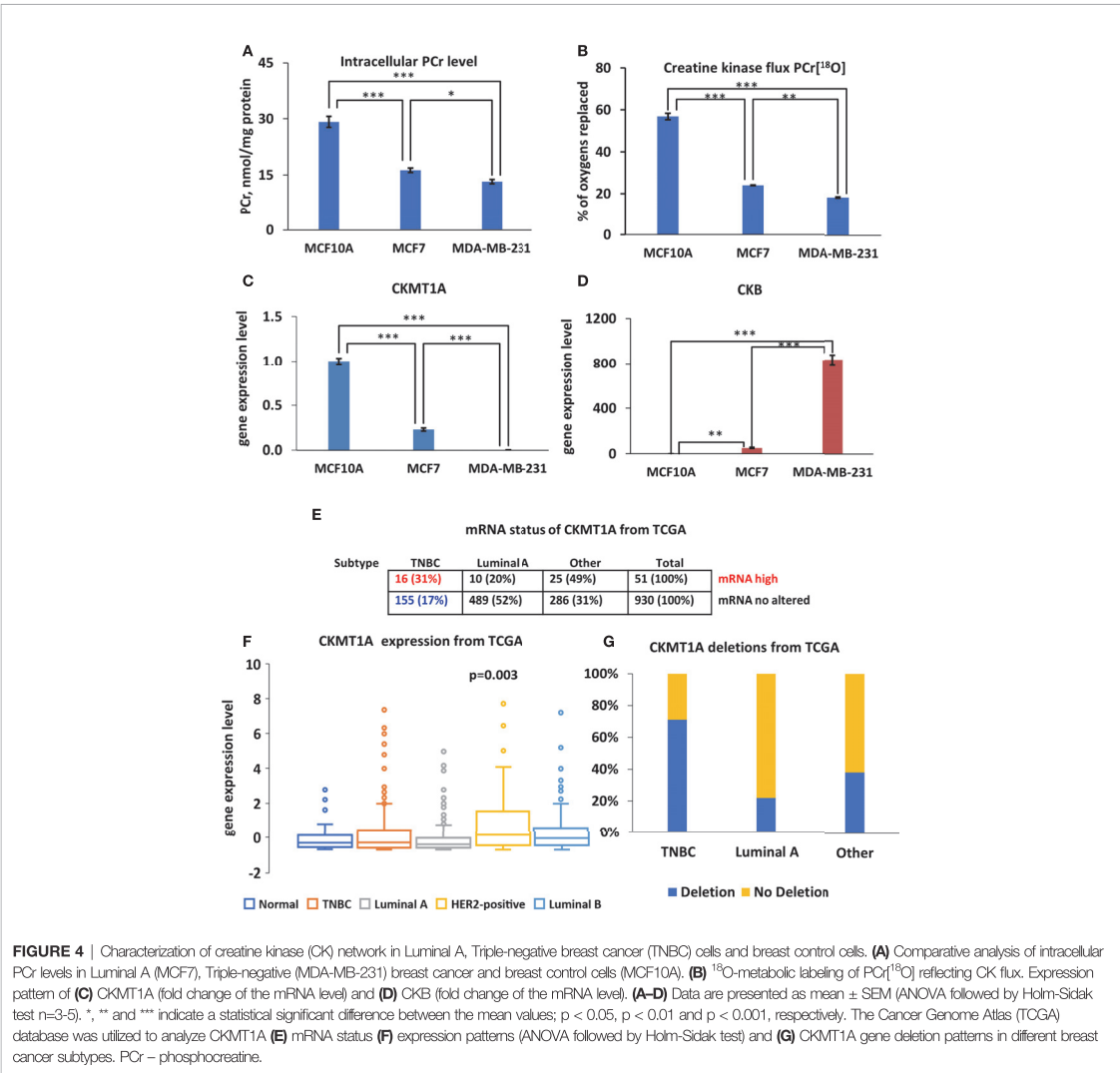


FIGURE 4 | Characterization of creatine kinase (CK) network in Luminal A, Triple-negative breast cancer (TNBC) cells and breast control cells. **(A)** Comparative analysis of intracellular PCr levels in Luminal A (MCF7), Triple-negative (MDA-MB-231) breast cancer and breast control cells (MCF10A). **(B)** ¹⁸O-metabolic labeling of PCr[¹⁸O] reflecting CK flux. Expression pattern of **(C)** CKMT1A (fold change of the mRNA level) and **(D)** CKB (fold change of the mRNA level). **(A–D)** Data are presented as mean ± SEM (ANOVA followed by Holm-Sidak test n=3–5). *, ** and *** indicate a statistical significant difference between the mean values; p < 0.05, p < 0.01 and p < 0.001, respectively. The Cancer Genome Atlas (TCGA) database was utilized to analyze CKMT1A **(E)** mRNA status **(F)** expression patterns (ANOVA followed by Holm-Sidak test) and **(G)** CKMT1A gene deletion patterns in different breast cancer subtypes. PCr – phosphocreatine.

which are associated with shifting their energy metabolism towards the glycolytic pathway, compared to the control breast epithelial cell line. Other investigators have also noted that several cancer cell lines, including HBC, have increased ATP levels (34). High ATP level in cancer cells may be related with the serine/threonine protein kinase (AKT) activation. *In vitro* study has shown that AKT regulates intracellular ATP level *via* increasing activity and expression of glycolytic enzymes (35). Moreover, a higher intracellular ATP could be beneficial to cancer cells in order to keep the intracellular ATP/ADP ratio low. *In vitro* studies demonstrated that low intracellular ATP/ADP allows cancer cells to maintain a high glycolytic activity in conditions where OXPHOS activity is suppressed or altered (36).

The present study demonstrated that in HBC cell lines, decline in OXPHOS and low intracellular ATP/ADP ratio enhanced glycolytic activity of cancer cells. In MCF7 cells, glycolysis was accompanied by increased flux through the G-3-P shuttle, while MDA-MB-231 cells had overexpressed HK2 instead. In current study, we did not observe a correlation between HK2 expression and G-6-P[¹⁸O] fluxes for MDA-MB-231 cells. It is known that enzyme expression level or activity sometimes is different from metabolic flux. Enzyme activity represents the upper metabolic limit, yet actual flux depends on current metabolic needs. For example, in the heart muscle with high AK and CK activities, ¹⁸O-measured metabolic flux represents only a fraction of total activity (37). Moreover, in failing hearts, the total activity of

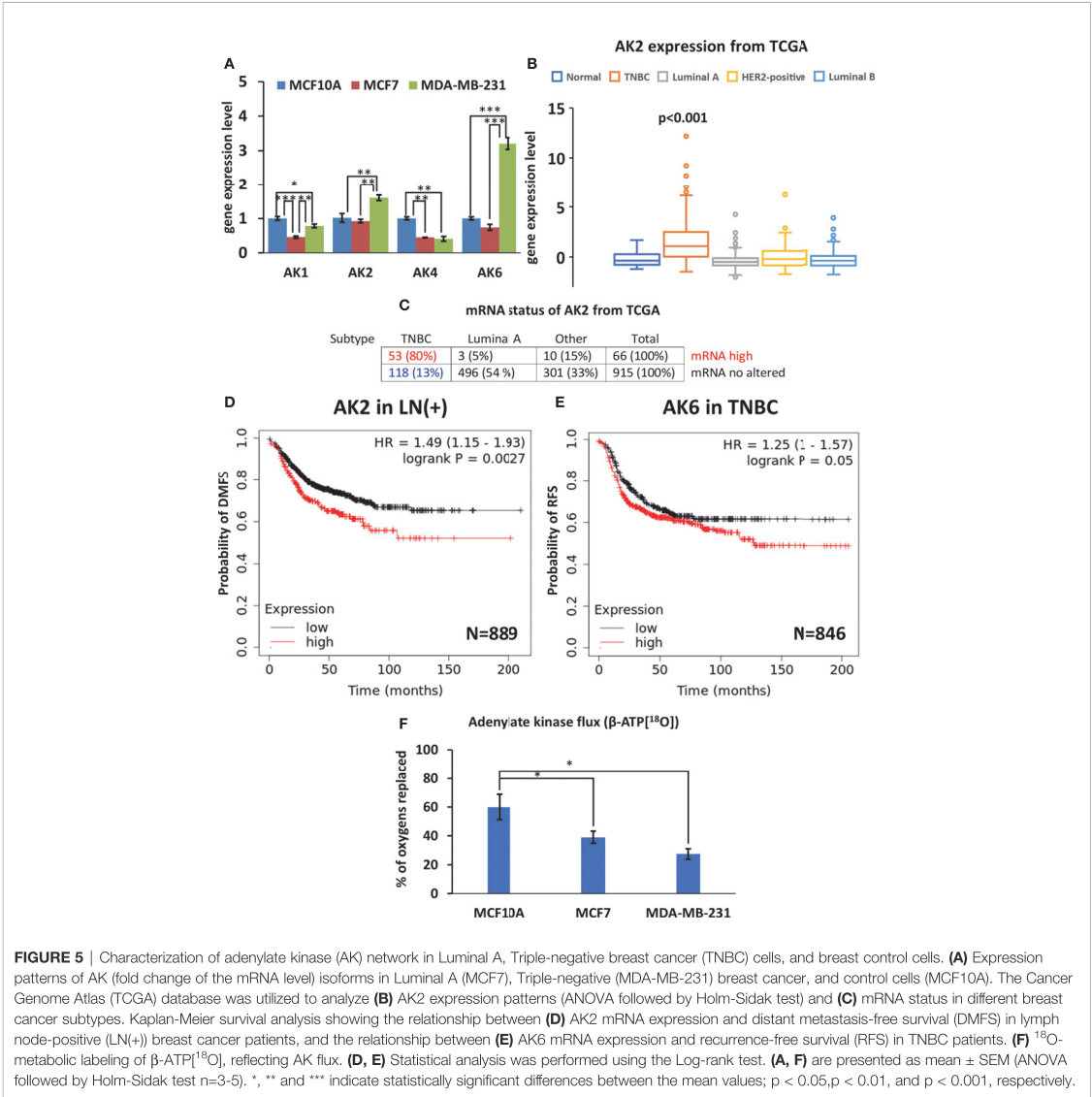


FIGURE 5 | Characterization of adenylate kinase (AK) network in Luminal A, Triple-negative breast cancer (TNBC) cells, and breast control cells. **(A)** Expression patterns of AK (fold change of the mRNA level) isoforms in Luminal A (MCF7), Triple-negative (MDA-MB-231) breast cancer, and control cells (MCF10A). The Cancer Genome Atlas (TCGA) database was utilized to analyze **(B)** AK2 expression patterns (ANOVA followed by Holm-Sidak test) and **(C)** mRNA status in different breast cancer subtypes. Kaplan-Meier survival analysis showing the relationship between **(D)** AK2 mRNA expression and distant metastasis-free survival (DMFS) in lymph node-positive (LN(+)) breast cancer patients, and the relationship between **(E)** AK6 mRNA expression and recurrence-free survival (RFS) in TNBC patients. **(F)** ¹⁸O-metabolic labeling of β -ATP^[18O], reflecting AK flux. **(D, E)** Statistical analysis was performed using the Log-rank test. **(A, F)** are presented as mean \pm SEM (ANOVA followed by Holm-Sidak test n=3-5). *, ** and *** indicate statistically significant differences between the mean values; p < 0.05, p < 0.01, and p < 0.001, respectively.

adenylate kinase is decreased, yet metabolic flux is increased. Metabolic fluxes catalyzed by adenylate kinase, creatine kinase, and hexokinase correlate with heart functional load at the same level of total activity (38). Another possible explanation could be the different intracellular localization of HK2 in studied cells. It has been demonstrated that HK2 binding to mitochondria facilitates the G-6-P channeling into glycolysis in cancer cells. At the same time, when HK2 is localized in the cytosol, the G-6-P is directed into the pentose phosphate shunt (16). Further studies are needed to clarify how HK expression pattern and localization influence the glycolytic flux in breast cancer cells.

Metabolic reprogramming in breast tumors usually depends on HBC molecular subtypes. It was recently reported, that the PCr energy shuttle has an important role in maintaining cell homeostasis in HER2+ positive HBC (20). Our study shows that the suppression of PCr energy shuttle in MCF7, and MDA-MB-231 cells, is associated with CKMT1A downregulation in both cell lines. Diminishing of CKMT1 is probably not specific for

TNBC and Luminal A alone but is also common for other cancers like colorectal cancer (39), neuroblastoma (13), prostate cancer (40), and sarcomas (41). Recent studies have shown that inhibition of CKMT1 decreased intracellular ATP levels in leukemia and HER2+ type of HBC (20, 42). However, in the current study, no such reduction in ATP level were noticed in breast cancer cells. On the contrary, we observed increased intracellular ATP levels in MDA-MB-231 and MCF7 compared to MCF10A, normal epithelial cells. The absence of CKMT1A could be compensated by cytosolic CK-B, which has been shown to be overexpressed in some tumors, including HBC (43, 44). In the current study, CKB was up-regulated in both MCF7 and MDA-MB-231 cells. A study on colon cancer cell line SW480 demonstrated that overexpression of CKB increased intracellular PCr levels (45). In our case, the elevation of the CKB level did not protect breast cells from diminishing of PCr levels. Since cytosolic CK functionally and structurally coupled with glycolysis (7) then overexpression/diminishing of BB-CK can alter glycolytic rate in cancer cells. It was found that knockdown of CKB cells decreased glycolysis in ovarian cancer (19). Due to this fact increased glycolysis in MCF7 and MDA-MB-231 may be associated with overexpression of CKB in those cells. Further studies are needed to understand how CK network is integrated into glycolytic network in breast cancer cells.

Our previous study showed that HBC tissue had increased AK activity compared to normal breast tissue (46). We found that in normal breast tissue, most of the total AK activity (80%) is performed by the cytosolic AK1 isoform, and the mitochondrial AK2 isoform activity is about four-fold lower. At the same time, in human HBC tissue, the proportion of AK1 decreases slightly, and the proportion of AK2 increases. The current experiment demonstrates that HBC cells have a low AK-mediated metabolic flux accompanied by downregulation of cytosolic AK1 and mitochondrial AK4 genes in both HBC cell lines. Previously, a similar effect on AK-mediated flux was observed in AK1-knockout skeletal muscle. ^{18}O labeling study demonstrated that knockout of AK1 in skeletal muscles suppressed β -ATP flux (47). Another study showed that knockout of mitochondrial AK4 disrupt mitochondrial ability to maintain normal intracellular nucleotide level (48). They found that in cancer cells silencing of AK4 gene increase intracellular ATP level as well as ATP/ADP ratio *via* enhancing glycolytic flux. Similarly, in the current study, we detected high ATP levels and ATP/ADP ratios in MCF7 and MDA-MB-231 cells with the raised glycolytic rate in those cells. This demonstrates that significant type-specific changes and metabolic adjustments in the AK phosphotransfer network occur in HBC cells.

Specific differences in Ak2 and Ak6 gene expression in Luminal A and TNBC could reflect the different malignant potential of these cells. On the one hand, it has been shown that AK2 is a repressor protein of growth for breast tumor cell lines (49). On the other hand, specific overexpression of AK2 has been demonstrated in ER-negative breast tumors (50). The current study, similarly to Speers et al. work, confirmed that AK2 is up-regulated in TNBC cell line. Our analysis of AK2

mRNA status in different HBC types, based on the TCGA database, shows that HBC tumors with a high AK2 mRNA expression are likely to be of the TNBC type. Moreover, dataset analysis showed that AK2 was a prognostic marker for aggressive breast cancer with positive lymph node. Recent studies demonstrated that AK2 is overexpressed in Lung cancer cells (51) and T-cell acute lymphoblastic leukemia cells (52). For Lung cancer, the positive expression of AK2 is associated with poor prognosis of pulmonary adenocarcinoma patients (51).

In this study, we found that not only the AK2, but also the AK6 gene is up-regulated in MDA-MB-231 cells. Recently, the AK6 high expression level was found in breast cancer and colorectal cancer (53, 54). In the case of colorectal cancer, the high AK6 is also correlated with a worse patient prognosis (53). In cells, the AK6 is predominantly located in the nuclear compartment, where it is required for ribosome formation and thus promotes protein synthesis and cell growth (53). It was demonstrated that reduction of AK6 expression in cancer cells disrupts ribosome assembly and abolishes tumorigenesis of cancer cells (53). Moreover, experiments on colon cancer cell line SW480 and human testicular carcinoma NT2 revealed that AK6 gene silencing or overexpression suppressed or promoted cancer cells' invasion potential, respectively (54, 55). Furthermore, the same studies demonstrated that knockout of AK6 induces apoptosis in malignant cells (54, 55). Therefore, AK6 could also reflect more significant malignant potential of TNBC. Interestingly, when located at the cytosolic compartment, AK6 behaves as a metabolic modulator of the cancer cells. A study on colorectal cells demonstrated that in colorectal cancer cells the AK6 can hyperactivate glycolytic metabolism by phosphorylating lactate dehydrogenase A (54). It is likely that AK6 upregulation is specific to TNBC where it supports aerobic glycolysis in malignant cells.

Recently, we have hypothesized that alteration in the AMP signaling is a key event of malignant transformation of a cell (56). Mainly, disruption of AMP signaling through AMP-activated protein kinase (AMPK) leads to reduced control over cell cycle and proliferation. The AMPK is a master regulator of anabolic and catabolic processes which activity is managed by intracellular AMP/ADP : ATP level (57). The main activator of AMPK is AK-catalyzed pathway which allosterically activates AMPK *via* increasing intracellular AMP level (58). Our current study demonstrates that breast cancer cells have low AK-mediated metabolic flux associated with diminished Ak1 and AK4 expression. A study on mice revealed that knockout of AK1 decreased AMPK activation in muscle cells (59). Recent, *in vitro* experiments on cancer cells have demonstrated that AK4 silencing increases intracellular ATP and decrease ATP/ADP ratio which leads to AMPK activation (48). Our current work and other studies (23, 24) demonstrated that ^{18}O stable isotope labeling method is sensitive enough to identify specific changes in AK network at different pathological conditions, including cancer. Further studies are needed to clarify which members of AK network (AK1-AK9) possess in the most regulation of intracellular nucleotide levels and how they are associated with the activity of AMPK in TNBC.

5 CONCLUSIONS

In summary, the introduction of a ^{18}O stable isotope-based analytical methodology to cancer research allowed us to detect subtle changes in ATP generation and energy transfer pathways in HBC cells. Altered ATP levels, decreased $\gamma/\beta\text{-ATP}[^{18}\text{O}]$, and G-6-P[^{18}O] turnovers indicate a profound rearrangement of breast cancer cell energy metabolism. Increased mitochondrial substrate shuttle flux (G-3-P[^{18}O]), and overexpression of HK2 suggest a tight relationship between the glycolytic phosphotransfer network and mitochondria in breast cancer cells. Alteration in the CK network is associated with decreased CK metabolic flux and lower PCr levels with downregulation of mitochondrial CK isoform CKMT1A in HBC cell lines. Despite a decreased overall AK flux in TNBC (MDA-MB-231) cells, overexpression of AK2 and AK6 was observed which could support energy metabolism in mitochondrial and nuclear microcompartments. Current work indicates that transformation of ATP generation and energy transport pathways in HBC cells is designed to support the energetic needs of specific cellular compartments (mitochondria and nuclear). Specifically, in aggressive breast cancer cells phosphoryl ^{18}O isotope-labeling reveals hidden rearrangements of energy metabolism which could be modulated and targeted by therapeutic agents in the future.

DATA AVAILABILITY STATEMENT

The raw data supporting the conclusions of this article will be made available by the authors, without undue reservation.

AUTHOR CONTRIBUTIONS

Conceptualization, AK, PD, and TK; methodology, AK, SM, HV, and SZ; validation, AK, SM, and SZ; formal analysis, AK and SM; investigation, AK, SM, IR, MP, ER-K, and LK; resources, AT, PD, and TK; data curation, AK and SM; writing—original draft preparation, AK, MP, and PD; writing—review and editing, AK, IR, MP, AT, PD, and TK; visualization, AK and SM; supervision, PD and TK; project administration, IR, PD, and TK; funding acquisition, AK, IR, PD, and TK. All authors have read and agreed to the published version of the manuscript.

REFERENCES

- Hanahan D, Weinberg RA. Hallmarks of Cancer: The Next Generation. *Cell* (2011) 144:646–74. doi: 10.1016/j.cell.2011.02.013
- Tasdogan A, Faubert B, Ramesh V, Ubellacker JM, Shen B, Solmonson A, et al. Metabolic Heterogeneity Confers Differences in Melanoma Metastatic Potential. *Nature* (2020) 577(7788):115–20. doi: 10.1038/s41586-019-1847-2
- Pavlova NN, Zhu J, Thompson CB. The Hallmarks of Cancer Metabolism: Still Emerging. *Cell Metab* (2022) 34:355–77. doi: 10.1016/j.cmet.2022.01.007
- Bray F, Ferlay J, Soerjomataram I, Siegel RL, Torre LA, Jemal A. Global Cancer Statistics 2018: GLOBOCAN Estimates of Incidence and Mortality Worldwide for 36 Cancers in 185 Countries. *CA Cancer J Clin* (2018) 68(6):394–424. doi: 10.3322/caac.21492
- Jia D, Lu M, Jung KH, Park JH, Yu L, Onuchic JN, et al. Elucidating Cancer Metabolic Plasticity by Coupling Gene Regulation With Metabolic Pathways.

FUNDING

This work was supported by the Estonian Research Council grants PRG1035, PSG11, PUTJD963 and the mobility grant MOBTP51; the National Institutes of Health (R01 HL134664 and R01 HL85744) and Marriott Family Foundation; as well as Estonia national scholarship program Kristjan Jaak, which is funded and managed by Archimedes Foundation in collaboration with the Estonian Ministry of Education and Research.

ACKNOWLEDGMENTS

The authors are grateful to Cambridge ISOTOPE Laboratories, Inc for their support with H_2^{18}O , donated to the authors as part of Cambridge ISOTOPE Laboratories, Inc Research Award.

SUPPLEMENTARY MATERIAL

The Supplementary Material for this article can be found online at: <https://www.frontiersin.org/articles/10.3389/fonc.2022.892195/full#supplementary-material>

Supplementary Figure 1 | CKMT1A copy number amplification associated with CKMT1A mRNA expression level from TCGA database. Each dot represents individual patient samples. Two-tailed Student's t-test two-samples unequal variance was used.

Supplementary Figure 2 | Original data from TCGA database represents CKMT1A expression profile of breast cancer patients. Each dot represents CKMT1A mRNA expression level of individual patient sample.

Supplementary Figure 3 | Original data from TCGA database represents AK2 expression profile of breast cancer patients. Each dot represents AK2 mRNA expression level of individual patient sample.

Supplementary Figure 4 | (A) AK2 and (B) AK6 expression level in breast cancer cells detected by western blotting. Homogenized cells containing 35 μg total protein was applied. Alpha tubulin was used as a control for equal loading. Mouse kidney homogenate was applied as a positive control for AK2, whereas MCF7 cell line lysate serves as a positive control for AK6 recommended by the antibody manufacturer. To compare the size of the proteins, the position of the marker proteins with given molecular mass is shown on the left side of each panel.

Proc Natl Acad Sci USA (2019) 116(9):3909–18. doi: 10.1073/pnas.1816391116

- Roth KG, Mambetsariev I, Kulkarni P, Salgia R. The Mitochondrion as an Emerging Therapeutic Target in Cancer. *Trends Mol Med* (2020) 26:119–34. doi: 10.1016/j.molmed.2019.06.009
- Wallimann T, Wyss M, Brdiczka D, Nicolay K, Eppenberger HM. Intracellular Compartmentation, Structure and Function of Creatine Kinase Isoenzymes in Tissues With High and Fluctuating Energy Demands: The “Phosphocreatine Circuit” for Cellular Energy Homeostasis. *Biochem J* (1992) 281:21–40. doi: 10.1042/bj2810021
- Dzeja PP, Zeleznikar RJ, Goldberg ND. Adenylate Kinase: Kinetic Behavior in Intact Cells Indicates it is Integral to Multiple Cellular Processes. *Mol Cell Biochem* (1998) 184(1/2):169–82. doi: 10.1023/A:1006859632730
- Dzeja PP, Terzic A. Phosphotransfer Networks and Cellular Energetics. *J Exp Biol* (2003) 206:2039–47. doi: 10.1242/jeb.00426

10. Schlattner U, Tokarska-Schlattner M, Wallimann T. Mitochondrial Creatine Kinase in Human Health and Disease. *Biochim Biophys Acta - Mol Bas Dis* (2006) 1762:164–80. doi: 10.1016/j.bbadis.2005.09.004
11. Chung S, Arrell DK, Faustino RS, Terzic A, Dzeja PP. Glycolytic Network Restructuring Integral to the Energetics of Embryonic Stem Cell Cardiac Differentiation. *J Mol Cell Cardiol* (2010) 48(4):725–34. doi: 10.1016/j.jymcc.2009.12.014
12. Noma T. Dynamics of Nucleotide Metabolism as a Supporter of Life Phenomena. *J Med Invest J Med Invest* (2005) 52:127–36. doi: 10.2152/jmi.52.127
13. Klepinin A, Chekulayev V, Timohhina N, Shevchuk I, Tepp K, Kaldma A, et al. Comparative Analysis of Some Aspects of Mitochondrial Metabolism in Differentiated and Undifferentiated Neuroblastoma Cells. *J Bioenerg Biomembr* (2014) 46(1):17–31. doi: 10.1007/s10863-013-9529-5
14. Ounpuu L, Klepinin A, Pook M, Teino I, Peet N, Paju K, et al. 2102Ep Embryonal Carcinoma Cells Have Compromised Respiration and Shifted Bioenergetic Profile Distinct From H9 Human Embryonic Stem Cells. *Biochim Biophys Acta - Gen Subj* (2017) 1861(8):2146–54. doi: 10.1016/j.jbbagen.2017.05.020
15. Klepinina L, Klepinin A, Truu L, Chekulayev V, Vija H, Kuus K, et al. Colon Cancer Cell Differentiation by Sodium Butyrate Modulates Metabolic Plasticity of Caco-2 Cells via Alteration of Phosphotransfer Network. *PLoS One* (2021) 16(1):e0245348. doi: 10.1371/journal.pone.0245348
16. Wilson JE. Isozymes of Mammalian Hexokinase: Structure, Subcellular Localization and Metabolic Function. *J Exp Biol J Exp Biol* (2003) 206:2049–57. doi: 10.1242/jeb.00241
17. Patra KC, Wang Q, Bhaskar PT, Miller L, Wang Z, Wheaton W, et al. Hexokinase 2 Is Required for Tumor Initiation and Maintenance and Its Systemic Deletion Is Therapeutic in Mouse Models of Cancer. *Cancer Cell* (2013) 24(2):213–28. doi: 10.1016/j.ccr.2013.06.014
18. Yang T, Ren C, Qiao P, Han X, Wang L, Lv S, et al. PIM2-Mediated Phosphorylation of Hexokinase 2 Is Critical for Tumor Growth and Paclitaxel Resistance in Breast Cancer. *Oncogene* (2018) 37(45):5997–6009. doi: 10.1038/s41388-018-0386-x
19. Li XH, Chen XJ, Ou W-B, Zhang Q, Lv ZR, Zhan Y, et al. Knockdown of Creatine Kinase B Inhibits Ovarian Cancer Progression by Decreasing Glycolysis. *Int J Biochem Cell Biol* (2013) 45(5):979–86. doi: 10.1016/j.biocel.2013.02.003
20. Kurmi K, Hitosugi S, Yu J, Boakye-Agyeman F, Wiese EK, Larson TR, et al. Tyrosine Phosphorylation of Mitochondrial Creatine Kinase 1 Enhances a Druggable Tumor Energy Shuttle Pathway. *Cell Metab* (2018) 28(6):833–847.e8. doi: 10.1016/j.cmet.2018.08.008
21. Nier AO. A Redetermination of the Relative Abundances of the Isotopes of Carbon, Nitrogen, Oxygen, Argon, and Potassium. *Phys Rev* (1950) 77(6):789–93. doi: 10.1103/PhysRev.77.789
22. España S, Sánchez-Parcerisa D, Ibáñez P, Sánchez-Tembleque V, Udias JM, Onecha VV, et al. Direct Proton Range Verification Using Oxygen-18 Enriched Water as a Contrast Agent. *Radiat Phys Chem* (2021) 182:109385. doi: 10.1016/j.radphyschem.2021.109385
23. Nemutlu E, Zhang S, Gupta A, Juranic NO, Macura SI, Terzic A, et al. Dynamic Phosphometabolomic Profiling of Human Tissues and Transgenic Models by 18O-Assisted 31P NMR and Mass Spectrometry. *Physiol Genomics* (2012) 44(7):386–402. doi: 10.1152/physiolgenomics.00152.2011
24. Nemutlu E, Gupta A, Zhang S, Viqar M, Holmuhamedov E, Terzic A, et al. Decline of Phosphotransfer and Substrate Supply Metabolic Circuits Hinders ATP Cycling in Aging Myocardium. *PLoS One* (2015) 10(9):e0136556. doi: 10.1371/journal.pone.0136556
25. Livak KJ, Schmittgen TD. Analysis of Relative Gene Expression Data Using Real-Time Quantitative PCR and the 2- $\Delta\Delta CT$ Method. *Methods* (2001) 25(4):402–8. doi: 10.1006/meth.2001.1262
26. Sikk P, Käämbre T, Vija H, Tepp K, Tiivel T, Nutt A, et al. Ultra Performance Liquid Chromatography Analysis of Adenine Nucleotides and Creatine Derivatives for Kinetic Studies. *Proc Est Acad Sci* (2009) 58(2):122. doi: 10.3176/proc.2009.2.04
27. Dzeja PP, Bortolon R, Perez-Terzic C, Holmuhamedov EL, Terzic A. Energetic Communication Between Mitochondria and Nucleus Directed by Catalyzed Phosphotransfer. *Proc Natl Acad Sci USA* (2002) 99(15):10156–61. doi: 10.1073/pnas.152259999
28. Györfly B, Lanczky A, Eklund AC, Denkert C, Budczies J, Li Q, et al. An Online Survival Analysis Tool to Rapidly Assess the Effect of 22,277 Genes on Breast Cancer Prognosis Using Microarray Data of 1,809 Patients. *Breast Cancer Res Treat* (2009) 123(3):725–31. doi: 10.1007/s10549-009-0674-9
29. Lane AN, Higashi RM, Fan TW. NMR and MS-Based Stable Isotope-Resolved Metabolomics and Applications in Cancer Metabolism. *TrAC - Trends Anal Chem* (2019) 120:115322. doi: 10.1016/j.trac.2018.11.020
30. Eylem CC, Baysal İ, Eriksi A, Yabanoglu-Ciftci S, Zhang S, Kir S, et al. Gas Chromatography-Mass Spectrometry Based 18O Stable Isotope Labeling of Krebs Cycle Intermediates. *Anal Chim Acta* (2021) 1154:338325. doi: 10.1016/j.aca.2021.338325
31. Fioletta VC, Palmieri M, Kloehn J, Mason S, Previs SF, McConville MJ, et al. Analysis of Mammalian Cell Proliferation and Macromolecule Synthesis Using Deuteratedwater and Gas Chromatography-Mass Spectrometry. *Metabolites* (2016) 6(4). doi: 10.3390/metabo6040034
32. Farthing DE, Buxbaum NP, Lucas PJ, Maglakelidze N, Oliver B, Wang J, et al. Comparing DNA Enrichment of Proliferating Cells Following Administration of Different Stable Isotopes of Heavy Water. *Sci Rep* (2017) 7(1):1–12. doi: 10.1038/s41598-017-04404-2
33. Fiorillo M, Scatena C, Naccarato AG, Sotgia F, Lisanti MP. Bedaquiline, an FDA-Approved Drug, Inhibits Mitochondrial ATP Production and Metastasis *In Vivo*, by Targeting the Gamma Subunit (ATP5F1C) of the ATP Synthase. *Cell Death Diff* (2021) 28:1–21. doi: 10.1038/s41418-021-00788-x
34. Zhang C, Liu Z, Liu X, Wei L, Liu Y, Yu J, et al. Targeted Metabolic Analysis of Nucleotides and Identification of Biomarkers Associated With Cancer in Cultured Cell Models. *Acta Pharm Sin B* (2013) 3(4):254–62. doi: 10.1016/j.apsb.2013.06.002
35. Hahn-Windgassen A, Nogueira V, Chen CC, Skeen JE, Sonenberg N, Hay N. Akt Activates the Mammalian Target of Rapamycin by Regulating Cellular ATP Level and AMPK Activity. *J Biol Chem* (2005) 280(37):32081–9. doi: 10.1074/jbc.M502876200
36. Maldonado EN, Lemasters JJ. ATP/ADP Ratio, the Missed Connection Between Mitochondria and the Warburg Effect. *Mitochondrion* (2014) 19(Part A):78–84. doi: 10.1016/j.mito.2014.09.002
37. Dzeja PP, Vitkevicius KT, Redfield MM, Burnett JC, Terzic A. Adenylate Kinase-Catalyzed Phosphotransfer in the Myocardium: Increased Contribution in Heart Failure. *Circ Res* (1999) 84(10):1137–43. doi: 10.1161/01.RES.84.10.1137
38. Pucar D, Dzeja PP, Bast P, Juranic N, Macura S, Terzic A. Cellular Energetics in the Preconditioned State: Protective Role for Phosphotransfer Reactions Captured by 18O-Assisted 31P NMR. *J Biol Chem* (2001) 276(48):44812–9. doi: 10.1074/jbc.M104425200
39. Kaldma A, Klepinin A, Chekulayev V, Mado K, Shevchuk I, Timohhina N, et al. An *In Situ* Study of Bioenergetic Properties of Human Colorectal Cancer: The Regulation of Mitochondrial Respiration and Distribution of Flux Control Among the Components of ATP Synthasome. *Int J Biochem Cell Biol* (2014) 55:171–86. doi: 10.1016/j.biocel.2014.09.004
40. Amamoto R, Uchiyama T, Yagi M, Monji K, Song YH, Oda Y, et al. The Expression of Ubiquitous Mitochondrial Creatine Kinase Is Downregulated as Prostate Cancer Progression. *J Cancer*. (2016) 7(1):50–9. doi: 10.7150/jca.13207
41. Patra S, Bera S, SinhaRoy S, Ghoshal S, Ray S, Basu A, et al. Progressive Decrease of Phosphocreatine, Creatine and Creatine Kinase in Skeletal Muscle Upon Transformation to Sarcoma. *FEBS J* (2008) 275(12):3236–47. doi: 10.1111/j.1742-4658.2008.06475.x
42. Fenouille N, Bassil CF, Ben-Sahra I, Benajiba L, Alexe G, Ramos A, et al. The Creatine Kinase Pathway Is a Metabolic Vulnerability in EVI1-Positive Acute Myeloid Leukemia. *Nat Med* (2017) 23(3):301–13. doi: 10.1038/nm.4283
43. Zarghami N, Gai M, Yu H, Roagna R, Ponzzone R, Katsaros D, et al. Creatine Kinase BB Isoenzyme Levels in Tumour Cytosols and Survival of Breast Cancer Patients. *Br J Cancer*. (1996) 73(3):386–90. doi: 10.1038/bjc.1996.66
44. Kazak L, Cohen P. Creatine Metabolism: Energy Homeostasis, Immunity and Cancer Biology. *Nat Rev Endocrinol*. (2020) 16:421–36. doi: 10.1038/s41574-020-0365-5
45. Loo JM, Scherl A, Nguyen A, Man FY, Weinberg E, Zeng Z, et al. Extracellular Metabolic Energetics Can Promote Cancer Progression. *Cell* (2015) 160(3):393–406. doi: 10.1016/j.cell.2014.12.018
46. Klepinin A, Ounpuu L, Guzun R, Chekulayev V, Timohhina N, Tepp K, et al. Simple Oxygenographic Analysis for the Presence of Adenylate Kinase 1 and 2 in

- Normal and Tumor Cells. *J Bioenerg Biomembr* (2016) 48(5):531–48. doi: 10.1007/s10863-016-9687-3
47. Janssen E, Dzeja PP, Oerlemans F, Simonetti AW, Heerschap A, De Haan A, et al. Adenylate Kinase 1 Gene Deletion Disrupts Muscle Energetic Economy Despite Metabolic Rearrangement. *EMBO J* (2000) 19(23):6371–81. doi: 10.1093/emboj/19.23.6371
 48. Lanning NJ, Looyenga BD, Kauffman AL, Niemi NM, Sudderth J, DeBerardinis RJ, et al. A Mitochondrial RNAi Screen Defines Cellular Bioenergetic Determinants and Identifies an Adenylate Kinase as a Key Regulator of ATP Levels. *Cell Rep* (2014) 7(3):907–17. doi: 10.1016/j.celrep.2014.03.065
 49. Kim H, Lee HJ, Oh Y, Choi SG, Hong SH, Kim HJ, et al. The DUSP26 Phosphatase Activator Adenylate Kinase 2 Regulates FADD Phosphorylation and Cell Growth. *Nat Commun* (2014) 5. doi: 10.1038/ncomms4351
 50. Speers C, Tsimelzon A, Sexton K, Herrick AM, Gutierrez C, Culhane A, et al. Identification of Novel Kinase Targets for the Treatment of Estrogen Receptor-Negative Breast Cancer. *Clin Cancer Res* (2009) 15(20):6327–40. doi: 10.1158/1078-0432.CCR-09-1107
 51. Liu H, Pu Y, Amina Q, Wang Q, Zhang M, Song J, et al. Prognostic and Therapeutic Potential of Adenylate Kinase 2 in Lung Adenocarcinoma. *Sci Rep* (2019) 9(1):1–10. doi: 10.1038/s41598-019-53594-4
 52. Maslah N, Latiri M, Asnafi V, Féroul M, Bedjaoui N, Steimlé T, et al. Adenylate Kinase 2 Expression and Addiction in T-ALL. *Blood Adv* (2021) 5(3):700–10. doi: 10.1182/bloodadvances.2020002700
 53. Bai D, Zhang J, Li T, Hang R, Liu Y, Tian Y, et al. The ATPase hCINAP Regulates 18S rRNA Processing and Is Essential for Embryogenesis and Tumour Growth. *Nat Commun* (2016) 7(5):1–15. doi: 10.1038/ncomms12310
 54. Ji Y, Yang C, Tang Z, Yang Y, Tian Y, Yao H, et al. Adenylate Kinase hCINAP Determines Self-Renewal of Colorectal Cancer Stem Cells by Facilitating LDHA Phosphorylation. *Nat Commun* (2017) 8:15308. doi: 10.1038/ncomms15308
 55. Shengwei K, Zhang R, He Y, Mu H, Sun F, Liu W, et al. Human Adenylate Kinase 6 Regulates WNK1 (With No Lysine Kinase-1) Phosphorylation States and Affects Ion Homeostasis in NT2 Cells. *Exp Cell Res* (2021) 402(1):112565. doi: 10.1016/j.yexcr.2021.112565
 56. Klepinin A, Zhang S, Klepinina L, Rebane-Klemm E, Terzic A, Kaambre T, et al. Adenylate Kinase and Metabolic Signaling in Cancer Cells. *Front Oncol* (2020) 10:660. doi: 10.3389/fonc.2020.00660
 57. Jeon SM. Regulation and Function of AMPK in Physiology and Diseases. *Exp Mol Med* (2016) 48:e245. doi: 10.1038/emmm.2016.81
 58. Takaine M, Imamura H, Yoshida S. AMP-Activated Protein Kinase and Adenylate Kinase Prevent the ATP Catastrophe and Cytotoxic Protein Aggregation. *bioRxiv* (2019) 801738. doi: 10.1101/801738
 59. Hancock CR, Janssen E, Terjung RL. Contraction-Mediated Phosphorylation of AMPK Is Lower in Skeletal Muscle of Adenylate Kinase-Deficient Mice. *J Appl Physiol* (2006) 100(2):406–13. doi: 10.1152/japplphysiol.00885.2005

Conflict of Interest: The authors declare that the research was conducted in the absence of any commercial or financial relationships that could be construed as a potential conflict of interest.

Publisher's Note: All claims expressed in this article are solely those of the authors and do not necessarily represent those of their affiliated organizations, or those of the publisher, the editors and the reviewers. Any product that may be evaluated in this article, or claim that may be made by its manufacturer, is not guaranteed or endorsed by the publisher.

Copyright © 2022 Klepinin, Miller, Reile, Puurand, Rebane-Klemm, Klepinina, Vija, Zhang, Terzic, Dzeja and Kaambre. This is an open-access article distributed under the terms of the Creative Commons Attribution License (CC BY). The use, distribution or reproduction in other forums is permitted, provided the original author(s) and the copyright owner(s) are credited and that the original publication in this journal is cited, in accordance with accepted academic practice. No use, distribution or reproduction is permitted which does not comply with these terms.

Appendix 3

Publication III

Kaup, K. K; Toom, L; Truu, L; **Miller, S**; Puurand, M; Tepp, K; Käämbre, T; Reile, I (2021). A line-broadening free real-time ^{31}P pure shift NMR method for phosphometabolomic analysis. *The Analyst*, 146(22):7034. doi:10.1039/d1an90092g.



Cite this: DOI: 10.1039/d1an01198g

Received 5th July 2021,
Accepted 20th August 2021

DOI: 10.1039/d1an01198g

rsc.li/analyst

A line-broadening free real-time ^{31}P pure shift NMR method for phosphometabolomic analysis†

Karl Kristjan Kaup,^{a,b} Lauri Toom,^{ib} Laura Truu,^a Sten Miller,^a Marju Puurand,^{id} Kersti Tepp,^{id} Tuuli Käämbre^{id} and Indrek Reile^{id}*^a

Phosphometabolomics by ^{31}P NMR can be challenging, since overlapping multiplets of homonuclear coupled phosphorus nuclei complicate spectral analysis. Pure shift NMR allows to simplify such spectra by collapsing multiplets into singlets, but most pure shift methods require substantially elongated measurement times or cause disturbing spectral line broadening. Herein, we combine established pure shift NMR and artefact suppression techniques to record ^{31}P pure shift NMR spectra without penalties in measurement time or line width. Examples are demonstrated in resolution of a mixture of nucleotide triphosphates and a biological sample of ^{18}O labelled ATP isotopomers.

NMR spectroscopy has established itself as a powerful and versatile tool in biochemical and biomedical research, giving access to easily interpretable and quantifiable information. It holds particular relevance for bioenergetics and phosphometabolomics, where ^{31}P NMR is used to visualise the chemical energy carrying phosphometabolites that are involved in cellular energy production, transport and utilization.¹

^{31}P NMR is used to detect high-energy nucleotides, *i.e.* ATP (adenosine triphosphate), whose concentrations help to evaluate the energetic status and health of muscle tissue.^{2,3} The evaluation of nucleotides is also believed to have an impact in cancer research in the near future.⁴ Application of NMR in phosphometabolomics is, however, often held back by the general limitations of NMR spectroscopy: its sensitivity and resolution. Although ^{31}P is one of the more sensitive MR active nuclei, measuring of dilute metabolites is time consuming and often takes multiple hours,³ limiting throughput.

Spectral resolution is a common limitation in 1D ^1H NMR, but is usually less of an issue for other nuclei, including ^{31}P NMR, where signals are dispersed across >400 ppm chemical shift range. In phosphometabolite analysis, however, ATP ^{31}P signals are further split into multiplets by approximately 20 Hz 2J -

couplings between adjacent phosphate residues. While this is not an issue for measuring pure ATP, it becomes a challenge when different nucleotide triphosphates are involved: their ^{31}P chemical shift differences are of similar magnitude to their mutual J -coupling, giving rise to partially overlapping multiplets (Fig. 1b

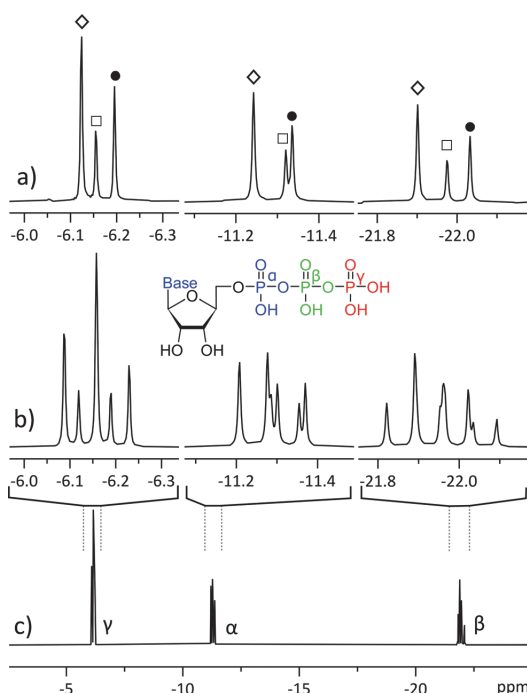


Fig. 1 ^{31}P NMR spectra of a mixture of 20 mM ATP (adenosine triphosphate, \diamond), 10 mM CTP (cytidine triphosphate, \bullet) and 5 mM UTP (uridine triphosphate, \square): (a) ^{31}P pure shift spectra, acquired with the method reported in this study; (b) magnification of the three phosphate sites from trace c; (c) normal ^{31}P 1D NMR spectrum. All spectra were acquired using 256 scans, with trace (a) acquired in four 64-scan experiments of different SAPHIRE orders and the FIDs were added after LP processing.

^aNational Institute of Chemical Physics and Biophysics, Akadeemia tee 23, Tallinn 12618, Estonia. E-mail: indrek.reile@kbfi.ee

^bInstitute of Chemistry, University of Tartu, Ravila 14A, 50411 Tartu, Estonia

†Electronic supplementary information (ESI) available. See DOI: 10.1039/d1an01198g

Communication

& c). Consequently, mixtures of different phosphates have also been studied by MS, which resolves them somewhat more easily, but requires more elaborate sample preparation and quantification routines.²

We encountered a similar problem in mapping the concentrations and turnover rates (fluxes) of different ATP synthesis and utilization sites.^{1,3} These experiments rely on the small (approx. 0.025 ppm) chemical shift difference between ATP isotopomers: dynamic ^{18}O labelling introduces isotopomer signals into the ^{31}P spectra (Fig. 2b & c), forming a complex pattern of overlapping multiplets that can be difficult to interpret.⁵ The biochemical meaning of all isotopomers is known⁶ and the relative intensities of $^{16}\text{O}/^{18}\text{O}$ related ^{31}P signals at any ATP phosphate (α , β , γ) can be related to activities of different ATP processing pathways.⁵ However, isotope shifts are of similar magnitude to J -coupling and can overlap with right-hand multiplet components, complicating analysis.⁶

Furthermore, signal intensity is dispersed among numerous isotopomers, increasing necessary measurement time.

Such spectra could be resolved by 2D ^{31}P spectroscopy, but this experiment would also be undesirably long for dilute biological samples.^{5–7} Herein we demonstrate a different approach, where resolution is achieved by pure shift NMR methodology, yielding better resolved and easier to interpret spectra.

Experimental

Spectra were acquired with a 5 mm BBO (broad band observe) probe on a 700 MHz Bruker Avance III spectrometer, corresponding to 283 MHz ^{31}P frequency. All experiments were recorded in 10 000 Hz bandwidth with ^1H decoupling. 16k complex points were recorded in a 0.82 s acquisition time, with a relaxation delay of 2 s. Sample temperature was regulated at 6 °C (2 °C above the freezing point of D_2O) and RF pulses were calibrated for each sample (typically around 14.7 μs hard 90° pulse). Samples were measured either in 5 mm tubes or in Shigemi tubes (^{18}O labelled samples). Samples were prepared by dissolving solid reagents or lyophilized biological material in D_2O and adjusting the pH to 9.5 with NaOH solution. ^{18}O labelled sample was prepared by perfusion of rat heart,⁸ followed by preparative LC separation of ATP (details in ESI†). Animal experiments were approved by the Estonian National Board of Animal Experiments in accordance with the European Community Directive (86/609/EEC). LP extrapolation of data chunks was performed in Bruker Topspin and final spectral processing was performed in Topspin or MestreNova software packages. Pulse sequence code, processing macro and further details are available in ESI.†

Pure shift NMR

Pure shift,^{9,10} or homonuclear decoupling, techniques have been extensively developed^{11–13} and are included in the modern NMR toolbox. They gain in resolution by sacrificing information embedded in multiplet patterns, collapsing them into singlets. This can also yield added sensitivity, as the intensities of multiplet components add. Methodology has been published for simplification of 1D spectra of small molecules,⁹ diastereomers¹⁴ or peptides¹⁵ and for added resolution in 2D NMR.^{16–18} While the majority of pure shift methods focus on ^1H NMR and there are a few examples available for heteronuclei,¹⁹ phosphometabolomics by ^{31}P NMR presents an opportunity to expand the application scope of pure shift.

The first¹⁰ and best quality^{20,21} pure shift techniques rely on interferogram (or pseudo-2D)⁹ acquisition where the homonuclear decoupled FID is constructed from “chunks” from tens of individual 1D measurements. This generally yields good quality spectra but is not applicable to phosphometabolomics, where acquiring a single 1D spectrum takes hours and recording tens of spectra would make the experiment prohibitively long. The alternative is real-time (RT) pure shift, where a single FID is recorded,¹² but acquisition is periodically inter-

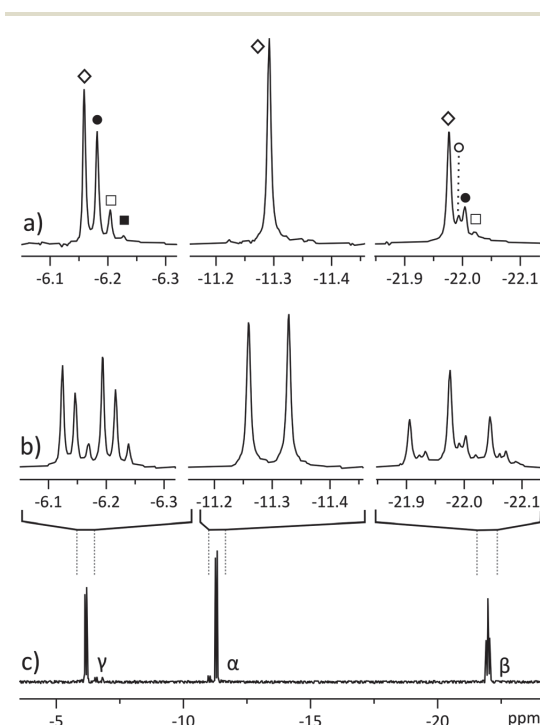


Fig. 2 ^{31}P NMR spectra of partially ^{18}O -labelled ATP, isolated from a perfused rat heart. (a) Pure shift spectrum displays a singlet for each isotopomer: \diamond for all ^{16}O isotopomer, \bullet for phosphate with one oxygen ^{18}O -labelled, \square for two labelled oxygens and \blacksquare for three labelled oxygens. β -Phosphate also yields a signal (\circ) corresponding to a ^{18}O label in the bridging position between adjacent phosphates;⁶ (b) segments from regular ^{31}P spectrum displaying overlapping multiplets; (c) regular ^{31}P spectrum of the sample. All spectra were acquired in 2048 scans, with spectrum (a) acquired in four 512-scan experiments of different SAPHIRE orders and the FIDs were added after LP extrapolation.

rupted to refocus the J-evolution and chemical shifts by RF pulses.²² While the measurement time penalty of interferogram pure shift is overcome, undesired spectral line broadening occurs. This is caused by relaxation between recorded "data chunks" as the time during RF pulses is omitted from the acquired signal, causing shortening of the FID.²²

The best current solution is called semi-RT pure shift,²³ which involves conducting two 1D measurements and combining the results into one continuous FID. Consequently, it introduces a two-fold increase in measurement time, a potential issue in dilute samples where even a single 1D measurement requires thousands of scans to be acquired. Here, we build on the principles of semi-RT, but instead of two experiments, we record only one discontinuous FID and fill in the gaps by linear prediction (LP) from adjacent data chunks to obtain a ³¹P pure shift spectrum with natural linewidth (Fig. 1 & 2a).

Pulse sequence and data processing

The pulse sequence (Fig. 3) is based on the 1st row of the band selective semi-RT experiment.²³ Spins are divided into two subgroups: active spins, which are the spins whose signal we want to measure, and passive spins, which cause the J-evolution of active spins. A series of pulsed field gradient spin echoes select the active spins with a band-selective soft pulse and set the starting point of J-evolution in the FID. Chemical shift is allowed to evolve unperturbed throughout acquisition, while the receiver is blanked periodically to invert passive spins with band-selective soft pulses to refocus the J-evolution in the midpoint of the following data chunk. Note that when measuring the β -ATP signal, two band-selective pulses are applied at the same time at passive α and γ phosphate frequencies. Data points are acquired during the FID gaps, but since the receiver is blanked, they do not carry meaningful information. This process is repeated multiple times during acquisition, resulting in a chunked FID (Fig. 4a).

Gaps in the discontinuous FID are filled computationally (Fig. 4b). A similar problem has been solved previously in EXACT^{16,24} experiments by algorithmic reconstruction of the missing data points, requiring specialized software not always

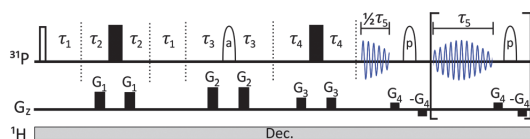


Fig. 3 The pulse sequence is effectively a combination of SAPHIRE²⁰ and semi-RT²³ sequences, with one additional delay τ_2 . G_2 describes gradient pulses. Filled rectangles stand for 180° hard pulses, unfilled rectangle for 90° hard pulse. Ellipses denote 180° RSnob soft pulses for (a) active spins (that will be detected) and (p) for passive spins. Hence, prior knowledge of the spectral position of passive and active spins is required. Following the semi-RT example,²³ Tycko-7/MLEV-4 supercycle is used for passive spin RSnob pulses. Explanations for delays τ_1 – τ_5 and further details are given in ESI†

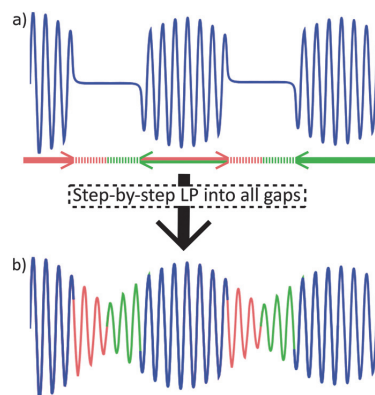


Fig. 4 Linear prediction to fill the FID gaps in trace (a): red segments are predicted forwards, based on the full length of the preceding data chunk (blue). Green segments are predicted backwards. Resulting continuous FID (b) can be processed as usual. In present work, data chunk and gap durations were 20 ms and 5.6 ms, respectively.

available at NMR laboratories. Instead, we extrapolate the information from within chunks into FID gaps by using standard linear prediction (LP) methodology that is commonly available in the software toolbox of modern spectrometers.

Every chunk is used to extrapolate half of the duration of the following and half of the preceding gap (with the exception of the 1st chunk that predicts only into the following gap). This way, J-coupling evolution is kept symmetrical about the centre of data chunks. It also relieves the conditions set on the relative lengths of chunks and gaps, as it allows to predict less points from the limited number of experimental points available. Repeating this procedure for all gaps produces a continuous FID that can be processed by usual means.

As is common in pure shift, the resulting FID will be periodically modulated by J-evolution that is centred around the midpoint of every data chunk (Fig. 4b).^{13,22} Fourier transform of such FID creates a spectrum with "chunking sideband" artefacts (Fig. 5b–e) positioned around the signals at distances inversely proportional to the sum of the data chunk and gap lengths (the periodically repeating unit in the FID). This issue is alleviated by the SAPHIRE²⁰ method that shifts the phase of the J-modulation across different scans (Fig. 5b–e; discussion in ESI†). Accordingly, the desired number of scans should be recorded in an even number of experiments where the artefacts are positioned in opposite phases. Adding the FIDs of such experiments will add the desired signals constructively, while "cancelling out" artefacts (Fig. 5a).

Theoretically, it is possible to extend SAPHIRE to an arbitrary order (measured in an infinite number of experimental pairs), cancelling out all sidebands and producing clean

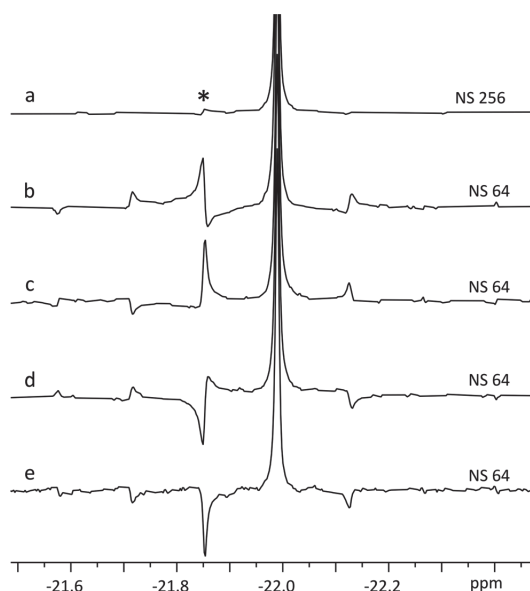


Fig. 5 Fourier transform after LP of four SAPPHERE experiments (b–e) on ATP β -phosphate (20 mM). Note how the artefacts are pairwise in opposite phases in traces b & d and c & e. Trace (a) displays FT of the sum of FID-s from b–e, where the chunking artefacts have been largely cancelled out,²⁰ with the most prominent artefact (*) having <2% intensity of the main signal.

spectra. However, since the experiment herein requires LP from the 1st data chunk (half the duration of following chunks) into the 1st gap, it cannot be implemented beyond the second order – there would not be enough data points available for reliable LP. Even so, artefact intensity decreases rapidly and it is seldom necessary to use higher order canceling.²⁰ In the experiment of Fig. 5a, SAPPHERE reduces artefact intensity approx. thirtyfold, yielding a pure shift spectrum with virtually identical linewidth to the original spectra and increased sensitivity as multiplet components add constructively. The resulting experiment compares favourably to other pure shift approaches, especially when time efficiency is considered (Fig. S4 and Table S1†).

Phosphometabolomics analysis

Applying the method to a mixture of similar concentrations of nucleotide triphosphates, a realistic scenario in phosphometabolomics of biological material,² allows to resolve signals of different nucleotides (Fig. 1), whose multiplets would otherwise overlap. The method gives excellent spectral quality, with line shape being indistinguishable from regular 1D NMR (Fig. 6). The experiment being band selective, two separate measurements must be conducted to cover all ATP phosphorus sites. This does not necessarily cost additional measurement time since decoupling provides a slight sensitivity increase, allowing to accumulate less scans to achieve similar SNR.

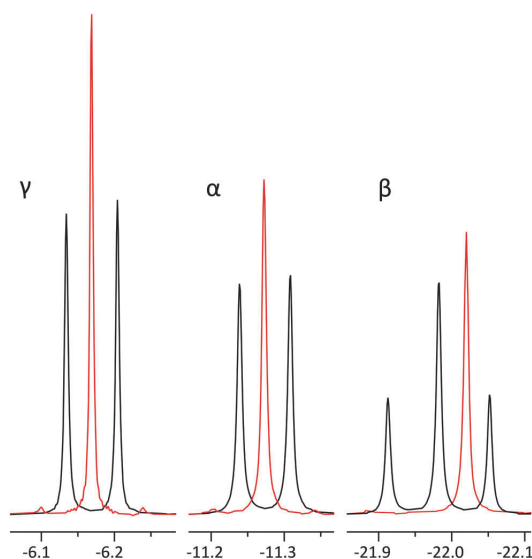


Fig. 6 Comparison of regular ^{31}P spectra of ATP α , β and γ phosphates (black) and their corresponding pure shift spectra (red) with identical line width. The β phosphate signal has been offset slightly to allow for better comparison of signals. In order to acquire all three positions, two separate experiments have to be recorded: one for α and γ phosphate and one for β phosphate. Signal intensities increase in pure shift spectra: 1.6-fold for γ , 1.4-fold for α and 1.2-fold for β . We suggest the differences are due to relaxation weighting during the pulse sequence. γ -Phosphate displays the largest artefact intensity of 1.5–2% of main signal.

Moreover, in the case of a mixture of Fig. 1, acquiring pure shift spectra of only one phosphate site suffices to characterize the ratio of all components.

In parallel, we applied the methodology to analysis of a mixture of $^{16}\text{O}/^{18}\text{O}$ labelled ATP isotopomers that were extracted from a perfused rat heart (Fig. 2).¹ Such experiments are usually sample limited and analysis has to be performed on dilute mixtures that are prepared from animal tissue and require thousands of scans to achieve sufficient SNR. Applying the method reported in this study reduces overlapping ATP isotopomer signals into singlets, making the spectra easier to interpret (Fig. 2a). One could argue that overlap is not an issue in this case and it is possible to simply count the rightmost signals of the multiplets. This might, however, cause misinterpretation, since left hand multiplet components of some isotopomers may overlap with those of the right multiplet components of other isotopomers. This issue would be corroborated if one moves to an even higher field spectrometer, where the frequency differences of isotopomers increase while coupling remains constant.

Analysing these isotopomer singlets gives a time-freeze overview of the phosphometabolomic state of the cells at the time of labelling, as has been described by Nemetlu *et al.*²⁵ The slightly added sensitivity allows to spot the less abundant

isotopomers that can go unnoticed in simple 1D NMR in equal number of scans (■, $^{18}\text{O}_3$ in Fig. 2). In the case of β -ATP we observe very closely resonating signals from bridging and peripheral labelled isotopomers (O , $^{18}\text{O}_1$ in Fig. 2), but still benefit from simplification of multiplet patterns along with an increase in sensitivity. While the sample of Fig. 2 was prepared by LC purification of a perfused rat heart extract, the method is also applicable directly to the extract, yielding simultaneous pure shift spectra of nearby ATP and ADP signals (Fig. S5†).

Conclusions

Combining the concepts of semi-RT-pure shift, SAPPHIRE and chunk extrapolation by LP allowed to demonstrate a heteronuclear application of pure shift NMR in phosphometabolomic analysis. Although spectral resolution is rarely as prominent an issue in ^{31}P NMR as it is in ^1H NMR, resolution of highly similar nucleotides and their isotopomers presents a strong case for developing methodology and expanding the application envelope of pure shift methodology for heteronuclei. We foresee using this and related methods in the metabolomic study of challenging diseases,²⁶ including cancer,⁴ in the near future. We suggest the method reported in this study is also applicable to ^1H NMR, especially when additional resolution is sought after for very dilute samples, where line broadening and sensitivity penalties have to be avoided. The developed method gives access to homonuclear decoupled spectra in real-time, with natural linewidth, and utilizes only software and functionalities that are commonly built into any modern NMR software package.

Author contributions

K. K. K. developed pulse program and processing software, performed NMR measurements. L. Truu, M. P., K. T., S. M. and T. K. carried out biological sample preparation. The project was conceptualized and supervised by L. Toom, T. K. and I. R. The manuscript was written by K. K. K. and I. R. and edited by all authors.

Conflicts of interest

There are no conflicts to declare.

Acknowledgements

The authors acknowledge financial support from the personal research grant PSG11, the mobility grant MOBTP51 and institutional funding scheme IUT23-1 of the Estonian Research Council, as well as from the Center of Excellence TK134 of the Archimedes Foundation. The authors are grateful to Cambridge Laboratories, Inc. for their support with H_2^{18}O and D_2O . NMR work was carried out using the instrumentation at

the Estonian Center of Analytical Chemistry (<http://www.akki.ee>).

Notes and references

- 1 D. Pucar, P. P. Dzeja, P. Bast, N. Juranic, S. Macura and A. Terzic, *J. Biol. Chem.*, 2001, **276**, 44812–44819.
- 2 E. Nemutlu, S. Zhang, A. Gupta, N. O. Juranic, S. I. Macura, A. Terzic, A. Jahangir and P. Dzeja, *Physiol. Genomics*, 2012, **44**, 386–402.
- 3 D. Pucar, P. P. Dzeja, P. Bast, R. J. Gumina, C. Drahl, L. Lim, N. Juranic, S. Macura and A. Terzic, *Mol. Cell. Biochem.*, 2004, **256**, 281–289.
- 4 N. N. Pavlova and C. B. Thompson, *Cell Metab.*, 2016, **23**, 27–47.
- 5 E. Nemutlu, N. Juranic, S. Zhang, L. E. Ward, T. Dutta, K. S. Nair, A. Terzic, S. Macura and P. P. Dzeja, *Anal. Bioanal. Chem.*, 2012, **403**, 697–706.
- 6 N. Juranic, E. Nemutlu, S. Zhang, P. Dzeja, A. Terzic and S. MacUra, *J. Biomol. NMR*, 2011, **50**, 237–245.
- 7 A. Majumdar, Y. Sun, M. Shah and C. L. Freel Meyers, *J. Org. Chem.*, 2010, **75**, 3214–3223.
- 8 D. Pucar, E. Janssen, P. P. Dzeja, N. Juranic, S. Macura, B. Wieringa and A. Terzic, *J. Biol. Chem.*, 2000, **275**, 41424–41429.
- 9 J. A. Aguilar, S. Faulkner, M. Nilsson and G. A. Morris, *Angew. Chem., Int. Ed.*, 2010, **49**, 3901–3903.
- 10 K. Zangger and H. Sterk, *J. Magn. Reson.*, 1997, **124**, 486–489.
- 11 K. Zangger, *Prog. Nucl. Magn. Reson. Spectrosc.*, 2015, **86–87**, 1–20.
- 12 L. Castañar, *Magn. Reson. Chem.*, 2017, **55**, 47–53.
- 13 R. W. Adams, in *eMagRes*, John Wiley & Sons, Ltd, Chichester, UK, 2014, vol. 3, pp. 295–310.
- 14 R. W. Adams, L. Byrne, P. Király, M. Foroozandeh, L. Paudel, M. Nilsson, J. Clayden and G. A. Morris, *Chem. Commun.*, 2014, **50**, 2512–2514.
- 15 J. Ying, J. Roche and A. Bax, *J. Magn. Reson.*, 2014, **241**, 97–102.
- 16 I. E. Ndukwe, A. Shchukina, V. Zorin, C. Cobas, K. Kazimierzczuk and C. P. Butts, *ChemPhysChem*, 2017, **18**, 2081–2087.
- 17 M. Foroozandeh, P. Giraudeau and D. Jeannerat, *Magn. Reson. Chem.*, 2013, **51**, 808–814.
- 18 C. Mauve, S. Khelifi, F. Gilard, G. Mouille and J. Farjon, *Chem. Commun.*, 2016, **52**, 6142–6145.
- 19 A. B. Jones, G. C. Lloyd-Jones and D. Uhrin, *Anal. Chem.*, 2017, **89**, 10013–10021.
- 20 P. Moutzouri, Y. Chen, M. Foroozandeh, P. Kiraly, A. R. Phillips, S. R. Coombes, M. Nilsson and G. A. Morris, *Chem. Commun.*, 2017, **53**, 10188–10191.
- 21 M. Foroozandeh, R. W. Adams, N. J. Meharry, D. Jeannerat, M. Nilsson and G. a. Morris, *Angew. Chem., Int. Ed.*, 2014, **53**, 6990–6992.

- 22 L. Castañar and T. Parella, *Magn. Reson. Chem.*, 2015, **53**, 399–426.
- 23 P. Kiraly, M. Nilsson and G. A. Morris, *J. Magn. Reson.*, 2018, **293**, 19–27.
- 24 I. E. Ndukwe, A. Shchukina, K. Kazimierzczuk, C. Cobas and C. P. Butts, *ChemPhysChem*, 2016, **17**, 2799–2803.
- 25 E. Nemutlu, S. Zhang, N. O. Juranic, A. Terzic, S. Macura and P. Dzeja, *Croat. Med. J.*, 2012, **53**, 529–534.
- 26 M. A. Siddiqui, S. Pandey, A. Azim, N. Sinha and M. H. Siddiqui, *Biophys. Chem.*, 2020, **267**, 106462.

Appendix 4

Publication IV

Reinsalu, L; Puurand, M; Chekulayev, V; **Miller, S**; Shevchuk, I; Tepp, K; Rebane-Klemm, E; Timohhina, N; Terasmaa, A; Kaambre, T (2021). Energy Metabolic Plasticity of Colorectal Cancer Cells as a Determinant of Tumor Growth and Metastasis. *Frontiers in oncology*, 11:698951. doi: 10.3389/fonc.2021.698951.



Energy Metabolic Plasticity of Colorectal Cancer Cells as a Determinant of Tumor Growth and Metastasis

Leenu Reinsalu^{1,2}, Marju Puurand¹, Vladimir Chekulayev¹, Sten Miller^{1,2}, Igor Shevchuk¹, Kersti Tepp¹, Egle Rebane-Klemm^{1,2}, Natalja Timohhina¹, Anton Terasmaa¹ and Tuuli Kaambre^{1*}

¹ Laboratory of Chemical Biology, National Institute of Chemical Physics and Biophysics, Tallinn, Estonia, ² Department of Chemistry and Biotechnology, School of Science, Tallinn University of Technology, Tallinn, Estonia

OPEN ACCESS

Edited by:

Miriam Martini,
University of Turin, Italy

Reviewed by:

Tatiana Rostovtseva,
National Institutes of Health (NIH),
United States
Wael Rabeh,
New York University Abu Dhabi,
United Arab Emirates

*Correspondence:

Tuuli Kaambre
tuuli.kaambre@kbfi.ee

Specialty section:

This article was submitted to
Cancer Metabolism,
a section of the journal
Frontiers in Oncology

Received: 22 April 2021

Accepted: 08 July 2021

Published: 26 July 2021

Citation:

Reinsalu L, Puurand M,
Chekulayev V, Miller S,
Shevchuk I, Tepp K,
Rebane-Klemm E, Timohhina N,
Terasmaa A and Kaambre T
(2021) Energy Metabolic
Plasticity of Colorectal
Cancer Cells as a Determinant of
Tumor Growth and Metastasis.
Front. Oncol. 11:698951.
doi: 10.3389/fonc.2021.698951

Metabolic plasticity is the ability of the cell to adjust its metabolism to changes in environmental conditions. Increased metabolic plasticity is a defining characteristic of cancer cells, which gives them the advantage of survival and a higher proliferative capacity. Here we review some functional features of metabolic plasticity of colorectal cancer cells (CRC). Metabolic plasticity is characterized by changes in adenine nucleotide transport across the outer mitochondrial membrane. Voltage-dependent anion channel (VDAC) is the main protein involved in the transport of adenine nucleotides, and its regulation is impaired in CRC cells. Apparent affinity for ADP is a functional parameter that characterizes VDAC permeability and provides an integrated assessment of cell metabolic state. VDAC permeability can be adjusted via its interactions with other proteins, such as hexokinase and tubulin. Also, the redox conditions inside a cancer cell may alter VDAC function, resulting in enhanced metabolic plasticity. In addition, a cancer cell shows reprogrammed energy transfer circuits such as adenylate kinase (AK) and creatine kinase (CK) pathway. Knowledge of the mechanism of metabolic plasticity will improve our understanding of colorectal carcinogenesis.

Keywords: tumor energy metabolism, aerobic glycolysis, oxidative phosphorylation, VDAC, creatine kinase, adenylate kinase, mitochondria

INTRODUCTION

Analysis of mitochondrial function is central to the study of intracellular energy metabolism and pathophysiological mechanisms of various human diseases, including cancer. The metabolism of cancer cells is adapted to meet their needs to survive and proliferate in a hypoxic and also in a well-oxygenated microenvironment and thus must acquire metabolic flexibility. At the molecular level,

Abbreviations: ADP, adenosine diphosphate; AMPK, adenosine 5'-monophosphate-activated protein kinase; AK, adenylate kinase; ANT, adenine nucleotide translocator; CK, creatine kinase; CRC, colorectal cancer; HK, hexokinase; HIF, hypoxia-inducible factor; ISC, iron-sulfur clusters; OMM, outer mitochondrial membrane; TCA, tricarboxylic acid; OXPHOS, oxidative phosphorylation; ROS, reactive oxygen species; VDAC, voltage-dependent anion channel.

metabolic flexibility relies on the configuration of metabolic pathways, which are regulated by key metabolic enzymes and transcription factors. Reprogramming of cellular energetics is recognized as a distinctive hallmark of cancer (1). The first theory on the peculiarities of cancer metabolism was formulated by Otto Warburg in the early 20th century. He concluded that tumors, unlike normal cells, obtain their energy mainly from aerobic glycolysis, while normal cells usually favor oxidative phosphorylation (OXPHOS), which is much more efficient in terms of ATP gain. This observation is coined as the Warburg effect (2, 3) and became the central model for oncobienergetics for most of the 20th century. The glycolytic part of the Warburg hypothesis was firmly and thoroughly confirmed for many cancer types, in contrast to the OXPHOS part, which was and still is a matter of intense research and controversy. Verified evidence indicates that in reality, both anaerobic (glucose to lactate) and aerobic (glucose to pyruvate) glycolysis operate in cancer cells simultaneously like in normal cells, although at higher rates than in non-tumor cells (4). In addition, tumor cells often exhibit high rates of OXPHOS (5, 6). Transcriptomics and end-product metabolites analyses of complex molecular pathways converge into a three-node minimum regulatory network consisting of hypoxia-inducible factor 1 (HIF-1), adenosine monophosphate-activated protein kinase (AMPK), and reactive oxygen species (ROS). Therefore, the coexistence of three distinct cellular metabolic phenotypes is revealed in cancer cells: 1) glycolytic, characterized by high activity of HIF-1 α and high activity of the glycolytic pathway; 2) OXPHOS state, characterized by high activity of AMPK and high activity of OXPHOS pathways such as glucose oxidation and fatty acid oxidation; 3) hybrid metabolic state, characterized by high activity of AMPK and HIF-1 α and concomitant functioning of glycolysis and OXPHOS pathways. In contrast, normal cells exhibit only two metabolic states, namely, glycolytic and OXPHOS, and lack the hybrid state (7, 8). In this regulatory network, HIF-1 and AMPK are the master regulators of glycolysis and OXPHOS, respectively (9), and both cytosolic and mitochondrial ROS mediate the complex interplay between AMPK and HIF-1. Accordingly, the hybrid metabolic state in cancer cells can be promoted by the stabilization of HIF-1 α and elevated production of mitochondrial ROS. Hypoxia activates glycolysis *via* stabilization of HIF-1 α and HIF-2 α , which in turn upregulates the activity of several members of the glycolytic pathway and increases glucose uptake (10, 11). In addition, the elevation of HIF-1 α levels could be induced by high concentrations of succinate (pseudohypoxia) (12). A striking feature of cancer cells is their ability to switch their metabolic phenotypes to glycolysis or OXPHOS in response to changes in their microenvironment or inhibition of one of these pathways, giving survival advantage during tumor progression (8, 13). This metabolic plasticity is promoted by the hybrid phenotype of cancer cells and is linked with metastasis and chemoresistance (14). However, it is still largely unknown how cancer cells regulate gene expression to maintain their hybrid metabolic state and metabolic plasticity.

Implementation of the hybrid metabolism paradigm may reveal new therapeutic targets and opportunities for the treatment of cancer. It was previously shown that administration of glycolytic inhibitors alone may be ineffective to eradicate tumors, and targeting the hybrid state to eliminate metabolic plasticity could be a new therapeutic strategy to eliminate cancer aggressiveness (15, 16). We review the changes in OMM permeability and intracellular energy transfer pathways in connection with the metabolic plasticity of CRC cells.

METABOLIC REPROGRAMMING OF COLORECTAL CANCER

Colorectal cancer has been regarded as a purely hypoxic tumor of the Warburg phenotype for many years. This was confirmed by increased expression of several glycolytic enzymes, pentose phosphate pathway, and glucose transporters associated with elevated rates of glucose consumption and lactate production as compared with normal surrounding tissues (17–25). Normal colonocytes use the OXPHOS system as the primary energy source (26, 27). Short-chain fatty acids undergo β -oxidation to form acetyl-CoA, which enters into the tricarboxylic acid (TCA) cycle to yield citrate, NADH, and finally ATP. But, unlike normal colonocytes, colorectal carcinomas cannot utilize butyrate as an energy source and carbon donor (26, 28), implying the truncated TCA cycle in CRC. Importantly, some metabolites of the TCA cycle, such as succinate, fumarate, and α -ketoglutarate, act as “oncometabolites” that support tumor growth *via* oncogenic signaling, *inter alia via* upregulation and stabilization of HIF-1 α (29).

Metabolic reprogramming during large intestine carcinogenesis is largely mediated by (a) altered expression of several oncogenes and a loss of tumor suppressor genes, encoding usually various transcriptional factors and protein kinases (30, 31), (b) adaptation to nutrient and oxygen availability in the local tumor microenvironment (metabolic plasticity) (32), and (c) metabolic cross-talk with stromal, adipose tissue and immune cells (31, 33–37).

Data on molecular mechanisms of the metabolic reprogramming of CRC are mostly obtained from studies using cell culture models, while the number of functional studies using clinical material is limited. Moreover, cell culture conditions have variations that could significantly affect the metabolic profile of the cells. For example, cells grown in glucose-free medium display a relatively high rate of oxygen consumption, while cultivation of cells in a high-glucose medium results in hyperglycolytic profile and declined respiratory flux (38–42). Our recent studies revealed remarkable differences in the regulation of outer mitochondrial membrane (OMM) permeability between cultured tumor cells and clinical material from cancer patients (5, 43). Comparative analysis of the biopsy or surgical cancer material and surrounding healthy tissue showed almost unchanged glycolytic activity and upregulation of OXPHOS in CRC, which is inconsistent with the data obtained by using cell culture (43–47). In addition, two widely

used breast cancer cell lines MCF7 and MCF-MDA-231 failed to replicate mitochondrial function in respect to metabolic activity and OXPHOS as seen in respective human samples (43, 46).

Why the CRC cells shift their metabolism in favor of OXPHOS? Perhaps, under normal conditions, the amount of ATP produced through aerobic glycolysis is insufficient to support cell proliferation and migration. There is a growing body of evidence that CRC is characterized by stimulated mitochondrial biogenesis expressed as an increase in mitochondrial DNA copy number (48) and elevated ADP-dependent oxygen consumption in CRC tissue (5, 6, 43–45). Activated mitochondrial biogenesis can be an adaptive response of tumor cells to overcome the chronic energy crisis caused by glucose starvation or defects in the function of their respiratory enzymes due to pathogenic nuclear or mtDNA mutations (49–51). The elevated lactate level may act as a signaling molecule to affect genes and proteins known to be involved in mitochondrial biogenesis (52), *via* upregulation of AMPK- and SIRT1-associated PGC-1 α activation (53). Nuclear Respiratory Factor 1 (NRF1) (54) and some cytokines, IL-6/8 (55, 56), activate the AMPK signaling pathway as well as apoptotic resistance of cancer cells (56–58). Some types of tumor cells support their high rates of OXPHOS and drug resistance by transferring mtDNA or even the entire mitochondria from surrounding healthy tissues; this intercellular mitochondrial transfer may occur through exosomes or tunnel nanotubes (59, 60). The signaling pathways responsible for the stimulation of mitochondrial biogenesis can have both intracellular and external origins.

THE ROLE OF VDAC AND THE REGULATION OF OUTER MITOCHONDRIAL MEMBRANE PERMEABILITY IN METABOLIC PLASTICITY

The flux of water-soluble metabolites into and out of the mitochondria occurs through a variety of inner mitochondrial membrane (IMM) carriers, but the flux of ATP, ADP, and Pi across the OMM occurs through a single pathway, the VDAC, and therefore the regulation of OXPHOS is largely mediated by the VDAC permeability control (61). Based on studies of muscle permeabilized fibers, cellular respiration and associated ATP synthesis are regulated by a protein complex called Mitochondrial Interactosome (MI), which is located at the junction of mitochondrial membranes (62, 63). Restrictions for adenine nucleotides in VDAC are evident by measuring an apparent affinity of mitochondria for exogenous ADP [K_m (ADP)] in permeabilized cells and tissues by using high-resolution respirometry (64, 65). These barriers appear only in permeabilized cells and not in isolated mitochondria and disappear during mild proteolytic treatment with trypsin (66). Therefore, the metabolic plasticity of cancer cells is associated

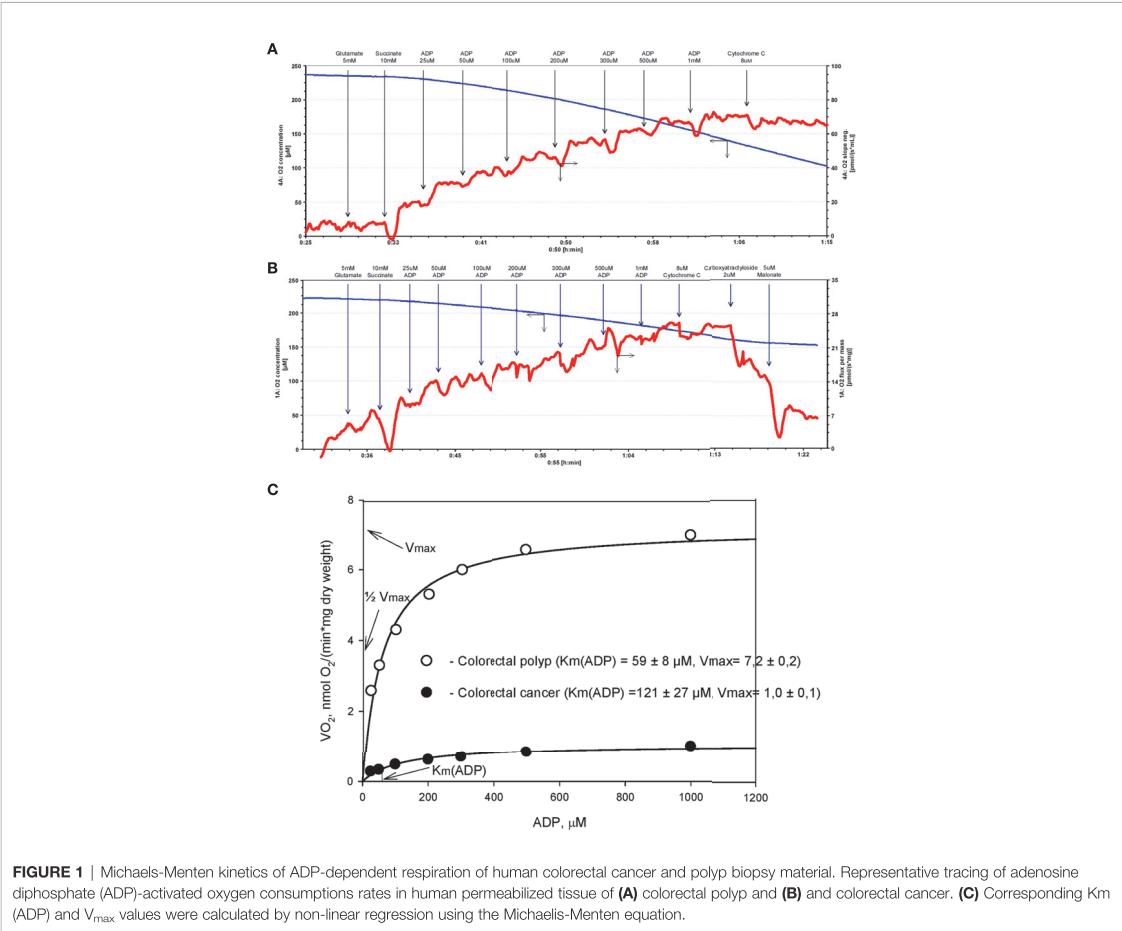
with the protein-mediated control of VDAC permeability towards ADP.

Cancer Metabolic Plasticity Is Functionally Defined by Changes in ADP Dependent Oxygen Consumption

Analysis of respirometry data provides instant functional profiling of metabolic plasticity. Dependence of mitochondrial O_2 consumption upon ADP concentration follows Michaelis-Menten kinetics and allows evaluation of apparent Michaelis-Menten constant for ADP K_m (ADP) in different tissues, cancers, and cell cultures (Figure 1). Determined in permeabilized cells and tissues, K_m (ADP) is the affinity of the mitochondria for exogenous ADP and characterizes permeability of OMM for adenine nucleotides and, thus, VDAC permeability. Measured K_m (ADP) values for human colon mucosa is $\sim 110 \mu M$ (47), $\sim 100 \mu M$ for CRC (5, 44, 47), $\sim 60 \mu M$ for colon polyps (47), and $\sim 40 \mu M$ for Caco2 CRC cell line (43), indicating the alteration of control mechanisms over VDAC permeability and OXPHOS during the progression of CRC. Thus, the regulation of OMM permeability to adenine nucleotides in cancer tissues is different from that in normal cells (5, 67, 68). Notably, K_m (ADP) values measured in cell cultures are much lower than in tissue biopsies and are similar to K_m (ADP) values for isolated mitochondria (69). This illustrates the shortcomings of cell culture studies and highlights the importance of using clinical material for the evaluation of the mechanism of cancer metabolic plasticity.

The cell-specific differences in K_m (ADP) are likely caused by the specific structural and functional organization of energy metabolism. For example, cells with a low K_m (ADP) value ($\sim 10 \mu M$), like glycolytic muscle, possess less structural and functional restrictions for ADP/ATP movement through OMM as compared to the oxidative muscles (K_m (ADP) $\sim 300 \mu M$) (64). Thus, relatively low K_m (ADP) for colorectal polyps indicates a metabolic reprogramming towards the glycolytic phenotype with functional OXPHOS (as in glycolytic muscle), and an increase in K_m values in the CRC reflects a shift to OXPHOS phenotype with increased intracellular complexity (analogy with oxidative muscle). Hence, K_m (ADP) value is an important parameter describing metabolic plasticity. According to the model proposed by Saks V. et al, the proportion of mitochondria with low oxidative capacity in the tissue can be inferred from the K_m (ADP) value (70). For example, the proportion of mitochondria with high oxidative capacity is 67% in CRC tumors and only 38% in colorectal polyps (47).

In addition to K_m (ADP), the maximal ADP-dependent oxygen consumption (V_{max}) is a defining characteristic of metabolic plasticity and is correlated to mitochondrial content (density) in the tissue. V_{max} values are higher in CRC than in normal colon tissue (5, 6, 47), indicating a vigorous metabolic activity. Moreover, V_{max} values in biopsy material from patients that succumbed to colon cancer were significantly higher than in patients staying in remission (5). However, the extent to which high V_{max} values correlate with tumor aggressiveness needs to be confirmed in further studies.



The Possible Mechanisms of VDAC Permeability Regulation

Several studies show that VDAC isoform 1 (VDAC1) is the dominant isoform in most malignant tumors including CRC (44, 71, 72). VDAC1 is crucial in communication between the mitochondria and the cytosol. Cancer cells display high levels of metabolic flexibility combined with apoptosis resistance, which provides a survival advantage for these cells. VDAC1 is well recognized as a metabolic checkpoint at the crossroad of these two processes (72, 73). VDAC mediates and regulates the transport of metabolites, ions, and ROS across OMM. Thus, VDAC1 plays a major role in the control of mitochondrial function. Transport of ADP through OMM is mediated *via* VDAC1 and through the inner membrane *via* ANT. Metabolic control analysis of the OXPHOS system of CRC revealed that ANT does not exert exclusive control over the mitochondrial ADP-dependent oxygen consumption (5, 43). Therefore, the rate-limiting step of ADP transport into the mitochondria appears to be VDAC. Therefore, the alteration of K_m (ADP)

value depends on the changes in interactions of VDAC1 with other proteins or on the modification of VDAC1 itself.

As the name implies, VDAC is regulated by a change of membrane potential. Studies of isolated VDAC1 reconstituted into planar lipid bilayers reveal sharp and symmetrical voltage dependence of VDAC1 permeability (72, 74, 75). At membrane potentials close to zero (between -20 to $+20$ mV), VDAC1 is open and displays low anionic selectivity. At more positive or more negative membrane potentials ($+30$, $+60$ mV or -30 , -60 mV), VDAC1 shows diminished permeability to large anions and becomes more selective to small cations (72). However, it is unknown whether the voltage dependence of VDAC1 is relevant in physiological conditions, as the value of membrane potential across OMM is unknown. It is generally believed that any membrane potential generated at OMM will be offset by a relatively undisturbed movement of small ions across OMM. However, there is a theoretical possibility that OMM can be polarized to potentials large enough to alter the permeability of VDAC1 (2, 3). Although the role of OMM potential in the

regulation of VDAC1 permeability is unlikely, it remains to be investigated whether potential across OMM changes in CRC and whether such change can alter $K_m(\text{ADP})$.

Hexokinase-VDAC Interaction Regulates the Permeability of VDAC to Adenine Nucleotides

Although the VDAC-hexokinase (HK) binding was demonstrated by several groups using different experimental approaches, it still remains somewhat speculative, and there are different hypothesis on its functional consequences. Research activities of Prof. Pedersen and his colleagues resulted in the discovery of the binding of HK-II to VDAC with the conclusion that this phenomenon could play a pivotal role in the “Warburg Effect” (76–80). Review paper of V. Shoshan-Barmatz et al. proposed the hypothesis that HK-II binds to VDAC and promotes VDAC closing (81). Neumann et al. demonstrated the binding of the cytosolic protein HK-I to VDAC by two-color STED microscopy (82). Our group showed the colocalization of VDAC1 and hexokinase II in cell cultures and clinical cancer samples by confocal microscopy imaging (6, 67). Based on these studies, two models of VDAC permeability control have been proposed. The model proposed by Pedersen et al. states that the binding of HK-II to VDAC plays a pivotal role in maintaining the Warburg phenotype in cancer cells (77, 83). In such a setting, mitochondrial ATP is preferentially directed to glycolysis (HK reaction) and the produced ADP is channeled back to the OXPHOS (Figure 2). At the same time, VDAC is assumed to be in an open state and mitochondria have free access to exogenous ADP (84, 85), thus low $K_m(\text{ADP})$ values are expected. Glucose-stimulated increase of mitochondrial respiration shows the amount of ADP released in the HK reaction that passes through VDAC and is utilized in

mitochondrial ATP synthesis (86). Such glucose effect comprises a fraction of total ADP-stimulated respiration and is higher in cancer cells as compared to normal cells. Accordingly, the glucose effect is about 20% for CRC tissue, about 12% for normal colon tissue samples (6), and about 48% for Caco-2 CRC cell line (43). These results show that the lower affinity of mitochondria for ADP could be related to the weaker ability for glucose to stimulate respiration. CRC displays elevated levels of VDAC1 as compared with surrounding healthy tissues (43), and this is in good agreement with the fact that V_{\max} for ADP-dependent respiration is higher in CRC (44). The total HK activity and expression levels of HK1 and HK2 in CRC do not differ from that of normal tissue (6, 44). In both the normal mucosa and the CRC, HK2 is colocalized with VDAC (6, 43). The interaction of HK1 or HK2 with VDAC1 gives numerous advantages to cancer cells: (1) it mediates the increased permeability of the OMM to adenine nucleotides; (2) it increases the rate of aerobic glycolysis and thereby allows the cells to adapt to hypoxic conditions; (3) it mediates elevated resistance to apoptosis and protection from oxidative stress as VDAC1-bound HK acts as an anti-apoptotic protein (73, 87–89). VDAC-HK interaction is reversed with inhibitors of HK2 (e.g., 3-bromopyruvate), and agents that disrupt the VDAC-HK interaction have been tested as anticancer drugs (73, 90–93). It was also reported that silencing of VDAC1 expression by siRNA inhibited the proliferation of several cancer cell lines (including CRC) (94).

Free Beta-Tubulins Controlling VDAC Permeability in CRC

According to the free-tubulin model, the binding of free tubulin blocks VDAC and thereby regulates respiration (95). The

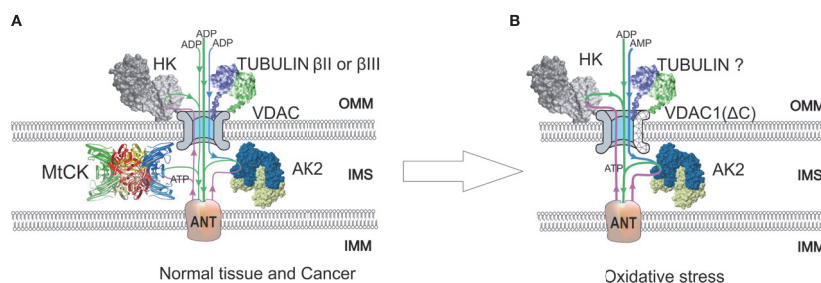


FIGURE 2 | A model of regulation of outer mitochondrial membrane (OMM) permeability for adenine nucleotides in normal and colorectal cancer (CRC) cells. Voltage-dependent anion channel (VDAC) is the pore through which adenine nucleotides move into and out of the mitochondria. **(A)** In normal and possibly some cancer cells, a minor amount of hexokinase (HK) is bound to VDAC and utilizes mitochondrial ATP to initiate glycolysis. Produced ADP is channeled back to the mitochondrial matrix via VDAC and adenine nucleotide translocase (ANT) for use in oxidative phosphorylation (OXPHOS). VDAC permeability is also regulated by tubulin binding. As a result of beta-tubulin-VDAC interaction, the VDAC is less permeable to adenine nucleotides. This in turn promotes cells to use creatine kinase (CK) and adenylate kinase (AK) energy transfer networks for intracellular distribution of high-energy phosphates. Mitochondrial intermembrane space (IMS)-residing mitochondrial CK (MtCK) is functionally coupled to ANT, turning OXPHOS to be dependent on ADP originating from MtCK reaction. Mitochondrial AK isoform AK2 uses AMP passing through VDAC and ATP passing through ANT to produce ADP, which stimulates OXPHOS. These energy transport systems provide feedback between ATP consumption and synthesis. **(B)** Redox stress may induce an increased amount of HK bound to VDAC. In addition, VDAC can be truncated at C-terminus by proteases activated in response to oxidative stress. The role of tubulin in the regulation of VDAC permeability remains unclear, as the interaction of truncated VDAC with tubulin might be impaired. The AK2 activity in cancer cells is increased, resulting in enhanced utilization of extra-mitochondrial AMP to OXPHOS. IMM, inner mitochondrial membrane; IMS, intermembrane space.

rationale behind this model is the observation that proliferating cancer cells have high levels of free tubulin for mitotic spindle formation. Free tubulin dimers bound to VDAC induce a closed state of VDAC (**Figure 2**) and cause a suppression of mitochondrial metabolism; thus, aerobic glycolysis will become the main source of energy. Maldonado and Lemasters's group shows at HepG2, A549, and UM-SCC-1 cells that tubulin binding closes the VDAC channel (95). It sounds like the hypothesis in this review contradicts Maldonado's publications (95, 96). However, in fact, the results of both works are in agreement. The amount of dimeric and polymerized tubulin in cells is nearly constant, but the ratio could change significantly. In both cases it is dimeric tubulin, which affects VDAC permeability, but this effect depends on the polymerization state. Also, it should be definitely noted that the regulation of VDAC permeability is tissue specific. Unlike striated muscles, where the main regulator of VDAC is beta-II tubulin (97), in CRC the VDAC and beta-II tubulin colocalization is absent (6). Instead, beta-III tubulin (TUBB3) could be the partner of VDAC in CRC cells. Beta-III tubulin overexpression has been reported in several intestinal cancers like carcinoids of the small intestine and rectal carcinoids (98), gastric cancer (99), colon neoplasias like polyps, and CRC (6, 100). *TUBB3* expression has been associated with the resistance to drugs perturbing the microtubule dynamics (e.g., paclitaxel) and studied as a prognostic biomarker in various cancers (101, 102). It has been demonstrated that in non-small-cell lung cancer, the expression of beta-III tubulin decreases the dependence of cells on glycolysis and thus improves the tumor's ability to cope with the changing nutrient supply in the microenvironment (103). From a functional analysis of the network of proteins forming disulfide bonds with beta-III tubulin, it appears that some of them are involved in oxidative stress and glucose deprivation response (104). It was shown that hypoxia *via* HIF-1 α can induce the expression of *TUBB3* (105). Beta-III tubulin is likely part of a complex pathway induced by hypoxia and shortage of nutrients (101). However, our recent study revealed that microtubule destabilizing (colchicine) and stabilizing (taxol) agents do not affect the Km(ADP) in glioblastoma and sarcoma cells (67). Hence, the actual role of beta-tubulins in cancer metabolism and mitochondrial respiratory control needs further investigation.

Regulation of VDAC1 by Protein-Protein Interactions and Redox Stress

In addition to the two previous models, the modifications of VDAC1 protein induced by oxidative stress could be responsible for alterations of apparent value of Km(ADP). Tumor cells are well adapted to a hypoxic environment, and VDAC1 is regulated by oxygen tension in HIF-1 α -dependent manner at the levels of transcription and protein modification. Transcription of the *VDAC1* gene is regulated by HIF-1 α and NRF-1 (nuclear respiratory factor 1), which leads to increased levels of VDAC1 in response to hypoxia or nutrient deprivation of the cells (106). Along with VDAC1 expression regulation, HIF-1 α is also involved in the cleavage of VDAC1, resulting in a truncated form of VDAC1 (107). In normoxic conditions, VDAC1 is

expressed as a full-length protein of molecular weight of approximately 30 kDa, while in response to hypoxia, there is a larger proportion of a shorter VDAC1 variant lacking C-terminal part (VDAC1- Δ C) with a molecular weight of approximately 25 kDa (107). The shorter variant is a product of the cleavage of VDAC1 at asparagine 214 by the asparagine endopeptidase Legumain (LGMN), which in turn is activated in a HIF-1 α -dependent way upon hypoxia (107). The electrophysiological properties of VDAC1- Δ C are similar to full-length protein; however, its permeability is slightly reduced (107). Levels of VDAC1- Δ C were higher in late-stage lung tumors (107), and it was suggested that HIF-1 α mediated induction of VDAC1- Δ C provides protection from apoptosis and enhances cell survival in hypoxia (107, 108). Hypoxia-induced VDAC1- Δ C lacks a phosphorylation site at serine 215, and therefore its interaction with tubulin is impaired (108). Notably, *HIF-1 α* overexpression was significantly associated with higher CRC-specific mortality in a cohort of 731 patients (109). Consequently, inhibition of HIF-1 α is proposed as a possible treatment strategy for CRC (110). Moreover, the expression of endopeptidase LGMN is elevated in CRC and is associated with a poor prognosis (111). Furthermore, a meta-analysis revealed the overexpression of *LGMN* to be correlated with the aggressiveness of different cancer types, with higher levels of LGMN in late-stage tumors (112).

It is currently unknown whether VDAC1- Δ C is present in CRC cells and whether truncation-induced impairment of VDAC1 interaction with tubulin affects apparent affinity for ADP (**Figure 2**). Given the role of tubulin in the regulation of VDAC1 and the discovery of VDAC1- Δ C in lung cancer, VDAC1 truncation may also play a role in metabolic alterations of CRC. Future studies should reveal whether the truncated form of VDAC1 plays a role in metabolic adaptations of CRC.

Recent studies indicate a link between iron-sulfur cluster (ISC) synthesis and regulation of VDAC1. Biogenesis of ISC is an ancient process, and ISCs are important redox-sensitive cofactors for many enzymes involved in energy homeostasis. Synthesis of ISC starts within the mitochondrial matrix, and depletion of proteins involved in mitochondrial ISC assembly leads to accumulation of VDAC1- Δ C in normoxic conditions independent of HIF-1 α (113). Depletion of the iron-sulfur cluster containing protein C1SD2 also resulted in the accumulation of truncated VDAC1- Δ C (113). Therefore, mitochondria-associated membrane-localized Fe-S protein C1SD2 acts as a link between ISC machinery and accumulation of VDAC1- Δ C (113).

Another iron-sulfur cluster protein, mitoNEET, was found to interact with VDAC1 in a redox-sensitive way (114). MitoNEET harbors [2Fe-2S] cluster and binds to VDAC1 when its cluster is oxidized, thus inhibiting VDAC1 conductivity. Such interaction does not occur when mitoNEET-bound ISC cluster is reduced (114). Therefore, mitoNEET governs VDAC1 permeability in a redox-sensitive way, inhibiting VDAC1 in high redox stress conditions. Oxidative stress is increased in CRC (115); thus, the interaction of mitoNEET with VDAC1 can be altered in CRC.

It remains to be investigated whether such redox-sensitive mitoNEET-VDAC1 interaction can alter the apparent K_m (ADP) value and is involved in the metabolic plasticity of CRC.

There is a large number of proteins that were found to interact with VDAC1 and are therefore potentially able to modulate VDAC permeability. Interacting partners of VDAC1 are involved in the regulation of apoptosis (Bax, Bcl2, Bak, etc.), energy metabolism (HK1, HK2, ACSL, CPT1, ANT, etc.), cytoskeletal organization (Tubulin, actin, dynein, etc.), and other cellular functions [Parkin, alpha-synuclein, APP, gamma-secretase] [reviewed in (116)]. However, the role of these interactions in the modulation of cellular respiration needs to be further investigated.

ENERGY TRANSPORT PATHWAYS IN CRC CELLS—THE PARTICIPANTS IN THE METABOLIC PLASTICITY

In addition to the altered transport of adenine nucleotides through OMM alterations of energy transport circuits formed from creatine kinase (CK) and adenylate kinase (AK) isoenzymes are also involved in the development of metabolic plasticity. Cancer cells have uncontrolled cell division, which is accompanied by a high energy need for anabolic processes and large cell structure rearrangements. Therefore, it is hypothesized that energy transport pathways are also reprogrammed in cancer cells to meet these demands. Previous data show downregulation of the CK pathway and mitochondrial CK (MtCK) in CRC cells, which results in functional uncoupling between the CK circuit and OXPHOS (6, 44). In contrast, total AK activity is higher in CRC than in normal intestinal tissue, and it also reflects enhanced coupling between AK and OXPHOS (i.e., AMP can affect the rate of oxygen consumption) (Figure 2) (6, 44). This is in agreement with the observation that expression of AK mitochondrial isoform AK2 is increased in several cancers including lung adenocarcinoma (117) and breast cancer (118, 119). Also, there is evidence that another mitochondrial isoform, AK4, is involved in the regulation of mitochondrial metabolism in cancer cells. In HeLa cells, AK4 forms complexes with ANT, VDAC, and HK2 for the efficient recycling of ADP (120). Further, AK4 expression is induced by hypoxia, and protein complex AK4-ANT-VDAC-HK2 complex supports the high glycolytic activity of cancer cells (120). Intestinal cells are able to switch off the CK circuit and turn on the AK pathway to establish metabolic plasticity. Such flexibility of phosphotransfer networks in Caco2 CRC cell lines depends on the availability of key metabolic substrates and is associated with the cell differentiation state (121). The abovementioned data indicate a possible role of the phosphotransfer networks related to the regulation of VDAC permeability for adenine nucleotides and metabolic plasticity.

The function of energy transfer pathways is well characterized in striated muscle cells where its role is to overcome the diffusion restrictions for ATP and ADP, thereby directing the energy-rich phosphate groups to the CK, AK, and glycolytic energy transfer circuits. This way of energy transfer allows the formation of micro-compartments at energy consumption sites where high ATP/ADP levels are maintained for maximal performance.

Similarly, in the compartment where energy is produced (e.g., mitochondrial membranes), favorable levels of ADP are maintained to ensure efficient ATP synthesis [reviewed in (65, 122)]. In the case of CRC, downregulation of MtCK leads to the inability to produce phosphocreatine and a loss of functional coupling between the VDAC-MtCK-ANT complex, accompanied by the formation of other regulating combinations like VDAC-HK-ANT. In this aspect, more studies are required to determine the profile of HK, AK, ANT, and VDAC isoform expression in human CRC.

In addition to their role in energy transfer among cellular processes, AKs are an integral part of intracellular energy sensing and metabolic signaling (123, 124). Due to its catalytic reaction ($2\text{ADP} \leftrightarrow \text{AMP} + \text{ATP}$), it can amplify a small change in the ATP/ADP ratio into relatively large changes in AMP concentration. This relates AKs to the activation of cellular AMP-sensitive components like AMPK. In general, activation of AMPK switches on catabolic pathways that generate ATP, while switching off biosynthetic pathways and cell-cycle progress (125). The role of AMPK in cancer is controversial; it has been recognized as a tumor suppressor in some cancers (126–129) and in some cases described as a contextual oncogene, as the AMPK activation promotes tumor progression and chemoresistance (130–132). Downregulation of $\text{AK} \rightarrow \text{AMP} \rightarrow \text{AMPK}$ signaling could lead to loss of control over the cell cycle, growth, and proliferation (124). A recent in-depth review about AKs and metabolic signaling in cancer cells by Klepinin et al. (124) highlights the role of suppression of AK phosphotransfer and signaling through AMPK as a potential target for cancer metabolism. How different AK isoforms are distributed in CRC cells and how their activities affect AMPK activation and metabolic plasticity need further investigation.

Adenylate kinases network promotes cancer growth and metastasis through participating in AMPK metabolic signaling and regulating mitochondrial adenine nucleotide exchange.

CONCLUSION AND PROSPECTS

Metabolic plasticity is a defining characteristic of the cancer cells that allow undisturbed proliferation in changing environment. At the functional level, different metabolic states of the cancer cells can be identified and characterized by measuring the dependence of mitochondrial respiration upon ADP concentration using the classical Michaelis-Menten kinetic model. The apparent affinity of ADP provides an integrated assessment of cell metabolic state, which is functionally determined by the permeability of VDAC1. Regulation of VDAC1 involves many protein-protein interactions, as well as hypoxia- and redox-sensitive mechanisms. The regulation of OMM permeability for adenine nucleotides is presumably more complex than the binding between the VDAC1 channel and some single type of protein molecule. Unraveling the molecular mechanisms of metabolic plasticity will reveal new therapeutic targets for the development of novel cancer treatments. This knowledge combined with relatively simple

functional evaluation of cancer metabolism in biopsy material can form a new prospect for personalized medicine.

AUTHOR CONTRIBUTIONS

Conceptualization, LT, MP, AT, and TK. Funding acquisition, TK. Project administration, AT and TK. Visualization, LR and IS. Writing—original draft, MP, AT, VC, and TK. Writing—

review and editing, LR, SM, ER-K, NT, KT, IS, and TK. All authors contributed to the article and approved the submitted version.

FUNDING

This work was supported by the Estonian Research Council grant PRG1035 and NICPB institutional Development Fund grant.

REFERENCES

- Hanahan D, Weinberg RA. Hallmarks of Cancer: The Next Generation. *Cell* (2011) 144(5):646–74. doi: 10.1016/j.cell.2011.02.013
- Lemeshko SV, Lemeshko VV. Metabolically Derived Potential on the Outer Membrane of Mitochondria: A Computational Model. *Biophys J* (2000) 79(6):2785–800. doi: 10.1016/S0006-3495(00)76518-0
- Lemeshko VV. Model of the Outer Membrane Potential Generation by the Inner Membrane of Mitochondria. *Biophys J* (2002) 82(2):684–92. doi: 10.1016/S0006-3495(02)75431-3
- Moreno-Sanchez R, Marin-Hernandez A, Saavedra E, Pardo JP, Ralph SJ, Rodriguez-Enriquez S. Who Controls the ATP Supply in Cancer Cells? Biochemistry Lessons to Understand Cancer Energy Metabolism. *Int J Biochem Cell Biol* (2014) 50:10–23. doi: 10.1016/j.biocel.2014.01.025
- Koit A, Shevchuk I, Ounpuu L, Klepinin A, Chekulayev V, Timohhina N, et al. Mitochondrial Respiration in Human Colorectal and Breast Cancer Clinical Material Is Regulated Differently. *Oxid Med Cell Longev* (2017) 2017:1372640. doi: 10.1155/2017/1372640
- Kaldma A, Klepinin A, Chekulayev V, Mado K, Shevchuk I, Timohhina N, et al. An *In Situ* Study of Bioenergetic Properties of Human Colorectal Cancer: The Regulation of Mitochondrial Respiration and Distribution of Flux Control Among the Components of ATP Synthasome. *Int J Biochem Cell Biol* (2014) 55:171–86. doi: 10.1016/j.biocel.2014.09.004
- Yu L, Lu M, Jia D, Ma J, Ben-Jacob E, Levine H, et al. Modeling the Genetic Regulation of Cancer Metabolism: Interplay Between Glycolysis and Oxidative Phosphorylation. *Cancer Res* (2017) 77(7):1564–74. doi: 10.1158/0008-5472.CAN-16-2074
- Paudel BB, Quaranta V. Metabolic Plasticity Meets Gene Regulation. *Proc Natl Acad Sci USA* (2019) 116(9):3370–2. doi: 10.1073/pnas.1900169116
- Vander Heiden MG, Cantley LC, Thompson CB. Understanding the Warburg Effect: The Metabolic Requirements of Cell Proliferation. *Science* (2009) 324(5930):1029–33. doi: 10.1126/science.1160809
- Libby CJ, McConathy J, Darley-Usmar V, Hjelmeland AB. The Role of Metabolic Plasticity in Blood and Brain Stem Cell Pathophysiology. *Cancer Res* (2020) 80(1):5–16. doi: 10.1158/0008-5472.CAN-19-1169
- Berridge MV, Herst PM, Tan AS. Metabolic Flexibility and Cell Hierarchy in Metastatic Cancer. *Mitochondrion* (2010) 10(6):584–8. doi: 10.1016/j.mito.2010.08.002
- Garrigue P, Bodin-Hullin A, Balasse L, Fernandez S, Essamet W, Dignat-George F, et al. The Evolving Role of Succinate in Tumor Metabolism: An (18)F-FDG-Based Study. *J Nucl Med* (2017) 58(11):1749–55. doi: 10.2967/jnumed.117.192674
- Lin Y, Ma C, Bezabeh T, Wang Z, Liang J, Huang Y, et al. 1h NMR-Based Metabolomics Reveal Overlapping Discriminatory Metabolites and Metabolic Pathway Disturbances Between Colorectal Tumor Tissues and Fecal Samples. *Int J Cancer* (2019) 145(6):1679–89. doi: 10.1002/ijc.32190
- Jia D, Park JH, Jung KH, Levine H, Kaipappattu BA. Elucidating the Metabolic Plasticity of Cancer: Mitochondrial Reprogramming and Hybrid Metabolic States. *Cells* (2018) 7(3):21. doi: 10.3390/cells7030021
- Jia D, Lu M, Jung KH, Park JH, Yu L, Onuchic JN, et al. Elucidating Cancer Metabolic Plasticity by Coupling Gene Regulation With Metabolic Pathways. *Proc Natl Acad Sci* (2019) 116(9):3909–18. doi: 10.1073/pnas.1816391116
- Sotgia F, Oszvari B, Fiorillo M, De Francesco EM, Bonuccelli G, Lisanti MP. A Mitochondrial Based Oncology Platform for Targeting Cancer Stem Cells (CSCs): MITO-ONC-Rx. *Cell Cycle* (2018) 17(17):2091–100. doi: 10.1080/15384101.2018.1515551
- Altenberg B, Greulich KO. Genes of Glycolysis Are Ubiquitously Overexpressed in 24 Cancer Classes. *Genomics* (2004) 84(6):1014–20. doi: 10.1016/j.ygeno.2004.08.010
- Kawada K, Toda K, Nakamoto Y, Iwamoto M, Hatano E, Chen FS, et al. Relationship Between F-18-FDG PET/CT Scans and KRAS Mutations in Metastatic Colorectal Cancer. *J Nucl Med* (2015) 56(9):1322–7. doi: 10.2967/jnumed.115.160614
- Iwamoto M, Kawada K, Nakamoto Y, Itatani Y, Inamoto S, Toda K, et al. Regulation of 18F-FDG Accumulation in Colorectal Cancer Cells With Mutated KRAS. *J Nucl Med* (2014) 55(12):2038–44. doi: 10.2967/jnumed.114.142927
- Rubie C, Kempf K, Hans J, Su T, Tilton B, Georg T, et al. Housekeeping Gene Variability in Normal and Cancerous Colorectal, Pancreatic, Esophageal, Gastric and Hepatic Tissues. *Mol Cell Probes* (2005) 19(2):101–9. doi: 10.1016/j.mcp.2004.10.001
- Shonk CE, Arison RN, Koven BJ, Majima H, Boxer GE. Enzyme Patterns in Human Tissues. 3. Glycolytic Enzymes in Normal and Malignant Tissues of the Colon and Rectum. *Cancer Res* (1965) 25:206–13.
- Hennipman A, Smits J, van Oirschot B, van Houwelingen JC, Rijksen G, Neyt JP, et al. Glycolytic Enzymes in Breast Cancer, Benign Breast Disease and Normal Breast Tissue. *Tumor Biol* (1987) 8(5):251–63. doi: 10.1159/000217529
- Hennipman A, van Oirschot BA, Smits J, Rijksen G, Staal GEJ. Glycolytic Enzyme Activities in Breast Cancer Metastases. *Tumor Biol* (1988) 9(5):241–8. doi: 10.1159/000217568
- Groheux D, Cochet A, Humbert O, Alberini J-L, Hindié E, Mankoff D. 18F-FDG PET/CT for Staging and Restaging of Breast Cancer. *J Nucl Med* (2016) 57(Supplement 1):17S–26S. doi: 10.2967/jnumed.115.157859
- Hirayama A, Kami K, Sugimoto M, Sugawara M, Toki N, Onozuka H, et al. Quantitative Metabolome Profiling of Colon and Stomach Cancer Microenvironment by Capillary Electrophoresis Time-of-Flight Mass Spectrometry. *Cancer Res* (2009) 69(11):4918–25. doi: 10.1158/0008-5472.CAN-08-4806
- Donohoe DR, Garge N, Zhang X, Sun W, O'Connell TM, Bunger MK, et al. The Microbiome and Butyrate Regulate Energy Metabolism and Autophagy in the Mammalian Colon. *Cell Metab* (2011) 13(5):517–26. doi: 10.1016/j.cmet.2011.02.018
- Fleming SE, Fitch MD, DeVries S, Liu ML, Kight C. Nutrient Utilization by Cells Isolated From Rat Jejunum, Cecum and Colon. *J Nutr* (1991) 121(6):869–78. doi: 10.1093/jn/121.6.869
- Donohoe DR, Collins LB, Wali A, Bigler R, Sun W, Bultman SJ. : The Warburg Effect Dictates the Mechanism of Butyrate-Mediated Histone Acetylation and Cell Proliferation. *Mol Cell* (2012) 48(4):612–26. doi: 10.1016/j.molcel.2012.08.033
- Martinez-Reyes I, Chandel NS. Mitochondrial TCA Cycle Metabolites Control Physiology and Disease. *Nat Commun* (2020) 11(1):102. doi: 10.1038/s41467-019-13668-3
- Rodriguez-Enriquez S, Marin-Hernandez A, Gallardo-Perez JC, Pacheco-Velazquez SC, Belmont-Diaz JA, Robledo-Cadena DX, et al. Transcriptional Regulation of Energy Metabolism in Cancer Cells. *Cells* (2019) 8(10):1225. doi: 10.3390/cells8101225

31. Neitzel C, Demuth P, Wittmann S, Fahrer J. Targeting Altered Energy Metabolism in Colorectal Cancer: Oncogenic Reprogramming, the Central Role of the TCA Cycle and Therapeutic Opportunities. *Cancers (Basel)* (2020) 12(7):1731. doi: 10.3390/cancers12071731
32. Epstein T, Gatenby RA, Brown JS. The Warburg Effect as an Adaptation of Cancer Cells to Rapid Fluctuations in Energy Demand. *PLoS One* (2017) 12(9):e0185085–e0185085. doi: 10.1371/journal.pone.0185085
33. Brown RE, Short SP, Williams CS. Colorectal Cancer and Metabolism. *Curr Colorectal Cancer Rep* (2018) 14(6):226–41. doi: 10.1007/s11888-018-0420-y
34. Gandhi N, Das MG. Metabolic Reprogramming in Breast Cancer and Its Therapeutic Implications. *Cells* (2019) 8(2):89. doi: 10.3390/cells8020089
35. Dai C, Arceo J, Arnold J, Sreekumar A, Dovichi NJ, Li J, et al. Metabolomics of Oncogene-Specific Metabolic Reprogramming During Breast Cancer. *Cancer Metab* (2018) 6:5. doi: 10.1186/s40170-018-0175-6
36. D'Esposito V, Ambrosio MR, Giuliano M, Cabaro S, Miele C, Beguinot F, et al. Mammary Adipose Tissue Control of Breast Cancer Progression: Impact of Obesity and Diabetes. *Front Oncol* (2020) 10(1554):1554. doi: 10.3389/fonc.2020.01554
37. Tian W, Zhang W, Zhang Y, Zhu T, Hua Y, Li H, et al. FABP4 Promotes Invasion and Metastasis of Colon Cancer by Regulating Fatty Acid Transport. *Cancer Cell Int* (2020) 20(1):512. doi: 10.1186/s12935-020-01582-4
38. Swerdlow RH, L E, Aires D, Lu J. Glycolysis-Respiration Relationships in a Neuroblastoma Cell Line. *Biochim Biophys Acta* (2013) 1830(4):2891–8. doi: 10.1016/j.bbagen.2013.01.002
39. Jose C, Rossignol R. Rationale for Mitochondria-Targeting Strategies in Cancer Bioenergetic Therapies. *Int J Biochem Cell Biol* (2013) 45(1):123–9. doi: 10.1016/j.biocel.2012.07.005
40. Gnaiger E, Kemp RB. Anaerobic Metabolism in Aerobic Mammalian Cells: Information From the Ratio of Calorimetric Heat Flux and Respirometric Oxygen Flux. *Biochim Biophys Acta* (1990) 1016(3):328–32. doi: 10.1016/0005-2728(90)90164-y
41. Gstraunthaler G, Seppi T, Pfaller W. Impact of Culture Conditions, Culture Media Volumes, and Glucose Content on Metabolic Properties of Renal Epithelial Cell Cultures. Are Renal Cells in Tissue Culture Hypoxic? *Cell Physiol Biochem* (1999) 9(3):150–72. doi: 10.1159/000016312
42. Sherr CJ, DePinho RA. Cellular Senescence: Mitotic Clock or Culture Shock? *Cell* (2000) 102(4):407–10. doi: 10.1016/s0092-8674(00)00046-5
43. Ounpuu L, Truu L, Shevchuk I, Chekulayev V, Klepinin A, Koit A, et al. Comparative Analysis of the Bioenergetics of Human Adenocarcinoma Caco-2 Cell Line and Postoperative Tissue Samples From Colorectal Cancer Patients. *Biochem Cell Biol* (2018) 96(6):808–17. doi: 10.1139/bcb-2018-0076
44. Chekulayev V, Mado K, Shevchuk I, Koit A, Kaldma A, Klepinin A, et al. Metabolic Remodeling in Human Colorectal Cancer and Surrounding Tissues: Alterations in Regulation of Mitochondrial Respiration and Metabolic Fluxes. *Biochem Biophys Rep* (2015) 4:111–25. doi: 10.1016/j.bbrep.2015.08.020
45. Kaambre T, Chekulayev V, Shevchuk I, Karu-Varikmaa M, Timohhina N, Tepp K, et al. Metabolic Control Analysis of Cellular Respiration *In Situ* in Intraoperative Samples of Human Breast Cancer. *J Bioenerg Biomembr* (2012) 44(5):539–58. doi: 10.1007/s10863-012-9457-9
46. Koit A, Timohhina N, Truu L, Chekulayev V, Gudlawar S, Shevchuk I, et al. Metabolic and OXPHOS Activities Quantified by Temporal Ex Vivo Analysis Display Patient-Specific Metabolic Vulnerabilities in Human Breast Cancers. *Front Oncol* (2020) 10:1053. doi: 10.3389/fonc.2020.01053
47. Rebane-Klemm E, Truu L, Reinsalu L, Puurand M, Shevchuk I, Chekulayev V, et al. Mitochondrial Respiration in KRAS and BRAF Mutated Colorectal Tumors and Polyps. *Cancers (Basel)* (2020) 12(4):815. doi: 10.3390/cancers12040815
48. Feng S, Xiong LL, Ji ZN, Cheng W, Yang HJ. Correlation Between Increased Copy Number of Mitochondrial DNA and Clinicopathological Stage in Colorectal Cancer. *Oncol Lett* (2011) 2(5):899–903. doi: 10.3892/ol.2011.322
49. Richter C, Gogvadze V, Laffranchi R, Schlapbach R, Schweizer M, Suter M, et al. Oxidants in Mitochondria: From Physiology to Diseases. *Biochim Biophys Acta* (1995) 1271(1):67–74. doi: 10.1016/0925-4439(95)00012-S
50. Lee HC, Yin PH, Chi CW, Wei YH. Increase in Mitochondrial Mass in Human Fibroblasts Under Oxidative Stress and During Replicative Cell Senescence. *J BioMed Sci* (2002) 9(6 Pt 1):517–26. doi: 10.1007/BF02254978
51. Lee HC, Yin PH, Lu CY, Chi CW, Wei YH. Increase of Mitochondria and Mitochondrial DNA in Response to Oxidative Stress in Human Cells. *Biochem J* (2000) 348 Pt 2:425–32. doi: 10.1042/bj3480425
52. Genders AJ, Martin SD, McGee SL, Bishop DJ. A Physiological Drop in pH Decreases Mitochondrial Respiration, and HDAC and Akt Signaling, in L6 Myocytes. *Am J Physiol Cell Physiol* (2019) 316(3):C404–14. doi: 10.1152/ajpcell.00214.2018
53. Canto C, Auwerx J. PGC-1 α , SIRT1 and AMPK, an Energy Sensing Network That Controls Energy Expenditure. *Curr Opin Lipidol* (2009) 20(2):98–105. doi: 10.1097/MOL.0b013e328328d0a4
54. Das KJ, Feltz Q, Poppiti R, Jackson MR, Roy D. Nuclear Respiratory Factor 1 Acting as an Oncoprotein Drives Estrogen-Induced Breast Carcinogenesis. *Cells* (2018) 7(12):234. doi: 10.3390/cells7120234
55. Wang G, Wang Q, Huang Q, Chen Y, Sun X, He L, et al. Upregulation of mtSSB by Interleukin-6 Promotes Cell Growth Through Mitochondrial Biogenesis-Mediated Telomerase Activation in Colorectal Cancer. *Int J Cancer* (2018) 144:2516–28. doi: 10.1002/ijc.31978
56. Kumari N, Dwarakanath BS, Das A, Bhatt AN. Role of Interleukin-6 in Cancer Progression and Therapeutic Resistance. *Tumor Biol* (2016) 37(9):11553–72. doi: 10.1007/s13277-016-5098-7
57. Kumari N, Das A, Bhatt AN. Interleukin-6 Confers Radio-Resistance by Inducing Akt-Mediated Glycolysis and Reducing Mitochondrial Damage in Cells. *J Biochem* (2019) 167(3):303–14. doi: 10.1093/jb/mvz091
58. Ham I-H, Oh HJ, Jin H, Bae CA, Jeon S-M, Choi KS, et al. Targeting Interleukin-6 as a Strategy to Overcome Stroma-Induced Resistance to Chemotherapy in Gastric Cancer. *Mol Cancer* (2019) 18(1):68. doi: 10.1186/s12943-019-0972-8
59. Berridge MV, McConnell MJ, Grasso C, Bajzikova M, Kovarova J, Neuzil J. Horizontal Transfer of Mitochondria Between Mammalian Cells: Beyond Co-Culture Approaches. *Curr Opin Genet Dev* (2016) 38:75–82. doi: 10.1016/j.gde.2016.04.003
60. Sahinbegovic H, Jelinek T, Hrdinka M, Bago JR, Turi M, Sevcikova T, et al. Intercellular Mitochondrial Transfer in the Tumor Microenvironment. *Cancers (Basel)* (2020) 12(7):1787. doi: 10.3390/cancers12071787
61. Lemasters JJ, Holmuhamedov E. Voltage-Dependent Anion Channel (VDAC) as Mitochondrial Governor—Thinking Outside the Box. *Biochim Biophys Acta* (2006) 1762(2):181–90. doi: 10.1016/j.bbadis.2005.10.006
62. Guzun R, Kaambre T, Bagur R, Grichine A, Usson Y, Varikmaa M, et al. Modular Organization of Cardiac Energy Metabolism: Energy Conversion, Transfer and Feedback Regulation. *Acta Physiol (Oxf)* (2015) 213(1):84–106. doi: 10.1111/apha.12287
63. Saks V, Guzun R, Timohhina N, Tepp K, Varikmaa M, Monge C, et al. Structure-Function Relationships in Feedback Regulation of Energy Fluxes *In Vivo* in Health and Disease: Mitochondrial Interactosome. *Biochim Biophys Acta* (2010) 1797(6-7):678–97. doi: 10.1016/j.bbabo.2010.01.011
64. Kuznetsov AV, Tiivel T, Sikk P, Kaambre T, Kay L, Daneshrad Z, et al. Striking Differences Between the Kinetics of Regulation of Respiration by ADP in Slow-Twitch and Fast-Twitch Muscles *In Vivo*. *Eur J Biochem* (1996) 241(3):909–15. doi: 10.1111/j.1432-1033.1996.00909.x
65. Puurand M, Tepp K, Klepinin A, Klepinina L, Shevchuk I, Kaambre T. Intracellular Energy-Transfer Networks and High-Resolution Respirometry: A Convenient Approach for Studying Their Function. *Int J Mol Sci* (2018) 19(10):2933. doi: 10.3390/ijms19102933
66. Kay L, Li Z, Merickay M, Olivares J, Tranqui L, Fontaine E, et al. Study of Regulation of Mitochondrial Respiration *In Vivo*. An Analysis of Influence of ADP Diffusion and Possible Role of Cytoskeleton. *Biochim Biophys Acta* (1997) 1322(1):41–59. doi: 10.1016/s0005-2728(97)00071-6
67. Klepinin A, Ounpuu L, Mado K, Truu L, Chekulayev V, Puurand M, et al. The Complexity of Mitochondrial Outer Membrane Permeability and VDAC Regulation by Associated Proteins. *J Bioenerg Biomembr* (2018) 50(5):339–54. doi: 10.1007/s10863-018-9765-9
68. Puurand M, Tepp K, Timohhina N, Aid J, Shevchuk I, Chekulayev V, et al. Tubulin betaII and betaIII Isoforms as the Regulators of VDAC Channel Permeability in Health and Disease. *Cells* (2019) 8(3):239. doi: 10.3390/cells8030239

69. Saks VA, Belikova YO, Kuznetsov AV. *In Vivo* Regulation of Mitochondrial Respiration in Cardiomyocytes: Specific Restrictions for Intracellular Diffusion of ADP. *Biochim Biophys Acta* (1991) 1074(2):302–11. doi: 10.1016/0304-4165(91)90168-g
70. Saks VA, Veksler VI, Kuznetsov AV, Kay L, Sikk P, Tiivel T, et al. Permeabilized Cell and Skinned Fiber Techniques in Studies of Mitochondrial Function *In Vivo*. *Mol Cell Biochem* (1998) 184(1-2):81–100. doi: 10.1023/A:1006834912257
71. Messina A, Reina S, Guarino F, De Pinto V. VDAC Isoforms in Mammals. *Biochim Biophys Acta (BBA) - Biomembr* (2012) 1818(6):1466–76. doi: 10.1016/j.bbame.2011.10.005
72. Shoshan-Barmatz V, Mizrahi D. VDAC1: From Structure to Cancer Therapy. *Front Oncol* (2012) 2:164. doi: 10.3389/fonc.2012.00164
73. Shoshan-Barmatz V, Ben-Hail D, Admoni L, Krelm Y, Tripathi SS. The Mitochondrial Voltage-Dependent Anion Channel 1 in Tumor Cells. *Biochim Biophys Acta (BBA) - Biomembr* (2015) 1848(10, Part B):2547–75. doi: 10.1016/j.bbame.2014.10.040
74. Mangan PS, Colombini M. Ultrasteepest Voltage Dependence in a Membrane Channel. *Proc Natl Acad Sci* (1987) 84(14):4896. doi: 10.1073/pnas.84.14.4896
75. Colombini M, Mannella CA. VDAC, The Early Days. *Biochim Biophys Acta (BBA) - Biomembr* (2012) 1818(6):1438–43. doi: 10.1016/j.bbame.2011.11.014
76. Mathupala SP, Ko YH, Pedersen PL. Hexokinase II: Cancer's Double-Edged Sword Acting as Both Facilitator and Gatekeeper of Malignancy When Bound to Mitochondria. *Oncogene* (2006) 25(34):4777–86. doi: 10.1038/sj.onc.1209603
77. Pedersen PL, Warburg, M and Hexokinase 2: Multiple Discoveries of Key Molecular Events Underlying One of Cancers' Most Common Phenotypes, the "Warburg Effect", i.e., elevated glycolysis in the presence of oxygen. *J Bioenerg Biomembr* (2007) 39(3):211–22. doi: 10.1007/s10863-007-9094-x
78. Pedersen PL. The Cancer Cell's "Power Plants" as Promising Therapeutic Targets: An Overview. *J Bioenerg Biomembr* (2007) 39(1):1–12. doi: 10.1007/s10863-007-9070-5
79. Mathupala SP, Ko YH, Pedersen PL. Hexokinase-2 Bound to Mitochondria: Cancer's Stygian Link to the "Warburg Effect" and a Pivotal Target for Effective Therapy. *Semin Cancer Biol* (2009) 19(1):17–24. doi: 10.1016/j.semcancer.2008.11.006
80. Mathupala SP, Pedersen PL. Voltage Dependent Anion Channel-1 (VDAC-1) as an Anti-Cancer Target. *Cancer Biol Ther* (2010) 9(12):1053–6. doi: 10.4161/cbt.9.12.12451
81. Shoshan-Barmatz V, Maldonado EN, Krelm Y. VDAC1 at the Crossroads of Cell Metabolism, Apoptosis and Cell Stress. *Cell Stress* (2017) 1(1):11–36. doi: 10.15698/cst2017.10.104
82. Neumann D, Buckers J, Kastrup L, Hell SW, Jakobs S. Two-Color STED Microscopy Reveals Different Degrees of Colocalization Between Hexokinase-I and the Three Human VDAC Isoforms. *PMC Biophys* (2010) 3(1):4. doi: 10.1186/1757-5036-3-4
83. Pedersen PL, Mathupala S, Rempel A, Geschwind JF, Ko YH. Mitochondrial Bound Type II Hexokinase: A Key Player in the Growth and Survival of Many Cancers and an Ideal Prospect for Therapeutic Intervention. *Biochim Biophys Acta* (2002) 1555(1-3):14–20. doi: 10.1016/S0005-2728(02)00248-7
84. Rostovtseva TK, Tan W, Colombini M. On the Role of VDAC in Apoptosis: Fact and Fiction. *J Bioenerg Biomembr* (2005) 37(3):129–42. doi: 10.1007/s10863-005-6566-8
85. Majewski N, Nogueira V, Bhaskar P, Coy PE, Skeen JE, Gottlob K, et al. Hexokinase-Mitochondria Interaction Mediated by Akt Is Required to Inhibit Apoptosis in the Presence or Absence of Bax and Bak. *Mol Cell* (2004) 16(5):819–30. doi: 10.1016/j.molcel.2004.11.014
86. Eimre M, Paju K, Pelloux S, Beraud N, Roosimaa M, Kadaja L, et al. Distinct Organization of Energy Metabolism in HL-1 Cardiac Cell Line and Cardiomyocytes. *Biochim Biophys Acta* (2008) 1777(6):514–24. doi: 10.1016/j.bbabi.2008.03.019
87. Ahmad A, Ahmad S, Schneider BK, Allen CB, Chang LY, White CW. Elevated Expression of Hexokinase II Protects Human Lung Epithelial-Like A549 Cells Against Oxidative Injury. *Am J Physiol Lung Cell Mol Physiol* (2002) 283(3):L573–84. doi: 10.1152/ajplung.00410.2001
88. Zaid H, Abu-Hamad S, Israelson A, Nathan I, Shoshan-Barmatz V. The Voltage-Dependent Anion Channel-1 Modulates Apoptotic Cell Death. *Cell Death Differ* (2005) 12(7):751–60. doi: 10.1038/sj.cdd.4401599
89. Pastorino J, Hoek J. Regulation of Hexokinase Binding to VDAC. *J Bioenerg Biomembr* (2008) 40(3):171–82. doi: 10.1007/s10863-008-9148-8
90. Wei L, Zhou Y, Dai Q, Qiao C, Zhao L, Hui H, et al. Oroxynin A Induces Dissociation of Hexokinase II From the Mitochondria and Inhibits Glycolysis by SIRT3-Mediated Deacetylation of Cyclophilin D in Breast Carcinoma. *Cell Death Dis* (2013) 4:e601. doi: 10.1038/cddis.2013.131
91. Ikeda S, Abe F, Matsuda Y, Kitadate A, Takahashi N, Tagawa H. Hypoxia-Inducible Hexokinase-2 Enhances Anti-Apoptotic Function via Activating Autophagy in Multiple Myeloma. *Cancer Sci* (2020) 111:4088–101. doi: 10.1111/cas.14614
92. Fan T, Sun G, Sun X, Zhao L, Zhong R, Peng Y. Tumor Energy Metabolism and Potential of 3-Bromopyruvate as an Inhibitor of Aerobic Glycolysis: Implications in Tumor Treatment. *Cancers (Basel)* (2019) 11(3):317. doi: 10.3390/cancers11030317
93. Woldetsadik AD, Vogel MC, Rabeh WM, Magzoub M. Hexokinase II-derived Cell-Penetrating Peptide Targets Mitochondria and Triggers Apoptosis in Cancer Cells. *FASEB J* (2017) 31(5):2168–84. doi: 10.1096/fj.201601173R
94. Arif T, Vasilkovsky L, Refaely Y, Konson A, Shoshan-Barmatz V. Silencing VDAC1 Expression by siRNA Inhibits Cancer Cell Proliferation and Tumor Growth *In Vivo*. *Mol Ther - Nucleic Acids* (2014) 3:e159. doi: 10.1038/mtna.2014.9
95. Maldonado EN, Patnaik J, Mullins MR, Lemasters JJ. Free Tubulin Modulates Mitochondrial Membrane Potential in Cancer Cells. *Cancer Res* (2010) 70(24):10192–201. doi: 10.1158/0008-5472.CAN-10-2429
96. Maldonado EN, Lemasters JJ. ATP/ADP Ratio, the Missed Connection Between Mitochondria and the Warburg Effect. *Mitochondrion* (2014) 19 Pt A:78–84. doi: 10.1016/j.mito.2014.09.002
97. Varikmaa M, Bagur R, Kaambre T, Grichine A, Timohhina N, Tepp K, et al. Role of Mitochondria-Cytoskeleton Interactions in Respiration Regulation and Mitochondrial Organization in Striated Muscles. *Biochim Biophys Acta* (2014) 1837(2):232–45. doi: 10.1016/j.bbabi.2013.10.011
98. Jirasek T, Mandys V, Viklicky V. Expression of Class III Beta-Tubulin in Neuroendocrine Tumours of Gastrointestinal Tract. *Folia Histochem Cytobiol* (2002) 40(3):305–10.
99. Urano N, Fujiwara Y, Doki Y, Kim SJ, Miyoshi Y, Noguchi S, et al. Clinical Significance of Class III Beta-Tubulin Expression and Its Predictive Value for Resistance to Docetaxel-Based Chemotherapy in Gastric Cancer. *Int J Oncol* (2006) 28(2):375–81. doi: 10.3892/ijo.28.2.375
100. Oztop S, Isik A, Guner G, Gurdal H, Karabulut E, Yilmaz E, et al. Class III Beta-Tubulin Expression in Colorectal Neoplasms Is a Potential Predictive Biomarker for Paclitaxel Response. *Anticancer Res* (2019) 39(2):655–62. doi: 10.21873/anticancer.13160
101. Mariani M, Karki R, Spennato M, Pandya D, He S, Andreoli M, et al. Class III Beta-Tubulin in Normal and Cancer Tissues. *Gene* (2015) 563(2):109–14. doi: 10.1016/j.gene.2015.03.061
102. Mariani M, Shahabi S, Sieber S, Scambia G, Ferlini C. Class III Beta-Tubulin (TUBB3): More Than a Biomarker in Solid Tumors? *Curr Mol Med* (2011) 11(9):726–31. doi: 10.2174/156652411798062368
103. Parker AL, Turner N, McCarroll JA, Kavalarris M. betaIII-Tubulin Alters Glucose Metabolism and Stress Response Signaling to Promote Cell Survival and Proliferation in Glucose-Starved Non-Small Cell Lung Cancer Cells. *Carcinogenesis* (2016) 37(8):787–98. doi: 10.1093/carcin/bgw058
104. Cicchillitti L, Penci R, Di Michele M, Filippetti F, Rotilio D, Donati MB, et al. Proteomic Characterization of Cytoskeletal and Mitochondrial Class III Beta-Tubulin. *Mol Cancer Ther* (2008) 7(7):2070–9. doi: 10.1158/1535-7163.MCT-07-2370
105. Raspaglio G, Filippetti F, Prislei S, Penci R, De Maria I, Cicchillitti L, et al. Hypoxia Induces Class III Beta-Tubulin Gene Expression by HIF-1alpha Binding to its 3' Flanking Region. *Gene* (2008) 409(1-2):100–8. doi: 10.1016/j.gene.2007.11.015
106. Guarino F, Zinghirino F, Mela L, Pappalardo XG, Ichas F, De Pinto V, et al. NRF-1 and HIF-1alpha Contribute to Modulation of Human VDAC1 Gene Promoter During Starvation and Hypoxia in HeLa Cells. *Biochim Biophys Acta Bioenerg* (2020) 1861(12):148289. doi: 10.1016/j.bbabi.2020.148289

107. Brahimi-Horn MC, Ben-Hail D, Ilie M, Gounon P, Rouleau M, Hofman V, et al. Expression of a Truncated Active Form of VDAC1 in Lung Cancer Associates With Hypoxic Cell Survival and Correlates With Progression to Chemotherapy Resistance. *Cancer Res* (2012) 72(8):2140–50. doi: 10.1158/0008-5472.CAN-11-3940
108. Meyenberg Cunha-de Padua M, Fabbri L, Dufies M, Lacas-Gervais S, Contenti J, Voyton C, et al. Evidences of a Direct Relationship Between Cellular Fuel Supply and Ciliogenesis Regulated by Hypoxic VDAC1-DeltaC. *Cancers (Basel)* (2020) 12(11):3484. doi: 10.3390/cancers12113484
109. Baba Y, Nosh K, Shima K, Irahara N, Chan AT, Meyerhardt JA, et al. HIF1A Overexpression is Associated With Poor Prognosis in a Cohort of 731 Colorectal Cancers. *Am J Pathol* (2010) 176(5):2292–301. doi: 10.2353/ajpath.2010.090972
110. Ioannou M, Paraskeva E, Baxeivanidou K, Simos G, Papamichali R, Papacharalambous C, et al. HIF-1alpha in Colorectal Carcinoma: Review of the Literature. *J BUON* (2015) 20(3):680–9.
111. Haugen MH, Boye K, Nesland JM, Pettersen SJ, Egeland EV, Tamhane T, et al. High Expression of the Cysteine Proteinase Legumain in Colorectal Cancer - Implications for Therapeutic Targeting. *Eur J Cancer* (2015) 51(1):9–17. doi: 10.1016/j.ejca.2014.10.020
112. Zhen Y, Chunlei G, Wenzhi S, Shuangtao Z, Na L, Rongrong W, et al. Clinicopathologic Significance of Legumain Overexpression in Cancer: A Systematic Review and Meta-Analysis. *Sci Rep* (2015) 5:16599. doi: 10.1038/srep16599
113. Ferecatu I, Canal F, Fabbri L, Mazure NM, Bouton C, Golinelli-Cohen MP. Dysfunction in the Mitochondrial Fe-S Assembly Machinery Leads to Formation of the Chemoresistant Truncated VDAC1 Isoform Without HIF-1alpha Activation. *PLoS One* (2018) 13(3):e0194782. doi: 10.1371/journal.pone.0194782
114. Lipper CH, Stoffeth JT, Bai F, Sohn YS, Roy S, Mittler R, et al. Redox-Dependent Gating of VDAC by mitoNEET. *Proc Natl Acad Sci USA* (2019) 116(40):19924–9. doi: 10.1073/pnas.1908271116
115. Basak D, Uddin MN, Hancock J. The Role of Oxidative Stress and Its Counteractive Utility in Colorectal Cancer (CRC). *Cancers (Basel)* (2020) 12(11):3336. doi: 10.3390/cancers12113336
116. Caterino M, Ruoppolo M, Mandola A, Costanzo M, Orru S, Imperlini E. Protein-Protein Interaction Networks as a New Perspective to Evaluate Distinct Functional Roles of Voltage-Dependent Anion Channel Isoforms. *Mol Biosyst* (2017) 13(12):2466–76. doi: 10.1039/c7mb00434f
117. Liu H, Pu Y, Amina Q, Wang Q, Zhang M, Song J, et al. Prognostic and Therapeutic Potential of Adenylate Kinase 2 in Lung Adenocarcinoma. *Sci Rep* (2019) 9(1):17757. doi: 10.1038/s41598-019-53594-4
118. Klepinin A, Ounpuu L, Güzün R, Chekulayev V, Timohhina N, Tepp K, et al. Simple Oxygraphic Analysis for the Presence of Adenylate Kinase 1 and 2 in Normal and Tumor Cells. *J Bioenerg Biomembr* (2016) 48(5):531–48. doi: 10.1007/s10863-016-9687-3
119. Speers C, Tsimelzon A, Sexton K, Herrick AM, Gutierrez C, Culhane A, et al. Identification of Novel Kinase Targets for the Treatment of Estrogen Receptor-Negative Breast Cancer. *Clin Cancer Res* (2009) 15(20):6327–40. doi: 10.1158/1078-0432.CCR-09-1107
120. Fujisawa K, Terai S, Takami T, Yamamoto N, Yamasaki T, Matsumoto T, et al. Modulation of Anti-Cancer Drug Sensitivity Through the Regulation of Mitochondrial Activity by Adenylate Kinase 4. *J Exp Clin Cancer Res* (2016) 35:48. doi: 10.1186/s13046-016-0322-2
121. Klepinina L, Klepinin A, Truu L, Chekulayev V, Vija H, Kuus K, et al. Colon Cancer Cell Differentiation by Sodium Butyrate Modulates Metabolic Plasticity of Caco-2 Cells via Alteration of Phosphotransfer Network. *PLoS One* (2021) 16(1):e0245348. doi: 10.1371/journal.pone.0245348
122. Dzeja PP, Terzic A. Phosphotransfer Networks and Cellular Energetics. *J Exp Biol* (2003) 206(Pt 12):2039–47. doi: 10.1242/jeb.00426
123. Dzeja P, Terzic A. Adenylate Kinase and AMP Signaling Networks: Metabolic Monitoring, Signal Communication and Body Energy Sensing. *Int J Mol Sci* (2009) 10(4):1729–72. doi: 10.3390/ijms10041729
124. Klepinin A, Zhang S, Klepinina L, Rebane-Klemm E, Terzic A, Kaambre T, et al. Adenylate Kinase and Metabolic Signaling in Cancer Cells. *Front Oncol* (2020) 10:660. doi: 10.3389/fonc.2020
125. Hardie DG, Ross FA, Hawley SA. AMPK: A Nutrient and Energy Sensor That Maintains Energy Homeostasis. *Nat Rev Mol Cell Biol* (2012) 13(4):251–62. doi: 10.1038/nrm3311
126. Wang W, Guan KL. AMP-Activated Protein Kinase and Cancer. *Acta Physiol* (2009) 196(1):55–63. doi: 10.1111/j.1748-1716.2009.01980.x
127. Faubert B, Boily G, Izreig S, Griss T, Samborska B, Dong Z, et al. AMPK Is a Negative Regulator of the Warburg Effect and Suppresses Tumor Growth *In Vivo*. *Cell Metab* (2013) 17(1):13–24. doi: 10.1016/j.cmet.2012.12.001
128. Rehman G, Shehzad A, Khan AL, Hamayun M. Role of AMP-Activated Protein Kinase in Cancer Therapy. *Archiv der Pharm* (2014) 347(7):457–68. doi: 10.1002/ardp.201300402
129. Hardie DG, Ross FA, Hawley SA. AMP-Activated Protein Kinase: A Target for Drugs Both Ancient and Modern. *Chem Biol* (2012) 19(10):1222–36. doi: 10.1016/j.chembiol.2012.08.019
130. Park HU, Suy S, Danner M, Dailey V, Zhang Y, Li H, et al. AMP-Activated Protein Kinase Promotes Human Prostate Cancer Cell Growth and Survival. *Mol Cancer Ther* (2009) 8(4):733–41. doi: 10.1158/1535-7163.MCT-08-0631
131. Khan AS, Frigo DE. Regulation, Role and Therapeutic Targeting of AMPK in Prostate Cancer. *Nat Rev Urol* (2017) 14(3):164–80. doi: 10.1038/nrurol.2016.272
132. Huang X, Li X, Xie X, Ye F, Chen B, Song C, et al. High Expressions of LDHA and AMPK as Prognostic Biomarkers for Breast Cancer. *Breast* (2016) 30:39–46. doi: 10.1016/j.breast.2016.08.014

Conflict of Interest: The authors declare that the research was conducted in the absence of any commercial or financial relationships that could be construed as a potential conflict of interest.

Publisher's Note: All claims expressed in this article are solely those of the authors and do not necessarily represent those of their affiliated organizations, or those of the publisher, the editors and the reviewers. Any product that may be evaluated in this article, or claim that may be made by its manufacturer, is not guaranteed or endorsed by the publisher.

Copyright © 2021 Reinsalu, Puurand, Chekulayev, Miller, Shevchuk, Tepp, Rebane-Klemm, Timohhina, Terasmaa and Kaambre. This is an open-access article distributed under the terms of the Creative Commons Attribution License (CC BY). The use, distribution or reproduction in other forums is permitted, provided the original author(s) and the copyright owner(s) are credited and that the original publication in this journal is cited, in accordance with accepted academic practice. No use, distribution or reproduction is permitted which does not comply with these terms.

Curriculum vitae

Personal data

Name:	Sten Miller
Date of birth:	31.03.1984
Place of birth:	Tallinn, Estonia
Citizenship:	Estonian

Contact data

E-mail:	millers4891@gmail.com
---------	-----------------------

Education

2020–2025	Tallinn University of Technology, PhD study, Department of Chemistry and Biotechnology
2018–2020	Tallinn University of Technology, M.Sc. in Applied Chemistry and Biotechnology
2015–2018	Tallinn University, B.Sc. in Biology with minor in Chemistry
2005–2007	The Police and Border Guard College of the Estonian Academy of Security Sciences in Paikuse, Vocational education
2001–2004	Viimsi High School

Language competence

English	Fluent
Estonian	Native
Finnish	Fluent
Spanish	Basic

Professional employment

2018–present	National Institute of Chemical Physics and Biophysics, Tallinn, Estonia, Junior Researcher
2017–2018	Estonian Marine Institute, University of Tartu, Tallinn, Diver and Laboratory Technician
2007–2014	Estonian Police and Border Guard Board Rapid Reaction Unit, Tactical Response Officer/Medic
2007–2008	Tallinn Emergency Services, Paramedic

Supplementary Courses

31.03.2022–30.05.2022	Salford University, Translational Medicine Laboratory (UK), Associate Researcher
-----------------------	--

Supervised dissertations

Jaanika Annuk, Bachelor's Degree, 2024, (sup) Sten Miller
Key enzymes involved in glycolysis in clinical material and cell culture of colorectal cancer, Tallinn University of Technology, School of Science, Department of Chemistry and Biotechnology

Publications

Reinsalu, L*; **Miller, S***; Auditano, G. L ; Puurand, M ; Moreno-Sanchez, R; Käämbre, T (2025). The Energy Metabolism Profiling of Human Colorectal Tumors. *Journal of cellular and molecular medicine*, 29(5):e70462. doi:10.1111/jcmm.70462.

Klepinin, A; **Miller, S**; Reile, I; Puurand, M; Rebane-Klemm, E; Klepinina, L; Vija, H; Zhang, S; Terzic, A; Dzeja, P; Kaambre, T (2022). Stable Isotope Tracing Uncovers Reduced g/b-ATP Turnover and Metabolic Flux Through Mitochondrial-Linked Phosphotransfer Circuits in Aggressive Breast Cancer Cells. *Frontiers in oncology*, 12:892195. doi: 10.3389/fonc.2022.892195.

Kaup, K. K; Toom, L; Truu, L; **Miller, S**; Puurand, M; Tepp, K; Käämbre, T; Reile, I (2021). A line-broadening free real-time ³¹P pure shift NMR method for phosphometabolomic analysis. *The Analyst*, 146(22):7034. doi:10.1039/d1an90092g.

Reinsalu, L; Puurand, M; Chekulayev, V; **Miller, S**; Shevchuk, I; Tepp, K; Rebane-Klemm, E; Timohhina, N; Terasmaa, A; Kaambre, T (2021). Energy Metabolic Plasticity of Colorectal Cancer Cells as a Determinant of Tumor Growth and Metastasis. *Frontiers in oncology*, 11:698951. doi: 10.3389/fonc.2021.698951.

Elulookirjeldus

Isikuandmed

Nimi:	Sten Miller
Sünniaeg:	31.03.1984
Sünnikoht:	Tallinn
Kodakondsus:	Eesti

Kontaktandmed

E-post:	millers4891@gmail.com
---------	-----------------------

Hariduskäik

2020–2025	Tallinna Tehnikaülikool, PhD Keemia ja biotehnoloogia instituut
2018–2020	Tallinna Tehnikaülikool, M.Sc. Rakenduskeemia ja biotehnoloogias
2015–2018	Tallinna Ülikool, B.Sc. Bioloogia keemia kõrvalerialaga
2005–2007	Sisekaitseakadeemia Politseikolledži Politseikool, kutseharidus
2003–2004	Viimsi Keskkool, keskharidus

Keelteoskus

Inglise keel	Kõrgtase
Eesti keel	Emakeel
Soome keel	Kõrgtase
Hispaania keel	Algtase

Teenistuskäik

2018–2024	Keemilise ja bioloogilise füüsika instituut, Tallinn, nooremteadur
2017–2018	Tartu Ülikooli Eesti mereinstituut, Tallinn, sukelduja ja laboritehnik
2007–2014	Politsei ja piirivalveameti kiirreageerimistalitus, kiirreageerija/meedik
2007–2008	Tallinna Kiirabi, parameedik

Lisakoolitused

31.03.2022–30.05.2022	Salford University, Translational Medicine Laboratory (UK), Külalisteadur
-----------------------	---

Juhendatud väitekirjad

Jaanika Annuk, bakalaureusekraad, 2023, (juh) Sten Miller
Glükolüüsis osalevad võtmeensüümid soolevähi kliinilises materjalis ja rakukultuuris,
Tallinna Tehnikaülikool, Loodusteaduskond, Keemia ja biotehnoloogia instituut

Publikatsioonid

Reinsalu, L*; **Miller, S***; Auditano, G. L ; Puurand, M ; Moreno-Sanchez, R; Käämbre, T (2025). The Energy Metabolism Profiling of Human Colorectal Tumors. *Journal of cellular and molecular medicine*, 29(5):e70462. doi:10.1111/jcmm.70462.

Klepinin, A; **Miller, S**; Reile, I; Puurand, M; Rebane-Klemm, E; Klepinina, L; Vija, H; Zhang, S; Terzic, A; Dzeja, P; Kaambre, T (2022). Stable Isotope Tracing Uncovers Reduced g/b-ATP Turnover and Metabolic Flux Through Mitochondrial-Linked Phosphotransfer Circuits in Aggressive Breast Cancer Cells. *Frontiers in oncology*, 12:892195. doi: 10.3389/fonc.2022.892195.

Kaup, K. K; Toom, L; Truu, L; **Miller, S**; Puurand, M; Tepp, K; Käämbre, T; Reile, I (2021). A line-broadening free real-time ³¹P pure shift NMR method for phosphometabolomic analysis. *The Analyst*, 146(22):7034. doi:10.1039/d1an90092g.

Reinsalu, L; Puurand, M; Chekulayev, V; **Miller, S**; Shevchuk, I; Tepp, K; Rebane-Klemm, E; Timohhina, N; Terasmaa, A; Kaambre, T (2021). Energy Metabolic Plasticity of Colorectal Cancer Cells as a Determinant of Tumor Growth and Metastasis. *Frontiers in oncology*, 11:698951. doi: 10.3389/fonc.2021.698951.

ISSN 2585-6901 (PDF)
ISBN 978-9916-80-304-2 (PDF)